Swansea University
Prifysgol Abertawe

IDENTIFICATION OF MICRO- AND SUBMICRON (NANO) PLASTICS IN WATER SOURCES AND THE IMPACT OF COVID-19 ON PLASTIC POLLUTION

Javier Delgado Gallardo

BSc (Biology, Salamanca University, Spain)

MBus (Quality, Environmental and Risk Management, EEN, Spain)

MSc (Water and Environmental Management, University of Brighton, UK)

Submitted to Swansea University in fulfilment of the requirements for the Degree of Doctor of Philosophy

Swansea University

2022

Abstract

One of the most significant environmental issues that our society may deal with this century could be plastics. The world's water bodies, as well as land and air, are becoming more and more contaminated by plastic due to the ongoing and expanding manufacturing of these synthetic materials, as well as the lack of an effective strategy for managing plastic waste. The fact that plastics break down into smaller particles (micro and nanoplastics) by action of environmental physical and chemical reactions, and do not degrade biologically in a reasonable time, is a cause of concern as plastics are believed to cause harm in animals, plants and humans.

To identify the types of plastics prevalent in aquatic habitats, a number of procedures have been developed, from sampling to identification. After a water body has been sampled using nets, pumps, or other tools, depending on the type of sample taken, it is usually necessary to treat the samples for separation and purification. The next stage is to employ analytical techniques to identify the synthetic contaminants. The most common approaches are microscopy, spectroscopy, and thermal analysis. This thesis gives an overview of where in the environment microplastics (MPs) and nanoplastics (NPs) can be found and summarizes the most important technologies applied to analyse the importance of plastics as a contaminant in water bodies. The development of standardised analytical procedures is still necessary as most of them are not suitable for the identification of particles below 50 μm due to resolution limitations. The preparation and analysis of samples are usually time-consuming factors that shall be considered. Particularly for MP and NP analysis in aqueous samples, thermal analysis methods based on sample degradation are generally not considered to be the most effective approach. Nevertheless, Pyrolysis - Gas Chromatography Time-of-Flight Mass Spectrometry (Py-GCToFMS) is used in this thesis to propose a novel approach as due to its unique detection abilities, and with a novel filtration methodology for collection, it enables the identification of tiny particle sizes (>0.1 μm) in water samples.

PTFE membranes were selected to filter the liquid samples using a glass filtration system. This way, the synthetic particles will be deposited on the membranes and will allow the study and analysis of the precipitated material. PTFE is a readily available, reasonably priced, and adaptable product that makes sample preparation quick and simple.

The three plastics under study—polypropylene (PP), polystyrene (PS), and polyvinyl chloride (PVC)—can be identified from complex samples at trace levels thanks to the employment of these widely used membranes and the identification of various and specific

(marker) ions. The technique was examined against a range of standards samples that contained predetermined concentrations of MPs and NPs. Detection levels were then determined for PVC and PS and were found to be below <50 µg/ L, with repeatable data showing good precision (RSD <20 %). The examination of a complex matrix sample taken from a nearby river contributed to further validate this innovative methodology; the results indicated the existence of PS with a semi-quantifiable result of 250.23 g/L. Because of this, PY-GCToFMS appears to be a method that is appropriate for the task of identifying MPs and NPs from complex mixtures.

This thesis also focuses on the environmental challenge that disposable plastic face masks (DPFMs) pose, which has been made significantly worse due to the COVID-19 pandemic. By the time this thesis was written, the production of disposable plastic facemasks had reached to approximately 200 million a day, in a global effort to tackle the spread of the new SARS-CoV-2 virus. This thesis investigates the emissions of pollutants from several different DPFM brands (medical and non-medical) that were submerged in water to replicate the conditions in the environment after these DPFMs have been discarded. The DPFM leachates were filtered using inorganic membranes type and characterized using Fourier transform infrared spectroscopy (FTIR), Scanning electron microscopy coupled with energy-dispersive X-ray spectroscopy (SEM-EDS), Light/Optical Microscopy (LM/OM), Inductively coupled plasma mass spectrometry (ICP-MS) and Liquid chromatography–mass spectrometry (LC-MS). Micro and nano scale polymeric fibres, particles, siliceous fragments and leachable inorganic and organic chemicals were observed from all of the tested DPFMs. For non-medical DPFMs, traces of concerning heavy metals were detected in association with silicon containing fragments (i.e. lead up to 6.79 µg/L). ICP-MS also confirmed the presence of other leachable metals like cadmium (up to 1.92 µg/L), antimony (up to 3.93 µg/L) and copper (up to 4.17 µg/L). LC-MS analysis identified organic species related to plastic additives; polyamide-66 monomer and oligomers (nylon-66 synthesis), surfactant molecules, and dye-like molecules were all tentatively identified in the leachate. The question of whether DPFMs are safe to use daily and what implications may be anticipated after their disposal into the environment is brought up by the toxicity of some of the chemicals discovered.

The previous approach is expanded to medical DPFMs with the utilisation of Field Emission Gun Scanning Electron Microscope (FEG-SEM) in order to get high resolution images of the micro and nanoparticles deposited on the membranes. It is also incorporated the use of

0.02 µm pore size inorganic membranes to better identify the nanoparticles released. Separated aqueous samples were also obtained by submerging medical DPFMs for 24 hours to be analysed using ICP-MS and LC-MS.

Both particles and fibres in the micro and nano scale were found in all 6 DPFMs brands of this study. EDS analysis revealed the presence of particles containing different heavy metals like lead, mercury, and arsenic among others. ICP-MS analysis results confirmed traces of heavy metals (antimony up to 2.41 µg/L and copper up to 4.68 µg/L). LC-MS analysis results identified organic species related to plastic additives and contaminants; polyamide-66 monomer and oligomers (nylon-66 synthesis), surfactant molecules, and polyethylene glycol were all tentatively identified in the leachate. The toxicity of some of the chemicals found raises the question of whether DPFMs are safe to be used on a daily basis and what consequences are to be expected after their disposal into the environment.

Declarations

This work has not previously been accepted in substance for any degree and is not being concurrently submitted in candidature for any degree.

Signed: Javier Delgado Gallardo 

Date 17/04/2023

This thesis is the result of my own investigations, except where otherwise stated. Other sources are acknowledged by footnotes giving explicit references. A bibliography is appended.

Signed: Javier Delgado Gallardo 

Date 17/04/2023

I hereby give consent for my thesis, if accepted, to be available for photocopying and for inter-library loan, and for the title and summary to be made available to outside organisations.

Signed: Javier Delgado Gallardo 

Date 17/04/2023

The University's ethical procedures have been followed and, where appropriate, that ethical approval has been granted.

Signed: Javier Delgado Gallardo 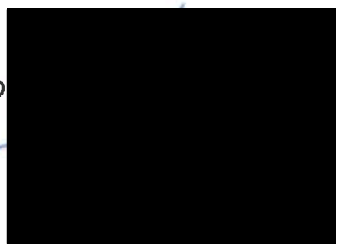

Date 17/04/2023

Table of Contents

Acknowledgements

I would like to express my very great appreciation to my supervisor Dr Sarper Sarp, for his invaluable guidance, enthusiastic encouragement, support, and useful critiques throughout the entirety of my study. Also, thanks to my colleague and friend Dr Geraint Sullivan for his important input, advice, and constructive suggestions during the developmentof this work.

I would also like to extend my thanks to Dr Eurig Wyn Jones and the technical staff Ian Matthews, Benjamin Harrison, and all the technicians that helped us during this project.

I wish to thank my parents Juan José and Eugenia, my brothers, sisters in law, cousins and friends for their constant support, love, motivation and care. All my love goes to Saúl, Martín and Alba my nephews and niece. This is for you, with the aim that you will continue this fight and try to make this world a better place.

My special thanks go to my friends and colleagues at Swansea University, Regina Khayrullina, Sandra Hernandez-Aldave, Diana Meza, Simona Ferraraccio, Becky Hudson and Aya Gallab for their support, encouragement, and constant belief in me.

I would like to express special thanks to EPSRC and Swansea University Faculty of Science and Engineering for funding this work. The Engineering and Physical Sciences Research Council (EPSRC) is the main funding body for engineering and physical sciences research in the UK.

List of Figures

List of Tables

Abbreviations

List of abbreviations used in this document:

Abbreviation	Definition
AF	Area of the filter
AFM	Atomic force microscopy
ANOVA	Analysis of variance
API	Atmospheric pressure ionization
AS	Area of sample shard
ATR	Attenuated total reflection
BEEP	Basic enzymatic purification process
BPA	Bisphenol A
BS	British Standard
CARS	Coherent anti-Stokes Raman scattering
CLSM	Confocal laser scanning microscopy
DAD	Diode-Array Detection
DEFRA	Department for Environment, Food and Rural Affairs
DNA	Deoxyribonucleic acid
DPFMs	Disposable plastic face masks
DSC	Differential scanning calorimetry
ECHA	European Chemicals Agency
EDS	Energy-dispersive X-ray spectroscopy
EI	Electron impact ionisation
ESI-MS	Positive electrospray mass spectrometry
EU	European Union
EVA	Ethylene vinyl acetate
FEG-SEM	Field Emission Gun Scanning Electron Microscope
FFP2	Filtering Face Piece 2
FITC	Fluorescent isophosphate
FPA	Focal plane array
GC-VUV	Gas chromatography–vacuum ultraviolet spectroscopy
FTIR	Fourier transform infrared spectroscopy
GPS	Global Positioning System
H	Hydrogen
H_2O	Water
H_2O_2	Hydrogen peroxide
H_2SO_4	Sulfuric acid
HCl	Hydrochloric acid
HDPE	high-density polyethylene

Abbreviation	Definition
HNO_3	Nitric acid
HPLC	High-performance liquid chromatography
HSI	Hyperspectral imaging
ICP-MS	Inductively coupled plasma mass spectrometry
IDH	Isocitrate dehydrogenase
KBr	Potassium bromide
Kg	Kilogram(s)
L	Litre
LC-MS	Liquid chromatography–mass spectrometry
LC-UV	Liquid chromatography–ultraviolet
LDH	lactate dehydrogenase
LOD	Limit of detection
MD	Medical devices
MeCN	Acetonitrile
MFFF	Magnetic field flow fractionation
MPs	Microplastics
MRFA	Met-Arg-Phe-Ala acetate salt
MSFD	European Marine Strategy Framework Directive
µg	Microgram(s)
µm	Micrometre(s)
NA	Non applicable
NaI	Sodium Iodide
ND	Not detectable
NMR	Nuclear magnetic resonance
NPs	Nanoplastics
OPA	Organic plastic additives
PA	Polyamide
PAN	Polyacrylonitrile
PBS	Phosphate-buffered saline
PC	Polycarbonate
PE	Polyethylene
PEG	Polyethylene glycol
PET	Polyethylene terephthalate
PFE	Pressurised fluid extraction
PHB	Poly(hydroxybutyrate)
PMMA	Polymethyl methacrylate
POM	Polyoxymethylene
PP	Polypropylene
PS	Polystyrene
PTFE	Polytetrafluoroethylene
PU	Polyurethane
PVC	Polyvinyl chloride
PVOH	Polyvinyl alcohol

Abbreviation	Definition
PY-GCMS	Pyrolysis gas chromatography mass spectrometry
PY-GCToF	Pyrolysis-gas chromatography time of flight mass spectrometry
REACH	Registration, Evaluation, Authorisation and Restriction of Chemicals
RF	Radio frequency
RGB	Red/green/blue
RP-HPLC	Reversed phases high-pressure liquid chromatography
RSD	Relative standard deviation
RT	Raman Tweezers
SDS	Sodium dodecyl sulphate
SEC	Size-exclusion chromatography
SEM	Scanning electron microscopy
SiMP	Micro silica particles
SiNPs	Nano silica particles
SMLM	Single molecule localization microscopy
SPM	Scanning probe microscopes
SPT	Sodium polytungstate
STA	Simultaneous thermal analysis
SVM	Support vector machine
TAF	Total atmospheric fallout
TD	Thermal desorption
TED	Thermal extraction desorption
TEM	Transmission Electron Microscopy
TGA	Thermogravimetric analysis
TOC	Total organic carbon
ToF	Time-of-flight
UEPP	Universal enzymatic purification protocol
UK	United Kingdom
UV-VIS	Ultraviolet (UV)-visible spectroscopy
WHO	World Health Organisation
WWTP	Wastewater treatment plant
$ZnCl_2$	Zinc chloride

Chapter 1: Introduction and literature review

1. General Introduction

Despite their vast applications, plastics are an environmental sensitive issue due to their resistance to biological and chemical degradation, which entail the accumulation of these materials in the environment[1]. Plastic debris is fragmented into smaller particles by action of natural ultraviolet radiation and other physical forces[2]. Microplastics (MPs) and nanoplastics (NPs) are synthetic materials below 5 mm[3] and 0.001 mm[4] respectively, whereby, the nanoscale is defined between 1nm to 100 nm[5]. Nevertheless, NPs differentiate from MPs not only in size, but also because of their bioavailability, interactions with light and natural colloids, diffusion times for the release of plastic additives and high fraction of particle molecules on the surface[6]. Because of their potential for faster fragmentation in the environment and the higher particle heterogeneity, NPs can also be distinguished from engineered nanomaterials. All these specific features have an effect on their environmental impact and fate, sampling, study and potential consequences on biota and human health[6].

Based on this information, and with increasing levels of plastic produced every year, the main goal of this project is to be a compendium of information concerning the actual situation of MPs and NPs worldwide and, most important, to develop a new standard methodology for the identification and quantification of MPs and NPs, given that there is still not such approach and it is an essential step in order to facilitate and unite the obtainment of results worldwide.

After a year of starting this project, the COVID-19 pandemic started, and all work was stopped for many months. Even when tasks could be resumed, every purchase of new material, every meeting with colleagues, the repair of equipment, and access to the labs have been laboriously complicated and it has affected the progress of this investigation.

Additionally, in August 2020 our lab was completely affected by a fire in the building it was allocated, with practically a total loss of all our equipment and samples. This unfortunate event delayed even more the attainment of results and the progress of this study. Even when several months extension was granted, the working pace and the achievement of set milestones have been utterly affected with multiple postponements and cancellations.

Nevertheless, this thesis includes information published in four different articles of relevant

impact and widely citated. These articles can be found at the end of this introduction, and they are also mentioned on every chapter.

1.1. MPs and NPs in the environment

1.1.1. Water

The investigation of MPs in water bodies is broad. MPs present a ubiquitous source of contamination in marine and freshwater environments[7]. Fresh water bodies are recently the focus of more investigations. A study reported the presence of MPs in channel bed sediments at 40 sites across urban, suburban, and rural river catchment areas in northwest England. MPs contamination was ubiquitous to all river channel beds, with the highest concentration of 517000 particles m^{-2} measured at one point[8]. They also studied the influence of severe flooding in these catchment areas and the fact that after one of these events, approximately 70% of the MPs load stored on these river beds (43 ± 14 billion particles) were exported and microbead contamination was eradicated on 7 sites. This report also points out the fact that the number of particles found in their studies equates to approximately 0.5% of the total estimated floating MPs load in the global ocean (4.85 trillion particles). Given the relatively small size of the catchment study, it is quite likely that the total MPs burden in the oceans across the globe may be far higher than this previous estimation[8].

Another report analysed large MP particles in sediments at four sites of tributaries of the river Thames, finding plastic pollution in all sites, with the highest concentration with an average of 66 particles 100 per gram, 91% of which were fragments. Sewage effluent input and population were chosen as predictors MPs presence[9].

Looking at data extracted from another article in relation to MPs contamination in the sediments of Edgbaston Pool (a shallow eutrophic lake in central Birmingham), the results are comparable with reported river sediment studies, adding evidence of the MPs ubiquity in all water environments[10].

The latter two articles also point out to the high concentration of MPs associated with paint used for road marking and the likelihood for it to be a widespread problem, affecting also animals in the habitat.

Related to this, the Norwegian Institute for Water Research has also released a study where they specify the most common sources for MPs in road dust. The worn surface of car tyres and marking paints are among them. They have also developed a model of potential pathways for road-associated MP particles that may end up in the aquatic or terrestrial environment.

However, there are many potential pathways, each of them governed by a set of transport and transformation processes. Since each of these processes are influenced by a wide range of factors, with spatial and temporal variations depending on local conditions, the complete picture is extremely complex[11].

The presence of MPs in urban stormwater has been also studied. Once the stormwater was collected in two ponds, optical and FTIR technologies were applied for the identification and quantification of MPs down to 48.5 μm. Among the synthetic particles found, PE was the most abundant plastic[12].

Aquaculture activities have also been subject to study as they are considered another source of MPs in aquatic environments. A study was done in a complex interconnected freshwater body, a pond-river-lake connection water system, where the abundance of MPs was evaluated for a 6-month period. The results suggest the increasing and decreasing of MPs on each water body depending on the month of study, although the rise of these pollutants into the whole water system is observed during the aquaculture period at it ponds receives a major inland-sourced plastic waste[13].

The contamination of groundwater by MPs and NPs has been broadly neglected, although some studies have proven this type of pollution with samples containing up to 15.2 particles/L[14] and 19.9 particles/L belonging to the principal polymer classes, which include, polyvinyl chloride, polyamide, polyester, polypropylene, and polyethylene[15].

Regarding NPs, it has been demonstrated they can also be subject to active degradation processes such as physical deterioration and photodegradation[16]. The depolymerization of plastic polymers into individual monomers occurs mostly in the water column where oxygen and hydroxyl radicals (OH) on the plastic surface play a significant role[17]. The porewater biogeochemical conditions (i.e., pH, ionic strength, natural organic matter content, microbial community composition, and geological background) as well as the properties of the plastics (e.g., polymer composition) and the physical characteristics of the sediments (i.e., density and particle size distribution) all have a significant impact on the degradation processes of NPs[18].

Environmental conditions may affect and modify the surface charges, reactivities, shape, chemical content, and morphology of NPs. The surface functional groups and surface charge of NPs are also impacted by the pH of the aquatic environment, either facilitating or impeding aggregation[19].

The charged NPs can interact with one another or experience electrostatic repulsion

depending on the pH of the surrounding environment[20]. Salinity alters NPs' stability by causing them to aggregate through electrostatic interactions. When NPs were subjected to a salinity (NaCl) >5%, the aggregation of positively and negatively charged NPs was observed; the hydrodynamic diameter of NPs significantly increased as NaCl concentrations increased[21].

Another positive correlation factor that has been documented is alkalinity, as pH can affect the competition between van der Waals force and electrostatic repulsion between particles, and thus, affecting the degree of spaciousness of clusters[22]. On the other hand, natural organic matter, aging and extracellular polymeric substances are among the reported factors that reduce the aggregation ability of NPs[23].

1.1.2. Air

The environmental fate of MPs and NPs in the air is a cause of increasing concern. One of the first investigations carried out estimated the appearance of fibrous MPs in total atmospheric fallout (TAF) between 2 and 355 fibres per m^2 per day, highlighting the probable importance of rainfall influence on fallout flux[24].

About this matter, a more recent study has proven that MPs do exist in rain, describing them as a new atmospheric pollutant. The most observed type of pollutant under a binocular microscope were plastics fibres, but also beads and shards were found. Although bigger amounts of MPs were found in samples collected from urban sites, the frequent occurrence of these polymers in samples of remote site suggest that the deposition of MPs via rainfall is pervasive and not only an urban phenomenon [25].

In the same vein, the atmospheric transport and deposition of MPs up over a distance of 95 km was demonstrated. Samples taken over five months in the French Pyrenees area contained MPs fibres up to ~750 µm long and fragments ≤300 µm. The article also reports daily deposition counts on the catchment of 249 fragments, 73 films and 44 fibres per square metre[26]. More recently, another study has demonstrated that up to 25.89% of atmospheric particles are synthetic MPs, with this amount decreasing exponentially from megacities to open oceans[27].

On another article, fibres in the air outdoors and indoors were analysed, including indoors settled dust. Concentrations fluctuate from 1.0 to 60 fibres per m^3 indoors and 0.3 to 1.5 per m^3 outdoors[28].

Furthermore, a recent article has demonstrated high concentrations of PET-based MPs of

38–120,000 μg/g in all the 286 indoor dust samples analysed collected from 12 different countries. A positive correlation was found between the concentrations of this polymer and other ones like polycarbonate (PC) and bisphenol A (a PC monomer). The study also calculates that an amount of 38–120,000 μg/kg bw (body weight) PET-based MPs is daily taken by infants via indoor ingestion[29].

Laundering synthetic textiles and clothes is a source MPs and NPs emissions into the environment. However, very little is known about mechanical drying as a source of MPs and NPs emissions. In a recent article, MP emissions from a household vented dryer into the surrounding air were proven. Microscopy was used for particle quantification and characterisation, followed by Fourier-Transform Infrared Spectroscopy (FTIR) and Pyrolysis Gas, to sample and analyse microfibres in the ambient air and while the dryer was operating[30].

MPs and have been identified in samples of air and are proven breathable by humans[31]. According to the authors, plastic particles and fibres suspended on air enter human respiratory system and are both inhalable (when they deposit on the upper airway via mouth and nose) and respirable (when they reach and accumulate in the deep lung).

Using a breathing thermal manikin, another study discuss how humans are exposed to airborne MPs indoors, where samples were analysed using focal plane array (FPA)-FTIR-Imaging spectroscopy followed by analyses down to 11 μm particle size. MP contamination was present in all samples at values ranging from 1.7 to 16.2 particles per m^3. Average synthetic fragment and fibre content was 4% of all identified particles, while non-synthetic protein and cellulose particles made up 91% and 4% of the total. All samples contained primarily polyester (81%), followed by polyethylene (5%), and nylon (3%). In general, MPs were smaller than non-synthetic particles[32].

MPs have been also detected in samples of human lower airway from bronchoalveolar lavage fluid (BALF), most of which were polyester and rayon fibres. This study also points at the inverse correlation between lung function and fibre concentration and suggest that MPs may be related with respiratory pathologies after inhaling them[33].

For NPs, it is usually assumed that these pollutants are formed when macro or microplastics physically degrade after being discharged into the environment, and atmospheric NPs are linked to different mechanical forces like aerosolization by wind. However, direct sources of NPs into the air are being identified. It has been recently discovered that technologies generally used to repair sewer pipes in urban areas may be releasing considerable amounts

of NPs into the atmosphere as steam-laden waste elements[34]. Still, the emissions and origin of unintended NPs are poorly understood and largely unaccounted[6].

1.1.3. Soil

MPs have been also found underground and on river banks. It is believed that, after further research, the soil in agricultural and urban areas will prove to be a higher environmental reservoir for MPs and NPs than in marine environments[35]. The physical parameters of the soil are negatively impacted by MPs by lowering bulk density, aggregate stability, and micropore volume while raising evaporation and desiccation rates. The chemical parameters are also impacted by decreases in cation exchange and hydraulic conductivity of the soil. Furthermore, biological parameters were also affected to the same extent[36].

The use of sewage sludge on farm soils has been pointed out as one of the largest sources of MPs introduction into the environment. In Europe and North America, around 50% of this sludge is processed for agricultural use as a fertilizer[37]. The estimated amount of MPs incorporated annually to European soils is ranged between 125 and 850 tonnes of MPs per million inhabitants, whilst between 1270 and 2130 tonnes of MPs per million inhabitants are released to urban environments[37].

The potential leaching of these contaminants into groundwater through biopores formation by earthworms is more than plausible, and fundamental reasoning suggests that NPs with a density higher than water can be an agent for a potential pathways to human exposure[38]. According to DEFRA's 2012 report, significant amounts of sewage sludge (80% of all sludge) are applied to land in the UK[39].

It has been demonstrated that soil wetting front (the region of rapid change in colour resulting from an increased water content) vertical and horizontal movements, dissolved organic carbon, and total nitrogen content can all be reduced by 14, 10, 9, and 7%, respectively by plastic waste and MPs. Not only that, in the presence of these, plant height and root biomass fell by 13 and 14%, respectively, while soil animals' body masses and reproduction rates fell by 5 and 11%, respectively[40]. Plant photosynthesis can also be altered in presence of MPs as they interfere with the microbial metabolism and the correlation among microbes in the soil[41].

Due to the ongoing increases in the global plastic manufacturing, the resilience of MPs and NPs, and the long-term degradation rate of existing plastic contamination, the current concerns posed by soil MP contamination to soil health are expected to persist[36].

In relation to NPs, it has been demonstrated how this particles combine with minerals and organic matter present in soil and it is believed these aggregations may last for centuries[42]. Nevertheless, there is still very little information about NPs in this environment, most likely due to the lack of appropriate analytical technologies in order to carry out analysis on heterogeneous and complex soil samples[43]. In a recent study, the extraction and identification of NPs from soil samples was performed by adding ultrapure water to the soil samples and filtered with 0.8 μm filters. The filtrates were fractionated by asymmetric flow-field flow fractionation coupled to UV spectroscopy and static light scattering and analysed using PY-GCMS afterwards[44].

1.1.4. Food and beverages

Food and drinking water have been also subject of study. In the past few years, MPs and fibres have been located in a wide range of worldwide commonly used products. The findings show that aquatic food products, such as fish and bivalves, provide a wide range, from 0–10.5 items/g for bivalves to 0–20 items/individual for fish[45]. Literature data on salt show that concentrations range from 0 to 13,629 particles/kg and drinking water has been demonstrated to have a concentration range of 0 to 61 particles/L for tap water and 0 to 6292 MPs/L for bottled water, making it another channel for human exposure to MPs[45]. Additionally, MPs have been discovered in packaged foods, sugar, honey, fruits, vegetables, and beverages. As a result, the ingestion of MPs by humans represents a non-negligible exposure pathway[45].

High concentrations have been found in honey and sugar[46], beer[47], table salt[48] and shellfish among others[49].

A study shows how MPs have been found in 93% of 259 bottled waters from different lots of international brands[50]. This outcome has led the World Health Organisation (WHO) to announce a review into the potential risks of plastic in drinking water.

Studies using spectroscopy analysis on samples from plastic food containers revealed that the plastic debris came from the plastic materials which were unintentionally produced during manufacturing. Particles with different forms were discovered using SEM scanning, which may be indication that the MP impact data models currently being employed do not accurately represent genuine MPs. Additionally, it was demonstrated that MPs and NPs are easily displaced by a conventional water wash, releasing particles that are typically less than 50 nm. It was also pointed out the possibility that the general population may be exposed to

MPs on a larger scale than is currently documented[51]. However, uncertainty persists on whether direct MP and NP pollution from plastic packaging poses a risk to human health. Investigations have been done with samples from the most popular plastic food packaging products from North America, Europe, and Asia-Pacific. It was determined that food containers exposed to high temperatures (up to 90 °C) emitted more than 10 million MPs per mL of water. It has also been shown that recycled plastic food packaging continuously releases MPs and NPs. Both leachates are easily ingested by murine macrophages (macrophages from rodents of the family Muridae), indicating that while exposure to NP significantly inhibited macrophage lysosomal activity, short-term MP exposure may cause inflammation. It was also suggested that the growing use of plastic packaging can offer serious health hazards to consumers, by demonstrating that MPs and NPs emitted from food containers can exhibit differentially detrimental impacts on macrophage activity[52].

1.1.5. Human health

Regarding potential risk for the fauna and humans, there is an increasing preoccupation about the effect of plastic fragments on seabirds, fish and other life in the oceans. Investigations are reporting the toxic effects of MPs in different species. A study has demonstrated the neurotoxicity, oxidative damage and energy-related changes caused by MPs in the European Seabass. They conclude that MPs alone caused neurotoxicity, lipid peroxidation in brain and muscle, and changed the activity of energy-related enzymes lactate dehydrogenase and isocitrate dehydrogenase (LDH and IDH)[53].

Apart from entering the human body via consumption or inhaled, the presence of MPs was discovered on human placentas using Raman Micro-spectroscopy. Several plastic fragments (ranging in size from 5 to 10 μm) with spherical or irregular shape were detected. All MP particles were characterised in terms of their morphology and chemical make-up. They were all pigmented and all are used in synthetic coatings, paints, adhesives, plasters, finger paints, polymers, cosmetics, and personal care products[54].

It is of special interest the fact that NPs, of a size small enough to cross the cell wall, could interact with the cell functions. An article about this issue expounded the different risks associated with plastics and their potentially dangerous additives. Those considered of concern to human health include phthalates, bisphenol A (BPA), brominated flame retardants, triclosan, bisphenone and organotins. The leaching of these toxic chemicals, from the core of the particle to the surface, could result in a long-term source of chemicals in body

fluids and tissues[55].

In order to give plastics flexibility, phthalates are widely utilised as plasticizers. They are an addition, and thus, because they are not chemically linked to the polymer (covalently bonded), they are more likely to be released into the environment. More than 80% of the plasticizers used globally are phthalates. It has been demonstrated that phthalate exposure has a biological effect in the utero and may be related to a shorter gestational period[56] and there is some evidence to suggest a connection between phthalate exposure and allergies and asthma, especially in children[57].

BPA is used in the production of polycarbonate plastics and epoxy resins and added in the process during polymerization. It has exceptional resistance to high temperatures and impacts[58]. By imitating or preventing the actions of natural hormones, this compound is an endocrine disruptor that has an influence on human health. This pollutant may also cause oxidative stress, damage to cell signalling pathways, inhibition of DNA methylation, direct effects on tissue or cells, reproductive toxicity, neurotoxicity, and a range of diseases in the human body, including diabetes, obesity, thyroid function changes, induced reproductive diseases, and even cancer. BPA can also disrupt the endocrine system's ability to function normally[59].

Another investigation reaffirms this idea pointing to the potential induction of physical damage through the particles itself and MPs/NPs alone producing biological stress or leaching of additives (inorganic and organic)[60].

Other study emphasises on the high surface curvature and the particular surface chemistry of NPs compared with MPs. NPs externally absorbed into cells might cause damage by interfering with several essential membrane processes related to the intracellular homeostasis of the exposed organism[61].

This concurs with investigations carried out on cerebral and epithelial human cells. Results confirmed that one of the mechanisms of cytotoxicity at cell level is the oxidative stress, as has been observed for both cell lines and contributes to the current knowledge of the effects of MPs and NPs[62].

Another study examined and compared the cytotoxicity of chlorinated polystyrene microplastics to that of unchlorinated polystyrene microplastics (PS-MPs) in order to imitate the reactions that take place during the treatment of drinking water[63]. Clean PS-MPs did not alter in size after being disinfected with chlorine, but their surface became rougher. On the surface of chlorinated PS-MPs, numerous carbon-chlorine bonds and persistent free radicals

were also produced. When compared to unchlorinated PS-MPs, chlorinated PS-MPs significantly reduced cell proliferation, altered cellular shape, disrupted the integrity of the cell membrane, triggered an inflammatory response in the cells, and caused apoptosis. The increased surface roughness and altered surface chemistry of these PS-MPs following chlorine disinfection could be the cause of the enhanced cytotoxicity[63].

Although there is currently a lack of conclusive evidence connecting the consumption of MPs to human health, results from correlative studies in individuals exposed to high concentrations of these pollutants, model animal and cell culture experiments, suggest that effects of MPs may include inducing toxicity to the reproductive and developmental systems as well as immune and stress responses[64]. More extensive clinical trials ought to be conducted in order to evaluate the possible effects of this recently discovered environmental pollutant[64]. More examples of the toxicity of MPs and NPs can be found in the introduction of every chapter in order to help with the narrative and present the cases that are more relevant to each section.

1.2. Review of Techniques Used in the Detection of Micro- and Nanoplastics in Aquatic Environments

As previously indicated, MPs and NPs are produced by the natural weathering of larger primal plastic precursors and represent one of the most recent and significant issues with regards to environmental pollution, since they are not biodegradable in the short and medium term due to their inert chemical features[1]. Proportionally, polyethylene (PE) is the most common polymer found in the environment, followed by polypropylene (PP) and polystyrene (PS). Other less frequently observed polymers are polyester, polyamide (PA), polyvinyl chloride (PVC), polyethylene terephthalate (PET), Ethylene vinyl acetate (EVA), polymethyl methacrylate (PMMA), polyacrylonitrile (PAN), polyvinyl alcohol (PVOH) and alkyd polymers[65]. The focus of current research is on the most frequent plastics, whose distribution in various ecosystems is not uniform. From the perspective of detection, the type of plastic present in a sample might be a good indicator of the environment it was taken from (i.e. plastic polymers presenting higher densities will be most likely found in benthic sediments rather than on the top layers of a water column)[66].

Oceanic plastic litter has been on the rise since the 1960's[67], and ever since then, a variety of strategies have been used to locate MP and NP particles worldwide in a variety of environmental matrices, with diverse degrees of success[31,38,68]. Amongst them, the most

commonly techniques used are spectroscopic approaches, including Fourier transform infrared (FTIR) spectroscopy and Raman spectroscopy, microscopy techniques (light and electron microscopy) and thermal analysis studies, including thermal gravimetric analysis (TGA) to coupled pyrolysis gas chromatography mass spectrometry (PY-GC/MS).

It has been shown that FTIR, Raman, light microscopy, and SEM all have associated constraints, such as the inability to identify between complex mixtures, despite being realistically effective for qualitative work. The detection levels of these devices have also been discovered to be restricted by resolution limitations. As a result, identifying and quantifying particles smaller than 50 μm presents an additional challenge[69,70].

Additionally, it has been established that thermal analysis techniques are generally not suitable methods for the analysis of MPs and NPs, particularly when investigating liquid samples, due to the small sample sizes acquired and consequent reduction in the detection levels. Recent studies are, however, getting over these restrictions and providing quicker and more reliable methods for identifying and quantifying MPs and NPs in the environment. For example, thermochemolysis in combination with pyrolysis coupled to gas chromatography-mass spectrometry has been proposed as an appropriate analytical method for the detection and quantification of these pollutants in environmental samples[71]. Differential scanning calorimetry (DSC) has been also suggested as a valid method for the identification and quantification of MPs in exemplary environmental matrices[72].

Further to these new advancements in analytical methods, it has been established that the processes of collection, separation, and purification performed before to identification analysis are essential in order to achieve the best results and preventing sample contamination. In general, the fact that many of the instruments and apparatus used to gather and examine the samples are made (wholly or partially) of plastic implies a high risk of contamination and biased study results[73].

This section aims to present a summary of the most common techniques for sampling, separation, purification and analysis of micro and nanoplastics in aqueous samples and an overview of the latest technologies applied in this area. The use of the different approaches in different environments is also presented to give a notion of the importance of this environmental issue.

In the paragraphs below, some images depict the analysis of MPs and NPs in bio-samples rather than in aqueous samples in order to provide a better visual experience and for the

benefit of better perception. The purpose of this research remains the same, nonetheless, since it presents a complete and inquisitive analysis of the methodologies utilised to examine MPs and NPs in aqueous environments.

The novelty of this study resides in the extent to which it examines sampling methods applied to samples taken from aquatic habitats, which constitutes nearly all of its focus. This piece combines numerous of the most recent studies concerning the environmental hazard that plastics represent, in comparison to earlier articles that have addressed related topics.

1.2.1. Sampling technologies

It is noticeable the pervasiveness of plastics everywhere. Almost everything, even the analytical equipment used daily, is produced entirely or mostly of synthetic polymers. The MPs and NPs sampling procedure, as well as the subsequent preparation and evaluation, can therefore be contaminated by outside sources. It is strongly advised that non-plastic materials and equipment are used during the entire investigation in order to prevent this[74].

Standardized sample methods for water analysis have been developed and are discussed below, especially for relatively clean waters like seas and large freshwater bodies. As a result of the low MP and NP concentrations in these habitats, considerable quantities of water must be sampled in order to produce a large enough sample size for analysis. Typically, this is carried out by placing different kinds of nets[74].

1.2.1.1. Nets and sieves

The sampling of MPs in large volume water surfaces is carried out using modified versions of conventional plankton collection methods. Since they are simple to deploy and operate and have a lower limit of detection of 333 μm, floating Neuston and trawling Manta nets (Figure 1.1) are widely employed[75,76]. These methods do, however, come at a significant price because they require the use of a vessel to carry out the labor-intensive sampling. Various other types of plankton nets have been used to sample water columns at depths and lower the limit of sampling level detection to 100 μm. These nets have demonstrated concentration recoveries that are up to 30 times higher than those for surface water sampling with Neuston or manta nets, even if lower volumes of water are sampled due to higher clogging rates[77].

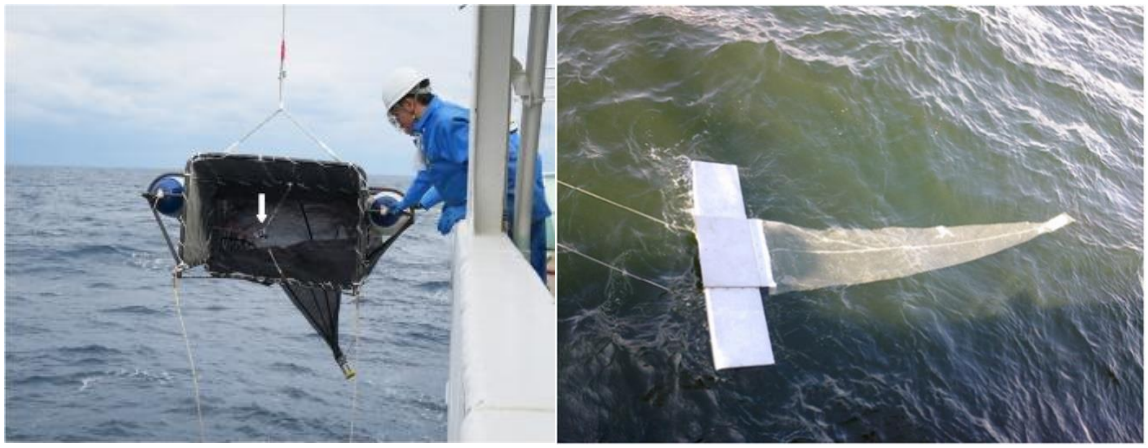

Figure 1.1. Neuston net (left) equipped with a flow meter (white arrow) and Manta net (right) [74]*. Reprinted with permission from* [75]*. Variability of swept area by sea-surface tows of a neuston net: Balance of resistance, clogging, and over-inflow effects. Fish. Res. Copyright 2019, Elsevier and* [76]*. Distribution and abundance of surface water microlitter in the Baltic Sea: A comparison of two sampling methods. Mar. Pollut. Bull. Copyright 2016, Elsevier, respectively.*

The surface microlayer method, which is manually carried out and applies a 2 mm sieve to sample the top 1 mm of surface water, as well as hand net sampling, have both been developed for sampling since MPs and NPs, which have a lower density than water, predominantly accumulate at the surface of waters. Pumps have also been installed in place because they are simple to use and let the operator select the mesh size, but they also need energy to work, and occasionally additional equipment is needed. Additionally, the application of these devices poses a high risk of contamination[78].

Despite the numerous methods for water sampling that are currently available, there is still a lack of studies on the study of MPs and NPs in complex wastewater that has a high level of solid and organic content, thus posing a difficulty in sample preparation and analysis[79]. As a result of the complexity and diversity of characteristics found in the waters under analysis, the devices that have been developed in recent years have emerged as being among the most sophisticated.

1.2.1.2. Filtration systems

MPs sampling has also been carried out at wastewater treatment plants (WWTPs), which have been found to be a significant entry site for these micropollutants into the marine environment [80]. A water sampling tool known as a Ruttner sampler was employed for the low matrix entering water and effluent water. This required using a vacuum suction pump to draw wastewater from the collection system and filter it through a 300 µm plankton net filter that was mounted in a stainless-steel holder. To gauge the volume of the filtered sample, a

flow meter was additionally employed. The findings demonstrated that, even when MPs were retained at very high levels (> 99%) in the WWTP, considerable amounts of MPs were nonetheless released into the environment, demonstrating the important role that WWTP play in terms of MP levels in ecosystems[80].

Another method uses a unique filtering system, made up of three translucent plastic cylinders of 60 mm diameter interconnected using threaded plastic joints (Figure 1.2)[81] and it was utilised in subsequent studies[82,83].

Figure 1.2. Filter device. Reproduced from [82]. Water Science & Technology 72(9) 1495-1504, with permission from the copyright holders, IWA Publishing.

A number of circular filters with an 80 mm diameter were fitted into the device at the threaded intersections using plankton nets with varying mesh sizes (Figure 1.3). The device's first connector was filled with a filter of 200 μm pore size, the next connector with a 100 μm pore size filter, and finally one with a 20 μm pore size filter.

Figure 1.3. Filter installed between joints. Reproduced from [82]. Water Science & Technology 72(9) 1495-1504, with permission from the copyright holders, IWA Publishing.

An electric pump was used to pump wastewater into the top of the filter unit at a flow rate of 1.0 ml/min, where it then went sequentially through filters with diameters of 200, 100, and 20 μm. As stated by the authors, this system made it possible to filter bigger amounts of wastewater. Depending on the amount of suspended organic matter, up to 100 ml of incoming wastewater and up to 8 litres of purified wastewater were filtered. The research verified the prior studies' findings suggesting that WWTPs continue to emit a significant amount of MPs into the environment.

Some other models have been developed and there is an apparatus consisting of four detachable stainless steel filter screens of 12 cm diameter and sizes of 500, 190, 100 and 25 μm (Figures 1.4a and 1.4b)[79].

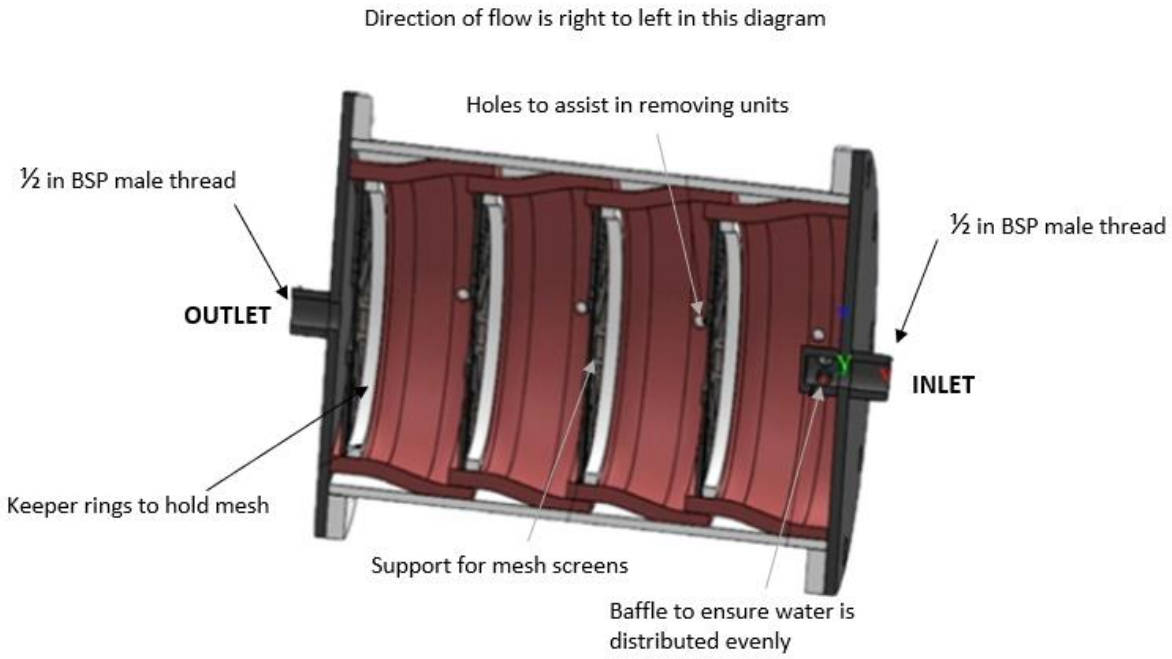

Figure 1.4a and 1.4b. Internal design of the filtering device [79]. Reprinted with permission from [79]. Wastewater treatment plants as a pathway for microplastics: Development of a new approach to sample wastewater-based microplastics. Water Res. 112, 93–99. Copyright 2017, Elsevier.

The filter screens were stacked within a PVC housing cover and mounted vertically onto a support (Figure 1.5) with the screen sizes descending in order with the smallest filter screen (25 μm) at the bottom.

Figure 1.5. External design of the filtering device [79]. Reprinted with permission from [79]. Wastewater treatment plants as a pathway for microplastics: Development of a new approach to sample wastewater-based microplastics. Water Res. 112, 93–99. Copyright 2017, Elsevier.

The authors state that, depending on the quality of the sample, this technology made it possible to continuously test significant amounts of wastewater, which were measured by a flow metre placed at the top feed inlet of the filter unit. Moreover, it allowed for the precise in-situ compartmentalization of MPs across a wide size range for a single sampling experiment[79].

A novel mobile pumping unit has been designed where the water sample is directly pumped from the wastewater effluent. This comprised a PVC hose, which could be lowered into the sample and was linked to a membrane pump, a polycarbonate filter receptacle containing a 10 μm stainless steel filter and a flowmeter (Figure 1.6). Under laboratory conditions, the samples underwent a further filtration step in a filter funnel with a diameter of 11 mm using aluminium oxide filters with 0.2 μm pore sizes in a laboratory setting[84].

Figure 1.6. Mobile pumping filtering device. Reprinted with permission from [84]. Identification of microplastic in effluents of wastewater treatment plants using focal plane array-based micro-Fourier-transform infrared imaging. Water Res. 108, 365–372. Copyright 2017, Elsevier.

The methods described above were introduced to assist with the challenging process of sampling in aqueous environments. The more sophisticated they are, the more likely they are to have plastic components that would elevate the potential risk of contamination of the sample and thus, lead to biased errors in the results.

Sampling methods for the collection of NPs are still under development and it has been indicated the need for standardization of these practices, including the use of filtration systems[85]. It has been argued that, due to the likelihood of the retention of a sizable amount of the NPs in the filter, this size-based filtration technique is only useful for verifying the existence of these nanoparticles and not for quantification[86].

Recently, the potential for sampling in terms of both size and density has been shown by utilizing continuous flow centrifugation on colloidal fraction water samples while simultaneously operating two centrifuges at various rotational speeds[87].

A summary of the information above can be found in Table 1.1.

Table 1.1. Summary of the information regarding sampling techniques discussed above showing advantages and disadvantages of each one. Adapted from Delgado-Gallardo et al., 2021[88].

Approach	Advantages	Disadvantages
Neuston and Manta nets	Easy to use; Large volumes of water can be sampled; Largely used (good to compare between locations).	Expensive equipment; Requires boat; Time-consuming; Lower limit of detection is 333 µm.
Plankton net	Easy to use; Lowest limit of detection 100 mm; Quick to use; Medium volumes of water can be sampled.	Expensive equipment; Requires boat; Static sampling requires water flow; May become clogged or break;
Sieving	Specialized equipment or boats are not required; Is easy to collect samples. Medium volumes of water can be sampled.	Laborious and time consuming; Samples medium volumes;
Pumps	Large volumes of water can be sampled; Effortless; Allows choice of mesh size.	Requires equipment; Requires energy to work; Potential contamination by the apparatus; May be difficult to carry between sampling locations.

1.2.1.3. Separation and purification of samples

The type and method of separation and purification used on water samples containing MPs and NPs is an important step after collection and depends on the selected analysis method. For instance, organic material and inorganic composites inside samples that adhere to the surface of these pollutants, must be eliminated in order to allow for a precise identification since they may prevent MPs and NPs within the sample from being recognised by the analytical technique.

Depending on the physical, chemical, or biological nature of the contaminants, researchers have employed various removal techniques, which are discussed in the following sections.

1.2.1.4. Separation

Due to the physical characteristics associated with MPs, such as low mass per volume, the primary separation techniques created and employed by researchers have typically involved density fractionation, where the collected sample is mixed with a fluid that presents a specified density[89]. Usually, a saturated salt suspension constitutes this fluid having a higher density[7]. The combined solutions are stirred and/or aerated, followed by a waiting period to allow for settling. Because of this procedure, particles with a higher density can be submerged while particles with a lower density, such as MPs and NPs, can float to the surface. Once the micro- and nanopollutants have reached the surface, they can be easily

separated by collecting and filtering the top layer[7].

Sodium chloride (NaCl) with a density of 1.2 kg/L is one of the most commonly used saturated suspensions due to its affordable price, non-toxicity, ideal recovery rates, and easy accessibility[78,89]. The only drawback reported for this approach is the inability of separating certain MPs polymers that present higher densities including PVC, which displays densities ranging from 1.16–1.58 kg/L, and polyoxymethylene (POM), with densities ranging 1.41–1.61 kg/L[7].

Another study, motivated by the density limitation demonstrated by using sodium chloride, used sodium iodide (NaI) and generated densities of up to 1.8 kg/L while employing an Air Induced Overflow technique to separate and collect MPs rising to the top of the mixed solution. In addition, experiments employing mixtures of NaI and NaCl have demonstrated that, depending on the MPs' properties, they can achieve high recovery rates of up to 99%.[78]. However, NaI, as all other higher density salts, can be an expensive option and must be handled with care as it may cause eye and skin irritation[90].

Furthermore, solutions containing zinc chloride ($ZnCl_2$) with concentrations as high as 1.6 kg/L have been used to separate MPs. Depending on the kinds of plastics in the sample, experimental results using zinc chloride in combination with a developed technology named a Munich Plastic Sediment Separator have demonstrated recovery rates close to 100%. $ZnCl_2$ is inexpensive, but since it causes environmental contamination, it must be recycled or reused, which complicates the process and raises the costs[91,92].

The use of non-toxic sodium polytungstate (SPT) has also been reported [93], with densities in the range of 1.4 kg/L and 3.1 kg/L. However, this is an expensive method in comparison with others solutions and also does not separate plastics components like PVC or POM[7].

In contrast to density fractionation, pressurised fluid extraction (PFE) is an alternative separation method, a technique that involves the use of solvents under certain pressure and subcritical temperature conditions to recover semi-volatile organic molecules from solid substrates. Initial trials with spiked polymers on glass beads revealed recovery rates of up to 111%. The range for wastewater samples was 85-94% recovery. The technique demonstrated effective extraction of plastic particles smaller than 30 μm, which were previously challenging to measure by flotation and other physical separation techniques. The disadvantages of this strategy include that MPs' morphology is affected after extraction, making it challenging to determine the size distribution[94].

A summary of the most common separation procedures found in literature are shown in Table

1.2.

Table 1.2. Characteristics of the different solutions commonly used for separation of MPs. The density and recovery rate are facilitated. Adapted from Delgado-Gallardo et al., 2021.

Solution	Density (g cm^{-3})	Recovery rate
NaCl	1.20	80-100%
NaCl and NaI	1.20 (NaCl), 1.60 (NaI)	94-98% (spheres), 0-98% (fibres)
Air Induced Overflow	1.20 (NaCl), 1.80 (NaI)	91-99%
$ZnCl_2$	1.60-1.70	96-100%
CaCl2	1.30-1.35	> 50% (sizes 100 µm to 1 mm)
Pressurized fluid extraction	Solvents	85-94%
Sodium polytungstate (SPT)	1.4 - 3.1	Not specified
Solution	**Advantages**	**Disadvantages**
NaCl	Cheap, available and no toxic	High density polymers not separated
NaCl and NaI	Good recovery rate	Expensive. It must be handle with care
Air Induced Overflow	Good recovery rate	Expensive. It must be handle with care
$ZnCl_2$	Cheaper than other solutions	Environmentally hazardous
CaCl2	Cheaper than other solutions	Causes interferences in measurement
Pressurized fluid extraction	Small particles can be separated	Morphology of MPs is altered
		Undetermined size distribution
Sodium polytungstate (SPT)	High density	High costs
		Not all plastic types are separated

The European Marine Strategy Framework Directive (MSFD), in order to bring some level of standardisation into the purification process, recommended using NaCl as a density fractionation separation method despite its drawbacks and the fact that many polymers (like PVC due to higher densities) could not be taken into consideration[95].

Nevertheless, to achieve the best mass recovery for MPs under 1 mm, the application of $ZnCl_2$ under recycling/reuse conditions has been recommended. In order to avoid the more expensive, time-consuming, and repetitive separation processes involved with conventional techniques, where the recovery range sharply declines with lower MP size, this method is suggested for both practical and economic reasons[7].

The adaptation of techniques developed for engineered nanoparticles has been suggested as a possibility for the separation of NPs[86]. Magnetic field flow fractionation (MFFF) is one of these methods, in which a magnetic field pulls and isolates the nanoparticles moving across a canal. This process may become challenging though, due to the need for NPs to be

magnetised and the possibility that the employed magnetic nanoparticles are too big to effectively bind to the nanopollutants[86]. Gel electrophoresis is a different option since it can separate NPs by dragging them through a gel with an electric field. Gels act as nanoporous structures; therefore, this method could be used to separate NPs. This procedure might also be difficult because electrophoresis is not plastic-specific. It has also been proposed that NPs can be separated using size-exclusion chromatography (SEC), which runs the material through a column of porous beads. The smaller particles are trapped in the porous matrix of the beads, which slows down their travel, while the larger particles pass by around the beads. SEC is not plastic-specific, like gel electrophoresis. Another challenge to be considered in the application of this techniques is the low concentration of NPs that can be expected to be found in environmental samples[86].

1.2.1.5. Purification

As it has already been indicated, enhancing the identification and analysis procedure depends on the earlier removal during the purification step of organic and inorganic materials attached to the MP surface. For the purpose of removing surface pollutants, two techniques have been identified in the literature that integrate chemical and enzymatic degradation.

Hydrogen peroxide (H_2O_2) in varying doses from 10 to 35% has been employed in chemical treatment methods and has been shown to cause minimal degradation of MPs. Nevertheless, significant colour fading has been reported at concentrations above 30%[90].

Other researchers went a step further and combined H_2O_2 and sulphuric acid (H_2SO_4), with results that indicated a 90% efficacy (based on statistical analysis ANOVA with Tukey post-hoc analysis, $P < 0.05$). However, the addition of intense oxidising acids could degrade or dissolve some types of MPs that are less resistant under low pH conditions[96].

A further study uses a combination of an ultrasonic bath with microfiltrated water and added sodium dodecyl sulphate (SDS)[97]. The breakdown of some brittle plastic materials would result in the formation of smaller MPs and NPs, which could potentially damage the samples, making this approach unsuitable[86].

The process of enzymatic degradation involves incubating samples with a combination of technical grade enzymes (amylase, cellulase, chitinase, lipase, and proteinase) to reduce to a minimum the biological matrix on the surface without harming the MP particle[74]. Even though the results demonstrated removal rates of up to 97% within hours after application, this initial investigation revealed that the methodology needed some modifications due to the

significant expenses involved[74].

Subsequent studies established the BEEP, or basic enzymatic purification process, for sample purification. The BEEP consists of a sequential seven-step process that employs both chemicals and enzymes. The application of chemicals like sodium dodecyl sulphate (SDS) detergent, phosphate-buffered saline (PBS) solution, and H_2O_2 determines the first steps, followed by density fractionation with $ZnCl_2$. The last step is the enzymatic degradation carried out using technical grade enzymes such as cellulase, chitinase, and protease, resulting in a 98.3% purification efficiency on plankton samples[98].

In the same study, it was discovered that MP samples with a biological surface matrix containing a high quantity of lipids or polysaccharides were only partially purified by the BEPP. This resulted in the development of the universal enzymatic purification protocol (UEPP), which includes two additional optional enzyme phases using amylase and lipase enzymes[98].

1.2.2. Methods for the detection of MPs and NPs

The most widely used methods for the identification and quantification of MPs and NPs are combination approaches using microscopy and spectroscopy, while recently the application of thermal analysis techniques has grown significantly.

1.2.2.1.Microscopy analysis

Due to the simplicity of sample preparation, microscopic detection provides a visual, direct, and quick method for detecting MPs. Microscopical techniques are frequently used in the investigation of this pollutants and vary from optical or light microscopes to scanning or tunnel electron microscopes. Even if the cost of instrumentation and sample preparation is relatively inexpensive, the typical optical microscope's insufficient resolution makes it generally unfavourable for the detection of MPs.

1.2.2.2. Stereo microscope

The use of the stereo microscope has been widely used to identify MPs from environmental samples, such as the sea surface and beach sand (Figure 1.8a)[70]. By employing a stereo microscope, which frequently uses reflected illumination from the sample's surface rather than transmitted illumination through a sample, greater surface and structural information

can be collected (as in optical or light microscopy). The larger working distance and depth of field are two of this type of microscope's primary elements. However, since this methodology is qualitative, it is challenging to differentiate between manufactured MPs and natural fibres using this technique (Figure 1.7)[70,99]. This is supported by a subsequent investigation, which revealed that more than 20% of plastic-like particles and 70% of clear particles were incorrectly detected by stereo-microscope[100]. The lack of resolution is another disadvantage of this approach, although, it has been proven to be effective for identifying bigger MPs exceeding 1 mm[70]. However, it is generally considered that the use of quantitative analysis of these contaminants by microscopic method is time consuming[99].

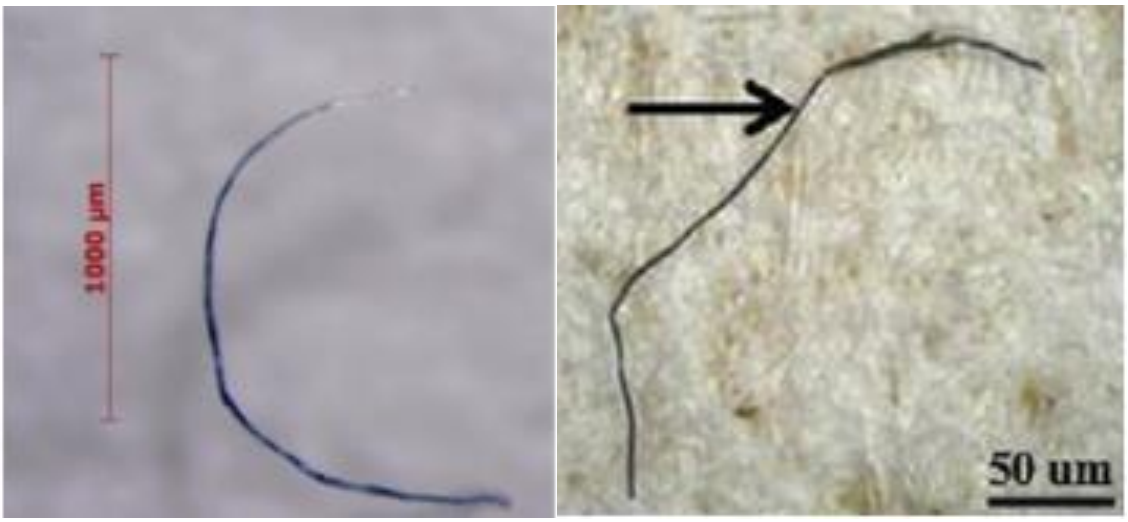

Figure 1.7. Non-plastic materials detected as microplastics by Stereo-microscope (Left: cotton; Right: rayon) [70,101]*. Reprinted and adapted with permission from* [70]*. A comparison of microscopic and spectroscopic identification methods for analysis of microplastics in environmental samples. Mar. Pollut. Bull. Copyright 2015, Elsevier and from* [101]*. Microplastics in freshwater systems: A review on occurrence, environmental effects, and methods for microplastics detection. Water Res. 137, 362–374. Copyright 2018, Elsevier.*

In another study, particles of high-density polyethylene (HDPE) were successfully identified on tissue from the blue mussel Mytilus edulis L. using a method utilising polarised optical microscopy (Figure 1.8d). These particles, which ranged in size from > 0 to 80 µm, were ingested into the stomach and accumulated in the lysosomal system. The scientists demonstrated that MPs are taken up by cells and have a major impact on tissues by using polarised optical microscopy to microscopically monitor plastic particles in intact gills and cryostat tissue sections of the mussel digestive gland[102].

1.2.2.3. Scanning microscopy

The development of the family of scanning probe microscopes (SPMs) has led to approaches like atomic force microscopy (AFM), which has a resolution on the order of fractions of a nanometre. Its main characteristics are topographic imaging, force measurement, and manipulation. AFM combined with infrared (IR) or Raman spectroscopy can produce IR absorption spectra and absorption images on the scale of 50–100 nm (subcellular level) and provides more information, including surface morphology, chemical content, and mapping of the IR absorption characteristics of polymers[103].

A suitable technique for assessing MPs and NPs is scanning electron microscopy with energy-dispersive X-ray spectroscopy (SEM-EDS), which can display the precise chemical and surface characteristics of even nanoscale microplastic particles (100-250 nm). However, dealing with aqueous samples might be challenging as the sample must be small to minimise the charging effects and they have to be properly prepared. The previously separated MP debris must be placed on double-sided adhesive carbon tape on aluminium SEM stubs and analysed as they are. Additionally, it has been reported that low voltages are incompatible with EDS[104,105].

As it provides a superior resolution (0.5 Å versus 0.4 nm of SEM), the use of transmission electron microscopy (TEM) can facilitate the examination of MPs from micro to nanoscale. While TEM uses transmitted electrons that are focused straight on the material, SEM relies on scattered electrons. TEM technology, as opposed to SEM, aims to expose what is inside or beyond the sample's surface and has a maximum magnification of 50 million X while SEM only has a maximum magnification of 2 million X (Figure 1.8e)[106,107].

1.2.2.4. Hyperspectral imaging

Hyperspectral imaging (HIS) employs the distinctive reflectance spectra of objects that are captured from the microscope to complete spectra for each pixel with a size as small as 128 nm. High resolution data is supplied (down to 2 nm), and it is presented as an RGB image and a spectral curve[108].

Brain damage and behavioural issues caused by nanoplastics in fish have been demonstrated employing this method. It was used to monitor the distinctive spectral characteristics of polystyrene nanoparticles that had been previously inoculated into the food chain of these fish. Several samples taken from the fish brains were analysed to get a wavelength spectrum

for each pixel of the light scattered by the samples[109]. This microscope featured components enabling visible-near infrared (400–1000 nm) hyperspectral imaging as well as an improved dark field illuminator. The previously homogenised brain samples were examined under a 60x magnification. Each acquired image of an exposed brain was converted into a spectral library that matched polystyrene. The Spectral Angle Mapper programme was then used to spectrally map and identify the polystyrene in the exposed brain images. The results revealed that polystyrene was found in the brains of all fish fed on these nanoparticles, but not in the brains of the control group[109].

In order to optically detect nanoscale features within a sample, enhanced dark field hyperspectral microscopy produces images with extremely high signal-to-noise ratios. These images can identify subcellular features smaller than 100 nm based on the scattering or emission properties of these features[108]. This technology was applied to confirm the translocation and foetal deposition of polystyrene nanoparticles during pregnancy. Pregnant Sprague Dawley rats were exposed to 20 nm rhodamine-labelled polystyrene nanobeads (2.64 x 1014 particles) via intratracheal instillation on gestational day 19. Maternal and foetal tissues were assessed after 24 hours using fluorescence optical imaging. The foetal tissues were fixed in order to view particles with hyperspectral microscopy. Polystyrene beads of a known concentration were inserted into the uterine arteries. The mother lung, heart, and spleen were then found to have polystyrene particles. Enhanced dark field imaging of foetal tissue revealed polystyrene nanoparticle accumulation in the placenta, foetus's liver, lungs, heart, kidney, and brain (Figure 1.8g), indicating that in late pregnancy, the mother's lungs may transfer nanoparticles to the foetus's tissue[110].

1.2.2.5. Dying methods in microscopy

A range of dye compounds have been utilized in combination with microscopy techniques to distinguish plastics from different matrices, where the plastic particles are marked with an organic dye or fluorescence molecule (Figure 1.8c). This method is considered to be a quick and inexpensive way to assess the MP load only in a sample, although it does not reveal the chemical components of the particles[111]. Chloroform, ethanol, n-heptane and xylene have also been applied in microbiology investigations[112]. Alternative solvents have been proposed in order to improve the staining approach. N-hexane has been proved to have recovery rates of 98% for PE[111]. More recently, a novel staining method was developed and used in the identification of 20-1000 µm MPs[77,113]. Nile Red (9-diethylamino-5H-benzo [α]

phenoxazine-5-one; hereafter), a lipophilic fluorescent dye, firstly applied in the detection of intracellular lipid droplets and cytofluorometry in microbiology studies[112], has been successfully demonstrated to interact with synthetic polymers in chemical samples[77,100] through hydrophobic interactions between the dye and polymer[114]. The benefits of using this approach are the intense fluorescence signal obtained and a rapid staining rate. Because dye molecules are only adsorbed to the MP's surface, this makes it simple for them to be desorbed. This is also a discriminatory method because not all plastics can always be stained. While some popular materials like PVC or PET are unaffected, Nile Red is suitable for PE, PS, PP, and nylon[115].

In order to address these difficulties regarding the previous approach being discriminatory and dye molecules being easily desorbed, a novel method was devised[115], by which the dye molecules are inserted inside the MPs by applying high temperatures to the samples and generate loosening of the macromolecular chain. As the temperature drops afterwards, the loose structure tightens up once more, encasing the dye molecules inside the MPs. This approach has also been used to stain MPs such as PE, PS, PVC, and PET using hydrophilic dyes like Safranine T and fluorescent isophosphate (FITC) in addition to Red Nile[115].

When samples are prepared for Fourier Transform Infrared Spectroscopy (FTIR), fluorescence microscopy and staining can also be employed as a pre-selection strategy to limit the level of misidentification and the time it takes to find each plastic-like particle. However, errors in staining cannot be totally avoided, especially when dealing with organic matter and natural lipids[116].

Confocal laser scanning microscopy (CLSM) is another fluorescence technique which is highly successful (Figure 1.8f). Studies utilising this technology show a number of significant benefits, including a simple, fairly priced, quick, and non-invasive method. With this technology, sample areas of 5 μm × 5 μm or 0.65 μm × 0.65 μm can be scanned[117,118]. The study of membrane samples with this technique provided 3D pore structural information, including pore diameter (smaller ones ~ or <10 μm) and porosity distribution, and pore connectivity. The advantages of this approach, such as its non-invasiveness, have been demonstrated. Additionally, sample preparation procedures that involved drying were avoided[118]. A recent investigation demonstrated the observation of fluorescently labelled PS microbeads in plant roots using this technology. Through a swelling method, Nile blue or 4-chloro-7-nitro-1,2,3-benzoxadiazole dyes were encapsulated into the microbeads and used

to detect the location of the PS beads in the root (Nile blue) and the green tissue [119].

A comparison of micro- or nano-plastics images detected by different microscopic methods is presented in Figure 1.8 (a to g).

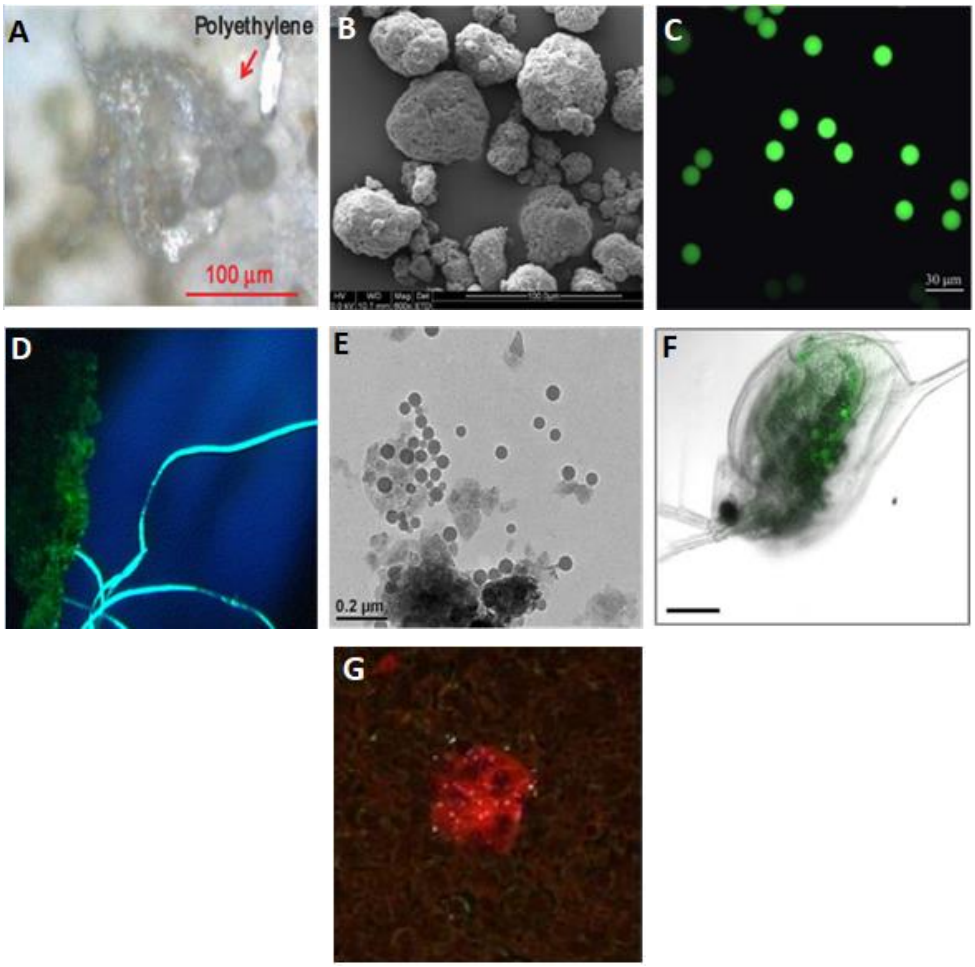

Figure 1.8. Detection of microplastics by microscopic methods.

(a) PE microplastics detected by Stereo-microscopy [70]. Reprinted with permission from Song, Y. K. et al. A comparison of microscopic and spectroscopic identification methods for analysis of microplastics in environmental samples. Mar. Pollut. Bull. Copyright 2015, Elsevier.

(b) PE microplastics detected by SEM [120]. Reprinted with permission from Razanajatovo et al. Sorption and desorption of selected pharmaceuticals by polyethylene microplastics. Mar. Pollut. Bull. Copyright 2018, Elsevier.

(c) PS microplastics detected by fluorescence microscopy [121]. Reprinted with permission from Yin et al. Polystyrene microplastics alter the behavior, energy reserve and nutritional composition of marine jacopever (Sebastes schlegelii). J. Hazard. Mater. Copyright 2018, Elsevier.

(d) Synthetic fibres detected by polarized light microscopy[122]. Reprinted with permission from Zubris & Richards. Synthetic fibers as an indicator of land application of sludge. Environ. Pollut. 138, 201–211. Copyright 2015, Elsevier.

(e) PS nano-plastics detected by TEM[107]. Reprinted with permission from Awet et al. Effects of polystyrene nanoparticles on the microbiota and functional diversity of enzymes in soil. Environ. Sci. Eur. Copyright 2018, Springer Nature.

(f) PS nanoplastics detected by CLSM[116]. Adapted with permission from Chae et al. Trophic transfer and individual impact of nano-sized polystyrene in a four-species freshwater food chain. Sci. Rep. Copyright 2018, Springer Nature.

(g) PS nanoplastics in foetal brain tissue detected by HSI[110]. Reprinted with permission from Fournier et al. Translocation of Engineered Nanomaterials from the Maternal Lungs to the Fetal Compartment After Instillation. FASEB J. Copyright 2018, Springer Nature.

1.2.2.6. Quantification of MPs using microscopy

MPs could be quantified utilising a variety of standard techniques that have been documented for the quantification of particles employing microscopy. One of them was introduced as a versatile and precise technique for detecting and counting particles on a fixed but heterogeneous substrate and can be applied in various applications. This method involves creating a picture of the fixed background by comparing various photos collected from the same experimental sample. To carry out the counting, this backdrop is eliminated in order to isolate the particles to be counted[123].

To count fluorescently labelled molecules, a different method based on single molecule localization microscopy (SMLM) has been adopted. Images and organic fluorophores are employed in photo-switching conditions. The amount of fluorescence flashing events observed in each spot are used to build a statistical model that extracts the number of fluorophores per spot. This technique makes quantitative high-resolution imaging easier[124].

1.2.2.7. Application of microscopy on MPs analysis

As previously mentioned, microscopy methods are frequently used in combination with other technologies to determine the kind of plastics that the sample contains. Nonetheless, numerous studies have successfully used microscopy as a quick method for identification when working with a type of polymer that is known in advance (for example, to prove the uptake of this polymer by an organism). This has been verified, for instance, by a recent work that used LC-MS to show how plants ingested PS plastic beads. After being exposed for 10 days, various encapsulated dyes (such Nile Blue) in beads of a variety of sub-micrometre to micrometre size were identified in the root and green tissue of wheat plants[125].

AFM-IR has been successfully applied on the identification of poly(hydroxybutyrate) (PHB) produced by the bacteria *Rhodobacter capsulatus*. PHB is a polymer of the polyester family, having analogous mechanical and thermoplastic properties of PE and PP[103].

SEM has been used to produce images of PE-MPs in water samples that displayed degrees of sorption and desorption of diverse pharmaceuticals (Figure 1.8b). These findings allude to the possible risk of bioaccumulation brought on by aquatic organisms ingesting MPs[120].

The authors of a previously cited article made assumptions regarding how well SEM-EDS may work for detecting MPs and even NPs in marine samples. Even though they point to

benefits like quick morphological analysis and the potential to use low voltages to conduct qualitative and quantitative elemental investigations without carbon or metal sputtering, the very low voltages used (0.5-1.5 kV) are insufficient for EDS analysis since they pose the risk of the sample being charged at higher voltages[105].

A different methodology using hyperspectral image and support vector machine (SVM) has been used with a size detection limit of 200 μm[126]. This approach is still in development for detection of smaller particles and, according to the authors, it could be not reliable when analysing environmental samples with naturally degraded plastics that can present chemical and physical alterations.

1.2.3. Spectroscopic analysis

Over the past few decades, spectroscopic methods have become more prevalent. The most popular techniques for analysing MPs at the moment are FTIR and Raman spectroscopy. Both of these techniques satisfy the requirement of qualitative and quantitative examination of plastic and non-plastic fibres, with FTIR being most frequently employed to identify MPs larger than 10-20 μm as well as for qualitative analysis[127,128].

When FTIR analysis was compared to stereo-microscopy, it revealed that some forms of MPs (fragments and expanded polystyrene) were more abundant on average whereas MP fibres and sheets were less prevalent[70].

FTIR assisted by microscopy (micro-FTIR) enables the non-destructive and qualitative analysis of these pollutants Micro-FTIR can be divided into measuring modes: attenuated total reflection micro-FTIR spectroscopy (ATR micro-FTIR) and focal plane array-based transmission micro-FTIR imaging (FPA micro-FTIR), both of which have advantages and disadvantages. For ATR micro-FTIR, thick and non-infrared-transparent samples can be identified, but the measurement may result in non-interpretable spectra if the shape of particles is irregular or particles of different sizes are too close together due to refractive errors[129,130].

A great advantage in FPA-based micro-FTIR measurement, which can record at the same time several thousand spectra automatically within one single measurement and which can be called chemical imaging, is the considerable time savings that can be achieved[131,132]. However, it is important to take particle thickness into account since, for instance, samples that are too thick can result in total absorbance. In contrast, if samples are too thin, they will

not be able to absorb enough infrared to reflect on the spectrum[132].

In recent years, one of the most frequently employed sampling methods has been attenuated total reflectance (ATR) where a portion of the light from an IR beam that is travelling from a high refractive index media (like a zinc selenide crystal) to a low refractive index medium (like a sample) is reflected back into the low refractive index medium. Nearly all light waves reflect back at a specific angle of incidence. The term "total internal reflection" refers to this phenomenon. In this situation, a little portion of the light energy escapes the crystal and travels 0.1 to 5 μm beyond the surface in the form of waves. This invisible wave is called evanescent wave. The intensity of the reflected light reduces at this point. This phenomenon is called attenuated total reflectance. When the sample is placed on the crystal, part of the IR radiation that penetrates past the crystal is absorbed by the sample. The IR spectrum of the sample is generated from this absorbance. Diamond, silicon, germanium, zinc selenide, and KRS-5 (thallium iodide or thallium bromide) are all frequently used materials for crystals[133].

In comparison to FTIR methodologies, greater accuracy and higher resolutions of detection have been achieved with Raman spectroscopy. Raman spectroscopy in combination with microscopy (micro-Raman spectroscopy) has been recorded[134], identifying down to a minimum size of one micron. The same study divided MP samples into five groups by size, and more than 80% were in the 5-20 μm range.

Plastics in the 50 nm–20 m range can be captured and identified using Raman spectroscopy in combination with optical tweezers denominated Raman Tweezers (RTs). RTs can be employed to evaluate the size and form of particles like beads, fragments, and fibres. Even when the spatial resolution is limited by diffraction, the sensitivity still reaches the level of a single nanostructure (∼250 nm)[135].

For the purpose of identifying 2-3 μm MPs in plankton, a coherent anti-Stokes Raman scattering (CARS) microscopy-based bioimaging technology has been developed. This technique performs better with wet materials and can produce stereo-chemical images[96,99]. However, some disadvantages have been observed, such as the deterioration of MPs by UV light, which has been shown to impact the Raman signal and subsequently exhibit a reduced characteristic peak, particularly for PE, PP and PVC[136]. Additionally, the Raman method can be interrupted by existing coloured pigments, fluorescence additives and carbon bonds[99].

1.2.3.1. Application of spectroscopy on MPs analysis

FTIR is being employed successfully in numerous investigations all around the world. To

date, more research has been done on marine ecosystems than any other aquatic environment. In one of these researches, MPs were detected in sediments collected from various sampling stations in the Belgian coastal zone using FTIR spectroscopy with an AutoIMAGE-microscope coupled to a spectrometer[137]. Concentrations of 390 MPs per kilo were reported, which are 15–50 times greater than those in comparable research, despite the fact that the size of the particles is not stated. By using FTIR analysis, the spherules discovered in the harbour sediments were all recognised as PS. All the examined plastic films were made of nylon, which was also identified as a component of the fibres as PP, nylon, and polyvinyl alcohol (PVOH). The granular particles were identified as PP, PE or PS[137].

In a different investigation, sediment samples were collected from the shore of north-eastern Italy, and the samples were then subjected to FTIR analysis to determine the presence of MPs. There were a total of ten different varieties of MP identified, including PE, PP, poly(ethylene-propylene), polyester, polyacrylonitrile, polystyrene, alkyd resin, polyvinyl chloride, and polyamide, with a most frequent size for 93% of the observed particles in the range of 30-500 μm[138] . Other collected samples from the Portuguese coast using the same approach demonstrated the presence of PE, PEst and PS retained on filters used for analysis[139].

In a similar manner, another study used FTIR to analyse beach sand samples from the Marina di Vecchiano (Tuscany, Italy) shoreline to locate MPs of sizes <2 mm, finding up to 30 mg MPs in 1 kg of sand. The material scraped from the surface of the sieved plastics debris was ground with KBr in a mortar and transformed into discs. FTIR spectra were collected at a resolution of 4 cm^{-1}, and the soluble fractions were examined as films cast onto KBr discs. There were only three polymer classes represented in the bigger fragments that were recovered from the sampling sites: PE, PS, and PP, indicating that higher density polymers like PVC and polyester are likely ending up in the benthic sediment rather than in the water[66].

In another article, 2D imaging-FTIR was used to analyse the frequency and severity of MPs contamination in sub-surface waters collected near-shore and offshore in the coastal region of the Ross Sea (Antarctica). PE, PP, polyamide, polytetrafluoroethylene (PTFE), and polymethyl methacrylate (PMMA) were among the materials discovered[129].

The aforementioned studies show just how pervasive and ubiquitous plastic pollution is in the environment, extending even to the most distant maritime areas. The existence of this environmental issue is confirmed by research that span as far as the ocean's deepest bottoms. One of them used micro-Raman spectroscopy to analyse samples he had taken from the

Mediterranean and Atlantic oceans' depths. Three different colours, copper phthalocyanine (blue), polychloro-copper phthalocyanine (green), and permanent red (red pigment), were examined in order to identify these particles. These are organic pigments with a non-natural origin, indicating the presence of anthropogenic particles in these samples[49].

Spectroscopic technologies have also been applied to other water bodies around the world. Analysis using μ-FTIR have been applied to samples collected from the surface sediments of the Beijiang River (China) littoral zone. This study demonstrated the presence of PE, PP, some other copolymers, and paint particles in concentrations ranging from 178 ± 69 to 544 ± 107 items/kg sediment. The chemical weathering of MPs could also be observed by the absorption peaks at about 1715 cm^{-1} (shown in the spectra with lower match degrees, 72.8% for PE and 74.4% for PP). A probable cause for this deterioration is the high availability to oxygen and exposure to sunlight in the surface zones[140].

Although rivers are frequently thought of as MPs transit channels from the land to the sea, new research has shown that fluvial catchments can also serve as sites of accumulation. MPs have been found even in the hyporheic zone compartment, which is 0.6 metres below the streambed. The use of focal plane array (FPA)- based μ-FTIR was key in order to analyse the smaller MPs (20-500 μm)[141].

There is a greater requirement for accurate analysis of MP in WWTP effluents due to the large levels of MP loading that are seen being discharged into the environment from treatment plants. When FTIR was utilised to analyse the MPs abundance in WWTPs, it was found that the majority of the identified MPs exhibited a profile like the blue PE particles found in toothpaste formulations[142].

ATR-FTIR and focal plane array FPA-based micro-FTIR were used in another investigation to analyse samples from 12 German WWTPs. With the aid of these methods, MPs as small as 20 μm could be identified. The most widespread polymers were PE and polyester fibres. The results of this analysis support the notion that, even when WWTP are retaining a sizable quantity of MPs, they should be regarded as substantial contributors to MP pollution since each WWTP is expected to discharge an annual amount of 9×10^7 to 4×10^9 MP particles and fibres into the environment[84].

1.2.4. Thermal analysis coupled to Gas Chromatography (GC) and Mass Spectrometry (MS)

Thermal analysis techniques have been developed, and they usually entail examining how

temperature affects a material's physical characteristics, including measurements of mass loss, changes in the material's heat flow throughout a temperature range, and/or evolved gas analysis. Depending on the characteristic that needs to be assessed, this necessitates the use of an extra analytical technique, such as mass spectrometry (MS) or FTIR (using a flow cell), for the evaluation of the produced gases.

Thermogravimetric analysis (TGA) and pyrolysis (PY) are two methods that are gaining popularity for the identification and analysis of MPs and NPs due to a number of advantages in the experiments. For a more detailed and reliable identification of these contaminants, these approaches are also typically integrated with gas chromatography (GC)[143].

Typically, the evolved gases produced by TGA and PY contain a fast mixture of organic breakdown products (analytes), which are subsequently separated into distinct bands by GC for simpler identification by an MS. The emerging analytes are separated within the GC, b based on the partitioning coefficient of the selected column phase and the characteristics of the emerging analytes. The partitioning into the gas phase is facilitated by a temperature gradient along the column inside the GC oven. For the GC to generate distinct and easily distinguishable emerging bands for MS analysis, good separation is required. Within each band, the emerging analytes from the GC enter the MS and are ionised. Typically, this is done with the use of an electron impact ionisation (EI) source, which bombards the emerging analytes with high energy electrons (70 eV), causing them to transform into product and fragment ions. The mass analyser subsequently separates the product and fragment ions depending on their masses, which are then converted by equipment inside the MS into a mass spectrum fingerprint. The data from this analyte fingerprint spectrum can then be compared to databases already in use that comprise information gathered through experiments and manual elucidation based on the idea of molecular fragmentation[143].

The organic breakdown products (tars), which have been studied in relation to thermal treatment of several plastic types, differ between different types and are essentially unique to each plastic. The different plastics' tars might be utilised as potential identifiers to distinguish various plastics in a complicated mixture or to distinguish plastics from samples with potentially challenging matrices, such as untreated water samples[144–146].

The difference in temperature at which each plastic degrade has been also investigated. PS, polymers start breaking down at 375 °C and it is completely degraded before reaching 450 °C. PP, as another example, starts decomposing at temperatures of 300 °C and presents a maximum mass loss in the interval of 400-475 °C where this material is completely

degraded. In case of PVC display two phases, the first one at temperatures between 250-350 °C where loss mass of around 65% are observed and the second phase at temperatures of 500 °C presenting a mass loss of around 95 % of the material. Total decomposition occurs at temperatures of 525 °C[144–146]. This has also been demonstrated in this thesis in Chapter 2, paragraph 2.3.2 Verification of thermal degradation.

For polymers, mechanism of thermal degradation depends not only on the thermal conditions, but also greatly influenced by the structural characteristics of the polymers, in particular the comonomer type (a polymerizable precursor to a copolymer aside from the principal monomer), content (short-chain branching) and distribution of short chain branching. The comonomer usually decreases the thermal stability of polymers. The longer side group and the bigger amount of comonomer are favourable to the thermal degradation[147].

1.2.4.1. Thermogravimetric analysis (TGA) coupled to GC/MS

TGA is a methodology for analysis that enables the identification of components from samples weighing between 10 and 50 mg and is based on the concept that all materials experience weight changes when heated to temperatures between 1100 and 1500 °C under constant inert conditions, employing purge gases like argon or nitrogen[148]. Samples are heated continuously over time and weighed accurately throughout the experiment (Figure 1.9) and the changes over temperature are then calculated and analysed.

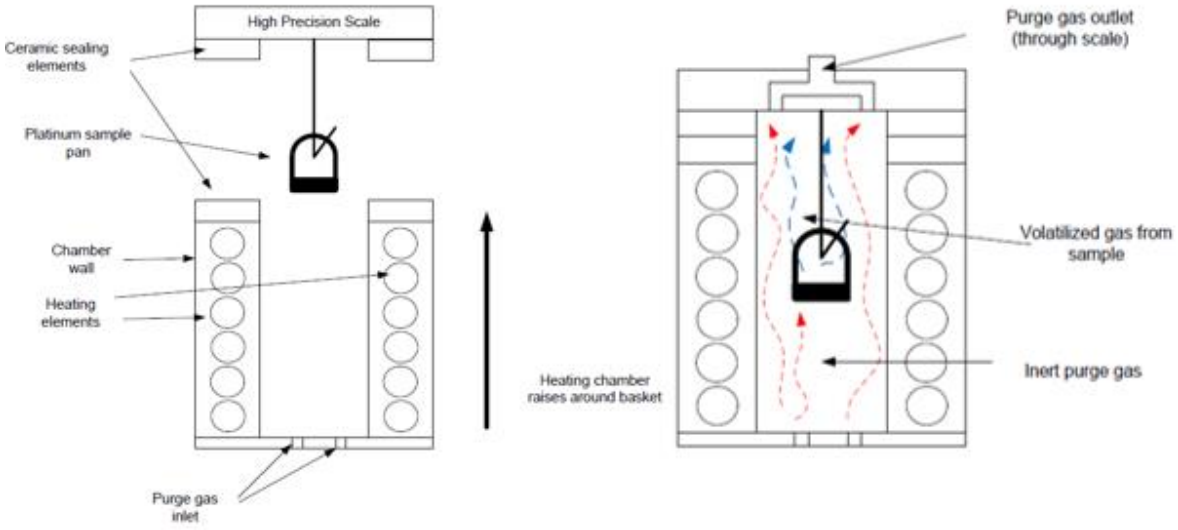

Figure 1.9. TGA apparatus [143]. Reprinted with permission from Gips, J. P. Shale Characterization Using TGA, Py-GC-MS, and NMR. Thesis, The University of Texan in Austin. December 2014. Copyright 2014.

With only a small sample size (below 1 g) needed for a single trial, this technology offers a number of advances and enables studies to be repeated using only a small quantity of the item being studied. Additionally, TGA is affordable and computerised, enabling the execution of many tests at a reasonably cheap cost. Another key feature is the collection of quantitative data, which provides accurate measurements of ±.001 mg over the whole temperature range and so, it provides results that are conclusive, repeatable, and have very low error margins[143].

1.2.4.2. Applications of TGA on MP analysis

TGA technology was used along with differential scanning calorimetry (DSC) to analyse the presence of MPs in wastewater from a municipal WWTP, where up to 39 mg of MPs were recovered and purified from 57 L of collected wastewater[149]. The temperature of the samples was raised at a rate of 5 K/min, from 20 to 800 °C, with a runtime for the experiment of 2.7 hours and using nitrogen as a purge gas. The quantification of masses for both PE and PP were determined in a single instrument run, however, due to the rest of the MP polymers within the sample having peak temperatures between 250-291 °C, these results overlaid, and identification was impracticable. That is the case with the broad peaks of two common plastics like PVC and Polyurethane (PU). When multiple polymers with phase transition temperatures above 200 °C were present, obtaining definitive identifications turned out a challenging task[149].

This issue was also observed in another article where it was indicated the need for a chromatographic separation step when dealing with complex combinations of materials [148]. In the same study, the authors proposed a novel technique known as thermal extraction desorption gas chromatography mass spectrometry (TED-GC-MS), which combines thermal extraction with TGA on solid-phase adsorbers (twisters) followed by the analysis of these adsorbers with thermal desorption (TD) coupled to GC-MS.

This new proposed methodology was implemented in a further study for the identification of MPs in 20 mg from complex environmental samples. Three separate rivers and a biogas facility provided samples for this study. 1500 litres of river water were filtered through a Teflon membrane with the aid of a centrifuge that was running constantly. After drying the samples, the suspended particles were ground into a powder. There are many different varieties of MPs, including PP, PE, and PS, and more research is still being done. Although the authors of this study did not provide information on the size and dispersion of the

particles, one reported benefit was that no time-consuming sample preparation was required[150].

1.2.4.3. Analysis with Pyrolysis (PY) coupled to GC/MS

PY is the thermal decomposition of a substance in an inert atmosphere, typically nitrogen or helium, followed by the characterization of the synthetic polymers and copolymers generated by the disintegration of the particles under controlled conditions of temperatures ranging from 500 to 1400 °C[151] (Figure 1.10).

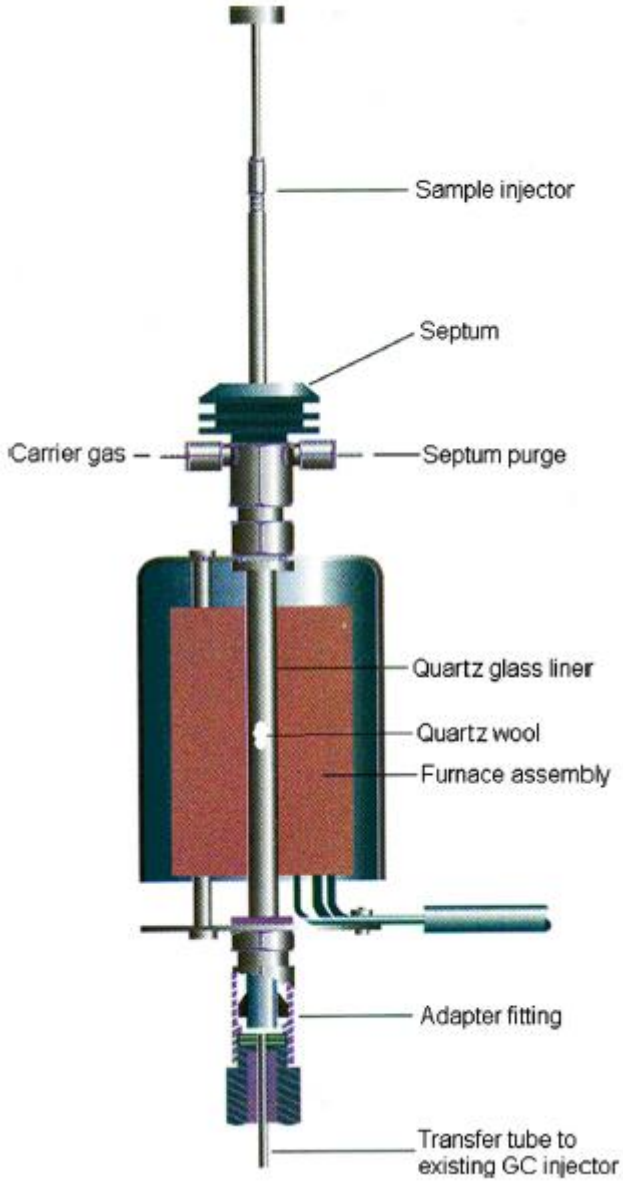

Figure 1.10. Schematic view of the furnace pyrolyser [152]. Reprinted with permission from Kusch, P. et al. Application of pyrolysis-gas chromatography/mass spectrometry for the identification of polymeric materials in failure analysis in the automotive industry. Eng. Fail. Anal. 35, 114–124. Copyright 2013, Elsevier.

With an improved method, based on raising the pyrolysis temperature to 700 °C, it was possible to carry out experiments that allowed the identification of copolymers like PE-PP or PE-PP-PA6 which are difficult to detect using conventional methods, and that can be examined as a whole MP particle[153].

There are a number of limitations to this method, including the sample size restriction (approximately 0.5 mg) that may be evaluated in a single run and the authors' claim that it is unsuitable for the analysis of environmental samples due to their complexity. Additionally, the study points out that performing single particle preselection is necessary, a procedure that is typically time-consuming because this method performs better for single particles. Another reported issue is the fact that the device needs to be frequently maintained due to the usual high-molecular-weight degradation products that condense and obstruct the small transfer capillary[150].

Other authors claimed that handling samples smaller than 50 μm can be challenging and prone to blowing away, and that tweezers are necessary in order to place the MP particle sample into an analytical receiver prior to PY-GC/MS inspection. Alternative approaches are suggested as potential remedies for handling particles, such as flow cytometry or staining methods like Red Nile[153].

More sensitive technologies, such as gas chromatography coupled with time-of-flight (ToF) mass spectrometry, can be applied to detect the type of MPs. A ToF analyser has an advantage over more widely used scanning mass spectrometers (quadrupole analysers) in that it has a superior acquisition rate and greater mass resolution, both of which are intended to lower sensitivity to sub part per billion levels[154,155].

1.2.4.4. Application of PY on MP analysis

Samples taken from sediments in Lower Saxony's Wadden Sea National Park were used in one of the first investigations using PY technique to analyse MPs in the environment. Comparing the resulting pyrograms to those produced by the pyrolysis of a few chosen standard polymers, allowed the identification of different types of polymers. According to the researchers, PY-GC/MS enables the analysis of polymer type, organic plastic additives (OPAs), plasticizers, antioxidants, and flavouring agents within MP particles in a single run without the need for solvents and without the possibility of contamination[156].

PY techniques have also been applied to the identification of MPs in aquatic environments, with recent studies of the occurrence of MPs in wastewater, suggesting that, even when

concentrations of MPs may be low (up to 99.9% removal with membrane bioreactor) after water treatment[81,82,157], given the high volumes of effluent discharged from WWTPs to the environment, they can be considered a significant pathway for the release of significant amounts of MPs into different water bodies[79].

Pyrolysis was used for the first time in the identification of PVC, PS, PE and PET at the nano-scales in the colloidal fractions of seawater samples[73]. The technique comprised ultrafiltering the water samples to create a concentrated solution. After that, there was a freeze-drying step, followed by crushing to produce samples that were about 25 mg. The samples were then heated to a temperature of 700 °C, followed by a 300 °C thermo-desorption step, and a 400 °C thermos-chemolysis step. Direct injection into a GC/MS device was used to analyse the gases created during these steps. The results revealed that while the large MPs were primarily formed of PE, which is allegedly the most durable polymer in marine ecosystems, the small MPs and NPs were made of a combination of PE, PS, PVC, and PET, suggesting that these compounds may breakdown more quickly than previously thought[73].

Table 1.3 summarizes the information in respect of the identification techniques discussed above.

Table 1.3. A summary of the different technologies used for the identification of MPs and NPs. Adapted from Delgado-Gallardo et al., 2021.

Approach	Basis	Minimum particle size	Advantages	Disadvantages
Stereo microscope	Illumination often employs reflected illumination from the surface of the sample instead of illumination transmitted through a sample	>1 mm	Larger working distance; Larger depth of field	Difficult to distinguish between synthetic microplastics and natural fibres; Lack of resolving power; Time-consuming
Scanning Electron Microscope (SEM)	Can show the exact chemical and surface properties of even nanosized microplastic particles	100–250 nm	High resolution images; Feasible	Sample charging may be significant; Quantification is difficult; Low voltages are incompatible with EDX
Transmission Electron Microscopy (TEM)	Allows investigation of what is inside nanoplastics as well as their shape and size	100–250 nm	Presents a better resolution (0.5 Å vs 0.4 nm of SEM)	Quantification is difficult;
Hyperspectral Imaging (HSI)	Works by capturing the unique reflectance spectra of objects from the microscope	2 nm	High resolution of images presented as an RGB image and a spectral curve	Expensive; Complex equipment
Raman Microspectroscopy (RM)	Allows investigation of the size and shape and chemical identification	100 nm	Higher resolution compared with that of FTIR; Allows investigation of the size, shape, and chemical properties simultaneously	Qualitative rather than quantitative; The diffraction limit of the laser spot hinders the imaging of smaller NPs
Fourier-Transform Infrared Spectroscopy (FT-IR)	Use of infrared radiation with a defined range; plastic polymers have highly specific IR spectra with distinct band patterns	20 nm	Easy to operate; Non-destructive methods; Well-established, fast, and quite reliable	Impossible to characterize a certain nanoplastic particle
Pyrolysis GC/MS	Spectra of pyrolysis products are linked to unique peaks in the chromatogram and then compared to a database of common plastic types	1 nm	Allows chemical identification; Sample can be analysed together with the organic plastic additives in one run without the use of solvents; Sensitive and reliable	Databases can be available for only certain polymers

1.3. Detection of MPs and NPs and other pollutants on textiles

The global fibre production—including both natural and synthetic fibres—rose from 57 million metric tonnes (MMT) in 2000 to 111 MMT in 2020, and it is expected that this growth will continue to 145 MMT by 2030[158]. Since 1995, synthetic fibres have dominated the textile industry, replacing cotton as the most generic form of fibre, with synthetic fibre alone accounting for over 65 % of global output by 2020. Natural and synthetic fibres are used in several products, including apparel, home textiles, filtration, and protective gear[158]. The main sources of MP fibres are the textile industry, industrial washing processes, and residential washing processes, all of which contribute to pollution. It is also known that washing variables like duration and temperature can affect microfibre release[159].

Polymers based on PE, PET, PP, and PA are most used in the textile industry. High-density polymers, like PET, generate plastics that do not float but sink instead depending on their movement and falling speed. Low-density plastics, like PP and PE, produce fragments with a density lower than water and hence float on the water[159].

Microfibres and microparticles are discharged into water, air, and soil during the production of textiles, during the wearing of clothing, and during end-of-life disposal[160]. The emission of MPs from textiles is frequently examined after they have been used, on the assumption that manufacturing losses of microplastics are typically low. The contamination of virgin plastic pellets used as a raw material for the production of synthetic fibres during shipment and processing may cause some losses. Microfiber release occurs during the spinning, weaving, and knitting of yarn as well as the brushing and cutting of cloth. Fast fashion is extremely susceptible to excessive microfibre release since it frequently has a large proportion of synthetic fibres, is used for a short time, requires a significant amount of first laundry, and deteriorates quickly[160].

The International Union for Conservation of Nature (IUCN) estimates that a single article of clothing produces about 1900 microfibres, whereas a single wash cycle can remove over 700,000 microfibres[161]. The predicted yearly amount of textile microfibres entering surface water in Europe is 13,000 tonnes, or 25 grammes per person, accounting for 8% of all primary microplastic emissions to water. About 60% of the textile microplastics lost during washing are captured by sludge used in wastewater treatment[162].

Whitening agents are the most widely used polymeric additives in the plastic synthesis and textile industries[163], and they have recently been found in marine, freshwater, and terrestrial

environments where they are quite persistent[164,165]. Along with these, the most common additives are dyes, flame retardants, plasticizers, antibacterial agents, antistatic agents, and antioxidants[166]. The majority of additives have not been adequately controlled and investigated as more and more novel additives (such synthetic phenolic compounds) have come into use[167]. The REACH (Registration, Evaluation, Authorization and Restriction of Chemicals) has placed restrictions or outright bans on certain chemicals that are used in textiles. These chemicals include phthalates (bis (2-ethylhexyl) phthalate (DEHP)), dibutyl phthalate (DBP), bisphenol A (BPA), nonylphenol ethoxylates (NPE), and flame retardants (tris (2,3-dibromopropyl)[168].

Commonly, the way that additives are attached to the plastic polymer is physically rather than chemically[169]. Therefore, during the processes of laundry, abrasion, and transportation, macro and MPs can easily leak additives to the environment[170]. Most of the chemicals found in clothing at the time of purchase are either by-products of manufacturing processes (such as dyeing, bleaching, or finishing) or were purposefully added with the intention of remaining in the fabric throughout the garment's lifespan. The textile business uses more than 2000 different chemicals, ranging from dyes to transfer agents[171].

The textile industry is currently very interested in the potential uses of metallic nanoparticles to enhance the production of fibres and create fabrics with new or improved qualities[172]. Thus, the term "nanofinishing" has been introduced to the list of textile finishing categories. An example of nanofinishing to enhance current textile production processes is the use of titanium dioxide (TiO_2) nanoparticles, specifically the scouring and bleaching of fibres (nanoscouring and nanobleaching).

Natural colouring and pigments in fabrics quickly degrade due to the photocatalytic activity of TiO_2 nanoparticles[173]. Some of the new features in textiles incorporating metallic nanoparticles include self-cleaning qualities (ZnO and TiO_2 nanoparticles)[174], UV blocking activity (TiO_2, ZnO, CeO_2, and Al_2O_3 nanoparticles)[175], antibacterial properties (Ag, CuO, ZnO, and TiO_2 nanoparticles)[176], hydrophobicity (SiO_2 and ZnO nanoparticles)[177], and electromagnetic wave shielding (Cu-, Ni-, Fe-, and Co-based nanoparticles)[173], among others.

Dyeing involves the largest range of chemicals with an estimated 800 dyes currently in use[178]. Because some dye intermediates are synthesized using catalysts, it is possible for antimony, copper, and chromium residues to appear in dyestuffs. Metal complexes including

those of copper, nickel, cobalt, and chromium are present in several reactive dyes. As a result of the manufacturing process's raw materials, dyestuffs with metal-free chromophores could also contain metallic impurities[171]. Phthalocyanines are complexes of copper that mimic the structure of porphyrins and are a type of synthetic organic pigment. In comparison, inorganic pigments are made up of a variety of substances, primarily oxides and sulphides. Some inorganic pigments, such ZnO and Sb_2O_3, act as white pigments as well as fungicides and synergists for flame retardants, respectively[179].

Some chemicals found in textiles are a result of packaging, transit, storage, and other procedures that take place between the time of manufacture and the time of purchase[178]. Metal-based additives can be in the form of partially soluble organic molecules, insoluble inorganic compounds, or liquid or salt organometallics. Concerns over their effects on human health and the environment have led to a steady movement away from inorganic and organometallic compounds in many industries, despite the higher heat resistance and weathering qualities and lower cost they can provide[180]. The chemicals employed in the production of conventional fabrics leave behind residues that are absorbed via the skin or evaporated into the air we breathe. Some of the chemicals can cause cancer or harm children even before they are born, while others can trigger allergenic reactions in some individuals. Long-term exposure to heavy metals can result in allergies, cancer, emphysema, kidney failure, and other health issues. Because of this, it is necessary to assess how much metal is present in textile fabrics[171].

The presence of heavy metals in synthetic textile fibres has been documented[171]. In one study, the examined fibres (acrylic, polyester, nylon, viscose, and polypropylene) shown concentrations of iron (Fe) in the range of 43.44 to 79.83 mg/kg, cadmium (Cd) in the range of 6.05 to 8.46 mg/kg, copper (Cu) in the range of 3.31 to 5.00 mg/kg, nickel (Ni) in the range of 0.53 to 2.42 mg/kg, antimony (Sb) in the range of 18.84 to 24.41 mg/kg, and chromium (Cr) in the range of 0.11 to 0.83 mg/kg. Cd was not detected in viscose and PP samples[171]. These results are in line with those of another study where garments made of PE, spandex, viscose, cotton, and polyamide were analysed in order to detect traces of heavy metals[181]. Of the various metals investigated, magnesium (Mg) showed the highest mean value (114 mg/kg), followed by Cr (45.7 mg/kg), zinc (Zn) (36.4 mg/kg), aluminium (Al) (28.5 mg/kg) and Sb (26.0 mg/kg). In viscose or polyamide materials with dark colours, chromium levels were comparably high (up to 754 mg/kg). All fabrics made of PE showed

high levels of Sb[181].

European Regulation 1007/2011 requires that information on fibre composition be provided, and textile products sold in Europe are not allowed to include certain amounts of metals. The legal limit in textiles for Cu is 5 µg/g and Sb have a limit of 3 µg/g. For lead, cadmium, chromium (VI), and arsenic (and their derivatives) the legal limit is 1 µg/g. Furthermore, it is prohibited to impregnate yarn with mercury-containing compounds. For verification and detection, ICP-MS or ICP-OES are the methodologies recomended[182].

Synthetic dyes used in the textile and other industries can contain up to 70% of azo dyes[183]. These are organic compounds bearing the functional group R−N=N−R′ in which R and R′ are usually aryl and substituted aryl groups (functional groups derived from an aromatic ring such as phenyl and naphthyl). The aromatic compounds allow for a fast and effective colour of the azo dyes and their production is unexpensive and a simple procedure[183]. While most azo pigments are non-toxic, some, including pigment oranges 1, 2, and 5, as well as dinitroaniline orange and ortho-nitroaniline orange, are mutagenic and carcinogenic. More than twenty different forms of aromatic amines can be produced when certain azo dye types degrade under specific conditions. Any azo dye that has the chemical ability to transform into aromatic amine compounds can be dangerous to humans and result in cancer[184]. Aquatic life, agricultural areas, running streams, and the ecosystem's integrity are all negatively impacted by the release of azo dye effluent as wastewater from various industries. Due to the persistence of azo dyes, which are difficult to break down naturally and by basic wastewater treatment methods, the entire marine biota of the discharged dye wastewater area is put under stress. This stress is primarily brought on by an increase in chemical oxygen demand (COD), which negatively affects biological oxygen demand (BOD)[183]. A range of countries have particular laws governing some azo dyes and dangerous aromatic amines. 22 aromatic amines produced from specific azo dyes are banned in the European Union (EU) from being used in products that may come into direct or extended contact with the skin or oral cavity of humans (EN 14362-1: Methods to determine azo colorants accessible with and without extracting the fibres and EN 14362-3: Methods to determine the use of certain azo colorants, which may release 4-aminoazobenzene). For all aromatic amines, the maximum concentration is 30 mg/kg[183]. Nevertheless, it has been demonstrated the presence of primary aromatic amines (PAAs) in textile and leather products exceeding EU regulatory limits with concentrations of benzidine of 45-593 mg/kg for some textiles and concentrations

of o-toluidine of 430 mg/kg, benzidine (31 mg/kg), and 3,3′-dimethylbenzidine (40 mg/kg) in leather products[185].

In addition to the chemicals above, various organic compounds like alkanes, aromatic amines, phthalates, aliphatic carboxylic acids, and linear aliphatic alcohols have been detected on textile effluents from a textile processing factory[186]. Additionally, textile wastewaters were found to contain glycol, polyethoxylated decyl alcohol, and linear alkylbenzene sulfonates. According to the authors, organic compounds in textile effluents often have a high structural variety and exhibit noticeable ecotoxicological consequences due to their considerable concentration level of emission[186]. With concentrations up to 1.2, 3.5, and 2.4 mg/l, respectively, polyethylene glycol (PEG), polyethoxylated decyl alcohol (AEO10), and 2-naphthalenesulfonate were determined to be the three main contaminants in textile wastewaters in another study[187]. This investigation also found that the concentrations of linear alkylbenzene sulfonates (LAS) in this fraction ranged from 14.2 μg/l for C10LAS to 39.1 μg/l for C11LAS. Auxiliaries for dye baths used in the textile industry, such as benzene (BS) and naphthalene sulfonates (NPS), were discovered to have higher concentration levels, up to 0.1 and 2.3 mg/l respectively[187]. The addition of PEG increases the tensile strength, resistance to creases, water absorption and abrasion resistance of the treated fabrics[188]. PEG is also known for its antifouling properties[189].

There are important considerations with the discharge of textile effluents into natural aquatic and terrestrial environments. The main source of the risk associated with these effluents is the presence of micropollutants. These chemical substances are bioactive and persistent contaminants, which means they cannot be eliminated by standard water treatment methods, and they are only partially biodegradable[186].

2019 saw the start of the SARS-CoV-2 outbreak, a new type of coronavirus that later spread throughout the world. The disease was given the name "COVID-19" and was classified as a pandemic by the World Health Organization (WHO) by March 2020. Globally, lockdowns, social distancing, and governmental regulations were implemented as measures and limits to stop the virus's spread. Wearing masks and other personal protective equipment (PPE) like face shields and gloves in particular became commonplace in public[190]. Most likely, these PPE will be disposed of improperly with other organic trash in typical municipal solid waste or, worse yet, will be dumped into the environment. Disposable gloves and masks have been

observed polluting public spaces (such parks and streets) all around the world[191]. The COVID-19 pandemic has increased pressure on waste management systems, resulting in inappropriate management techniques such local burnings and direct dumping. However, the unregulated treatment of even 1% of face masks corresponds to 10 million pieces of a mass between 30 and 40 tonnes. Additionally, plastic associated with COVID-19 has been seen in aquatic habitats, suggesting a potential new source of oceanic microplastics[192].

Face masks are available in a variety of styles, sizes, materials, and levels of quality. Masks are made of non-woven textiles made of mainly polyester, polypropylene, polycarbonate, polystyrene, and polyethene. Surgical masks often have three layers, with a polypropylene layer positioned in the middle of the non-woven fabric. Every layer has a distinct purpose (e.g., the melted brown inhibits microbial entry and acts as a microbial filter)[193]. In general, masks are assessed based on performance criteria such as filtration, exposure, mask airflow resistance, etc. Filtration is essential for catching exhaled aerosols as well as for microbiological and aerosol filtration. The effectiveness of the mask is also evaluated for its lack of aerosol transfer from the outside. Another important factor is breathability, which is determined by pressure variations that occur when breathing[193]. Multiple varieties of printed and semi-printed masks have increased in popularity as a result of the need for masks due to COVID-19 prevention measures. Fashion and branding logos have also grown in popularity[190]. As commented before, most commercially produced textiles use synthetic pigments and dyes, and it is believed the same products are used for dyeing DPFMs. It has also been demonstrated that single-use surgical face masks are able to act as dye carriers in water bodies[194].

1.3.1. Detection of heavy metals and organic compounds

For the textile business as well as for consumer safety, it is crucial to identify the metal contents of the different textile materials. It is well known that several metals found in textile fibres can affect the way yarn is produced, how it is bleached and dyed, and its quality when it is processed[195]. Therefore, more effort should be put into creating a quick, accurate, and sensitive method for identifying harmful metals in textile materials. For determining the total or extractable levels of heavy metals in textiles, a number of analytical methods have been proposed, including atomic absorption spectrometry, X-ray fluorescence spectrometry, spectrophotometry, and anodic stripping voltammetry. Each approach has benefits of its

own, but in general they are arduous, time-consuming, not sensitive enough, and not selective enough[195]. ICP-MS has been presented as a robust method for measuring ultratrace metals in a wide variety of sample types and is, without a doubt, the trace element method that is expanding the fastest right now. Approximately 11,000 units have been installed worldwide since its commercialization in 1983 for a wide range of applications[196]. In contrast to the molecules and compounds that other approaches like GC/MS measure, ICP-MS is an elemental analysis method, which means that it is used to analyse elements. ICP-MS transforms the sample into ions using an argon (Ar) plasma, the ICP, which are then examined using a mass spectrometer, the MS. Similar to inductively coupled plasma optical emission spectroscopy (ICP-OES), ICP-MS examines the elements (ions) directly as opposed to ICP-OES, which uses an optical spectrometer to measure the light emitted from elements as they travel through the plasma. Both methods swiftly analyse a variety of elements in a sample, however ICP-MS has much lower detection limits than ICP-OES, making it a superior option for analysing trace elements. ICP-OES, flame atomic absorption (FAA), electrothermal atomization (ETA), and other atomic spectroscopic methods can all approximately determine the same set of elements, but ICP-MS has distinct advantages due to its multielement characteristics, speed of analysis, detection limits, and isotopic capability[196].

ICP-MS is commonly used to investigate samples that are liquids (such as water) or that can dissolve or produce a liquid after being acid digested. ICP-MS is highly adaptable and may rapidly measure organic solvents, identify very small (nano)particles, or be coupled to accessories that enable direct investigation of solid materials or gases. For information on the many chemical forms or "species" of each element in a sample, ICP-MS can also be connected to a chromatographic separation tool like an HPLC, GC, or Field Flow Fractionation (FFF) [196]. Additionally, ICP-MS can detect and isolate each unique isotope of an element because it is a mass spectrometric technique, making it useful for applications where isotopic abundances or isotope ratios are relevant. Only a few elements cannot be measured by ICP-MS: F and Ne (which cannot be ionised in an argon plasma), Ar, N, and O (which are present at high levels in the plasma and air), and H and He (which are below the mass range of the mass spectrometer). Even F, one of these 'out of range' elements, can be indirectly studied using a triple quadrupole ICP-MS. The fact that ICP-MS offers incredibly low detection limits for almost all of the elements it can measure is one of the factors leading

to its increasing application. Many elements can be found using ICP-MS at concentrations as low as 0.1 parts per trillion[196].

ICP-MS has been utilised for the determination of total amount of trace metals (Cd, Cr, Cu, Ni and Pb) in four textile samples after microwave-assisted acidic digestion of samples at 300 °C for 28 min. The suggested method's precision was examined against approved comparable reference material. ICP-MS was reported to be highly suited for quick and accurate monitoring of trace metals in textile samples[195].

In another study it was discovered that the levels of lead and arsenic were higher than those permitted by European Regulation 1907/2006. Mercury (Hg) was also measured in several fabrics, despite the fact that impregnation of yarns with Hg compounds is prohibited. Some textile items that were sold commercially in Europe and were part of this study did not adhere to European Regulation[171].

Not only modern textile samples have been analysed using this technology. Historic and archaeological textiles have been also investigated and results showed that mordants including copper, iron, tin, aluminium, or uranium, as well as an organic dye with a substitutional bromine, were effectively identified[197].

ICP-MS has been also put in place to conduct a leaching test and different techniques to examine the release of nano-TiO2 and total Ti from five different types of commercially available conventional textiles with Ti contents ranging from 2.63 to 1448 μg/g. TEM was used in conjunction with traditional and single particle inductively coupled plasma mass spectrometry (SP-ICP-MS) to analyse the released particles in order to measure the total and particulate TiO2 release by mass and particle number, as well as size distribution. Depending on the type of fabric, a different percentage of nano-TiO2 was released, which ranged from 0-80% of the overall amount. Particle mode sizes ranged from 50 to 75 nm, while TEM imaging showed that the particles were 80 to 200 nm in size[198].

SP-ICP-MS is a relatively new technology and in the last decade has become a popular analytical approach for the quick characterisation of nanoparticles. In essence, diluted suspensions of nanoparticles are nebulized into the device, the time-resolved signal from the element (isotope) associated with the NPs is recorded, and the intensity of this signal is converted to matching particle size. This method has spread widely in recent years and is close to becoming a standard practise for nanoparticle analysis. It can give information on particle size distribution, particle number concentration, and mass concentration in diluted

samples requiring minimal to no sample preparation[198]. Its potential for the analysis of MPs has been demonstrated using spherical polystyrene microspheres of 1 and 2.5 μm to mimic MPs coming from plastic waste. The method used relies on ultra-fast transient signal monitoring when using a quadrupole-based ICP-MS unit in what is known as single-event mode and registering the signal spikes produced by individual microparticles by observing the signal intensity at a mass-to-charge ratio (m/z) of 13 ($^{13}C^+$)[199].

For the analysis of organic compounds, the online combination of mass spectrometry (MS) and liquid chromatography (LC) has developed into a reliable and widely used analytical method in recent decades[200]. Liquid chromatography (LC) typically separates a sample into its constituent parts based on differences in their affinity (or retention strength) for the stationary phase or mobile phase. Then, depending on the properties of the components, they are detected using UV, fluorescence, or electrical conductivity. These detectors primarily classify compounds according to retention time and quantitative substances according to peak area and intensity. Chromatography provides excellent resolution, but it can be challenging to precisely classify and quantify substances when several components elute approximately at the same time, as happens during simultaneous multianalyte analysis[200]. Present day liquid chromatography that generally utilizes very small packing particles and a relatively high pressure is referred to as high-performance liquid chromatography (HPLC). Normal phase liquid chromatography (NPLC) refers to techniques where the stationary phase is more polar than the mobile phase (for example, using toluene as the mobile phase and silica as the stationary phase), whereas reversed phase liquid chromatography (RPLC) applies the opposite (e.g., a water-methanol mixture as the mobile phase and C18 (octadecylsilyl) as the stationary phase)[201].

Mass spectrometry (MS), in contrast, provides an overly sensitive detection approach that ionises the sample individual components using a range of techniques, separates the resulting ions based on their mass-to-charge ratios in vacuum, and then calculates the intensity of each ion. It is very beneficial for qualitative analysis since the mass spectra produced by MS can display the concentration level of ions with a specific mass. This is so because mass is information that is specific to particular molecules, and MS provides the ability to access that information directly[200].

For the determination of complete azo dyes, LC-MS or LC-MS/MS with various interfaces have been widely employed[202,203]. The precise identification and quantification of aromatic

amines generated from textile samples dyed with azo dyes have been demonstrated, with the analysis 18 aromatic amine compounds including o-tolidine (3,3′-dimethylbenzidine) and 3,3′-dimethoxybenzidine[202]. This methodology has also been utilised for the quantification of arylamines, derived also from azo colorants[203]. A study performed on textile wastewater discharges demonstrated that ethoxylated surfactants (AEO) found in the samples collected may be oxidised or degraded, producing carboxylated AEO and polyethylene glycol (PEG), or even carboxylated PEG, according to LC-MS tests[204]. This technology has been used also to examine historical samples like 3000-year-old wool funerary textiles from Xinjiang, China or samples of silk that had been coloured yellow using flavonoid glycosides from Sophora japonica (pagoda tree) and curcumins from Curcuma longa (turmeric)[205].

Some of the contents of this section were published by ACS publications in February 2021 in the article 'From Sampling to Analysis: A Critical Review of Techniques Used in the Detection of Micro- and Nanoplastics in Aquatic Environments' [88] *of which the author of this thesis is first author.*

1.4. Highlights

Chapter 1 presents an exhaustive and detailed study of the fate of MPs and NPs in the environment and the potential risks for all organisms, including humans, along with the different approaches put in place from sampling to the final detection of MPs and NPS in water samples from different water bodies worldwide.

- MPs and NPs now can be found in every natural environment, and it has been demonstrated that they pose a risk for all organisms, including humans, as they can be inhaled and consumed, and NPs can even cross the cell wall and release chemicals that can interfere with the cell functionality.
- Depending on the technique employed for the final analysis, the process for identifying MPs and NPs in samples from aquatic settings can involve several distinct processes.
- The process of gathering samples can be laborious and could require

different equipment. To avoid contamination that could affect the results, extreme care must be used when choosing the contact material for the sampling equipment.

- For most analytical procedures, separation and purification—either physical, chemical, or biological—are essential and crucial steps that call for the removal of both inorganic and organic debris adhering to the surface of the plastic pollutants in order to enable accurate identification. However, they take a lot of time, and current research using more advanced analytical techniques has demonstrated that this phase can be skipped.

- Microscopy, spectroscopy, and thermal analysis are the three most often utilized tools for MP identification. Although the use of microscopy alone has its limitations, it has been widely employed in studies where the nature of the plastic particles is already known. In order to identify unidentified polymer types, spectroscopy and microscopy are frequently combined.

- The key to resolving the challenges now observed, especially in the analysis of NPs, may lie in the adoption and development of methodologies employed in other domains. To address the environmental issue that MPs and NPs represent, procedure standardization is crucial. To fully comprehend its magnitude and importance, both to us and to future generations, further research must be conducted.

1.5. Aims and Objective

There is a great debate about the role of MPs and NPs in the environment and how they can potentially affect the physiology of plants and animals, including humans. A general agreement exists in the scientific area claiming for further analysis and projects to be carried out on each area of expertise in order to elucidate the reality of the pollution posed by MPs and NPs.

To start with, it is necessary a standardized method for the detection, identification and

quantification of these contaminants, and it is one of the main aims of this thesis to develop and apply a straightforward, reliable, fast, and unexpensive method to detect, identify, and quantify MPs and NPs in water sources.
Secondly, in view of the rising in use and dispensation of disposable plastic face masks (DPFMs) due to the COVID-19 pandemic, and the fact that unregulated disposal of these item has been considered a new form of plastic pollution to the environment, this thesis initiated the analysis of these products in order to shed light on the potential hazard they pose to the environment due to their chemical and physical characteristics.
To achieve these aims, the following objectives were set:

1. To develop a methodology to separate MPs and NPs in aqueous which is also suitable for analysis using pyrolysis GC/MS.
2. To ensure this methodology accessible, reliable, able to avoid time-consuming tasks and straight forward.
3. To collect evidence of the release of MPs and NPs from disposable plastic face masks (DPFMs) into the environment once they are discarded.
4. To determine the potential risks to all organisms (including humans) derived from this novel form of global pollution.
5. To evaluate to what degree medical masks type IIR and FFP2 are also a source of MPs, NPs and other contaminants.

Based on the identified gap in research and current objectives, this work's research hypotheses include:

- The use of a glass filtration system and membranes of different pore size as a support for the samples, should be a valid approach for the purpose of separating and analysing MPs and NPs on aqueous samples.
- The use of an analytical mill should be sufficient to obtain particles in the nanoscale.
- Pyrolysis GC/MS is an approach that shows advantages and suitability to

develop a new MPs and NPs detection methodology.

- PTFE and aluminium oxide membranes will serve as a support for the different synthetic fibres and particles after filtration, with sizes down to 20 nanometres.
- Disposable plastic face masks can be proven to be a new and increasing source of MPs and NPs, chemicals, and other pollutants into de environment after the raising in production due to the COVID-19 pandemic.
- Medical DPFMs type II and FFP2 are also potential contaminants for the environment and pose a risk for human health.

This current thesis has been broken down into five chapters and their outline is described below:

Chapter 2: This chapter facilitates a summary of the use of thermal analysis approaches in the study of plastics and introduces a new methodology for the identification of MPs in aqueous samples using pyrolysis - gas chromatography – time of flight mass spectrometry (Py-GCToF). It also lay the foundations of a new protocol for grinding up and filtrating methodology for MPs and NPs using membranes of a very small pore size, down to 100 nanometres. Having the purpose of detecting the particles size, results are shown after using different technologies. Py-GCToF is suggested as a reliable and quick approach of detecting MPs and NPs.

Most of the contents of this chapter were published by ScienceDirect/Elsevier in February 2020 in the article 'Detection of trace sub-micron (nano) plastics in water samples using pyrolysis-gas chromatography time of flight mass spectrometry (PY-GCToF)' [206] *of which the author of this thesis is co-first author. The preparation of the samples was fully conducted by the author of this thesis. Microscopy, STA and Py-GCToF analyses were carried out by the author of this thesis and Dr. Geraint Sullivan.*

Chapter 3: This chapter introduces the recent environmental problem derived from the rising in use and dispense of disposable plastic face masks (DPFMs) into the environment, due to the SARS CoV-2 global pandemic that started by the end of 2019. It shows how, from several and different mask types, not only micro- and nanoparticles are released into the environment after physical degradation, but also chemical pollutants are also leaching from

DPFMs, some of them heavy metals like antimony and lead. This is the first time that this issue has been reported and published and corroborates the findings of other authors regarding the use and release of MPs, NPs, chemicals, and other contaminants from textile samples. It also remarks the fact that supposedly innocuous items that are used every day can pose a risk for the environment and human health and claims for further analyses to be carried on.

Most of the contents of this chapter were published by ScienceDirect/Elsevier in February 2021 in the article 'An investigation into the leaching of micro and nano particles and chemical pollutants from disposable face masks - linked to the COVID-19 pandemic' [207] *of which the author of this thesis is co-first author. The preparation of the samples was fully conducted by the author of this thesis. Microscopy and FTIR analyses were carried out by the author of this thesis and Dr. Geraint Sullivan. IPC-MS analyses were carried out at Tata Steel (Port Talbot) and LC-MS analyses were carried out at the National Mass Spectrometry Facility (Swansea University).*

Chapter 4: This chapter follows the findings of chapter 4 and focuses exclusively on the analysis of medical plastic face masks type II and FFP2. With the intention of providing further and more detailed results, new microscopical techniques are included and also the use of filtration membranes of 20 nanometres pore size in order to obtain better NPs images. Even when this type of masks appears to be less harmful, the results are not encouraging. MPs and NPs and chemical contaminants (including again heavy metals) are released from them as well. The author of this thesis recommends for more studies to be carried out as the potential damage for the environment and all organisms within is still unknown.

Most of the contents of this chapter were published by ScienceDirect/Elsevier in March 2022 in the article 'Disposable FFP2 and Type IIR Medical-Grade Face Masks: An Exhaustive Analysis into the Leaching of Micro- and Nanoparticles and Chemical Pollutants Linked to the COVID-19 Pandemic' [208] *of which the author of this thesis is first author. Microscopy analyses were carried out by the author of this thesis. IPC-MS analyses were carried out at Tata Steel (Port Talbot) and LC-MS analyses were carried out at the National Mass Spectrometry Facility (Swansea University).*

Final **Chapter 5** compiles and summarizes the findings of this thesis and also includes

suggestions for future work based on the methodology shown in the different chapters and gives recommendations on the application of other technologies that could improve the results obtained.

Chapter 2: Detection of trace sub-micron (nano) plastics in water samples using pyrolysis-Gas chromatography time of flight mass spectrometry (PY-GCToF).

2.1. Introduction

As commented above, MPs and NPs cannot yet be measured using an established standard method. The detection of micropollutants smaller than 50-100 μm using existing techniques is equally difficult. Some research claim that there is yet no methodology that is trustworthy enough to identify NPs in complex environmental samples such surface, ground, drinkable, and raw waters[209]. As indicated on the previous chapter, FTIR, Raman, light microscopy, and SEM are currently utilised as common analytical methods. Nevertheless, they present associated constraints, such as identification in complicated mixes, despite being effectively valuable for qualitative work[70,210], and detection levels of these instruments are limited by resolution. This makes it difficult to identify small particle sizes (>50 μm) and also to quantify low level material[70,210].

Using FTIR, the samples have to be IR-active and those below 20 μm might not present enough absorbance in order to get a suitable spectra[74]. Also, it is difficult to examine samples that are not transparent using FTIR and the formation of biofilm on the polymers affect the detection of these materials[78]. According to these authors, Raman spectroscopy can identify plastic particles as small as 1 μm, but a considerable disadvantage of this procedure is the sample preparation since organic and inorganic material considerably interferes in fluorescence and, consequently, the levels of MPs detection. This technique also requires a considerable amount of time for analysis. In both instances, however, the analysis of NPs is out of scope.

Scanning Electron Microscopy (SEM) and Transmission Electron Microscopy (TEM) can also analyse particles in the micro scale, but the need of coating at high vacuum for SEM complicates sample preparation. TEM does not seem to be a suitable approach due to the shapeless structure that NPs present and the requirement of heavy-metal stains[86].

Other improved techniques, like Nile Red coupled with an automated counting software MP-VAT, has been put in place for the identification of nanoparticles around 500 nm. Even when

results were satisfactory, the study points at the impossibility of determining the chemical composition of the samples and the need of pre-treat samples to eliminate organic material and produce more reliable results[77].

To overcome these limitations, this thesis focuses on the identification of MPs and NPs by analysis of their thermal degradation products using chromatographic and mass spectrometry, a highly sensitive technique commonly used to analyse complex samples and has been used in characterisation of synthetic polymers and copolymers[73,127,153,156].

The method employs a commonly used PTFE membranes (pore sizes 0.45 and 0.1 μm) to deposit MPs and NPs from aqueous samples working in the limit range of nanoscale. After processing, these filters are analysed using gas chromatography coupled to time-of-flight (ToF) mass spectrometry. The verification of MP and NP type is based purely on the identification of the evolved degradation products. The plastics studied in this article are known to breakdown at temperatures below 500 °C[144–146]. The degradation products produced from the different plastics may be used as potential markers to identify a variety of plastics in a complex mixture or identify plastics from samples containing potentially difficult matrices, such as untreated water samples. The choice of membrane was also decided based on PTFEs' higher thermal resistivity than common plastics, as it begins to degrade (>550°)[211] and is less likely to contribute to background interference.

The use of pyrolysis - gas chromatography time of flight mass spectrometry (Py-GCToF) is proposed as a methodology that facilitates a fast and suitable analysis of plastic pollutants. A schematic representation of the whole process is shown in Figure 2.1.

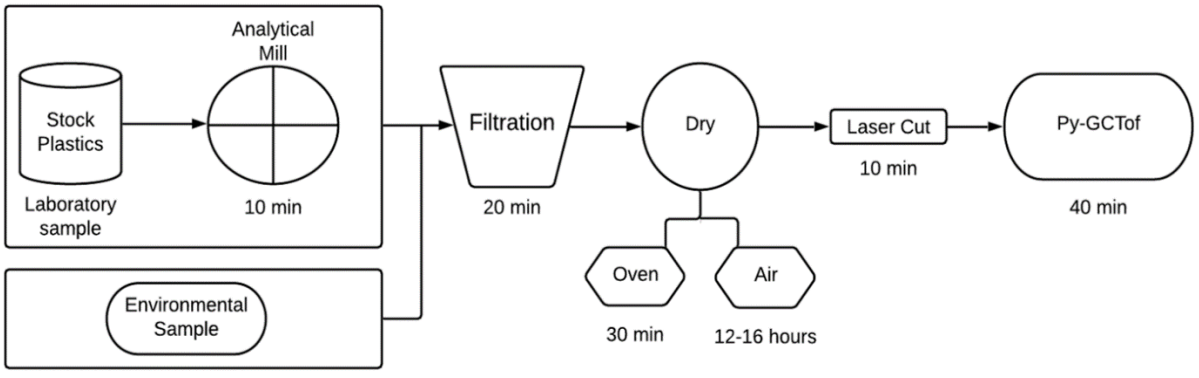

Figure 2.1. Illustration of the novel standard methodology proposed in this study for the identification of micro and nanoplastics using both laboratory and real environmental samples. Adapted from Sullivan et al., 2020.

2.2. Materials and methods

2.2.1. Standard reference materials

Powdered PVC (high and low molecular weight and bulk density of 1.4 g/ml), PP (pellets and bulk density of 0.9 g/ml), PE were purchased from Sigma-Aldrich UK. PS, on granules of 900 μm and a bulk density of 0.62 g/ml, was purchased from Goodfellow Cambridge Limited. Fluoropore® Polytetrafluoroethylene (PTFE) membranes (Merck Group UK) of 0.45 μm and 0.1 μm pore size were purchased for filtration purposes. Helium and nitrogen gases were purchased from BOC Gas & Gear (Port Talbot, UK).

2.2.2. Instrumentation

The plastic reference material was pulverized to a smaller than 100 μm using an IKA® England LTD M20 Universal Mill to produce material that is estimated to be between micro and nano in scale. Then, samples were poured through a glass vacuum filtration funnel and received flask during a filtration experiment under negative pressure using a Sparmax® vacuum pump (The Airbrush Company Ltd, UK). The filtration equipment was purchased from Sigma-Aldrich UK and included: a 1000 ml vacuum filtering conical flask, an aluminium spring clamp, a silicone stopper perforated size 8, a fritted glass membrane support base, a 300 ml glass beaker style funnel, a 500 ml beaker and a metal spatula. The vacuum pump was a model P630.V5A18, with a maximum vacuum of 740mmHg, an input operating vacuum of 675mmHg and an output flow of 32 L/min.

A brand new PURAIR P5-48 Nano (Air Science® Technologies Ltd) fume hood for particulates was employed to accomplish the grinding, filtering and overnight drying of the samples.

The dynamic light scattering analyses were carried out using a Zetasizer Nano ZS (Malvern Panalytical Ltd, Malvern, UK) (Figure A1.1 of Appendix A-1) and total organic carbon (TOC) measurements were obtained from a TOC-L analyser (Shimadzu UK Ltd, Milton Keynes, UK).

The filtrated membranes were cut using a TROTEC Speedy 300™ laser cutter (Trotec Laser, UK). Light microscopy of the membranes was used to determine coverage and particle size, these were done using Zeiss Primotech microscope (Carl Zeiss Ltd., Cambridge, UK) at 5 x and 10 x magnification.

The thermo-gravimetric analysis of the raw materials (plastics and membranes) was performed on a simultaneous thermal analysis (STA) 6000 by Perkin-Elmer 6000

(Llantrisant UK). This was used to determine the mass losses over a temperature range of 30 -700 °C.

The pyrolysis of the filtrate membranes was achieved using a CDS Pyroprobe® 5150 from Analytix Ltd (Boldon, UK). The pyrolysis products were then analysed using gas chromatography time of flight mass spectrometer (GC-ToF) that consisted of an Agilent 7890B GC (Agilent Technologies, Santa Clara, CA) and a Pegasus BT mass analyser (LECO Corporation, Saint Joseph, MI).

2.2.3. Microplastic preparation

The raw plastics were mechanically processed in an analytical mill to produce particles with cross sectional areas smaller than 100 µm. Preliminary studies in the literature demonstrated that the production of uniformly pulverised mixes with particles smaller than 1 mm can be accomplished by milling the samples[212]. Plastics were ground at 20,000 rotations per minute for this experiment in order to determine, by light scattering analysis, the minimum amount of time needed to produce MPs and NPs of the right size for the purposes of the project.

15 g of each plastic were placed in the grinding chamber. After a minute of grinding, the mill was paused for at least a minute to prevent the unit from overheating and the plastic particles from becoming agglomerated. According to light microscopy findings, MPs were uniformly distributed across the filter, and all seem to be under 100 µm in size as anticipated (Figure 2.2).

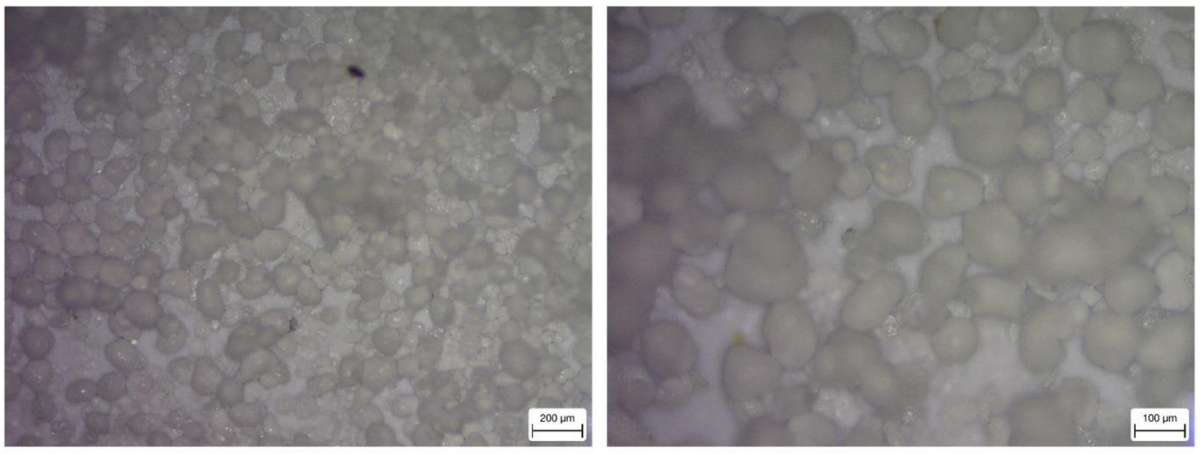

Figure 2.2. Light microscopy images of MPs generated by milling then filtered on to PTFE membrane. Left image is 5 x magnification and image on right is 10 x magnification. Adapted from Sullivan et al., 2020.

2.2.4. Microplastic filtration and sample preparation

Due to the previous commented ubiquity of MPs and NPs, all material employed in the preparation of the samples were plastic free and samples were prepared under an extraction hood for particulates, in order to avoid external contamination.

Aluminium weighing boats and metal spatulas were always used to manipulate the different type of plastics. Both the ground plastics and the aqueous samples obtained in each filtration were kept in glass bottles with a lid made of aluminium and natural rubber.

For the membrane samples containing only one of the plastics, 1 g of ground material was added to 500 ml of deionised water and stirred to ensure homogeneity of the solution and that sufficient material was deposited on the membrane. The same procedure was followed to prepared mixed samples of each plastic, reducing the quantity of material used to 0.25 g of each ground plastic.

A vacuum pump connected to the side arm of the receiver flask created a negative pressure of 675 mmHg which was used to draw through the sample (water containing MPs). The 500 ml aqueous sample was firstly filtered using a 0.45 μm pore PTFE or cellulose membrane. From each 500 ml of aqueous sample obtained, at least 3 smaller samples of 5 ml were stored in glass bottles for the subsequent scattering light and total organic carbon analysis. The rest of the liquid sample was then filtered again utilising this time 0.1 μm pore PTFE or cellulose membrane.

The 0.45 and 0.1 μm pore size membranes with the deposited ground plastics were afterwards introduced in brand new glass petri dishes and introduced for drying overnight in an isolated fume cupboard for particulates at room temperature under constant air flow to aid evaporation. The petri dishes were left covered to avoid any external contamination. This process can be accelerated by introducing the petri dishes in an oven at 80°C for 30 minutes. Once dried, several 10 mm x 1 mm shards of the membranes were cut systematically to give representative coverage of the filter. This process ensured high precision and repeatability of the filter cutting process. All samples were placed into plastic free glass bottles to keep from being contaminated.

2.2.5. Thermal analysis and analyte identification

This paragraph describes the use of Py-GCToFMS as an approach to identify MPs in aqueous samples that have been deposited on to PTFE membranes (pore sizes 0.45 and 0.1 μm). This type of membranes is widely used in industry and laboratory settings. The MPs will be

identified purely on the basis of the evolved tars generated. PS, PP and PVC are known to breakdown at temperatures below 500 °C[144–146]. The tars produced from the different plastics may be used as potential markers to identify a variety of plastics in a complex mixture or identify plastics from samples containing organic material and other chemical components such as untreated water samples. The choice of membrane was also decided based on PTFEs' higher thermal resistivity than common plastics, as it begins to degrade (>550°) [211] and is less likely to contribute to the final results with ion markers that could create a background interference in the outcome of the Py-GCTofMS apparatus.

The verification of MP type will be deduced using gas chromatography coupled to time-of-flight (ToF) mass spectrometry. The advantage of using a ToF analyser over more common scanning mass spectrometers (quadrupole analysers), is its superior acquisition speed and mass resolution[154,155], which is anticipated to bring sensitivity down to sub part per billion levels. The combination of gas chromatography and mass selectivity of the mass analysers allows us to match markers from reference materials to unknowns based on two parameters: retention time and mass spectra to further aid in plastic type identification. Together with the unprecedented low-level detection capability of the instrument and the small pore sizes of the membranes, it is anticipated the detection of MPs and NPs down to 0.45 and 0.1 μm in cross sectional size at part per billion level.

The marker ions for the distinctive chemicals produced by PS, PP, and PVC will be employed to limit the scope of the chromatographic data and facilitate the interpretation of the results. Light alkyl aromatics and polyaromatics like toluene, styrene, and naphthalene are expected to predominate in PS and PP[144]. These spectra are well defined and typically their fragmentation patterns produce high abundance fragment or precursor ions such as 91 mz for toluene, 104 mz for styrene and 128 mz for naphthalene[213]. For PP, the typical products generated are aliphatic[145] and fragmentation of these compounds generate very similar spectra predominant with low mass fragment ions (Stevensons rule for sigma cleavage)[213]. These ions with low fragmentation are very typical of many other substances. Therefore, as a compromise, and expecting it to be less abundant, a higher molecular weight fragment ion will be selected, such as 97, 111 or 125 mz as higher masses are deemed less common and more distinguishing. In order to characterise PP by overlaying samples with a reference material, the retention time will also be a major factor to consider.

2.2.5.1. STA analysis

Simultaneous thermal analysis (STA) of PP, PS and PVC and PTFE membranes were carried out utilizing nitrogen as the purge gas at a flow rate of 20 ml/min. The samples were heated up to a temperature of 700 °C at a heating rate of 15 °C/min. The main purpose of this analysis is to verify the temperature at which each plastic is degraded and confirm the information presented in the literature. Once it has been verified that PTFE is degrading at higher temperatures that the selected plastics, the limit temperature for the pyrolizer can be set.

2.2.5.2. Pyrolysis GC-ToFMS analysis

The samples were pyrolyzed using the CDS Pyroprobe. They were introduced into quartz tubes and heated from 30 °C to 500 °C at a rate of 20 °C/ms with a hold at 500 °C for 20 seconds. A nitrogen purge at 20 ml/minute around the probe ensures the sample is maintained in a pyrolytic environment. The pyrolysis products were captured using a Tenax® trap utilised for sorption of broad range of compounds (C6-C40). This was initially held at 50 °C. Prior injection, the trap was heated to 300 °C to desorb the captured analytes. The transfer lines connecting the pyroprobe unit to the GC were held at 300 °C to avoid analyte condensation. The trapped analytes are then exchanged into a gas flow of ultra-pure helium before being transferred to the GC unit.

To ensure good chromatography and analyte separation a 30-meter, a non-polar column with a 5 % diphenyl dimethyl polysiloxane phase was purchased from Restek Ltd (Worthing, UK) with a column id of 250 µm and a film thickness of 0.25 µm. The column flow was established at 1.2 mL minute (ultra-pure helium) and GC oven ramp of 40 to 300 °C at 10 °C/min as a smaller ramp rate would have taken too long for the different compounds to go through the column. This approach allows to steadily increase the temperature to efficiently separate high volatile compounds from less volatile ones.

The inlet conditions were set at 250 °C with the split vent open at ratio of 75:1 to prevent column overloading. The transfer line connecting the GC to the mass analyser was heated at 250 °C to minimise peak broadening. In the mass analyser the source (electron ionisation) operated at standardised 70 eV for reproducible spectra and source kept hot at 250 °C to limit source contamination. The MS acquisition parameters were set at 15 spectra/s with an extraction frequency of 15 kHz, collecting spectra between 50-500 *mz*. These parameters were chosen in order to get a good library match as a minimum of 10-15 spectra/s is required.

A quicker setting could result in not enough data obtained. On the contrary, a slower setting could translate in the acquisition of too much data. The parameters 15 spectra/s with an extraction frequency of 15 kHz were considered optimum to get quality data.
The data software package used to interpret the mass spectral information was ChromaTOF (LECO Corporation, Saint Joseph, MI).

2.2.5.3. Semi-quantification of PVC and PS breakdown products

A sample containing a mixture of PS and PVC was filtered and prepared following the methodology in paragraph 2.2.4 but on this occasion, prior to pyrolysis, each cut filter was spiked with 1 ng of chlorobenzene d5 internal standard and run in triplicate. An internal standard is a chemical compound that is nearly identical to the target analyte, but with sufficient differences in mass or functional groups to be discriminated from the target analyte by the analytical method. The internal standard is used to correct for matrix effects that affect polymer pyrolysis and fragment recovery. This correction is made by comparing the instrument response for the internal standard of known amount to the instrument response for the target analytes. The internal standard also corrects for changes in the mass spectrometer ion source condition and fluctuations in carrier gas flow rates[214].
Chlorobenzene d5 was selected to be used as internal standard as benzene is one of the breakdown products of PVC and PS. This internal standard has deuterium, a minor and stable isotope of hydrogen with one proton and one neutron and thus, it is easily recognizable as it has a mass difference with the compounds to be identified. As PP produces hydrocarbons, this internal standard is not suitable for semi-quantification purposes, and thus, semi-quantification results for this polymer are not included in this thesis. However, for future analysis, the author of this thesis recommends the use of an alkane or similar compound to be used as an internal standard for PP, like naphthalene d8, styrene d8 or a deuterated alkane mix, such as deuterated n-dodecane (n-C12D26).
Chlorobenzene d5 was then applied for the semi-quantitative analysis of the emerging plastic breakdown products of PVC and PS which are typically aromatic. The semi-quantification was based on the summation of the area count of the individual marker ions of PS and PVC, compared to the area count of the spiked internal standard (equation 1 below). Additionally, three blank PTFE samples were also run and spiked with 1 ng of chlorobenzene d5 for determination of analytical limit of detection (LOD) of PS and PVC. The LOD for each plastic was calculated by the 3x standard deviation of the marker ions in the PTFE filter

blank.

Equation 1:

$$\frac{\sum Area\ count\ of\ mircoplastic\ marker\ ions}{Area\ count\ of\ \text{chlorobenzene d5}} \times Mass\ of\ \text{chlorobenzene d5}$$

2.3. Results and discussion

2.3.1. Dynamic light scattering analysis

Three aqueous samples obtained from each filtration process (5-, 10- and 15-minutes ground plastics added to 500 ml of deionised water), where directly examined for dynamic light scattering results and 10 runs for every sample were carried out. The analysed plastics were PE, PET, PP and PVC.

One of the factors taken into account was the Polydispersity Index (PdI), a measure of the wideness of the molecular weight distribution of the particles. The larger the PdI, the broader the molecular weight. The possible values are in the range between 0 and 1, with 0 for samples presenting perfectly uniform sized particles and 1 being a highly polydisperse sample with a large number of different particle sizes.

Another factor that has been analysed is the correlation curve (correlogram) facilitated by the Zetasizer software. The correlogram from a measurement can give a lot of information about the sample. The time at which the correlation starts to significantly decay is an indication of the mean size of the sample. The steeper the line, the more monodisperse the sample is. Conversely, the more extended the decay becomes, the greater the sample polydispersity. For a sample with small particles, it is expected to have a correlation signal decaying very early in the graph given (Figure 2.3).

The software also assists with the creation of an 'Expert Advice' report where indications regarding the size measurements of the sample are given and whether or not the quality criteria has been met.

In order to avoid suspected agglomeration of sub-micron plastics particles with the consequent formation of larger bodies in the aqueous solution, the different samples were immediately analysed in the Zetasizer apparatus or vigorously agitated before the test was carried out.

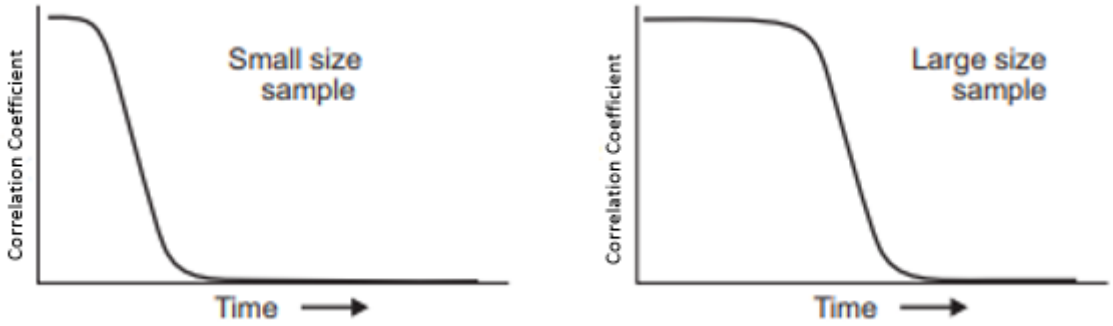

Figure 2.3. Standard correlogram of a sample containing small elements (left) versus a standard correlogram for samples containing large elements. The rapid decay of the correlation signal in the first case is only expected after a time in the second case. Standard correlogram of a sample containing small elements (left) versus a standard correlogram for samples containing large elements. The rapid decay of the correlation signal in the first case is only expected after a time in the second case.

Despite the results showing a uniform and defined size distribution curve and some samples meeting the quality criteria, the high PdI values obtained in the mayority of the runs together with the large size values obtained in all samples (>0.45 µm), suggest that the plastic particles within the solution are most probably aggregating after filtration, as pointed out by the 'Expert Advice' report from the Zetasizer software. This fact is not completely unexpected due to the hydrophobic characteristics that plastics display. The characteristics are presented in paragraph 1.1.1 and include the pH of the aquatic environment[19,20], salinity[21], alkalinity[22] or natural organic matter[23].

The agglomeration of small plastic particles in the water samples seems the cause for the formation of bigger conglomerates and the reason for the high polydispersion observed, leading to poor quality results. Nevertheless, these results reafirm the second hypothesis of this thesis and confirm the grinding method selected as being suitable for the purpose of this project, which is the target of this part of the investigation. On account of the hydrophobic properties of the plastics, these particles accumulate and form larger plastic aggregates inside aqueous solution, which does not interfere with the main objective of this stage of the research.

2.3.2. Verification of thermal degradation

For the purpose of confirming the information presented in the literature[215,216], thermo-gravimetric analyses were performed on the raw plastic materials and PTFE membranes using a Perkin-Elmer STA6000 apparatus. The outcome can be observed in Figure 2.4.

Results for PVC show the expected curve in two phases, with the first phase displaying a mass loss of approximately 65% at temperatures between 250 and 350 °C and the second phase presenting a mass loss of approximately 95% at temperatures of 500 °C, with a total decomposition at temperatures of 525 °C.

The observed curve for PP illustrates how this material begins to break down at temperatures of 300 °C, with a sharp mass loss occurring between 400 and 475 °C, where the entire amount of PP totally disintegrates.

Even more quickly than PP, PS began to degrade at 375 °C and was completely degraded before it reached 450 °C. Before reaching the temperature of 500 °C, PTFE membranes lost a negligible amount of mass, on the order of 3%. This material began to decompose once this limit was reached, and at 650 °C it was totally consumed. Therefore, it was decided that the analysis of MPs should be done at 500 °C. The increased mass transfer of the MP decomposition products to the column, will overall enhance the signal of plastic markers to that of the background noise contributed by the PTFE filter. These results, are the first step in order to achieve the first objective of this thesis.

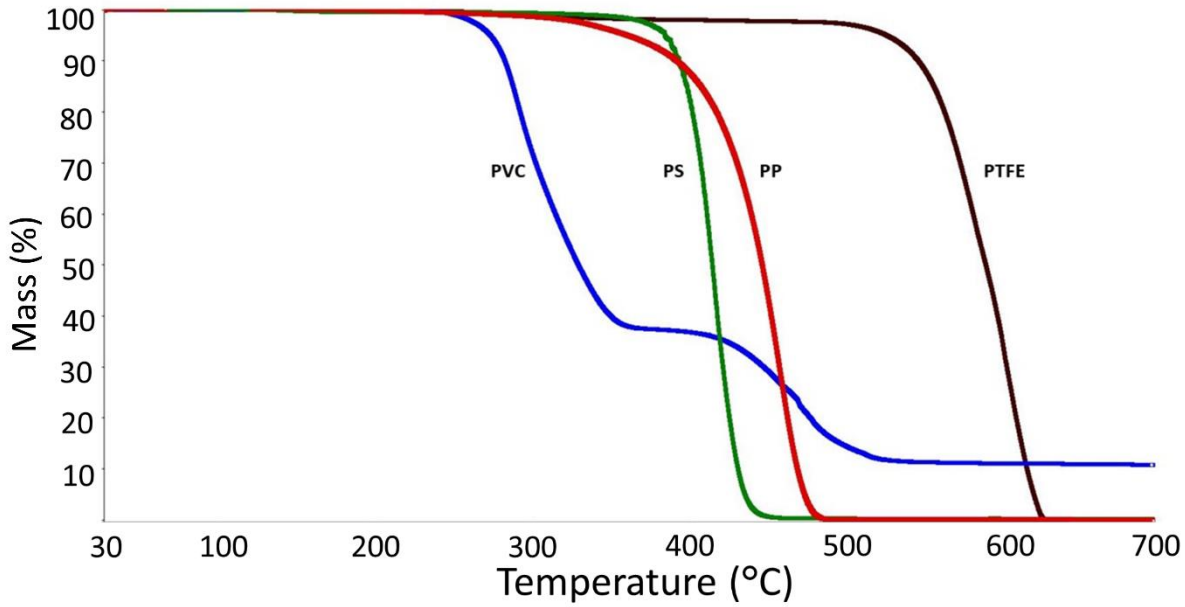

Figure 2.4. A thermo-gravimetric plot for different polymers; PVC (blue curve), PS (green curve), PP (red), and PTFE (black). The polymers are degraded at temperatures below 500 °C while PTFE degrades at higher temperature. Adapted from Sullivan et al., 2020.

2.3.3. Detection of plastic markers

Before being analysed with the Py-GCToF, samples of raw PTFE membranes (blanks) and PTFE membranes containing MPs (from filtering of water samples spiked with MPs) were

prepared. The samples contained PVC, PS and/or PP. The results of the filtered sample membranes were overlaid with the PTFE process blanks in order to identify the markers ions for these MPs. By comparing the markers to raw polymers processed under the same pyrolysis conditions, the markers were further validated. It is possible to clearly distinguish the individual plastics from the PTFE filter by contrasting the blank (PTFE filter only) with the MP samples (Figure 2.5). As stated before, some authors recommended the use of tweezers (or other alternatives such a flow cytometry) in order to place the micro- and nanoparticles into a receiver, and thus, handling samples smaller than 50 μm can present complication[153]. With the use of membranes, the necessity of any of these techniques is avoided as they are easy to handle and once the shards have been laser cut, they can be introduced into glass cylinders immediately after for PY-GC/ToFMS. The suitability of PY-GC/MS for the detection and analysis of MPs and NPs is then proven and confirms the third hypothesis contemplated in the Introduction.

One of the limitations encountered with the use of PTFE membranes was the contribution of this material (at 500 °C) to some of the ions present in the baseline. This ion contribution creates a background spectrum. Nevertheless, the MPs and NPs contribute to peaks with greater signal to noise ratio and therefore are distinguishable. Additionally, the instrument software is capable of remove this background from the results and show only the peaks belonging to MPs and NPs contained in the sample. However, in order to avoid this issue , it is recommended the use of inorganic membranes that will not interfere in any way, although it must be noted that this kind of membranes are more expensive.

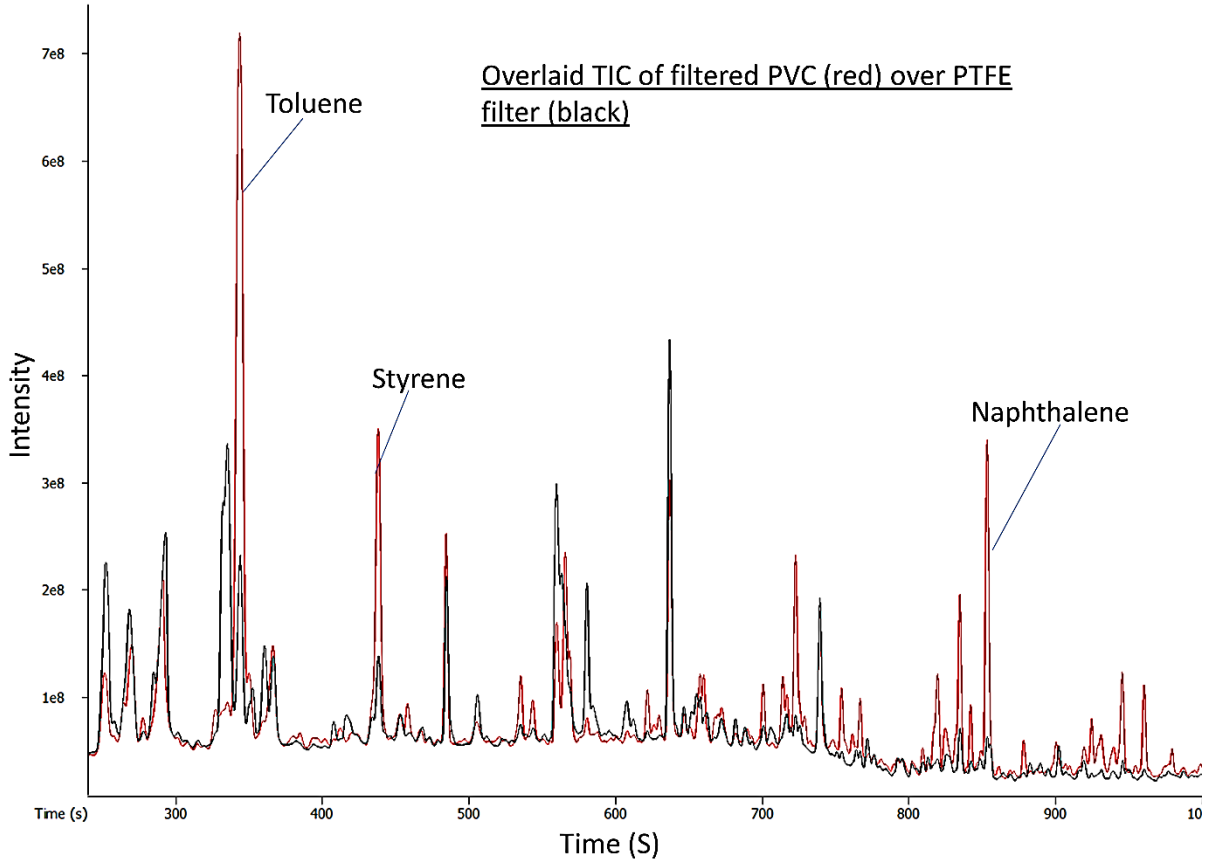

Figure 2.5. Demonstration of overlaid total ion chromatogram (TIC) of PVC deposited by filtration (in red) compared with PTFE filter blank (in black). There are identifiable ion markers coming from the PVC such as toluene, styrene and naphthalene that clearly present a larger peak and thus, these ion markers allow for the identification of PVC. Adapted from Sullivan et al., 2020.

2.3.4. PVC thermal decomposition

The thermal breakdown of PVC at 500 °C showed that over 50% of the material is lost as HCl gas and the remaining organic product (tar), light aromatic compounds such as benzene and toluene make up the majority of the liquid (80 %) [144]. Is at temperatures as low as 200 °C when Benzene and HCl emerge, and it is not until higher temperatures (above 300 °C) that the appearance of the other alkyl aromatics and polyaromatic hydrocarbons occurs. The most abundant of the aromatic compounds during the second loss is benzene, although lesser amounts of alkyl aromatic species (styrene, xylene) and poly-aromatic compounds (indene, naphthalene) can also be observed. The primary cause of PVC thermal breakdown is dechlorination, which generates initiation sites by the random scission of secondary chlorine atoms (Figure 2.6(3)). Benzene and alkyl benzenes are then formed through intramolecular cyclisation of the chain ends. A conjugated diene and an alkene (dienophile) react to generate unsaturated six-membered rings in the so known Diels-Alder reaction. It is also referred to

as a "cycloaddition" since the reaction results in the production of a cyclic product via a cyclic transition state. The inner part of PVC is cross-linked via Diels-Alder condensation reaction of double bonds belonging to other chains, at higher temperatures these structures degrade to produce aromatic hydrocarbons through cyclisation of free ends[144].

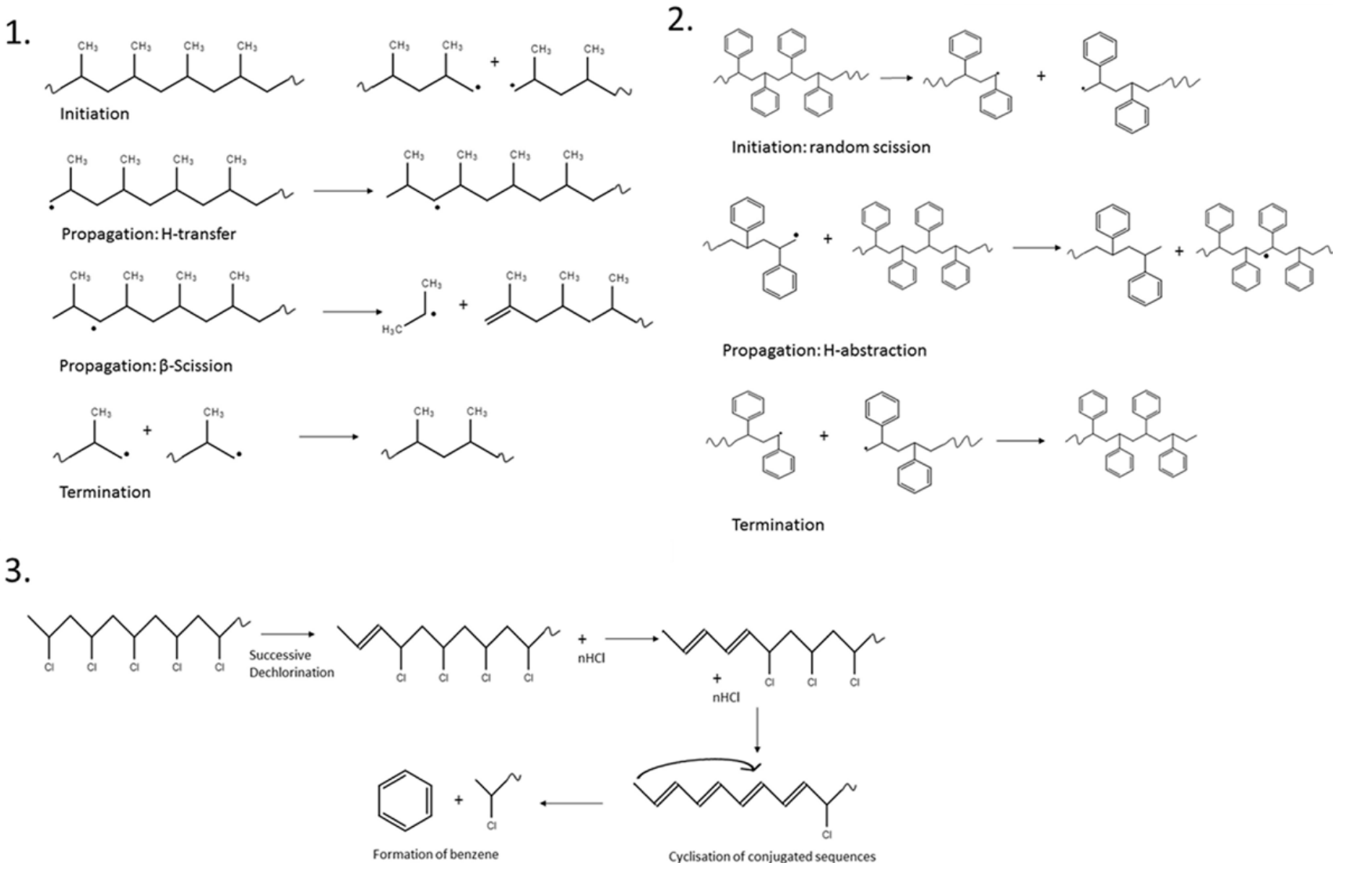

Figure 2.6. Image of the simplified mechanism for thermal decomposition of PP (1), PS (2), PVC (3), and degradation is initiated through formation of primary radicals. Reprinted with permission from McNeill, I. C., Memetea, L. & Cole, W. J. A study of the products of PVC thermal degradation. Polym. Degrad. Stab. ***49****, 181–191. Copyright 2005, Elsevier.*

Toluene, alkyl aromatics, and polyaromatic hydrocarbons, which are typical of PVC thermal degradation, were the primary chemicals found in filtered PVC[144] (Figure 2.7). Chlorobenzene was the only chlorinated substance detected, and it was present in low concentrations, as is typical for the thermal degradation of PVC[217]. The emergence of aromatic and poly aromatic compounds was then observed with an increase in pyrolysis temperature, and their synthesis is most likely the result of rearrangements of the scission products of the polymer backbone.

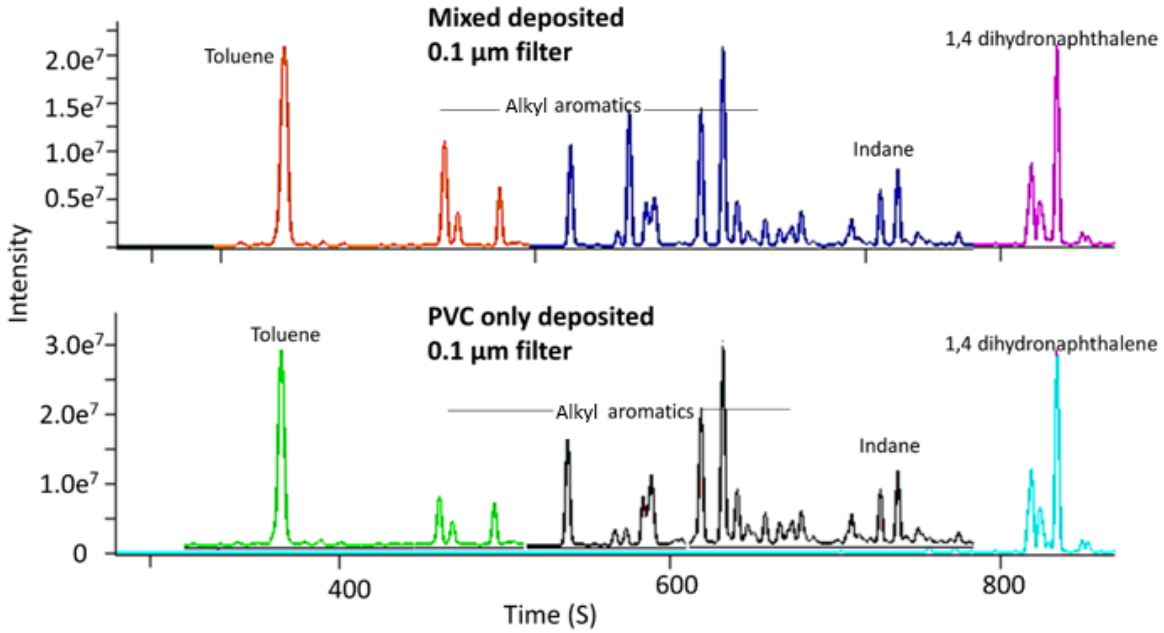

Figure 2.7. Comparison of extracted ions (91, 117, 130 m/z) for PVC from sample deposited with only PVC (bottom) particles and a sample deposited with a mix of plastics particles (PP, PS, PVC), (above) deposited on 0.1 µm. Adapted from Sullivan et al., 2020.

2.3.5. Polypropylene thermal decomposition

A repeating pattern of branched alkenes is noticeable for PP throughout the chromatogram (Figure 2.8). This is most likely the result of the polymer's backbone randomly and thermally breaking, which shows a homologous pattern[145]. In paragraph 2.3.2 it was verified that PP degrades above 400 °C into a large number of aliphatic compounds, the majority of which are branched and unsaturated hydrocarbons raging from C11 to C31. Some researchers have conducted studies on pyrolysis of PP and different chemical compositions have been obtained. The depolymerization reaction leading to the production of monomer (25%) is not the most important degradation reaction. The transfer reactions predominate and generate

the following products: 2,4-dimethyl-1-heptene (27–32%), pentane (ca. 8%), 2,4,6,8-tetramethyl-1-hendecene (7–18%) and 2,4,6-trimethyl-1-nonene (4–10%)[218].

In this experiment, the products 2,4,6-trimethyl-1-nonene and 2,4,6,8-tetramethyl-1-decene were identified. Both products belong to the class of organic compounds known as unsaturated aliphatic hydrocarbons[219]. These are aliphatic hydrocarbons that contain one or more unsaturated carbon atoms. The suggested process is a radical chain mechanism that is started by the polymer randomly splitting into primary radicals (Figure 2.6(1)). Propagation reactions progress with either beta (β) scission of the primary radicals to produce secondary radicals and ethane, or through cyclic intermolecular hydrogen transfer of the primary radicals. Intramolecular hydrogen transfer advances with another β scission generating predominantly alkenes. The chemistry of thermal hydrocarbon cracking and free radical production includes β scission as a significant reaction. The breaking of the carbon-carbon bond produces free radicals. Free radicals have a high reactivity and short lifetime. An olefin (ethylene) and a primary free radical with two fewer carbon atoms are produced when a free radical in a polymer chain undergoes a β scission, which separates two carbons from the charged carbon. At higher temperatures, more scissions lead to more primary radicals that can react with each other to form alkanes (termination reaction)[145].

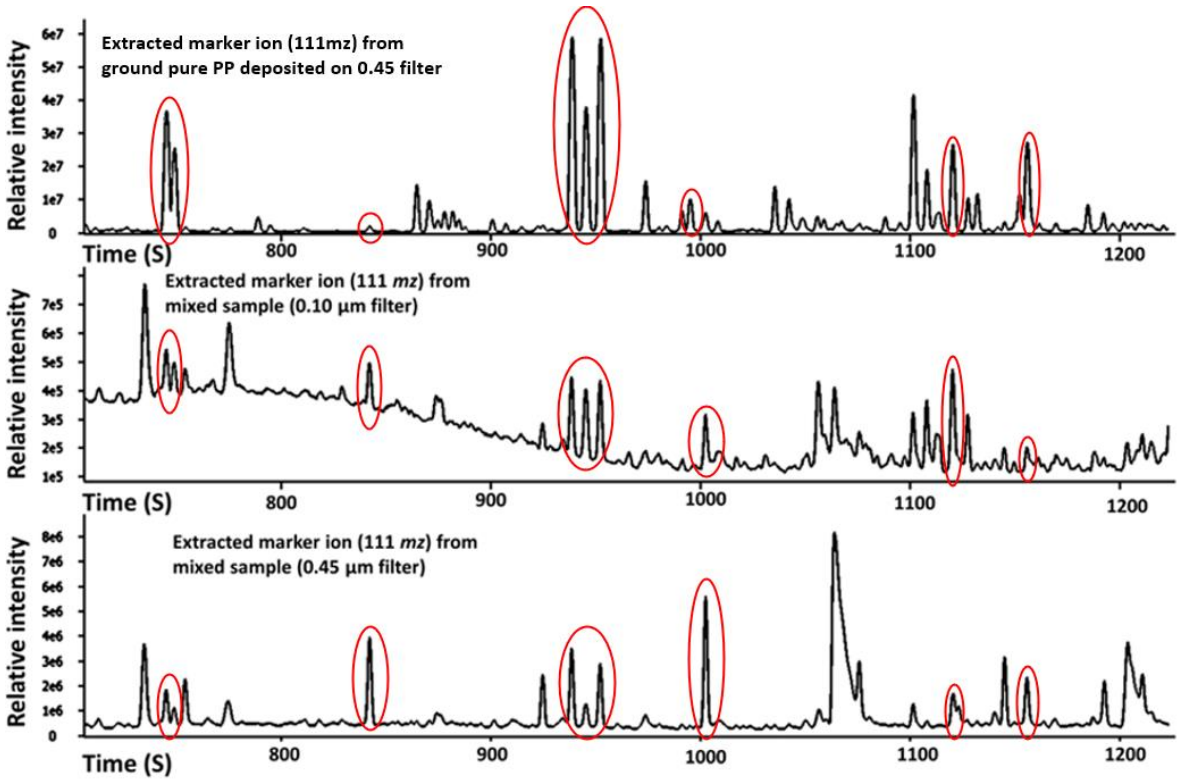

Figure 2.8. Comparison of PP ions from sample filtered with only PP (top), with sample containing a mix of plastics (PP, PS, PVC), filtered using 0.10 µm filter (middle) and sample containing a mix of plastics filtered using 0.45 µm (bottom). The chromatogram from the filter containing mixed plastic aligns neatly with the filter containing only PP. Retention, is therefore a good verification parameter for PP. Although peak intensity varies, this is directly linked to the amount of material deposited on the filter (PP deposited only having the greatest intensity, as more PP is present). Adapted from Sullivan et al., 2020.

2.3.6. Polystyrene thermal decomposition

Similar to PP, the thermal degradation of PS proceeds according to a conventional radical chain initiated mechanism, with the main mechanisms being initiation, propagation, and termination reactions[146]. For PS, the initiation reactions form radicals after the rupture of a C-C bond in the polymer and it can take place through either a random scission of the polymer chain, forming one primary radical (carbon adjacent to the benzyl group) and one secondary benzyl radical (carbon directly bonded to the benzene functional group) (Figure 2.6(2)) or through chain-end scission to form a benzyl radical as before, and a stabilized allyl benzyl radical. The propagation then consists of H-abstractions and β scissions. As explained in the previous paragraph, β scission is an important reaction in the chemistry of thermal cracking of hydrocarbons and the formation of free radicals. There are two forms of H-abstractions: intramolecular abstractions, in which primary radicals from random scission and chain end scission react to generate another molecule and radical, and intermolecular

abstractions, in which radicals abstract H from other molecules. The termination proceeds under second-order kinetics as either recombination or disproportionation reactions of radicals to form molecules.

In practice the thermal degradation of PS predominantly generates the monomer styrene (60-80 %) and to a lesser degree, aromatics, light hydrocarbons, alkyl aromatics and dimers and trimers (all below <10 %)[146]. More specifically, the main products obtained from the thermal degradation of PS have been reported to be single aromatic species (styrene ca. 70 wt.%, α-methyl styrene, toluene) and double aromatic species (1,3-diphenylpropane and 1,3-diphenylbutene)[220]. Therefore, not surprisingly, styrene being the most predominant due to the polymer being comprised of polymerized styrene monomers. However, a similarity between PS and PVC is the fact that they both contain toluene and styrene, but a distinguishing feature of PS, is the peak ion ratio of styrene to toluene is around >40 :1 and PVC has a peak ion ratio of toluene to styrene of 100 :1 with toluene peak at significant abundance (Figure 2.9). Notably with PS, is the increase in single ring aromatic compounds such as 1,2,3-trimethyl-benzene and 3-butenyl-benzene, each as a result of scission the PS polymer and rearrangements of side groups. Towards the later end of the chromatograms, PS degradation compounds have increased molecular mass and it is apparent these are larger units of the polymer such as stilbene, which appears to be a dimer of styrene (Figure 2.10).

A number of markers (ions) were identified for PVC, PS and PP and are listed in Table 2.1. These plastics markers were identifiable on 0.45 µm and 0.1 µm filters, putting the detection of cross-sectional area to as low as a 100 nm.

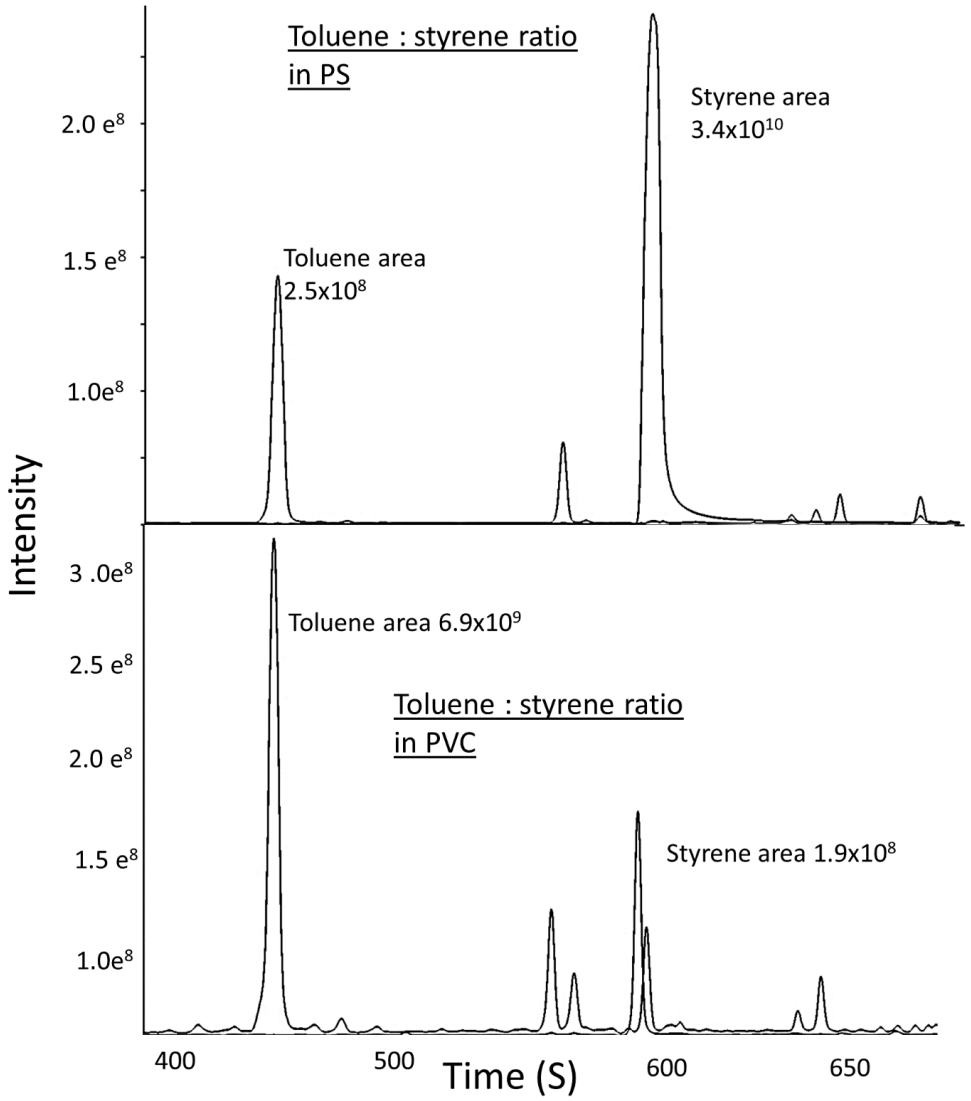

Figure 2.9. Image of the ions ratio of 104 mz (styrene): 91 mz (toluene), in PS (top) and PVC (bottom). PS contributes to significantly more towards styrene compared to PVC, whose main contribution is toluene. Adapted from Sullivan et al., 2020.

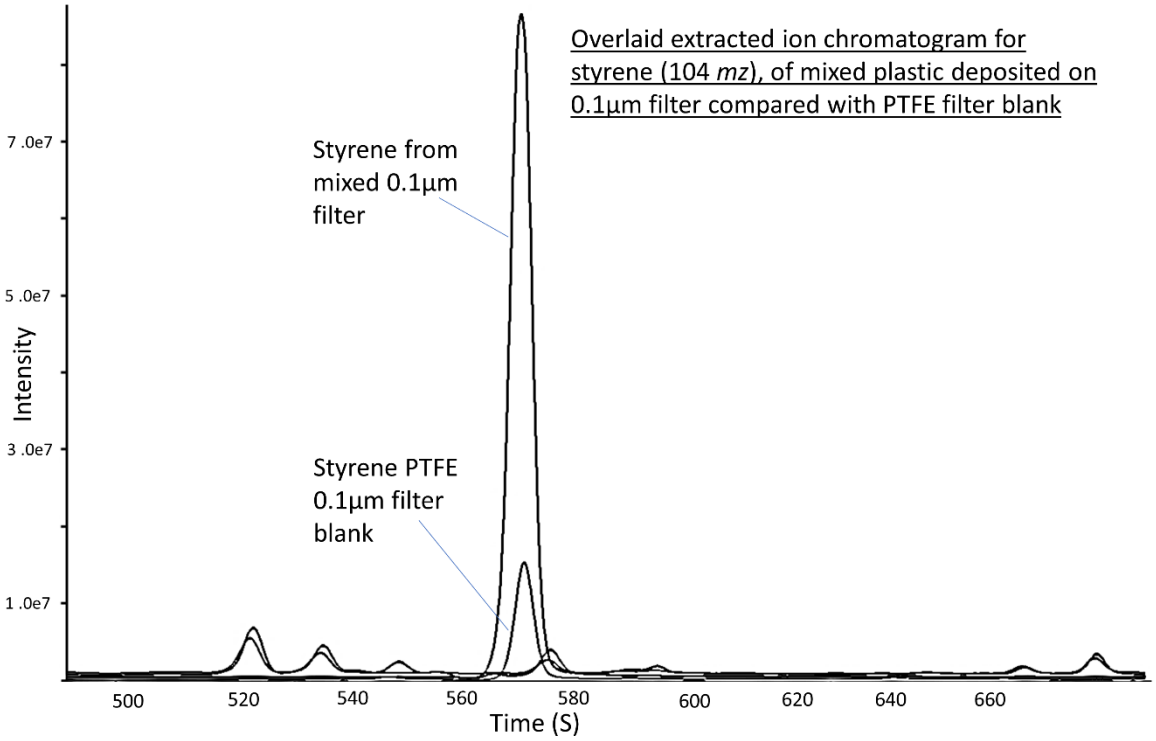

Figure 2.10. Image of the detection of styrene from plastic mixture deposited on 0.1 µm PTFE filter. Styrene peak (104 mz) is significantly greater in abundance compared to the process PTFE filter blank. Adapted from Sullivan et al., 2020.

Table 2.1. List of the compounds and marker ions for PVC, PP and PS plastics. Retention times and mz for each marker ion are also facilitated. It can be observed that some of the plastics share some of the marker ions. Nevertheless, that is not an impediment for identification. Adapted from Sullivan et al., 2020.

Sample	Compound identified	Retention time S^{-1}	*mz* marker ion.
PVC	**Toluene**	437	**91**
	Ethyl benzene	534	91
	Styrene	565	104
	Indane	714	**117**
	Indene	722	116
	1,4 dihydronaphthalene	834	**130**
	Naphthalene	852	**128**
	1-Methyl-naphthalene	945-960	**142**
	Biphenyl	1009	154
PP	**7-Methyl-decene**	706	**111**, 97
	3- Dodecane	709	**111**, 97
	2,4-Dimethyl-1-decene	711	**111**, 97
	5-Methyl-undecene	745	**111**, 97
	7-Methyl-1-undecene	788	**111**, 97
	7-Methyl-2-decene	864	**111**, 97
	1-Tridecene	924	**111**, 97
	2,6,8-Trimethyl-octene	1101	**111**, 97
	2,4,6-Trimethyl-nonene	1120	**111**, 97
	2,4,6,8-tetramethyl-1-decene	1244	**111**, 97
PS	Toluene	441	91
	Styrene	561	**104**
	1-Ethyl-2-methyl benzene	621	**117**
	1,2,3-Trimethyl-benzene	656	120, **105**
	2-Propenyl-benzene	697	**117, 91**
	3-Butenyl-benzene	716	132, **91**
	3-Phenyl-1-propyne	722	115
	1-Methylenepropyl-benzene	729	132, 117 ,91
	Bibenzyl	1112	182, 104, 91
	1,1'-(1-Methyl-1,2-ethanediyl)bis-Benzene	1138	105, 91
	Stilbene	1239	**180**, 165
	1,2-Dihydro-3-phenylnaphthalene	1311	191, 128, 91
	2,5-Diphenyl-1,5-hexadiene	1351	143, 130, 104, 91

2.3.7. Identification of microplastics in complex mixture through markers

Applying ion filters for PVC (91, 117, 128, 130, 142), PP (111, 97) and PS (91, 104, 105, 117, 180) on the software, individual MP types could be distinguished from a mixture that had been filtered using a 0.45 and 0.1 µm membrane. Each plastic could be identified by its respective PVC, PP, or PS markers, which could all be extracted from the chromatogram. This was confirmed by the comparison of samples of raw plastics that were previously run.

Figure 2.7 shows an example of PVC ions (91 *mz*) identified from a mixture of plastics deposited on 0.1 µm filter, while Figure 2.8 shows markers identified for PP in the mixture deposited on 0.45 µm filter and compared with raw PP for confirmation.

2.3.8. Semi-quantification of PVC and PS breakdown products

To determine the analytical limit of detection (LOD) and precision of the procedure, the samples prepared for semi-quantification were run in triplicate from randomised spots on the filters and processed in accordance with the marker ions for PVC and PS (Figure 2.11). By calculating the standard deviation of numerous blank samples (filter only and internal standards) and multiplying by a factor of three, the analytical LOD for PVC and PS marker ions was calculated, yielding values of 48.6 and 42.7 ng (per 10:1 mm shard), respectively (Tables 2.2 and 2.3).

Table 2.2. Analytical limit of detection (LOD) calculations for PVC. Information regarding intensity (of both the sample and internal standard), concentrations, means, standard deviation and limit of detection is facilitated.

PVC					
Ion Markers	**Mass-to-charge ratio (m/z)**	**Intensity sample 1**	**Intensity sample 2**	**Intensity sample 3**	**Mean Intensity**
Toluene	91	2.44E+09	1.25E+09	1.87E+09	1.85E+09
Naphthalene	128	6.74E+08	1.05E+08	1.87E+08	3.22E+08
Indene	116	3.07E+08	2.55E+08	6.48E+07	2.09E+08
1-Methyl-naphthalene	142	1.50E+08	1.42E+08	3.82E+07	1.10E+08
Biphenyl	154	2.45E+08	4.99E+07	2.81E+07	1.08E+08
Ion Markers	**Mass-to-charge ratio (m/z)**	**St Dev.**	**Intensity internal standard 1**	**Intensity internal standard 2**	**Intensity internal standard 3**
Toluene	91	4.85E+08	6.11E+07	6.11E+07	6.11E+07
Naphthalene	128	2.51E+08	6.11E+07	6.11E+07	6.11E+07
Indene	116	1.04E+08	6.11E+07	6.11E+07	6.11E+07
1-Methyl-naphthalene	142	5.09E+07	6.11E+07	6.11E+07	6.11E+07
Biphenyl	154	9.75E+07	6.11E+07	6.11E+07	6.11E+07
Ion Markers	**Mass-to-charge ratio (m/z)**	**Concentration 1 (ng)**	**Concentration 2 (ng)**	**Concentration 3 (ng)**	**Mean Concentration**
Toluene	91	3.99E+01	2.04E+01	3.06E+01	3.03E+01
Naphthalene	128	1.10E+01	1.72E+00	3.07E+00	5.28E+00
Indene	116	5.03E+00	4.18E+00	1.06E+00	3.42E+00
1-Methyl-naphthalene	142	2.45E+00	2.33E+00	6.26E-01	1.80E+00
Biphenyl	154	4.01E+00	8.18E-01	4.60E-01	1.76E+00
Ion Markers	**Mass-to-charge ratio (m/z)**	**St Dev. (±)**	**Limit of detection (LOD) (ng)**		
Toluene	91	7.95	23.84		
Naphthalene	128	4.11	12.34		
Indene	116	1.70	5.11		
1-Methyl-naphthalene	142	0.83	2.50	**Total LOD**	
Biphenyl	154	1.60	4.79	**48.59**	

Table 2.3. Analytical limit of detection (LOD) calculations for PS. Information regarding intensity (of both the sample and internal standard), concentrations, means, standard deviation and limit of detection is facilitated.

PS					
Ion Markers	**Mass-to-charge ratio (m/z)**	**Intensity sample 1**	**Intensity sample 2**	**Intensity sample 3**	**Mean intensity**
Styrene	104	8.46E+08	3.93E+08	1.17E+09	8.04E+08
1,2,3-Trimethyl-benzene	105	3.24E+07	4.56E+07	5.99E+07	4.59E+07
2-Propenyl-benzene	117	1.10E+07	2.02E+07	3.55E+07	2.22E+07
Stilbene	180	3.39E+06	1.48E+07	1.77E+07	1.20E+07
3-Butenyl-benzene	91	1.85E+09	7.26E+08	7.62E+08	1.11E+09
2,5-Diphenyl-1,5-hexadiene	91	7.32E+06	2.00E+06	2.32E+06	3.88E+06
Ion Markers	**Mass-to-charge ratio (m/z)**	**St Dev (±)**	**Intensity internal standard 1**	**Intensity internal standard 2**	**Intensity internal standard 3**
Styrene	104	3.19E+08	6.11E+07	6.11E+07	6.11E+07
1,2,3-Trimethyl-benzene	105	1.13E+07	6.11E+07	6.11E+07	6.11E+07
2-Propenyl-benzene	117	1.01E+07	6.11E+07	6.11E+07	6.11E+07
Stilbene	180	6.18E+06	6.11E+07	6.11E+07	6.11E+07
3-Butenyl-benzene	91	5.20E+08	6.11E+07	6.11E+07	6.11E+07
2,5-Diphenyl-1,5-hexadiene	91	2.43E+06	6.11E+07	6.11E+07	6.11E+07
Ion Markers	**Mass-to-charge ratio (m/z)**	**Concentration 1 (ng)**	**Concentration 2 (ng)**	**Concentration 3 (ng)**	**Mean Concentration**
Styrene	104	1.39E+01	6.44E+00	1.92E+01	1.32E+01
1,2,3-Trimethyl-benzene	105	5.30E-01	7.46E-01	9.81E-01	7.52E-01
2-Propenyl-benzene	117	1.80E-01	3.31E-01	5.81E-01	3.64E-01
Stilbene	180	5.55E-02	2.42E-01	2.90E-01	1.96E-01
3-Butenyl-benzene	91	3.02E+01	1.19E+01	1.25E+01	1.82E+01
2,5-Diphenyl-1,5-hexadiene	91	1.20E-01	3.28E-02	3.79E-02	6.35E-02
Ion Markers	**Mass-to-charge ratio (m/z)**	**St Dev (±)**	**Limit of detection (LOD) (ng)**		
Styrene	104	5.23	15.69		
1,2,3-Trimethyl-benzene	105	0.18	0.55		
2-Propenyl-benzene	117	0.17	0.50		
Stilbene	180	0.10	0.30		
3-Butenyl-benzene	91	8.51	25.52	**Total LOD**	
2,5-Diphenyl-1,5-hexadiene	91	0.04	0.12	**42.68**	

In order to back calculate the sample LOD value for PVC and PS for a 1 litre sample, all the known filtration process parameters, such as the filter's diameter (40 mm) and sample volume filtered (500 ml), are required. Once the total area of the membrane is calculated and divided by the area of the shard, we multiply by the LOD value previously obtained (48.6 ng for PVC and 42.7 ng for PS), divide by the volume filtered (500 ml). This result is divided by 1000 and gives the sample LOD values of 48.9 and 42.9 µg/l, respectively (see equation 2 for further clarification).

$$C = \frac{\left(\left(\frac{AF}{AS}\right) \times m\right)}{v}$$ Equation 2.

C is concentration of nano plastic material per volume of sample (ng/ml ~ µg/l)
AF is the area of the filter (mm^2)
AS is area of sample shard
M is mass calculated by semi-quantitation
V is volume of sample used in ml

Using this methodology, the semi-quantification of PVC and PS from the mixed sample on the 0.45 µm pore size filter determined an average mass for PVC markers 281.5 µg/l with a relative standard deviation (RSD) of 19.72% and 299.62 µg/l for PS with an RSD of 4.75% (Tables 2.4 and 2.5). The RSD, also known as the coefficient of variation, determines whether the standard deviation of a data set is small or large when compared to the mean. In other words, the relative standard deviation can provide with information about the accuracy of the average of the results and is often used as quality controls for quantitative laboratory assays. With RSD values obtained below 20%, the results are considered acceptable[221].
As before, in order to back calculate the sample average mass value for PVC and PS for a 1 litre sample, all the known filtration process parameters, such as the filter's diameter (40 mm) and sample volume filtered (500 ml), are required. Once the total area of the membrane is calculated and divided by the area of the shard, we multiply by the concentration value previously obtained (280.46 ng for PVC and 298.04 ng for PS), divide by the volume filtered (500 ml) and divided by 1000 (see equation 2 for further clarification). The RSD percentage for both MPs indicates that the analytical procedure is repeatable and that the MPs form a homogeneous layer on the PTFE filter, which is consistent with the images from the microscopy (Figure 2.2).

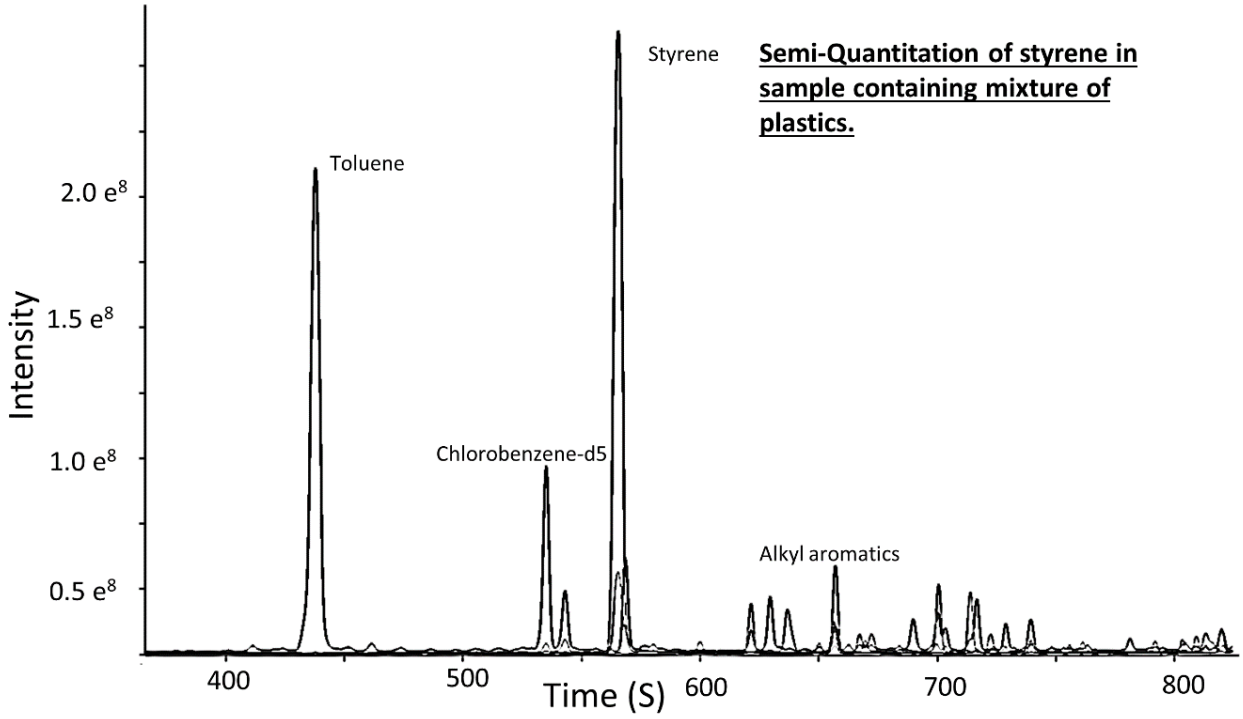

Figure 2.11. Example of semi-quantification of polystyrene from a sample containing a mixture of plastics. It is assumed that majority of toluene emerges from PVC and therefore ignored from styrene calculation, whist the main product from polystyrene degradation is styrene. Adapted from Sullivan et al., 2020.

Table 2.4. Concentration and relative standard deviation (RSD) for PVC on a mixed sample. Information regarding intensity (of both the sample and internal standard), concentrations, means, standard deviation and relative standard deviation is facilitated.

PVC					
Ion Markers	**Mass-to-charge ratio (m/z)**	**Intensity sample 1**	**Intensity sample 2**	**Intensity sample 3**	**Mean intensity**
Toluene	91	6.85E+09	1.18E+10	7.07E+09	8.57E+09
Naphthalene	128	5.18E+09	8.86E+09	5.84E+09	6.63E+09
Indene	116	1.25E+09	2.66E+09	1.33E+09	1.74E+09
1-Methyl-naphthalene	142	9.66E+08	3.02E+09	1.11E+09	1.70E+09
Biphenyl	154	1.12E+09	2.48E+09	1.32E+09	1.64E+09
Ion Markers	**Mass-to-charge ratio (m/z)**	**St Dev.**	**Intensity internal standard 1**	**Intensity internal standard 2**	**Intensity internal standard 3**
Toluene	91	2.28E+09	6.91E+07	8.12E+07	6.30E+07
Naphthalene	128	1.60E+09	6.91E+07	8.12E+07	6.30E+07
Indene	116	6.46E+08	6.91E+07	8.12E+07	6.30E+07
1-Methyl-naphthalene	142	9.35E+08	6.91E+07	8.12E+07	6.30E+07
Biphenyl	154	5.99E+08	6.91E+07	8.12E+07	6.30E+07
Ion Markers	**Mass-to-charge ratio (m/z)**	**Concentration 1 (ng)**	**Concentration 2 (ng)**	**Concentration 3 (ng)**	
Toluene	91	9.90E+01	1.45E+02	1.12E+02	
Naphthalene	128	7.50E+01	1.09E+02	9.26E+01	
Indene	116	1.80E+01	3.27E+01	2.11E+01	
1-Methyl-naphthalene	142	1.40E+01	3.72E+01	1.76E+01	
Biphenyl	154	1.62E+01	3.05E+01	2.09E+01	
	Totals	**2.22E+02**	**3.55E+02**	**2.64E+02**	
Ion Markers	**Mass-to-charge ratio (m/z)**	**Mean Concentration**	**St Dev. (±)**	**Relative St Dev (RSD) (%)**	
Toluene	91	1.19E+02	19.48	16.39	
Naphthalene	128	9.22E+01	13.92	15.09	
Indene	116	2.39E+01	6.33	26.43	
1-Methyl-naphthalene	142	2.29E+01	10.18	44.46	
Biphenyl	154	2.25E+01	5.96	26.46	
	Totals	**2.80E+02**	**55.31**	**19.72**	

Table 2.5. Concentration and relative standard deviation (RSD) for PS on a mixed sample. Information regarding intensity (of both the sample and internal standard), concentrations, means, standard deviation and relative standard deviation is facilitated.

PS					
Ion Markers	**Mass-to-charge ratio (m/z)**	**Intensity sample 1**	**Intensity sample 2**	**Intensity sample 3**	**Mean Intensity**
Styrene	104	1.13E+10	1.37E+10	1.24E+10	1.25E+10
1,2,3-Trimethyl-benzene	105	5.60E+08	4.53E+08	3.90E+08	4.67E+08
2-Propenyl-benzene	117	2.04E+09	1.10E+09	1.08E+09	1.41E+09
Stilbene	180	4.53E+08	2.32E+08	2.90E+08	3.25E+08
3-Butenyl-benzene	91	4.35E+09	9.68E+09	4.05E+09	6.02E+09
2,5-Diphenyl-1,5-hexadiene	91	6.24E+08	3.43E+08	6.22E+08	5.30E+08
Ion Markers	**Mass-to-charge ratio (m/z)**	**St Dev (±)**	**Intensity internal standard 1**	**Intensity internal standard 2**	**Intensity internal standard 3**
Styrene	104	9.85E+08	6.91E+07	8.12E+07	6.30E+07
1,2,3-Trimethyl-benzene	105	7.01E+07	6.91E+07	8.12E+07	6.30E+07
2-Propenyl-benzene	117	4.51E+08	6.91E+07	8.12E+07	6.30E+07
Stilbene	180	9.36E+07	6.91E+07	8.12E+07	6.30E+07
3-Butenyl-benzene	91	2.59E+09	6.91E+07	8.12E+07	6.30E+07
2,5-Diphenyl-1,5-hexadiene	91	1.32E+08	6.91E+07	8.12E+07	6.30E+07
Ion Markers	**Mass-to-charge ratio (m/z)**	**Concentration 1 (ng)**	**Concentration 2 (ng)**	**Concentration 3 (ng)**	
Styrene	104	1.64E+02	1.69E+02	1.97E+02	
1,2,3-Trimethyl-benzene	105	8.09E+00	5.57E+00	6.18E+00	
2-Propenyl-benzene	117	2.96E+01	1.36E+01	1.71E+01	
Stilbene	180	6.55E+00	2.85E+00	4.60E+00	
3-Butenyl-benzene	91	6.29E+01	1.19E+02	6.42E+01	
2,5-Diphenyl-1,5-hexadiene	91	9.03E+00	4.22E+00	9.87E+00	
	Totals	**2.80E+02**	**3.15E+02**	**2.99E+02**	
Ion Markers	**Mass-to-charge ratio (m/z)**	**Mean Concentration**	**St Dev (±)**	**Relative St Dev (RSD) (%)**	
Styrene	104	1.77E+02	14.65	43.96	
1,2,3-Trimethyl-benzene	105	6.62E+00	1.07	3.22	
2-Propenyl-benzene	117	2.01E+01	6.87	20.60	
Stilbene	180	4.67E+00	1.51	4.53	
3-Butenyl-benzene	91	8.21E+01	26.26	78.77	
2,5-Diphenyl-1,5-hexadiene	91	7.71E+00	2.49	7.46	
	Totals	**2.98E+02**	**14.17**	**4.75**	

2.3.9. Semi-Quantification of micro (nano)-plastics in river water

Following the same approach than in the previous paragraph and based on the same blanks/control samples of paragraph 2.3.8, it was possible to detect concentrations of PS in raw samples for a local river. Using a 0.45 m PTFE membrane, 200 mL samples of untreated river water from the river Tawe in South Wales at GPS coordinates 51.7265391, -3.8386937 were filtered before being dried, cut, spiked with an internal standard, and pyrolyzed following the previously described procedure. The 3 samples were analysed for the marker ions for PS and PVC. Multiple marker ions for PS (like styrene or 1,2,3-Trimethyl-benzene) were identified in the results (Figure 2.12 and Table 2.6), but markers for PVC were not detected (Table A-2.1 in Appendix A-2).

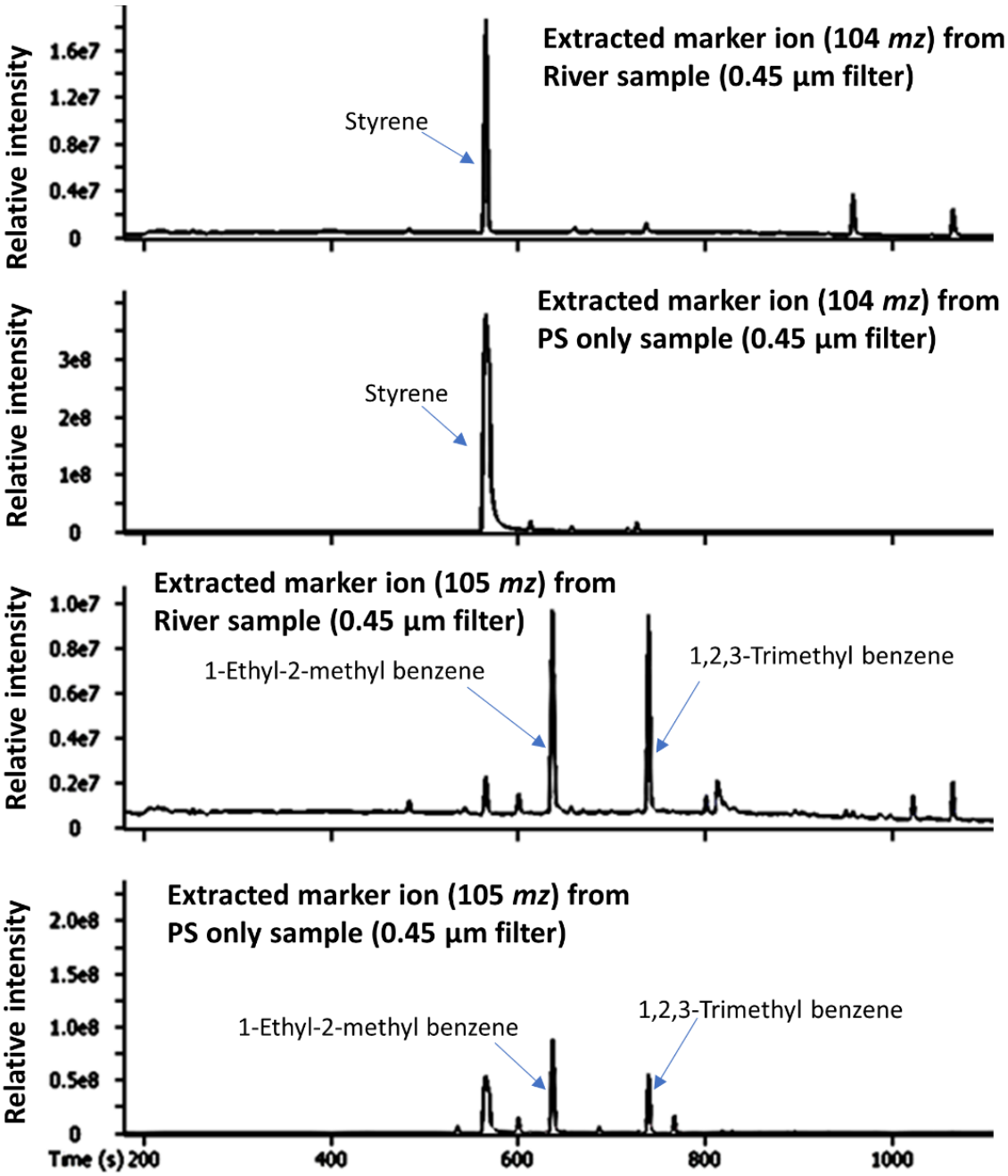

Figure 2.12. An example of the comparison of ion 104 and 105 mz from deposited PS on PTFE filter with filtered River Tawe sample. The ion 104 mz is associated with styrene and 105 mz for 1-ethyl-2-methyl benzene and 1,2,3-Trimethyl benzene, which are commonly found in polystyrene these have been identified in both samples. Adapted from Sullivan et al., 2020.

Table 2.6. Concentration and relative standard deviation (RSD) for PS on a river sample. Information regarding intensity (of both the sample and internal standard), concentrations, means, standard deviation and relative standard deviation is facilitated.

PS					
Ion Markers	**Mass-to-charge ratio (m/z)**	**Intensity sample 1**	**Intensity sample 2**	**Intensity sample 3**	**Mean intensity**
Styrene	104	2.81E+08	1.80E+08	1.72E+08	2.11E+08
1,2,3-Trimethyl-benzene	105	2.84E+09	4.73E+09	3.51E+09	3.70E+09
2-Propenyl-benzene	117	2.15E+08	3.96E+08	1.94E+08	2.68E+08
3-Butenyl-benzene	91	3.64E+08	1.05E+09	3.65E+08	5.93E+08
2,5-Diphenyl-1,5-hexadiene	91	1.01E+07	9.57E+06	9.35E+06	9.68E+06
Ion Markers	**Mass-to-charge ratio (m/z)**	**St Dev (±)**	**Intensity internal standard 1**	**Intensity internal standard 2**	**Intensity internal standard 3**
Styrene	104	4.94E+07	4.09E+07	7.75E+07	3.42E+07
1,2,3-Trimethyl-benzene	105	7.83E+08	4.09E+07	7.75E+07	3.42E+07
2-Propenyl-benzene	117	9.10E+07	4.09E+07	7.75E+07	3.42E+07
3-Butenyl-benzene	91	3.24E+08	4.09E+07	7.75E+07	3.42E+07
2,5-Diphenyl-1,5-hexadiene	91	3.16E+05	4.09E+07	7.75E+07	3.42E+07
Ion Markers	**Mass-to-charge ratio (m/z)**	**Concentration 1 (ng)**	**Concentration 2 (ng)**	**Concentration 3 (ng)**	
Styrene	104	6.85E+00	2.33E+00	5.02E+00	
1,2,3-Trimethyl-benzene	105	6.94E+01	6.11E+01	1.03E+02	
2-Propenyl-benzene	117	5.24E+00	5.11E+00	5.66E+00	
3-Butenyl-benzene	91	8.88E+00	1.36E+01	1.07E+01	
2,5-Diphenyl-1,5-hexadiene	91	2.47E-01	1.24E-01	2.74E-01	
	Totals	**90.61**	**82.21**	**124.38**	
Ion Markers	**Mass-to-charge ratio (m/z)**	**Mean Concentration**	**St Dev (±)**	**Relative St Dev (RSD) (%)**	
Styrene	104	4.73E+00	1.86	39.24	
1,2,3-Trimethyl-benzene	105	7.77E+01	18.01	23.16	
2-Propenyl-benzene	117	5.34E+00	0.23	4.38	
3-Butenyl-benzene	91	1.10E+01	1.93	17.46	
2,5-Diphenyl-1,5-hexadiene	91	2.15E-01	0.07	30.44	
	Totals	**9.91E+01**	**18.23**	**18.40**	

Once calculated, PS gave a semi-quantifiable result of 250.23 µg/L with an RSD of 18.4% for the repeated analysis. As before, in order to back calculate the sample average mass value for PS for a 1 litre sample, all the known filtration process parameters, such as the filter's diameter (40 mm) and sample volume filtered (in this case 200 ml), are required. Once the total area of the membrane is calculated and divided by the area of the shard, we multiply by the concentration value previously obtained (99.1 ng), divide by the volume filtered (in this case 200 ml) and divided by 1000 (see equation 2 for further clarification). With several markers being detected and a value over the LOD threshold of 48.9 g/L for PS markers, it is likely that PS micro (nano)-plastics have been identified using a real sample matrix. The river sample was carried out as a proof-of-concept test, and the positive outcomes indicate that this method is suitable for detecting low levels of MPs and NPs above 0.45 m in water samples with a complex matrix. These findings are in line with the and first and second objectives and also with the third hypothesis contemplated in the Introduction.

Even when the source of this pollution is unknown to the author of this thesis, this technique could allow its identification upstream by monitoring the river catchment taking samples in different locations. This system-scale approach could demonstrate the different composition of the pollutants along the river catchment. Not only the source of the contamination could be identified, but also information about spatial variation in plastic density, transport and polymer type could be determined, providing additional insights into the sources and sinks of plastic contamination.

As previously indicated, due to their interactions with chemicals in the environment, MPs and NPs are linked to a number of potential concerns for the health of both animals and people. It is impossible to disregard the presence of these micropollutants in rivers and water bodies, even at low concentrations, and appropriate methodology has been proposed to evaluate their wider environmental impact. Recently, the important hazardous risk that PS MPs and NPs pose to freshwater organisms in the tropic chain has been corroborated[222]. Using PS microbeads of 1 µm (considered borderline size between micro- and nanoplastic particles), and exposing in vivo several freshwater species to them (the rotifer Brachionus calyciflorus, the alga Raphidocelis subcapitata, , the crustacean Ceriodaphnia dubia and the benthic ostracod Heterocypris incongruens), it was demonstrated that reactive oxygen species (ROS) production and genetic material changes started to happen at concentrations in the order of µg /L, presumably as a result of inflammatory responses[222].

To summarise, this chapter validates the initial premises on which this part of the investigation is based. The effectiveness of membranes with different pore sizes (in this case PTFE membranes) as support for the deposition of MP's and NP's when incorporated to a glass filtration system has been demonstrated.

With regard to the limitations indicated on chapter 1, the requirement of large sample volumes or continuous filtration of liquid, due to the low concentrations of MPs and NPs in aqueous environmental samples[150], has certainly been avoided with the use of PY-GC/ToFMS given its unique detection capabilities. Samples of 200 ml were enough to give results as shown above.

The sample size of about 0.5 mg per run observed by other authors[150], has not been an impediment during the execution of this part of the project. The membrane shards of 10 mm x 1 mm dimensions kept the totality of the particles deposited after filtration and the whole shards were introduced in the glass cylinders and in the pyrolizer for analysis.

About the limitation due to the potential complexity of the samples and the requirement of preselection of single particles[150], the fact that a sample taken from a local river could be run straight away, without needing any pre-treatment, shows that PY-GC/ToFMS is a revolutionary approach for the detection of MPs and NPs in liquid samples and it does not present all the drawback experimented by previous investigators.

The use of inorganic/ceramic membranes was the next step of this project. Unfortunately, due to the fire that affected the university laboratory, the PY-GC/MS instrument that was planned to be used was left out of order and further analysis had to be put on standby until instrument recovery.

2.4. Highlights

Chapter 2 facilitates a summary of the use of thermal analysis approaches in the study of plastics and introduces a new methodology for the identification of MPs in aqueous samples using pyrolysis - gas chromatography – time of flight mass spectroscopy (Py-GCToF). It also lays the foundations of a new protocol for grinding up and filtrating methodology for MPs and NPs using membranes of a very small pore size, down to 100 nanometres.

- A solid and reliable approach for the identification of submicron particles with a cross sectional area down to 0.1 µm extracted from aqueous samples has been demonstrated by the deposition and analysis of MPs and NPs on PTFE membranes. MPs and NPs can be found in

complex aqueous samples at concentrations as low as 50 parts per billion thanks to the combined efforts of the higher sensitivity of Py-GCToF, the analytical tool utilized in this work.

- The use of PTFE membranes is due to the material's features, including its wide availability, low cost, and significant thermal resistance, which make it easy to apply this technology without complicated steps and with sample sizes as little as 500 ml.
- In less than an hour, the membranes holding the micropollutants can be prepared. It is possible to identify PS, PP, and PVC even when they are present in a combination thanks to the use of particular differential markers ions for plastics.
- With % RSD 20% for the PVC and PS, this analytical method's repeatability was good, which also suggests that the MPs were evenly applied on the membranes.
- The ability to detect PS on a membrane filtered with water from a nearby river proves that this technology is appropriate for the investigation of samples with complicated matrixes.

Most of the contents of this chapter were published by ScienceDirect/Elsevier in February 2020 in the article 'Detection of trace sub-micron (nano) plastics in water samples using pyrolysis-gas chromatography time of flight mass spectrometry (PY-GCToF)' [206] *of which the author of this thesis is co-first author. The preparation of the samples was fully conducted by the author of this thesis. Microscopy, STA and Py-GCToF analyses were carried out by the author of this thesis and Dr. Geraint Sullivan.*

Chapter 3: An investigation into the leaching of micro and nanoparticles and chemical pollutants from disposal facemasks - linked to the COVID-19 pandemic.

3.1. Introduction

Face mask use has increased significantly during the SARS CoV-2 pandemic in an unprecedented way to help control the transmission of this airborne viral disease[223], as recommended by the World Health Organisation (WHO)[224–226]. To meet the demand on a global scale, face coverings have experienced an upsurge in mass production. In order to safeguard just health care workers, the WHO estimated that an extra 89 million disposable plastic face masks (DPFMs) are needed each month[225,226]. With an estimated daily production of 200 million DPFMs, China is currently the world's leading producer and distributor of DPFMs[225], with up to a 1 billion DPFMs being used globally on a monthly basis[224]. This has resulted in a rise in the amount of DPFMs and clinical waste that is carelessly disposed on the streets and the environment and disposed of in landfills, with a significant fraction invariably ending up in waterways and the ocean[226]. The increase in DPFM waste is viewed as a new source of pollution that is directly related to the COVID-19 outbreak. The impact of the pollution brought on by DPFMs on the wider environment, however, is still largely unknown[192].

The majority of DPFMs are totally composed of plastic fibres[225,227], containing high percentages of polypropylene (PP) and polyethylene (PE), and other polymeric materials such as nylon and polystyrene[225–227] with novelty masks often coloured with dyes for customer appeal. The manufacturing of DPFMs often entails electrospinning micro and nanofibers fibres of plastic, into three layers[225,226]. Silica nanoparticles (SiNPs) may be used as filler in some production processes to improve the qualities of plastics, such as increasing the material's mechanical strength and toughness[228]. Additionally, Si compounds provide other benefits. Different compositions of SiO_2 hybrid sols have been proven suitable as precursors of high-quality fire-resistant coatings for textile materials[229]. In another study, the

antibacterial properties of silver nanoparticles attached to the surface of SiMPs have been demonstrated[230].

The fate of DPFMs in the environment and whether they leak pollutants such microscopic polymeric fibres, micro-crystalline silica, and other secondary pollutants, like leachable chemicals (dyes, surfactants and glues), are subjects of significant concern[225,226]. The effects of these contaminants on the ecosystem and whether they might go into the food chain is still subject to study, with little information available. Other components, like heavy inorganic metals are also linked to many of these chemical dyes[171], and are well known to negatively affect the environment and potentially human health. In the production of dyes, metals including antimony (Sb), copper (Cu), and chromium (Cr) are utilised as catalysts; occasionally, leftovers from these processes are discovered in textile materials as plastic additives[169,171]. Heavy metals including nickel (Ni), copper (Cu), and chromium (Cr) can also form complexes with some reactive dyes. These compounds may be incorporated into particles that are released from the masks and can be inhaled or absorbed through skin contact. These chemicals may dissolve in moisture droplets of sweat and saliva, which may serve as a vehicle for uptake into the body. There are documented risks connected with certain substances, especially heavy metals, ranging from mild allergic reactions, frequently from minimal exposure, to more serious health issues if repeated exposure happen, such as kidney disease, emphysema, cancer, and sometimes may be detrimental to unborn children during pregnancy[171,231].

Dye compounds themselves pose risk to environmental and public health[232]. Since many of them are organic compounds that can leach and dissolve in water, they can enter the water system and thus, the food chain. The majority of dyes are also chromophores, competing for light in the environment and decreasing aquatic plants' ability to photosynthesise, therefore disrupting the ecosystem[232]. Due to the polarity of these molecules, they are often difficult to remove by conventional water treatment methods, leading to their presence in drinking water. Since they are generally highly aromatic, the majority of these compounds have the potential to cause cancer and mutagenesis. Additionally, these dye molecules have the capacity to penetrate cells and crosslink with the DNA of those cells, impairing those cells' transcriptional activities. The majority of dyes are classified as persistent organic pollutants with the ability to bioaccumulate, which can have an impact on several trophic

levels, including entering human diet[232].

Not only chemical species but also the release of submicron particles from DPFMs are cause for concerns. Recent studies of MPs and NPs, which include polymeric fibres, showed that they have detrimental effects in animal models. MPs and NPs exhibit cytotoxic and genotoxic effects in terrestrial (including humans) and aquatic organisms[233–235]. Researchers have discovered that some MPs and NPs can be absorbed by the gut and then pass through the blood brain barrier[210,236] resulting in neurotoxic damage[237]. These particles often produce cellular damage by causing increased oxidative stress, as the particles are recognised by the organism as being foreign[237,238]. The emission of micro and nanofibers is of special importance. According to one study, fibres rather than spherical particles were shown to embed themselves more easily in tissues. This led to elevated superoxide dismutase levels in zebra fish gut tissue, an indication of oxidative stress and inflammation[238].

Additional to this, there is potential human health concern around the presence of micro silica particles (SiMP) between 1-10 µm and nano silica particles (SiNP) <1 µm, which is often used in manufacturing process of plastics[239,240]. Strong evidence exists that indicate the potential effects on human health of inhaling crystalline and amorphous silica particles. These nanosized silica particles can irritate the lungs and lead to silicosis, a lung fibrosis that can develop into emphysema and lung cancer[239–241]. SiMPs and SiNPs cause cell damage through oxidative stress, that leads to DNA damage, genotoxicity and cell death[240]. The toxicity of SiMP and SiNP is also evident in other tissues, where it causes cancer in bone and blood tissue and neurotoxicity in brain tissue[239,240,242]. However, SiMP and SiNP have less of an impact on the ecosystem and, if consumed, have only mildly harmful effects on terrestrial animals and aquatic organisms[243]. Nevertheless, the existence of these particles in DPFM's water leachates may be indicative of the ease of their discharge. Further questions may arise regarding their possible release when wearing facial protection, such as whether they might be easily inhaled or swallowed.

As this type of contamination also correlates with the main object of study of this thesis, that is, the fate of MPs and NPs in aqueous samples, it was decided to start a new investigation to clarify how DPFMs would behave once they enter the environment and the water bodies and try also to quantify the amount of MPs and NPS released from them.

One of the first limitations was the almost non-existent data on the effect of the pollution

caused by DPFMs on the wider environment.

The purpose of this research is to determine how inappropriate disposal of DPFMs affects the environment by formalising a workflow procedure to identify the different contaminants released or leached from DPFs under simulated environmental conditions (face mask gently agitated in deionised water). A diagram of this procedure can be observed below (Figure 3.1).

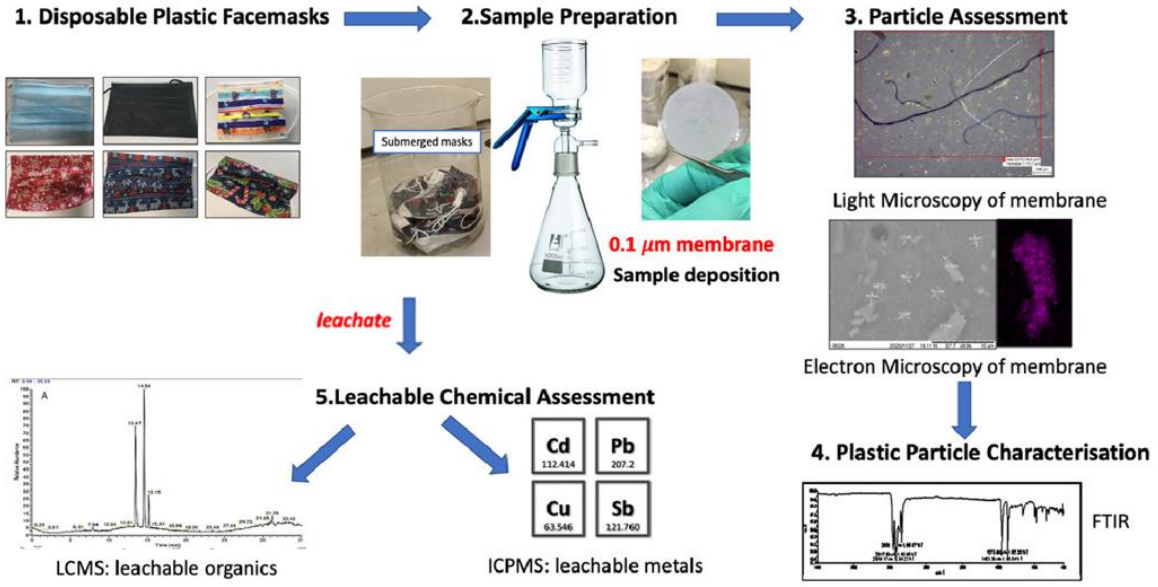

Figure 3.1 Diagram of the approach followed for this part of the investigation. The different DPFMs are submerged in deionised water to create two different types of samples: the leachates for ICP-MS and LC-MS analysis and the membranes with the deposited particles for microscopy and FTIR analysis.

3.2. Materials and Methods

This paragraph includes the consumables and instrumentation used in the investigation: 7 different DPFMs (some of them shown in Figure 3.2), numbered from 1 to 7 (including 7a, 7b, and 7c), were purchased from several manufacturers and suppliers as listed in Table 3.1, and contaminants extracted using deionised water dispensed from Milli Q® type 1 dispenser, procedural blanks were also prepared using the same deionised water source.

The term ‘reagent blank’ relates to the blank samples composed of deionised water only, directly obtained from the Milli Q® type 1 dispenser. The term ‘procedural blank’ relates to samples of deionised water that has been filtered through a membrane and analysed as the

rest of samples to identify any compound released from the membrane into the filtered water. For the leachates (ICP-MS and LC-MS samples) the term 'procedural blank' relates to samples of deionised water only that has been left in brand new beakers for 24 hours, as done with the samples, to analyse the release of any compounds from the beakers.

Whatman® Anodisc inorganic membranes of 0.1 µm pore size where purchased (Merck Group® UK) were used as membrane filters for particle deposition. A Glass vacuum manifold purchased from Sigma Aldrich®UK and vacuum pump Sparmax (The Airbrush Company Ltd, UK) was used to aid filtration of leachate. A brand new PURAIR P5-48 Nano (Air Science® Technologies Ltd) for particulates was employed to perform the filtering and overnight drying of the samples.

For microscopy analysis, a Zeiss Primotech light microscope (Carl Zeiss Ltd., Cambridge, UK) and TM3000 SEM electron microscope (Hitachi High-Technologies Corporation) was used for particle identification.

A Perkin Elmer® FTIR Frontier (UK) was used for chemical characterisation of solid materials (Figure A1.2 of Appendix A-1). A Perkin Elmer® ICP-MS NexIon 2000 metal leachate identification and quantification. A Dionex ultimate® (UK) 3000 was used for LCMS analysis of organic contaminates, these were tentatively identified using identification using Thermo LTQ Orbitrap XL accurate Mass spectrometer (Figure A1.3 of Appendix A-1). For chromatographic separation a reverse phase XBridge C18 column with dimensions: 3.5 µm x 2.1 mm x 150 mm and Guard column: XBridge C18 3.5 µm x 2.1 mm x 10 mm was used.

Figure 3.2. Images of the typical facemasks used in this investigation. Image 1 corresponds to mask 1; standard plain mask (similar to masks 3 and 6), image 2; Mask 2 (black colour), Image 4; mask 4 (novelty kids, similar to mask 5), Image 7a- c; masks 7a-c (festive masks).

Table 3.1. Information associated to the various DPFMs brands analysed in this study: the manufacturer, distributor, and supplier they were purchased from. The total number of masks used to obtain the samples is also facilitated. Adapted from Sullivan et al., 2021.

Sample	Description	Brand	Manufacturer	Distributor	Type	Supplier	Masks used for the filtration of fibres and particles	Masks used for analysis of leachate (IPC-MS and LC-MS)
Mask 1	Plain	NA	Huaxian Tiancheng Sanitary Material Co., Ltd	NA	NA	Amazon	3 batches of 10 masks (total of 3 samples)	1 mask per sample (total of 3 samples)
Mask 2	Black	PRO SFE	Shanghai Careus Medical Product Co., Ltd	Hunter Price International	NA	Poundland	3 batches of 10 masks (total of 3 samples)	1 mask per sample (total of 3 samples)
Mask 3	Plain children	PMS International	NA	NA	NA	CKs store	3 batches of 10 masks (total of 3 samples)	1 mask per sample (total of 3 samples)
Mask 4	Novelty children (paw patrol)	NA	Guangzhou Quantum Laser Intelligent Equipment co., Ltd	Sambro International Ltd.	Type I	Poundland	3 batches of 10 masks (total of 3 samples)	1 mask per sample (total of 3 samples)
Mask 5	Plain	TLS	Toiletry Sales Ltd	Toiletry Sales Ltd	Type IIR	Sainsbury	3 batches of 10 masks (total of 3 samples)	1 mask per sample (total of 3 samples)
Mask 6	Plain	CGM-3PLY	Foshan Suncare Medical Products Co., Ltd	Teucer (UK) Ltd	NA	Tesco	3 batches of 10 masks (total of 3 samples)	1 mask per sample (total of 3 samples)
Mask 7a	Festive Red	NA	Shanghai Ogo Medical Instrument Co., Ltd	Sambro International Ltd.	Type I	Poundland	3 batches of 10 masks (total of 3 samples)	1 mask per sample (total of 3 samples)
Mask 7b	Festive blue						3 batches of 10 masks (total of 3 samples)	1 mask per sample (total of 3 samples)
Mask 7c	Festive green						3 batches of 10 masks (total of 3 samples)	1 mask per sample (total of 3 samples)

3.2.1. Methodology

3.2.1.1. Leaching and filtration of particles

It is important to explain and distinguish the different methodology followed for the filtration of fibres and particles from the approach applied to obtain the leachate for LC-MS and ICP-MS analysis.

For fibres and particle analysis, in order to prepare 3 different samples for each brand, three sets of 10 masks of the same brand were placed into brand new glass beakers, submerged into 1.5 L of deionized water and gently stirred for 4 hours to ensure that all of the DPFMs were completely covered by the water. Following submersion, the eluent was filtered under vacuum using an Al_2O_3 membrane filter with a pore size of 0.1 µm. Once completed, the membranes were then placed on glass petri dishes and dried for two hours at 50 °C inside a drying cabinet. Each batch also included the running of procedural blanks, which required passing 1.5 L of deionized water through the membranes and then drying for two hours at 50 °C. The filtration process was carried out using a glass vacuum filtration funnel and receiving flask with samples drawn through under negative pressure. The whole procedure was carried out under a fume hood to avoid external contamination of samples. When stirring wasn't occurring, the beakers were covered with aluminium foil that had been washed with ethanol and completely dried afterwards.

To obtain the leachate samples for LC-MS and ICP-MS investigation, one mask of each brand was placed in brand new glass flasks containing 250 mL of deionised water and left submerged for 24 hours typical of leachate analysis in environmental laboratories. These flasks were also covered with aluminium foil that had been previously washed with ethanol and completely dried after washing.

In order to avoid contamination from clothes or lab coats, nitrile gloves were placed covering the sleeves and elastic bands were used to make sure no fibres were released.

3.2.1.2. Microscopy

Using a Zeiss Primotech microscope, light microscopy of the membranes was performed to assess the coverage of particle contamination (Carl Zeiss Ltd., Cambridge, UK) at 5 x, 10 x and 50 x magnification.

For scanning electronic microscopy (SEM) and energy-dispersive X-ray spectroscopy (EDS)

analysis, a Tabletop Microscope TM3000 was utilized (Hitachi High-Technologies Corporation), samples were mounted on carbon tape and placed in vacuums chamber prior.

3.2.1.3. FTIR characterisation of DPFMs and Membrane

Surface characterisation was carried out using a Perkin Elmer FTIR Frontier for rapid solid sample analysis Solid material placed over crystal housing and pressed down using the gauge with a force of 30 (arbitrary units). Scanning was between 650-4000 cm^{-1}, with 4 accumulations, to get an average spectrum. This apparatus utilises attenuated total reflectance (ATR), as discussed paragraph 1.2.4 of the introduction, one of the most frequently employed sampling methods nowadays. The Perkin Elmer FTIR Frontier also incorporates a diamond crystal.

3.2.1.4. ICP-MS elemental analysis

As stated in 3.2.1.1, a mask for each brand of DPFM were introduced in brand new glass flasks and submerged for 24 hours in 250 mL of deionized water after covering them with clean aluminium foil, as is customary for leachate investigation in environmental laboratories. For ICP-MS analysis, the leachate was subsampled afterwards and acidified with 1 mL of 1 M nitric acid and conducted to a standard elemental analysis on a Perkin Elmer ICP-MS NexIon 2000. A procedural blank (deionised water passed through membrane) and reagent blank (deionised water only) was run with samples to check for background interference. As stated before, the term ‘procedural blank’ relates to samples of deionised water only that have been left in brand new flasks for 24 hours, as done with the samples, to analyse the release of any compounds from the glass flasks. These two types of blanks, reagent and procedural, were run after highest calibration and after every sample to check for carryover and were also treated in the same conditions as the samples.

In order to represent all the analytes in the sample, multielement calibration standards were made up from PerkinElmer Pure single and multielement standards and diluted into 10% HNO3. Concentration range of 0 µg/L to 100 µg/L was preformed and standard curve required regression statistics above 0.9995 to be deemed acceptable, samples exceeding 100 µg/L were diluted accordingly to bring into dynamic range. Quality control samples prepared from separate batch of multielement standards and prepared at 50% of calibration range (10

µg/L or 10ppb and 5 µg/L or 5ppb for Hg), acceptance criteria for accuracy and precision were deemed acceptable below 15%. The calibration standards were prepared from a 1000ppm mixed standard and were manufactured and tested under ISO 17034 and ISO 17025 guidelines. The calibration curves for each element can be found in Figures A-3.9 to Figure A-3.21 of Appendix A-3.

Instrument parameters as follows: plasma gas flow set at 18 L/minute of argon, auxiliary gas flow set at 1.8 L /minute and nebuliser flow rate of set at 0.98 L/minute. Sample uptake was set at 300 µL/minute with 3 replicates per sample, the RF voltage was set a 1600 W.

3.2.1.5. LC-UV and LC-MS accurate mass of leachate[1]

For these experiments, no sample preparation, concentration or dilution was undertaken, all samples were analysed as submitted. The samples were kept in the freezer until time to be studied, then defrosted and an aliquot pipetted into a glass autosampler vial for examination. The analysis of a subsample of the leachate described in 3.2.1.4 for organic compounds was carried out by direct injection (5 µL) on LC-UV for initial sample contamination screening and LC-MS for compound identification. HPLC conditions were developed on the Agilent 1100 and transferred to the Dionex Ultimate 3000 LC on the Orbitrap MS with a slight reduction in flow rate (200µl/min reduced to 150µl/min) to optimise ionisation. A Waters XBridge C18 column: 3.5 µm x 2.1 mm x 150 mm and Guard column: XBridge C18 3.5 µm x 2.1 mm x 10 mm was used for analyte separation for both systems and used a Flow rate 200µl/min for LC/UV; 150µl/min for LC/MS. The composition of mobile phase A was 0.1% Formic acid, 2% (Acetonitrile) MeCN in (Water) H_2O and mobile phase B 0.1% Formic acid in MeCN for both instrument set-ups. The elution gradient started at 2 % B and increased to 90 % at 32 minutes before returning to 2% B ending with a total run time of 37 minutes. The gradient is standard for unknown samples, which these were, as it extends from low to high organic phase over a reasonably shallow linear gradient. The experiment was started at a low %B (2% in this case), hold it at this value for 2 mins so that all the salts and buffers in the samples that won't interact with the C_{18} stationary phase are eluted, then increase the organic solvent proportion over a period of 28 mins (2 - 30 mins) from 2 to 90% to elute the samples according to their partition with the stationary phase, with all being eluted by 90%B. This is

[1] Additional LC-UV and LC-MS information can be found in Appendix A-3.

then held at 90% for 2 mins to ensure elution of any particularly retentive components, then returned to 2% and allowed to equilibrate for a few minutes ready for the next run. The column was at RT (no column oven) and ramp rate just over 3.14 ^{o}C per minute.

For UV-VIS parameters the lamp was set at 254, 214 and 360 nm with bandwidth of 4, 16 and 32 nm respectively, compared to a reference cell set at 360 nm with bandwidth of 100 nm. The DAD spectrum operated at bandwidth of 190-700 with a refenced at bandwidth of 2 nm. Again, as these were unknown samples, it was operated at the different wavelengths to cover all the bases with the UV wavelengths monitored individually, as well as the whole UV-VIs range covered by the diode array detection. 254nm is the absorption wavelength for saturated or unsaturated hydrocarbons, especially pi-bonds, aryl compounds, etc. 214nm is an absorption wavelength for a variety of molecules, especially amino acids and peptides, and 360nm was included, but was used more as a reference than an informative wavelength in this case.

For analysis: reagent blanks (LC grade water) and procedural blanks (deionised water used in sample preparation) were run pre and post samples check background ions and potential carryover. A LC coumarin standard (an aromatic organic chemical compound) was also run pre and post sample analysis to verify the system suitability i.e. retention time drift, analyte response and peak profile for coumarin.

For MS parameters, the Dionex ultimate 3000 was connected in series to a Thermo LTQ Orbitrap XL with API ion spray source; sheath gas flow was set to 15 L/minute, auxiliary gas flow set at 2 L per minute, the probe was voltage was set at 4.3 kV with capillary and tube lens voltage of 43 and 150 V respectively. The MS scan conditions were full mass profile mode m/z 200-1000 with resolution of 60,000. LCMS was tuned and calibrated using infusion at low flow rate of tune mix, containing a mixture of caffeine, MRFA and ultra Mark (Cal mix) prior each analysis. A coumarin standard was also used to optimise parameters of LC flow rate. The reagent and procedural blanks were also run prior and post sample analysis to establish background of the system.

The analysis conditions for HPLC, UV-Vis / Diode Array and MS can be observed in Tables A-3.1, A-3.2 and A-3.3 in the Appendix A-3.

3.3. Results and discussion.

3.3.1. Mask and Filtrate characterisation: Microscopy and FTIR analysis[2]

Given their potential to leach dispersive contaminants into water, 9 different batches of DPFMs (from 7 brands) were examined (Table 3.1). The membranes from the filtration process were subsequently characterised using light microscopy, SEM-EDS microscopy and FTIR.

According to light microscopy, which was employed as an initial indicator of particle contamination, all nine batches of DPFMs (Mask 1 to 7c) released fibres which were believed to be PP and angular fragments that seemed crystalline and were likely composed of siliceous material. It appears that novelty children mask 4 and novelty festive masks 7a, 7b and 7c have significant fibre and particle contaminations. Images taken with a light microscope of samples 7 a to c reveal a variety of coloured fibres, indicating that some may have been stained with a dyeing agent. It also appears that the membrane filters have acquired a slight tarnish. This is true for Mask 2, although in less abundance than 4, 7 a-c, the fibres are predominantly black in line with physical mask appearance. Masks 1, 3, 5 and 6 appear to generate lower number of fibres, in comparison with 4, 7a, 7b and 7c, and are a mixture of clear and blue, which is also in line with overall appearance of the original masks (Figure 3.3).

These findings are in line with the fourth hypothesis contemplated in the introduction regarding DPFMs to be a new source of MPs. Even when the release of synthetic fibres and particles was expected, the high amount of released debris coming from some of the masks (e.g., mask 7b) was unpredicted. This way, it can be considered that DPFMs present indeed an additional cause of release of MPs into the environment when in contact with water. Further studies will be required in order to quantify and estimate the amount of fibres and particles released from each mask to better understand this new source of plastic pollution.

[2] Additional FTIR information can be found in Appendix A-3.

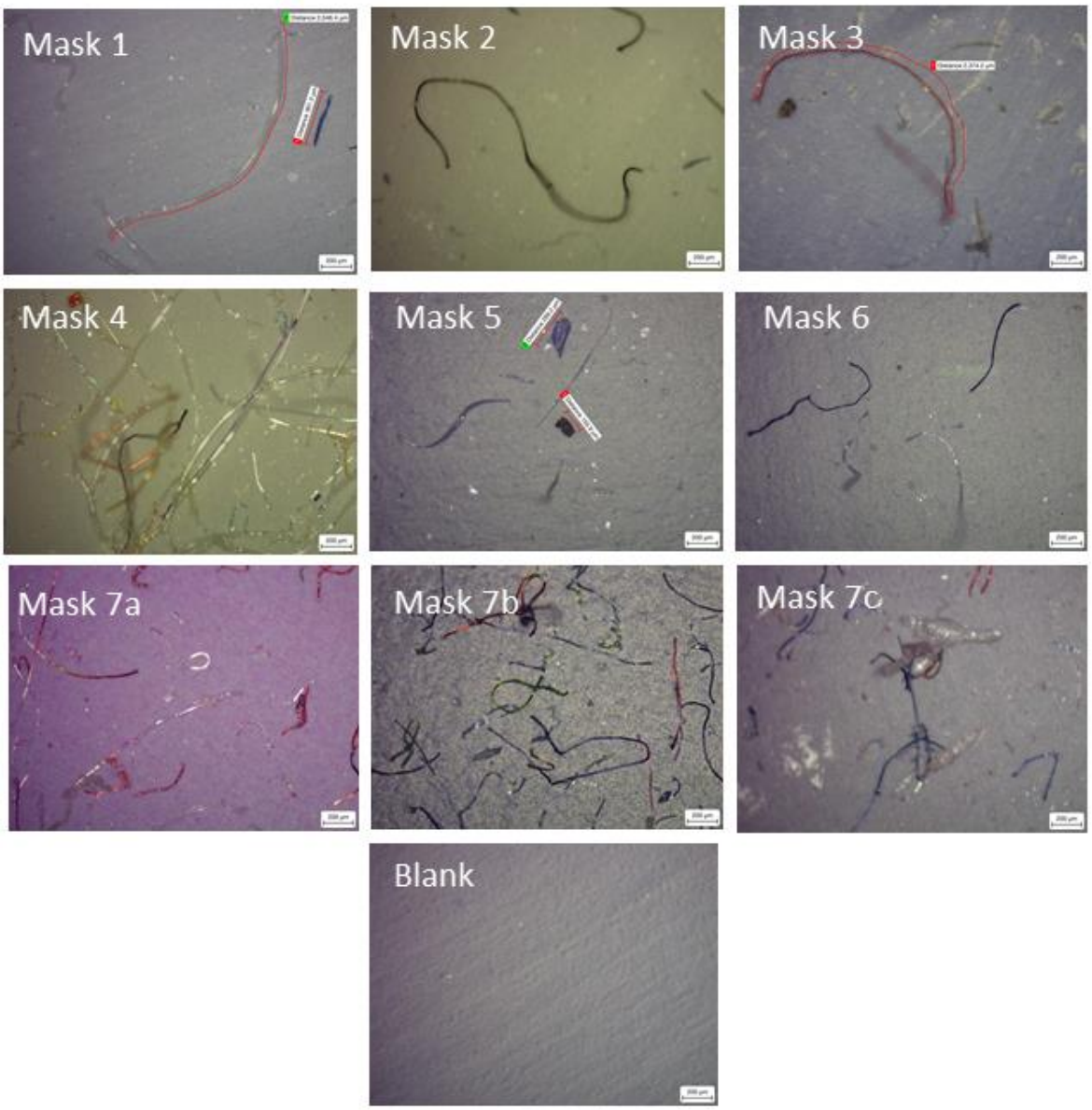

Figure 3.3. Light microscope images of the membrane filters post filtration of masks1-7c taken and blank membrane at 5 x magnification. Notably Mask 4 (paw patrol) and 7a-c (festive novelty) have what appears significant fibres and particle contamination.

The physical masks' FTIR examination reveals that they were predominantly made of PP, with some additional functionalization seen in the novelty masks (4, 7a, 7b and 7c), particularly on coloured sides. The main purpose of using FTIR was to corroborate that the different DPFMs were mainly composed of PP. Apart from the typical peaks for this synthetic material, some other peaks were detected in some DPFMs and subsequently analysed.

The white side presented spectrum indicative of PP, with absorbance peaks of 1375 cm^{-1},

1457 cm^{-1}, 2838 cm^{-1}, 2950 cm^{-1} and 2917 cm^{-1}. Most of these peaks are in the CH stretching group (Figure 3.4 and Table 3.2).

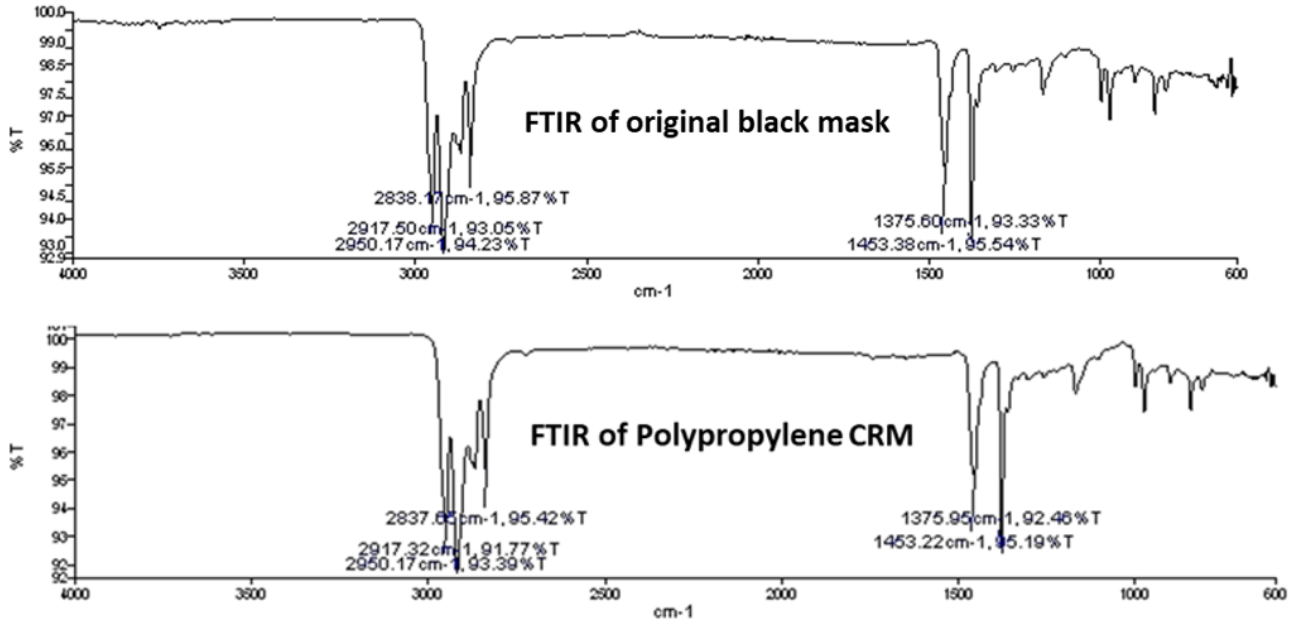

Figure 3.4. Example of FTIR spectrum comparing physical mask 2 (Black) with pure polypropylene. The absorbance peaks detected and their similarity can also be observed.

Covalent bond vibrations can be generated by radiation from the infrared (IR) region of the electromagnetic spectrum. Bonds stretch and bend due to the absorption of IR radiation. Stretches are equivalent to changes in the lengths of the bonds inside a molecule. Bends are the result of increases or decreases in the angle between bonds in a molecule. there are 3 vibrations: 2 stretches and 1 bend[244]. Traditionally, the CH stretching region has been defined as a range of wavenumbers that lies approximately between 2500 and 3400 cm-1 and consists primarily of fundamental transitions of the CH valence vibrational movements. Compared to the stretching vibrations of NH, OH, or SH that are also present in this interval, CH stretching bands are not prone to broadening by hydrogen bonding. Fundamental CH stretching energies are clearly distinguishable from other molecular vibrations and are well-separated from them in the spectra due to the strong relative strength of the CH bond and small hydrogen mass[245].

Back to the results, the coloured side showed primarily an absorption band at 1711 cm^{-1}, indicative of carboxylic acid or ketone functional (see Table 3.2). This is could possibly arise

from the side group of an acidic dye compound, polyamide used in synthesis of from nylon -66 and sometimes found in oxidised PP[246–248]. For Plain masks both blue and white side possessed peaks indicative of PP.

Table 3.2. Main FTIR absorbance peaks identified in the different DPFMs, along with the appearance, group, compound class and the samples they were found in.

FTIR main peaks	Appearance	Group	Compound Class	Sample
1095 cm-1	Strong	C-O stretching	Secondary alcohol	Mask 4, 7a, 7b, 7c
1242 cm-1	Strong	C-O stretching	Alkyl aryl ether	Mask 4, 7a, 7b, 7c
1375 cm-1	Medium	O-H bending	Phenol	Present in all samples
1457 cm-1	Medium	C-H bending	Alkane	Present in all samples
1711 cm-1	Strong	C=O stretching	Aliphatic ketone or carboxylic acid	Mask 4, 7a, 7b, 7c
2838 cm-1	Medium	C-H stretching	Alkane	Present in all samples
2950 cm-1	Medium	C-H stretching	Alkane	Present in all samples
2917 cm-1	Medium	C-H stretching	Alkane	Present in all samples

FTIR was also carried out on the membranes post filtration of all 9 batches; absorbance spectrum in line with main peaks of PP were identified on membranes from Mask 2, 3 and 7 a b c, further indicating that the fibres derived from the DPFMs are PP in composition. It was observed that, for some masks, less fibrous material was likely deposited on the surface of the membranes (i.e., masks 1, 5 and 6 were plain typical medical type masks as the detection of PP peaks were below the capabilities of the ATR-FTIR).

As like previous samples, masks 4, 7a, 7b and 7c presented additional peaks: 1711 cm^{-1} (carboxylic acid stretching), 1242 cm^{-1} (Alkyl aryl ether) and 1095 cm^{-1} (secondary alcohol stretch)[246,249]. They were also often seen as the primary peaks on the membranes post filtration, and are often common groups in dyes such as Eriochrome black and Congo red[249]. Since these membranes were often tarnished, it is likely that the inks or dyes used to manufacture the novelty designs are the source of these peaks.

3.3.2. SEM analysis[3]

A more in-depth analysis of the membrane filters was preformed using SEM-EDS. The size of the particles precipitated on the support were confirmed to be in the micro (1 <mm) and nano (submicron particle size 0.1–1 μm) range, with each mask releasing a significant amount of grain-sized particles measured between 360 nm - 500 μm on SEM, but likely to be even finer (limited by resolution of TM3000). These results confirm the fourth hypothesis regarding the use of ceramic membranes as a valid support for the samples analysed. Fibrous particles appeared to be in larger size range, often ranging from as little as 25 μm to several millimetres (2.5 mm). Fibres were found to be emitted from all masks in this study (Mask 1-7c). As previously mentioned in paragraph 3.2.1.1, great attention was put in place in order to avoid contamination from clothes or lab coats to make sure all the fibres and particles investigated came from the DPFMs in study. The results obtained are thought to be valid and in line with the purpose of this study. They also support the objectives and hypotheses contemplated in Chapter 1.

The elemental composition of the particles was further investigated with an EDS analysis employing back scattered electrons. It was observed that the fibrous particles had a high percentage of carbon and were probably generated from fibres of spun polypropylene. A high number of the grains contained high percentages of Si and oxygen and likely to be compositions of silica (Figure 3.5). However, some grains analysed (thought to be silica) were often high in carbon and likely even finer fragments of plastic (Figure 3.6).

The appearance of these particles was expected. As previously commented, SiNPs can be employed as filler in some manufacturing processes to enhance the properties of plastics, such as increasing the material's toughness and mechanical strength[228], also as a fire retardant[229] and is known for its antibacterial properties[230]. Nevertheless, as seen in the introduction of this chapter, strong evidence exists that indicate the potential effects on human health of inhaling crystalline and amorphous silica particles. If, apart from being released into the environment, there is a possibility of these particles entering the human body by breathing them while using DPFMs, there is then a direct exposure to this type of pollutants and further studies would be required to better comprehend this risk.

[3] Additional SEM information can be found in Appendix A-3.

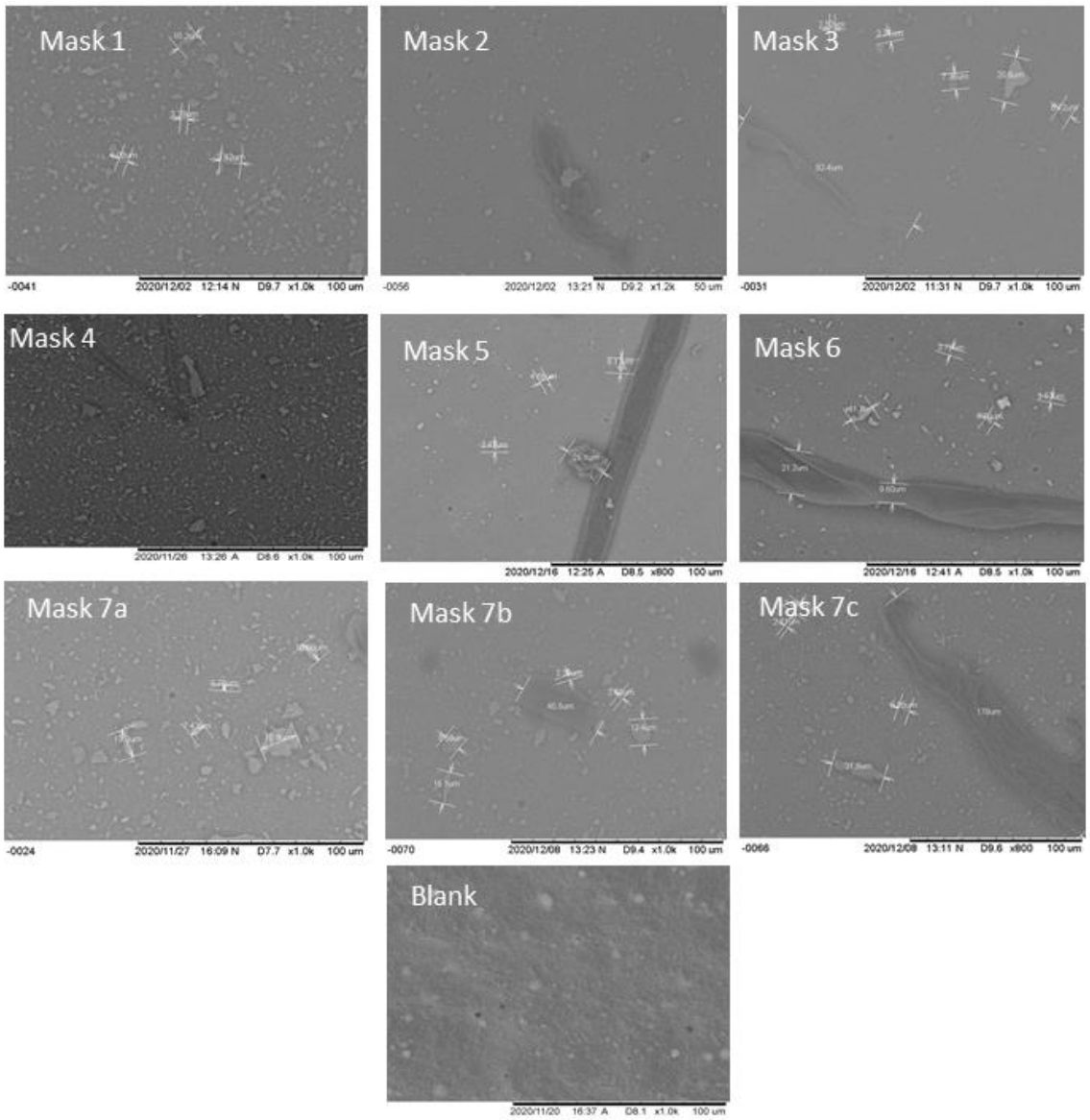

Figure 3.5. SEM images of fibres and particles from Mask 1-7C and blank membrane filter. Elemental compositions of fibres were found to be mainly carbon, whilst the small angular fragments found in all masks had high percentages of Silica and Oxygen.

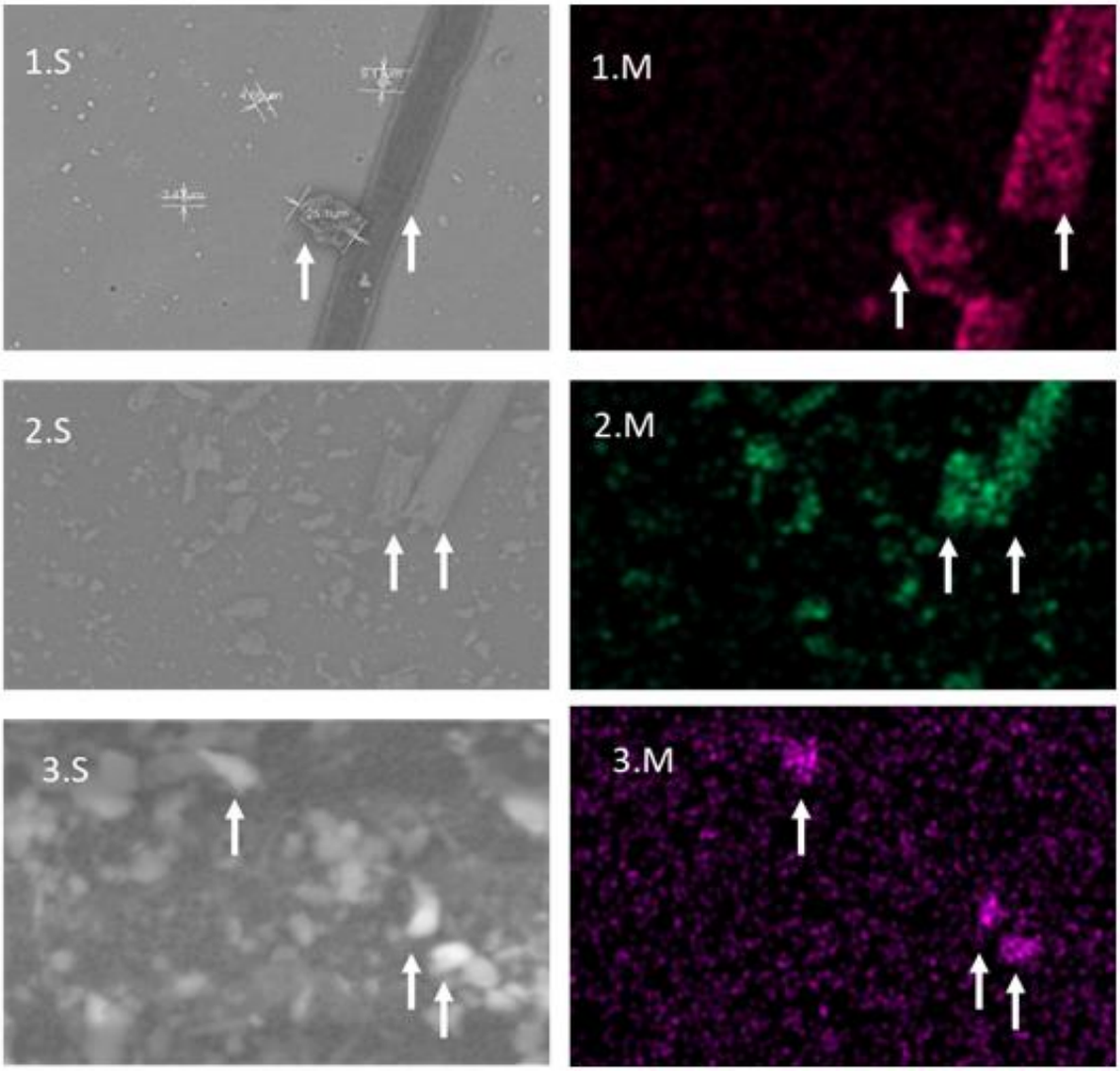

Figure 3.6. SEM images 1.S, 2.S and 3.S (masks 3, 7c and 4) and a corresponding elemental map (1.M, 2.M and 3M). 1.M coloured fuchsia representing carbon on a fibre and particle, 2.M is coloured green to represent silica on grains and 3.M is Purple indicating the presence of lead found on some of the grains.

Additionally, these particles frequently contained heavy metals, particularly in the novelty DPFMs such as masks 2, 4, 7a, 7b and 7c. Some heavy metals were located on grain particles as seen in masks child's novelty mask (4) and the festive masks (7 a, b, c) shown in Figures 3.7 and 3.8. They are most likely additives used in plastic manufacture. More EDS examples of the composition of particles and fibres found can be observed in Figures A-3.1 to A-3.4.

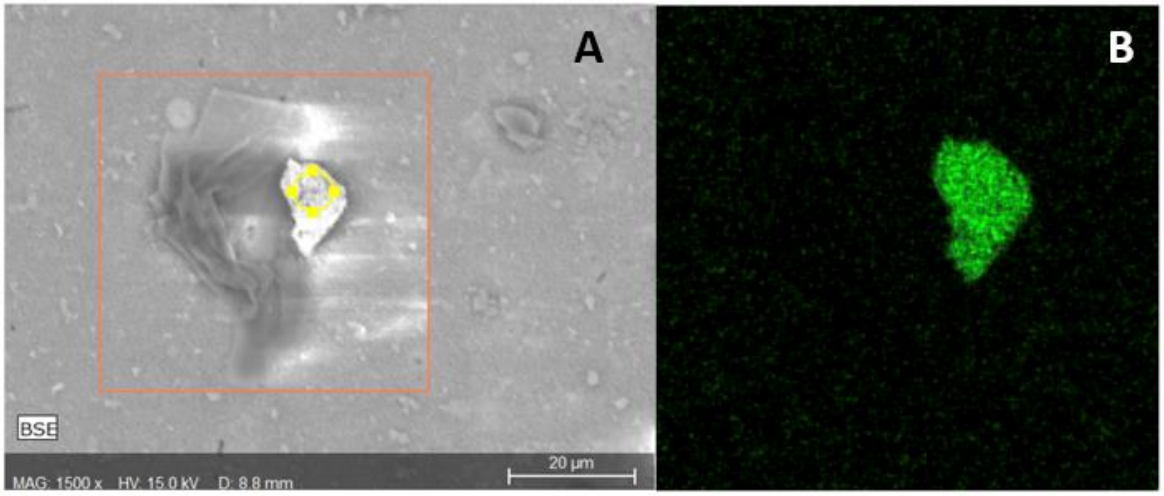

C

Spectrum: Point

Element	AN	Series	Net unn. C [wt.%]	norm. C [wt.%]	Atom. C [at.%]
Tin	50	L-series	1163	89.79	46.79	25.20
Cadmium	48	L-series	1010	70.60	36.79	20.92
Oxygen	8	K-series	62	18.38	9.58	38.26
Arsenic	33	L-series	74	7.61	3.97	3.38
Carbon	6	K-series	23	3.58	1.87	9.94
Silicon	14	K-series	41	1.93	1.00	2.28
Iron	26	K-series	0	0.00	0.00	0.00
Antimony	51	L-series	0	0.00	0.00	0.00
Lead	82	M-series	0	0.00	0.00	0.00
Copper	29	K-series	0	0.00	0.00	0.00
Zinc	30	K-series	0	0.00	0.00	0.00
Platinum	78	M-series	0	0.00	0.00	0.00
			Total:	191.90	100.00	100.00

D

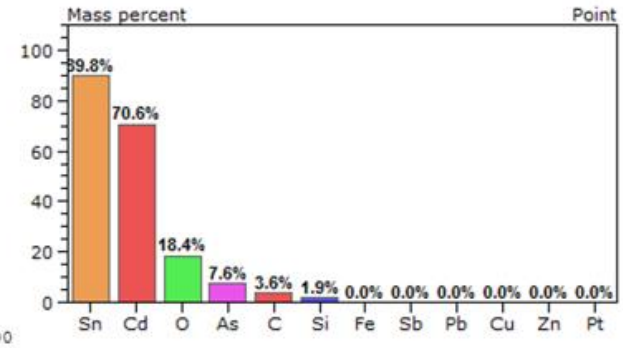

Figure 3.7. An example of EDS data referring to the composition of a grain particle found in Mask 4 (paw patrol). (A) is the image generated by the SEM at x1500, (B) is the false colour map for elemental Cd, (C) is tabulated elemental composition data and (D) shows the EDS data plotted graphically. It is noticeable the high concentration of Cd.

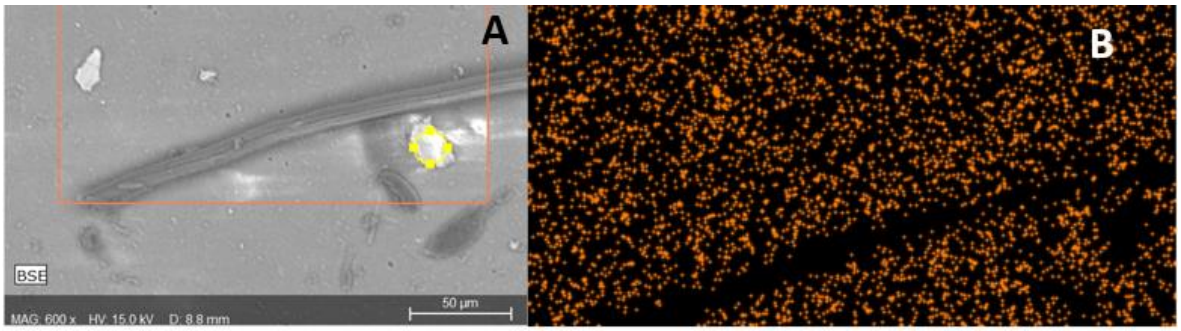

C

Spectrum: Point

Element	AN	Series	Net	unn. C [wt.%]	norm. C [wt.%]	Atom. C [at.%]
Arsenic	33	L-series	885	54.64	50.55	23.78
Iron	26	K-series	120	18.57	17.18	10.84
Carbon	6	K-series	36	14.66	13.56	39.79
Oxygen	8	K-series	59	11.03	10.20	22.48
Cadmium	48	L-series	124	8.67	8.02	2.52
Silicon	14	K-series	9	0.51	0.47	0.59
Antimony	51	L-series	0	0.00	0.00	0.00
Tin	50	L-series	0	0.00	0.00	0.00
Lead	82	M-series	0	0.00	0.00	0.00
Copper	29	K-series	0	0.00	0.00	0.00
Zinc	30	K-series	0	0.00	0.00	0.00
Platinum	78	M-series	0	0.00	0.00	0.00
			Total:	108.09	100.00	100.00

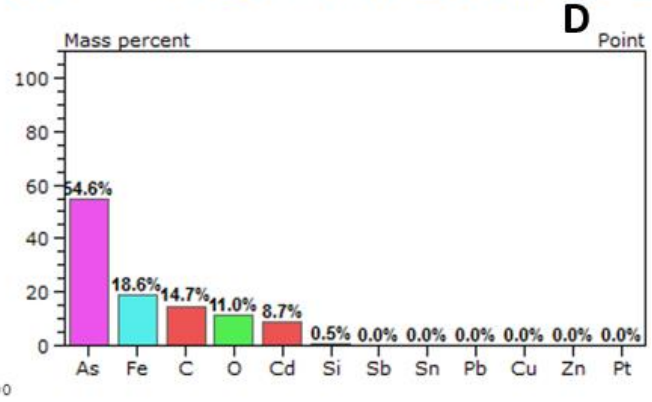

Figure 3.8. An example of EDS data referring to the composition of a grain particle found in Mask 7a. (A) is the image generated by the SEM at x600, (B) is the false colour map for elemental Si, (C) is tabulated elemental composition data and (D) shows the EDS data plotted graphically. It is noticeable the high concentration of As.

As pointed out in paragraph 1.3, metals like Fe, Cd, Cu, Ni, Sb, Cr, Mg, Zn, and Al in different concentrations have been proven to be released from diverse type of textile samples[171,181]. Some others high-risk contaminants like Pb are known to be amply used in the textile industry as components of dyestuffs[182]. As it was explained in the introduction of this chapter and in chapter 1, there are known dangers associated with some substances, especially heavy metals, ranging from mild allergic reactions, frequently from minimal exposure, to more serious health problems if exposure occurs repeatedly[171,231].

The environment and public health can be at risk from dye chemicals. Since many of them are organic substances, they can dissolve and leach into water, where they can then enter the water system and the food chain. Also, the majority of dyes are chromophores, competing with light in the environment and reducing the capacity of aquatic plants to engage in photosynthesis, which affects the ecology[232].

This fact connects with the third objective of this thesis, regarding the ascertain of the potential risk for ecosystems and human health and it also connects with the fourth

hypothesis of this thesis regarding DPFMs to be proven as a new source of MPs and NPs, chemicals and other pollutants.

In order to verify and measure the amount of heavy metals released from these DPFMs in study, it was decided that ICP-MS would be the best option to carry out the tests, following also the recommendations included in the European Regulation 1007/2011. The results are presented hereunder.

3.3.3. Leachable compounds: ICP-MS analysis[4]

According to EDS research, heavy metals were primarily linked to coloured novelty masks. It was therefore decided to conduct a heavy metal and organic compound leaching analysis (suspected organic dyes) on the coloured masks (DPFMs 2, 4, 7a, 7b and 7c).

Two plain standard masks type I and type II were employed for comparative tests, along with a blank control run using deionized water (the same used in the leaching method) (DPFMs 5, 6) to determine whether novelty and simple masks have any correlation. 7 DPFMs were selected in total, and they were all submerged for 24 hours in 250 mL of deionized water, as previously explained in paragraph 3.2.1.1.

To determine the quality of background interference coming from the deionizer and glassware, samples of reagent blank (deionized solely) and procedural blank (deionized water collected through filtration of unused membranes) were also prepared as previously explained in paragraph 3.2.1.5. The parameters listed in sections 3.2.1.4 and 3.2.1.5 were used to analyse a subsample of the leachate using ICP-MS and LC-MS.

In order to determine the analyte concentration for ICP-MS analysis of samples, a complete external calibration was performed. Additionally, the reagent and procedural blanks were performed before and after sample analysis to evaluate any potential carry over. The regression statistics determined were deemed acceptable with R^2 values for each determinant (Ag, As, Cd, Co, Cr, Cu, Mo, Ni, Pb, Sb, Ti and V) >0.09995 (figures A-3.9 to A-3.21 in Appendix A-3) and all blanks were below the instrument limit of detection (0.1 ppb) for heavy metal analytes. All quality control (QC) determinants passed acceptance criteria with precision and accuracy <15 % with sample concentration (injected in triplicate, RSD <15 %) and deemed valid (Supplementary information available in Appendix A-2). Table 3.3 shows

[4] Additional LC-MS information can be found in Appendix A-3.

the leachable heavy metals from the DPFMs determined by ICP-MS analysis of the sub sampled water. These given values in Table 3.3 are the averages of the triplicates examined for each sample as provided by the technicians at Tata Steel (Port Talbot). For a better comprehension of the data, the LOD has been included from the data supplied in Figures A-3.9 to A-3.21 in Appendix A-3. The average, standard deviation and RSD have been calculated from the three quality control measurements provided. RSD results for all metal elements are below 5% (apart from Mo with a value of 5.46%) and all are considered optimal. The different graphs representing each examined mask and the analysed concentration of the metals selected for this part of the investigation can be observed in Figures 3.9 to 3.15. With the aim of facilitate a graphical representation of the data variability and the validation of the results, the error bars for each element related to each of the standard deviations calculated from the QC data are also provided. The negative values, which are assumed as indicators of that element being absent in the sample, are also represented in order to give a better visualisation of those elements not detected. The values given are expressed in ppb. Table 3.4 shows the highlighted results for the main heavy metals found and calculated to µg/L.

Table 3.3. Raw data containing the averages of the triplicates examined for each sample as provided by the technicians at Tata Steel (Port Talbot), along with the limit of detection (LOD), quality controls (QC), QC averages, QC standard deviation and QC relative standard deviation (RSD).

Sample Id	Ag	As	Cd	Co	Cr	Cu	Mo	Ni	Pb	Sb	Ti	V	Hg
Reagent blank	0.03	-0.03	-0.04	0.01	-0.74	0.11	-0.74	0.39	-0.09	-0.59	-0.12	-0.02	0.05
Procedure blank	-0.03	-0.23	-0.07	-0.03	0.20	0.20	-0.65	1.94	-0.18	-0.62	-0.29	-0.05	0.03
Pro SFE black (Mask 2)	-0.03	-0.27	-0.06	0.27	-0.67	16.68	-1.51	1.27	0.04	4.24	2.56	-0.02	0.02
Paw patrol (Mask 4)	0.01	-0.23	0.16	2.16	-0.53	7.48	-1.58	8.53	3.56	0.84	1.08	-0.01	0.12
Type II R (Mask 5)	0.03	-0.15	-0.07	-0.01	-0.61	3.40	-1.69	13.79	3.05	12.28	0.11	0.01	0.01
Tesco (Mask 6)	0.05	0.14	7.68	0.05	-0.74	7.22	-0.11	0.87	6.79	0.51	0.11	0.06	0.06
Xmas Red (Mask 7a)	-0.05	-0.16	2.12	-0.02	-0.83	8.24	-1.37	0.39	6.49	444.50	0.04	-0.04	0.00
Xmas blue (Mask 7b)	-0.05	-0.14	-0.06	-0.02	-0.91	9.24	-1.93	0.35	-0.19	1572.26	0.44	-0.08	0.00
Xmas Green (Mask 7c)	-0.02	-0.22	-0.08	-0.01	-0.64	16.01	-1.69	0.39	-0.10	588.57	0.24	-0.01	0.04
LOD (ppb)	>0.003	>0.008	>0.01	>0.004	>0.06	>0.01	>0.03	>0.03	>0.002	>0.05	>0.18	>0.10	>0.01
QC (10 ppb)	10.18	10.28	10.10	9.95	9.78	10.11	10.12	10.24	10.37	9.60	10.09	10.29	5.34
QC (10 ppb)	10.15	9.62	10.26	10.16	9.99	9.78	10.23	10.24	10.38	10.33	10.29	10.36	4.93
QC (10 ppb)	10.76	10.63	10.75	10.09	9.79	10.34	9.05	10.27	10.13	10.40	9.65	10.01	4.89
Average QC	10.36	10.18	10.37	10.07	9.85	10.08	9.80	10.25	10.29	10.11	10.01	10.22	5.05
QC Standard Dev (±)	0.28	0.42	0.28	0.09	0.10	0.23	0.54	0.01	0.12	0.36	0.27	0.15	0.20
RSD	2.74	4.11	2.67	0.86	0.97	2.25	5.46	0.14	1.13	3.58	2.68	1.48	4.01

All the masks presented some degree of Cu. This was expected since, as commented in chapter 1, Cu compounds (like CuO), are used in textile industry due to their antibacterial properties[177]. It is plausible for CU residues and other metals like SB and Cr to appear in dyestuffs because some dye intermediates are synthesised utilising catalysts and levels of Cu in the range of 3.31 to 5.00 mg/kg have been reported[171]. Is being show in the literature that copper is a known environmental pollutant which can induce toxic effects a number of organisms including humans[250,251].

Different levels of Pb were also found in all masks apart from masks 7b and 7c. Even when it did not come as a surprise, the high concentrations of Pb in some masks (i.e., mask 6) were not expected. Lead is broadly used in the textile industry as a component of dyestuffs, but it has other applications as well. It can be referred as lead acetate for dyeing of textiles, lead chloride for the preparation of lead salts, lead molybdate for pigments used in dyestuffs and lead nitrate for mordant/oxidizer in dyeing[182]. High concentrations of this heavy metal in textile fibres samples have, nevertheless, been reported: cotton (1.57 mg/kg), acrylic (1.68 mg/kg), polyester (1.08 mg/kg), and polypropylene (1.37 mg/kg)[171]. As a neurotoxin, it has a significant impact on the development of the human brain and reproductive system. As a proven carcinogen with the ability to bioaccumulate, lead is a severe cause for concern. Even minimal exposures to lead can have negative side effects for humans, including neurological damage and impact to foetal development[231,252,253]. It specifically impacts reading and reasoning skills in children, and is associated with hearing loss, speech delay, balance issues, and violent inclinations. Children are especially vulnerable to long-term lead exposure. It's unlikely that neural damage, which can happen between the ages of 1 and 3, can be reversed. It's also necessary to be aware that a child's environment may contain lead from sources other than the tested products themselves. Because lead is an especially cumulative poison, the daily intake of lead is not as important a determinant of harm as is the duration of exposure and the total lead ingested over time[254].

The highest levels of Cd were found in mask 6. This heavy metal is used mostly in pigments and dyes; particularly red, orange, yellow and green and as a stabiliser for some plastics like PVC. As cadmium is relatively hard to oxidize, it is often used as a coating agent. Concentrations of Cd in the range of 6.05 to 8.46 mg/kg have been examined in fibres of different textiles (acrylic, polyester, nylon, viscose, and polypropylene)[171]. Long-

term exposure to cadmium can result in chronic anaemia. Under such circumstances, the deposition of Cd in the kidney can develop into cancer and cardiovascular problems[255]. Concentrations of Sb were also found in masks 2, 5, 7a, 7b and 7c, with the higher levels related to the latter three ones (highest concentration recorded for mask 7b at 1572.26 ppb). Sb is commonly found in polyester fibres due to its application as a catalyst in the manufacturing of polyethylene terephthalate and as a flame retardant synergist in multiple new and recycled polymers. Most of the world's PET production (about 60%) is used the manufacture of fibers for textiles. Samples of textiles produced for human use were found to have concentrations ranging from about 125 to 470 μg/g[256]. Due to having been discovered before, it was not unexpected to find this pollutant in the samples analysed, although the recorded levels were certainly unanticipated. As a contaminant, Sb and its compounds can produce pulmonary toxicity and chromosome aberrations and micronuclei have been observed. It is considered a carcinogen, and it can be toxic to the heart, lungs, liver and skin[257].

The graphs shown in Figures 3.13, 3.14, and 3.15 do not contain the concentrations of Sb as it would not have allowed a proper visualization of the rest of the chemical concentrations as Sb levels are much higher in comparison.

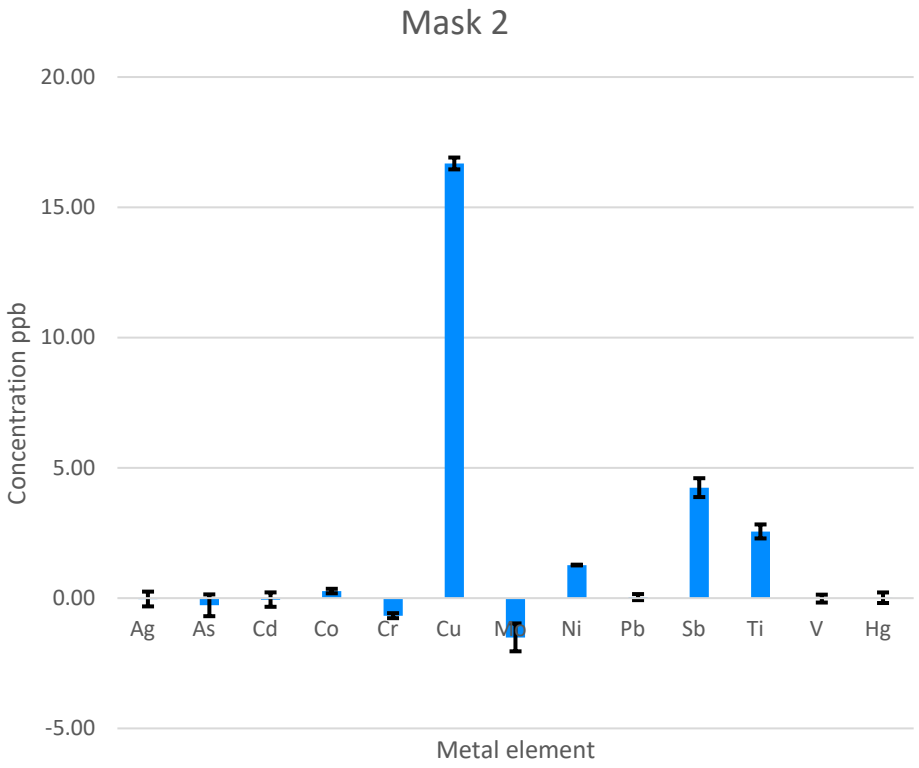

Figure 3.9. A graph with error bars for mask 2 representing the analysed concentration (ppb) of each of the metals selected. Cu is the metal with higher concentration.

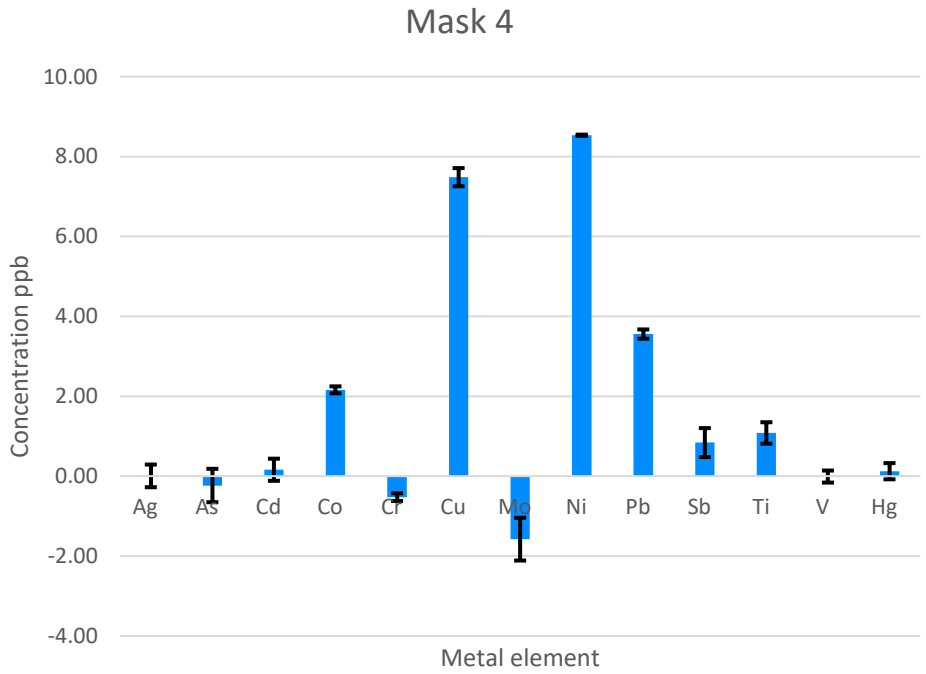

Figure 3.10. A graph with error bars for mask 4 representing the analysed concentration (ppb) of each of the metals selected. Cu and Ni are the metals with higher concentrations.

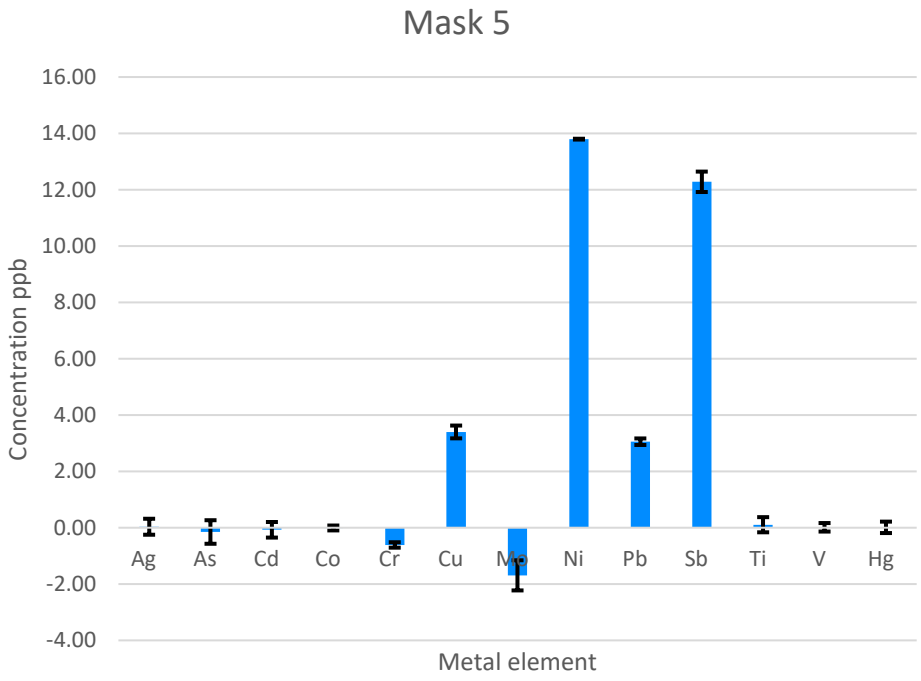

Figure 3.11. A graph with error bars for mask 5 representing the analysed concentration (ppb) of each of the metals selected. Ni and Sb are the metals with higher concentrations.

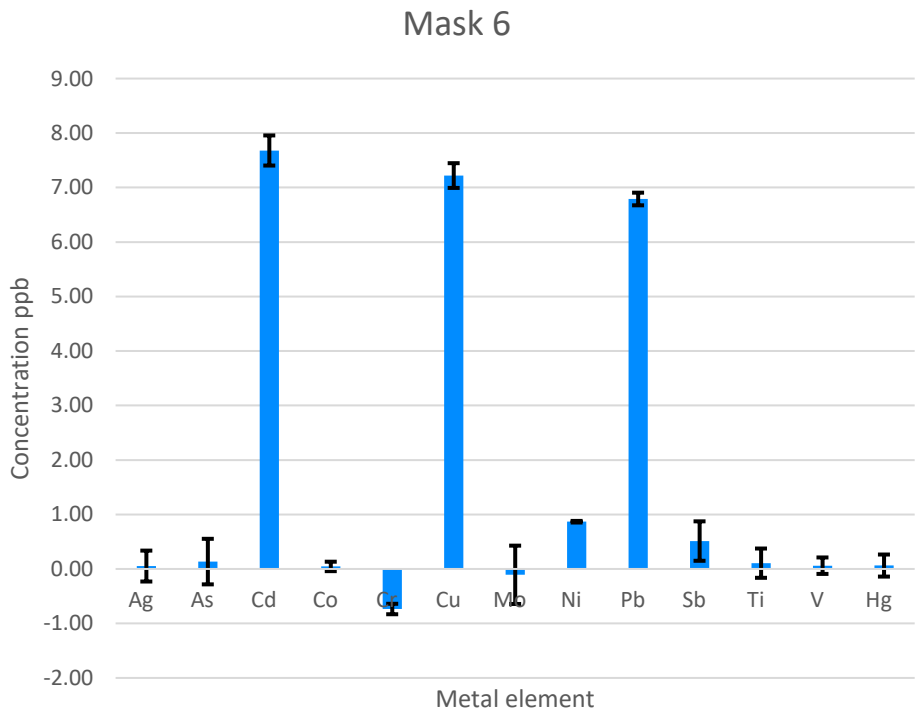

Figure 3.12. A graph with error bars for mask 6 representing the analysed concentration (ppb) of each of the metals selected. Cd, Ni and Sb are the metals with higher concentrations.

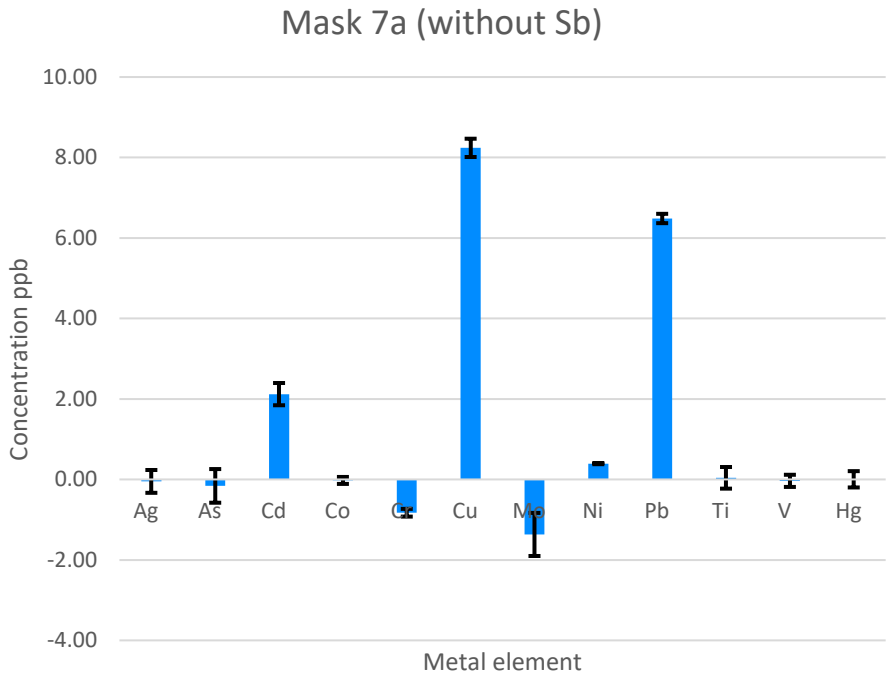

Figure 3.13. A graph with error bars for mask 7a representing the analysed concentration (ppb) of each of the metals selected. Due to its high value, Sb is not represented. Apart from Sb, Cu and Sb are the metals with higher concentrations.

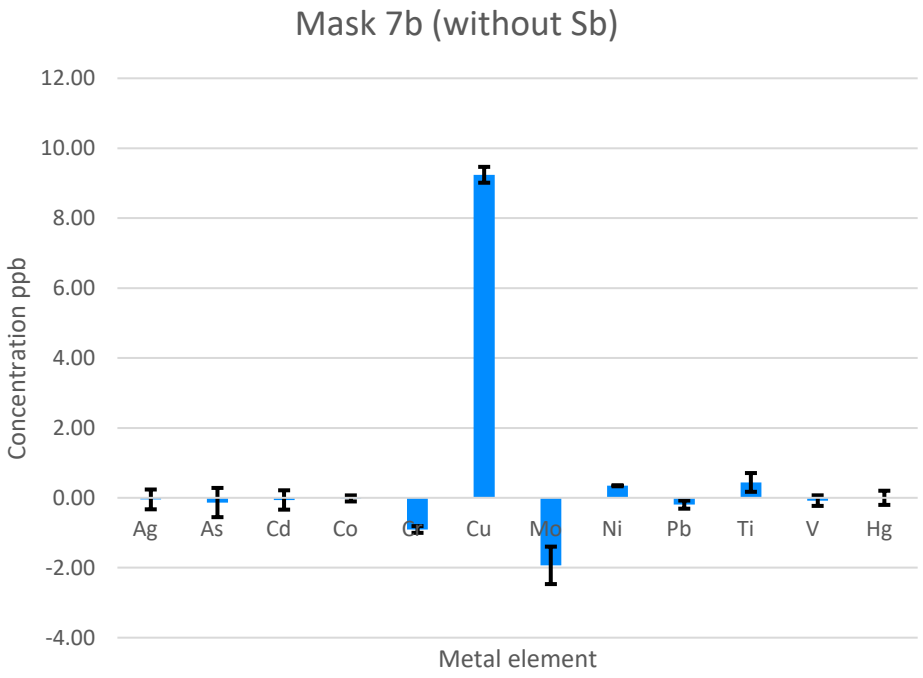

Figure 3.14. A graph with error bars for mask 7b representing the analysed concentration (ppb) of each of the metals selected. Due to its high value, Sb is not represented. Apart from Sb, Cu is the metal with higher concentration.

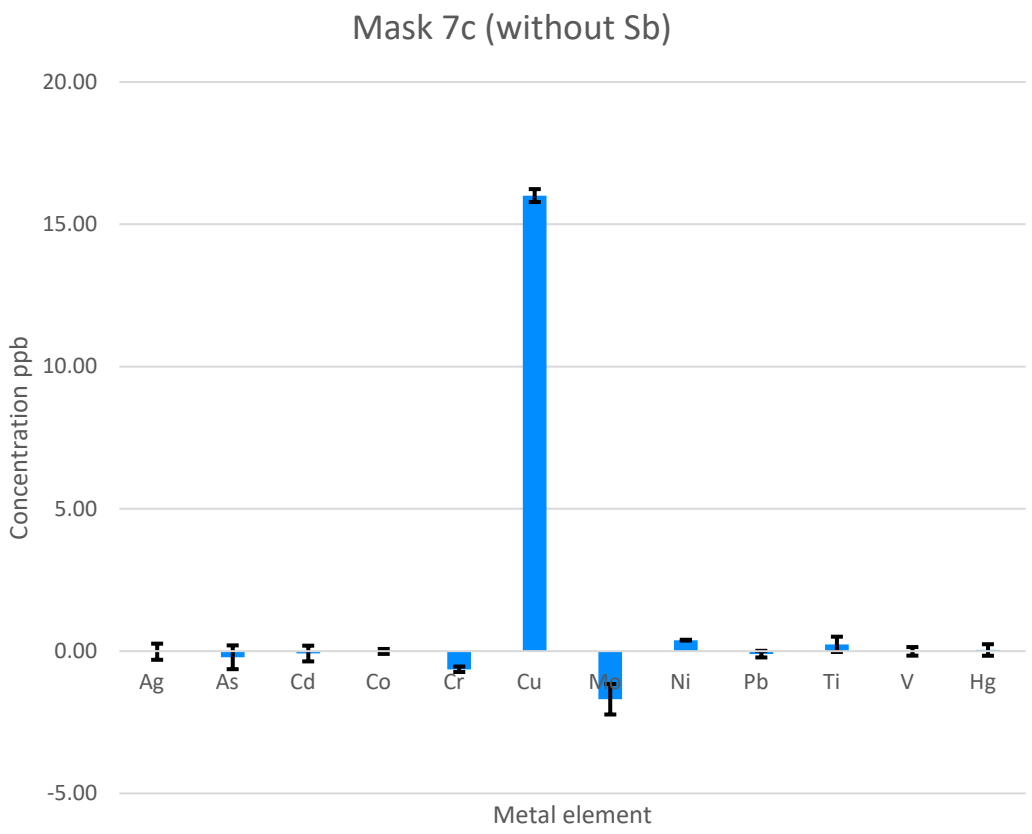

Figure 3.15. A graph with error bars for mask 7c representing the analysed concentration (ppb) of each of the metals selected. Due to its high value, Sb is not represented. Apart from Sb, Cu is the metal with higher concentration.

Once the results obtained have been calculated into µg/L by dividing by 4, concerning levels of Sb released from festive novelty masks (7a, 7b and 7c) and ranging from 111-393 µg/L were demonstrated. As previously commented, all masks appeared to release Cu, with calculated levels ranging from 0.85 µg/L (Mask 5) to highest levels of 4.17 µg/L (Mask 2). Lastly, leachable Pb was present in samples 2-7a, interestingly the highest value of 6.79 µg/L was associated with mask 6, the plain mask purchased from Tesco ©. Table 3.4 below shows the highlighted results for the main heavy metals found and calculated to µg/L.

Table 3.4. Lists some of the main heavy metals discovered in the DPFM leachate (250 mL). Mask 7a, 7b and 7c appears to have the highest release of Sb, whilst Cu is released from all masks. Adapted from Sullivan et al., 2021.

Sample	Cd (µg/L)	Co (µg/L)	Cu (µg/L)	Pb (µg/L)	Sb (µg/L)	Ti (µg/L)
Procedural Blank	N.D*	N.D	N.D	N.D	N.D	N.D
Mask 2 (Leachate)	N.D	N.D	**4.17**	**0.01**	**1.06**	**0.64**
Mask 4 (Leachate)	**0.04**	**0.59**	**1.87**	**0.89**	N.D	**0.27**
Mask 5 (Leachate)	N.D	N.D	**0.85**	**0.75**	**3.07**	N.D
Mask 6 (Leachate)	**1.92**	N.D	**1.80**	**6.79**	N.D	N.D
Mask 7 a (Leachate)	**0.53**	N.D	**2.06**	**1.62**	**111**	N.D
Mask 7 b (Leachate)	N.D	N.D	**2.31**	N.D	**393**	**0.12**
Mask 7 c (Leachate)	N.D	N.D	**4.00**	N.D	**147**	**0.06**

** Not Detected*

As established in Chapter 1, textile products supplied in Europe are not permitted to include particular levels of metals, and information on the composition of the fibres must be provided in accordance with European Regulation 1007/2011. Cu has a legal limit of 5 µg/g in textiles, while Sb has a limit of 3 µg/g. The legal limit is 1 µg/g for lead, cadmium, chromium (VI), and arsenic (and its compounds)[182].

Even when the concentrations found seem to be below the legal limits, the leaching of these chemicals into the environment is still a cause for concern. The bio-accumulative properties of these contaminants are one reason, but more importantly, the author of this thesis believes that these chemicals could be leaching into the vapor drops created while breathing using DPFMs and it could be a source of direct contamination if this polluted condensation is breathed back and inhaled during the time DPFMs are used. For these reasons, it is crucial that further investigation is conducted in order to determine the extent of this hazard for all organisms.

3.3.4. Leachable compounds: LC-MS analysis

All of the masks analysed by LCMS (accurate mass) released organic molecules in addition to heavy metals, some of which were tentatively identified as polyamide-66 ($[M+H]^+$ *mz*= 227.1754. $C_{12}H_{23}O_2N_2$), polyamide-6 and various oligomers of polyamide (PA), typically associated with nylon (Figure 3.16). Nylon may be interwoven in several layers of the face covering and is frequently utilised in the elasticized areas of DPFMs. PA-66 and PA-6

monomers and oligomers were identified ($[M+H]^+$ *mz*=340.2590 and 453.3421)[258], in novelty masks 4, 6, 7 a, b, c and in plain mask 6 purchased from Tesco©. Medical type II mask (Mask 5) and black colour mask (6) showed little evidence of PA emission and is therefore likely to contain little, if any, nylon parts used in their fabrication. Representative LC-MS spectra for the nylon-type ions in the data for mask 7a can be observe in Figure 3.17 and more information regarding peak identity is found in Table 3.5.

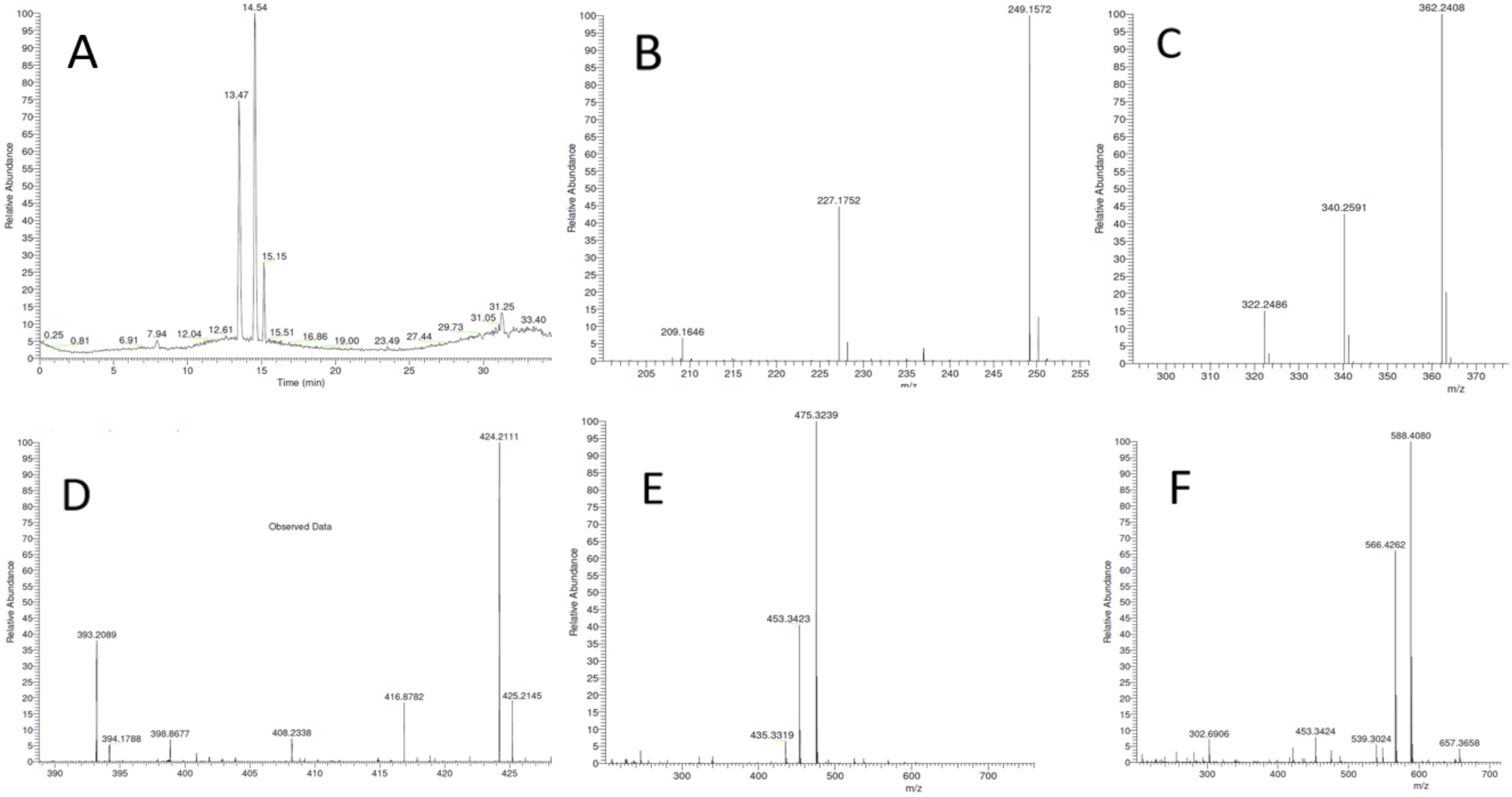

Figure 3.16. LC-MS data obtained from Leachate sample from mask 4. Top A is the total ion chromatogram (TIC), and B-F are mass spectrums for the associated peaks of the TIC. Peak at Rt 7.73 has a mz of 249.1572 (B) was tentatively identified as Caprolactam. Mass spectrums C, D, E and F are therefore, likely to be oligomers of Caprolactam. More information regarding peak identity is found in Table 3.5.

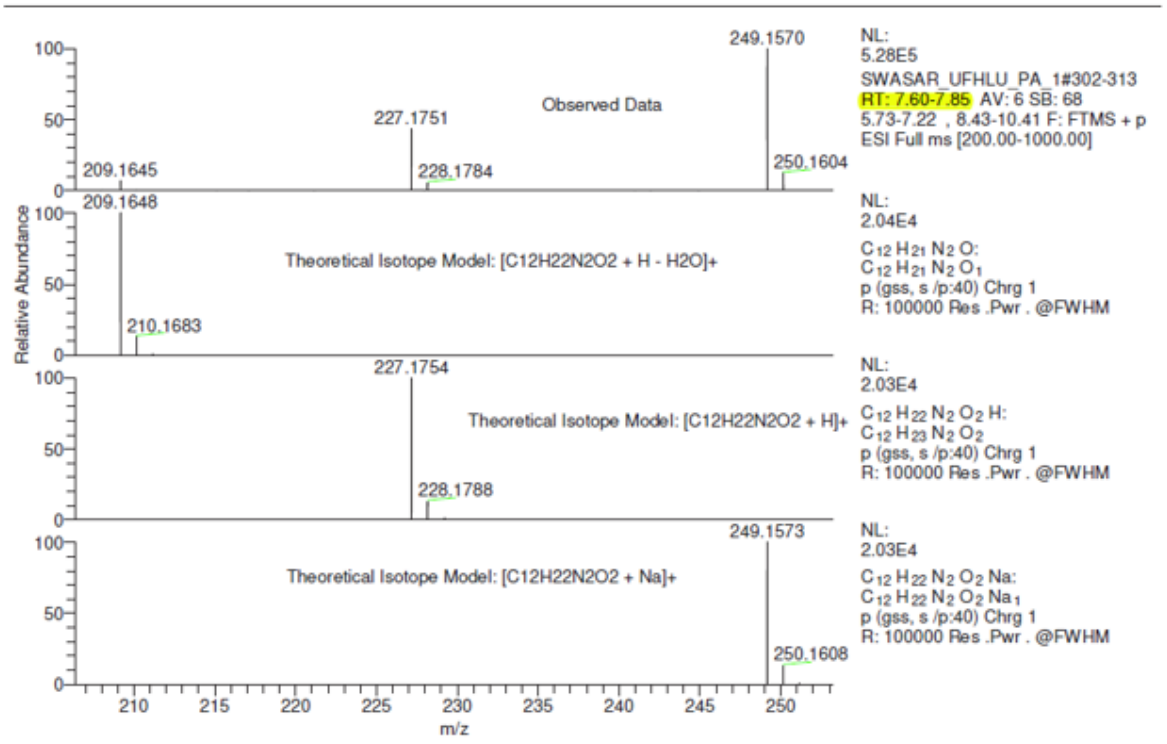

Isotope:	Min. .. Max.		
14 N	0....15		
16 O	0....15		
12 C	0....80		
1 H	0....100		
23 Na	0....1		
Tolerance Window:	+- 5.00 ppm		
Db/Ring Equiv:	-3.. 100	N-Rule:	Do not use
Fits:	300	Charge:	1

Mass	Theoretical Mass	Delta [ppm]	RDB	Composition
209.1645	209.1648	-1.6	3.5	$C_{12}H_{21}O_1N_2$
	209.1635	4.8	4.0	$C_{10}H_{13}N_5$
227.1751	227.1754	-1.3	2.5	$C_{12}H_{23}O_2N_2$
	227.1741	4.6	3.0	$C_{10}H_{21}C_1N_5$
249.1570	249.1571	-0.3	6.5	$C_{10}H_{17}N_8$
	249.1571	-0.3	1.0	$C_{11}H_{23}C_5N_1$
	249.1573	-1.4	3.0	$C_{12}H_{22}O_2N_2Na_1$
	249.1560	4.0	3.5	$C_{10}H_{20}C_1N_5Na_1$

Figure 3.17. Representative spectra for peaks with mz of 227.1754 and mz 249.1572 in the data for mask 7a, associated to nylon-type ions (highlighted in yellow).

Of the compounds identified in the leachates, none of these species were identified in the procedural blank. In order to evaluate any potential background and carryover, a procedural blank was injected in between samples. The blanks verified there was no sample carryover, and the background was clear of any ions from the samples. It was also observed the formation of sodiated adducts. Adducts are defined as the product of a direct addition of two

or more distinct molecules, resulting in a single reaction product containing all atoms of all components[259]. Sodium adduct formation is common in electrospray ionization (ESI), mainly because sodium is ubiquitous in solvent systems (exposure to glassware). The Na+ ions are already in solution and can readily adduct to neutral molecules during the electrospray ionisation/evaporation process through which the molecule ion species are generated[260]. Adduction to neutral molecules depends on several factors:

- Sample molecular structure, e.g., O bases, have a higher efficiency of Na+ adduct formation than N bases due to O atoms being more electronegative and the competition from protonation in the case of nitrogen.
- Na+ ion concentration in comparison with other adducts that can be formed during the ionisation process such as H+ NH4+, K+, Li+ etc. The level of Na+ adduction can vary.
- The ratio of organic:aqueous solvent system, usually the higher the organic content, the more Na+ adduction is promoted over H+ adduction[260].

Other compounds were also detected. In some samples polyethylene glycol-like (PEG) derivatives were tentatively identified; in black colour mask (2) plain masks (5, 6) and novelty masks (7 a, b, c). Figure 3.18 is an example of the LC-MS spectra for a peak with mz of 539.3025 for mask 7a, associated to a PEG ion. PEG was not found in novelty children mask 4 and in procedural blank sample. PEG ($C_{2n}H_{4n+2}O_{n+1}$) is typically represented by a homologous series with a repeating mass difference of *mz* 22 and 44. PEG is a typical membrane filter contaminant that is frequently detected in LCMS as multiple species on the chromatogram. However, due to the limited PEG speciation in the leachate samples, and that this compound was not present in all samples (i.e., novelty masks 4 and blank sample) it is therefore assumed that PEG was originated from DPFMs.

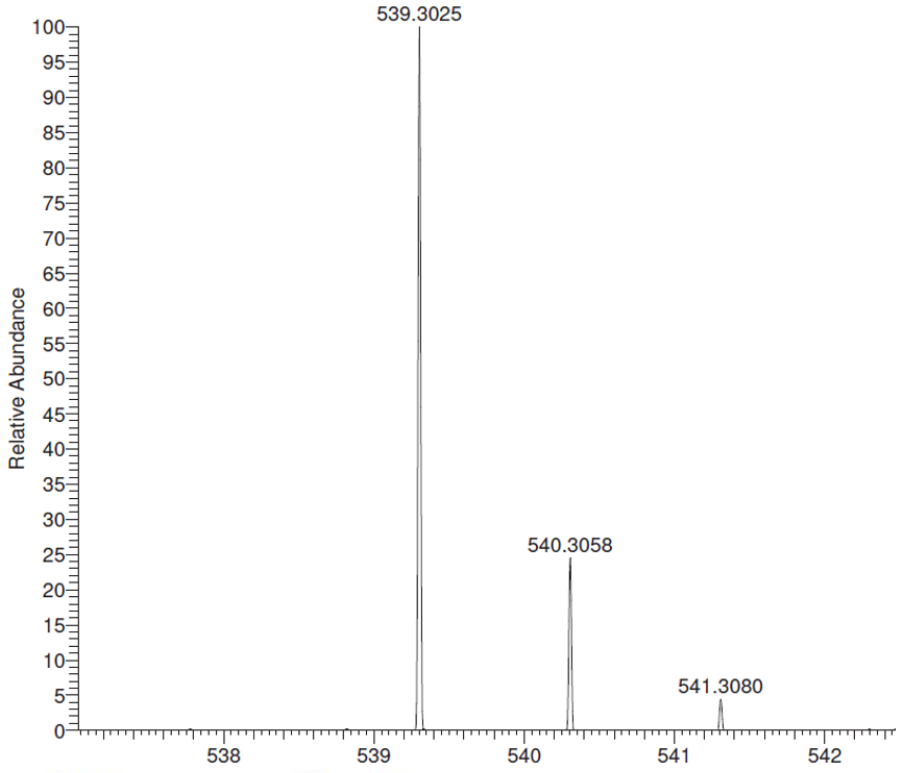

Isotope:	Min. .. Max.		
14 N	0....15		
16 O	0....15		
12 C	0....80		
1 H	0....100		
23 Na	0....1		
Tolerance Window:	+- 5.00 ppm		
Db/Ring Equiv:	-3.. 100	N-Rule:	Do not use
Fits:	300	Charge:	1

Mass	Theoretical Mass	Delta [ppm]	RDB	Composition
539.3025	539.3025	0.1	0.5	$C_{32}H_{68}O_{17}$
	539.3025	0.1	6.0	$C_{20}H_{40}O_{6}N_{10}Na_{1}$
	539.3022	0.6	-1.5	$C_{20}H_{47}O_{14}N_{2}$
	539.3022	0.6	4.0	$C_{19}H_{41}O_{9}N_{9}$
	539.3030	-0.9	16.0	$C_{35}H_{41}O_{4}N_{1}$
	539.3019	1.0	18.5	$C_{34}H_{38}N_{5}Na_{1}$
	539.3033	-1.5	18.0	$C_{36}H_{40}O_{1}N_{2}Na_{1}$
	539.3017	1.5	16.5	$C_{33}H_{39}O_{3}N_{4}$
	539.3035	-1.9	9.0	$C_{20}H_{37}O_{5}N_{13}$
	539.3035	-1.9	3.5	$C_{21}H_{43}O_{10}N_{6}$
	539.3038	-2.4	11.0	$C_{21}H_{36}O_{2}N_{14}Na_{1}$
	539.3038	-2.4	5.5	$C_{22}H_{42}O_{7}N_{7}Na_{1}$
	539.3038	-2.4	0.0	$C_{23}H_{48}O_{12}Na_{1}$
	539.3011	2.6	1.0	$C_{19}H_{44}O_{10}N_{6}Na_{1}$
	539.3011	2.6	6.5	$C_{18}H_{38}O_{5}N_{13}Na_{1}$
	539.3008	3.1	-1.0	$C_{18}H_{45}O_{13}N_{5}$

Figure 3.18. Representative LC-MS spectra for a peak with mz of 539.3025 in the data for mask 7a, associated to a PEG ion (highlighted in yellow).

Aromatic amines compounds (azo like) are other chemicals that were tentatively identified but difficult to confirm on DPFMs 2, 5, 6, 7a, 7b, and 7c. The peak corresponds to Rt 20.16 and also showed a similar peak in LC/UV at 21.95 mins. . LC/UV Spectra and representative

chromatograms of mask 7b and 4 (which does not present this peak) are shown in Figures 3.19 to 3.22 to illustrate this. More representative chromatograms showing these peaks can be found in Appendix A-3, Figures A-3.5 to A-3.8.

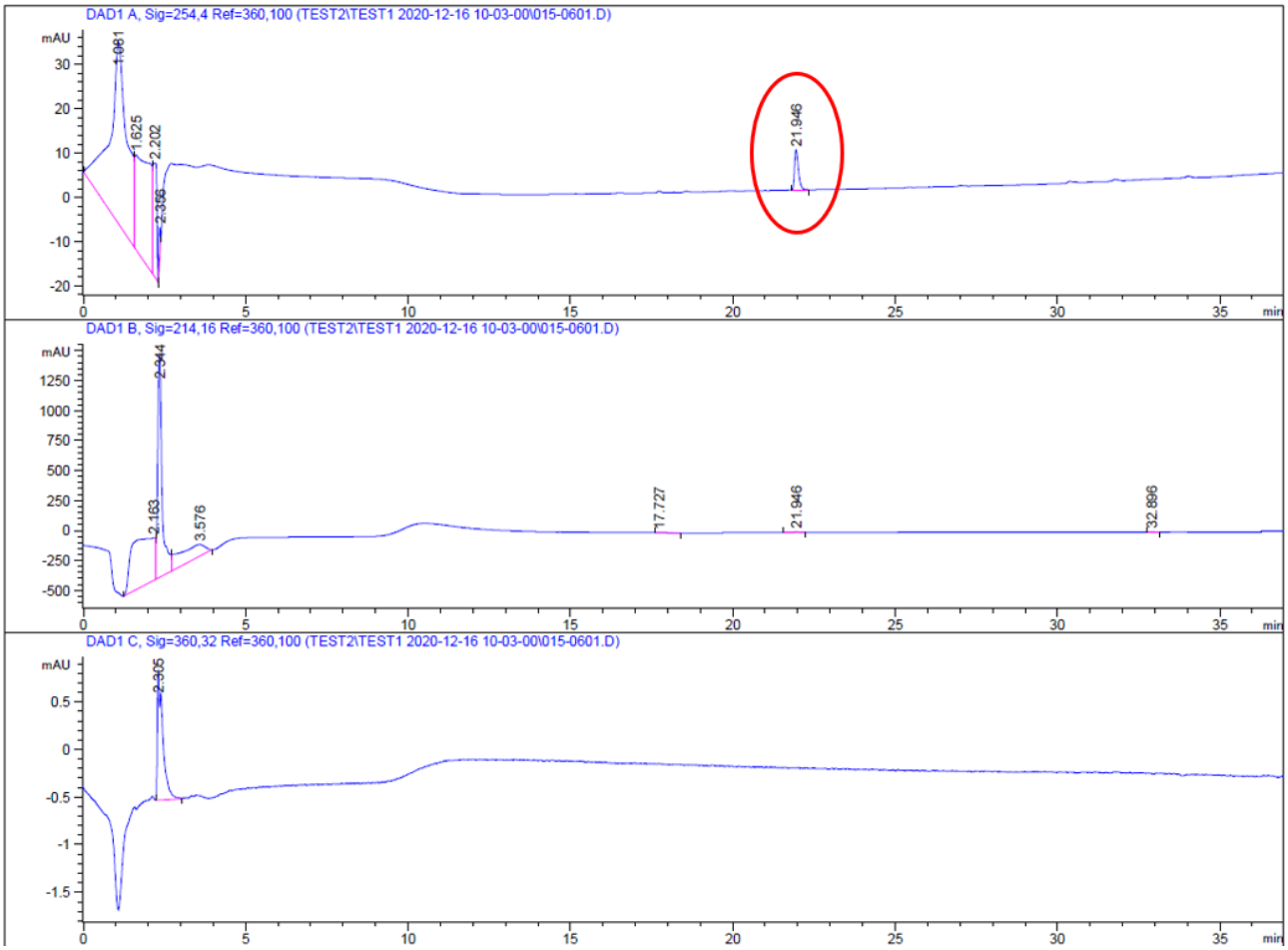

Figure 3.19. LC/UV Spectra of mask 7b showing a peak of interest for tentative identified azo like compound at 21.95 minutes.

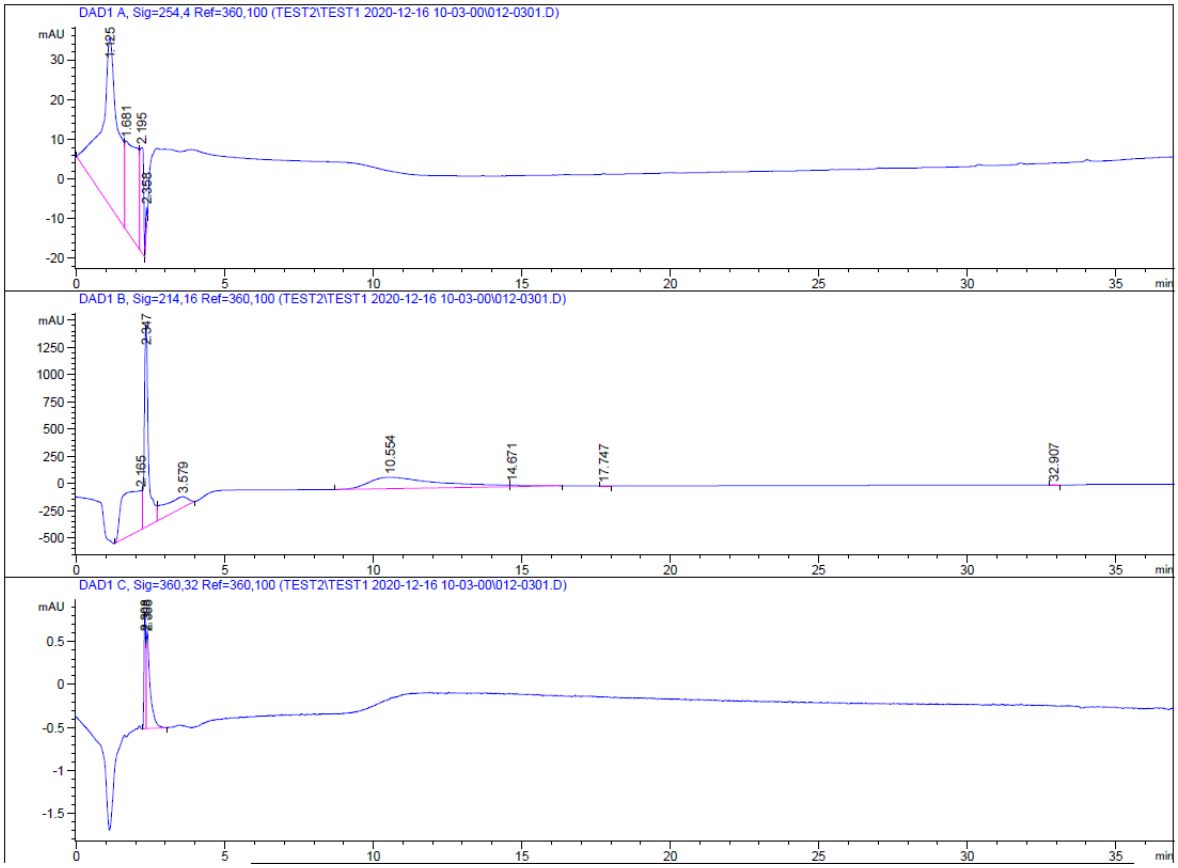

Figure 3.20. Comparative LC/UV Spectra of mask 4 were no peak of interest for tentative identified azo like was detected.

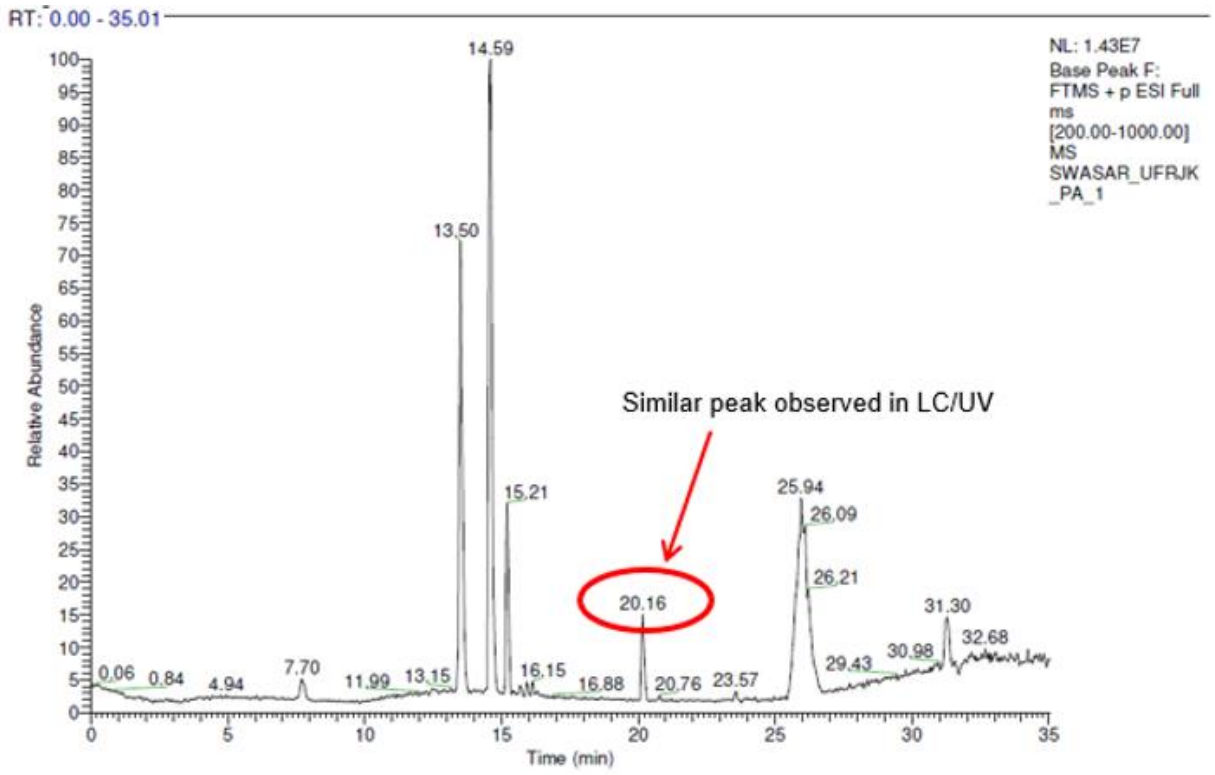

Figure 3.21. LC/MS chromatogram of mask 7b showing a similar peak detected with LC/UV at 21.95 mins.

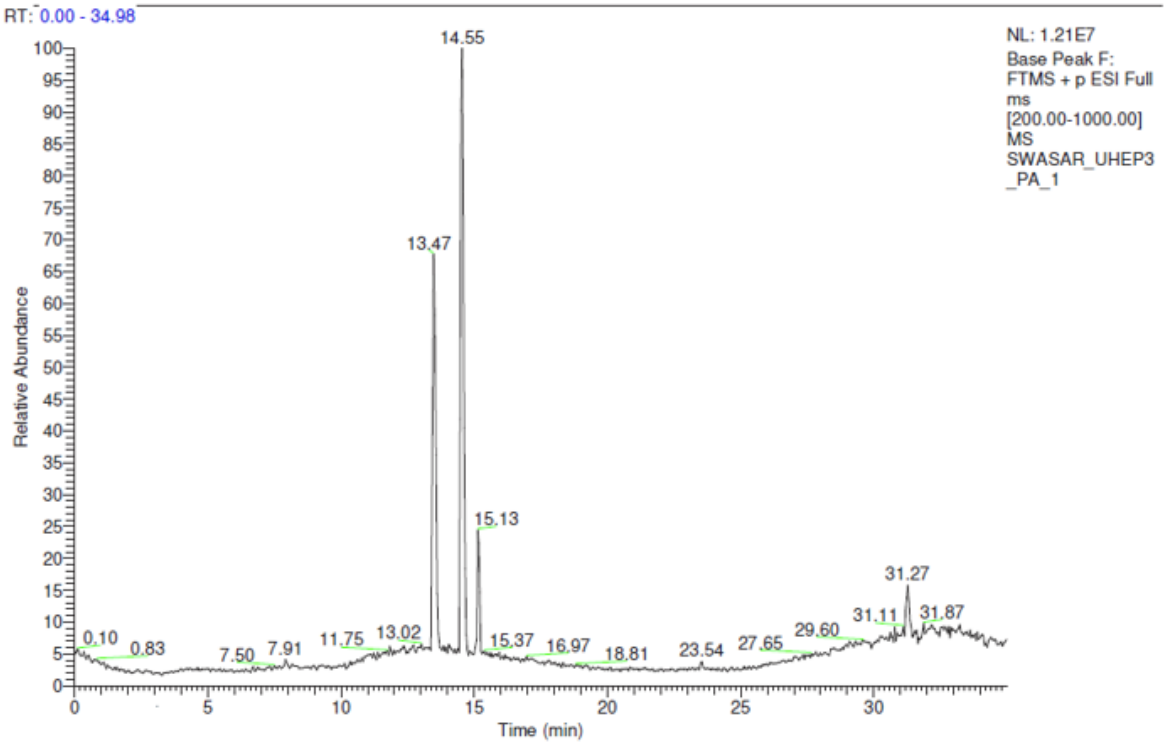

Figure 3.22. Comparative LC/MS chromatogram of mask 3 not showing the similar peak detected with LC/UV at 21.95 mins on other masks.

The main ions generating this peak have m/z values of 285 and 371. It can be assumed that the ion at m/z 371 is [+H]+ as it has a sodiated adduct, [+Na]+, at m/z 393. Measured accurate mass is m/z 371.2183. A list of potential elemental formulae matches to this m/z value can be observed in Figure 3.23. However, it must be noted that only C, H, N and O have been included, which of course is a limitation if other mono-isotopic heteroatoms such as F, P etc. are incorporated.

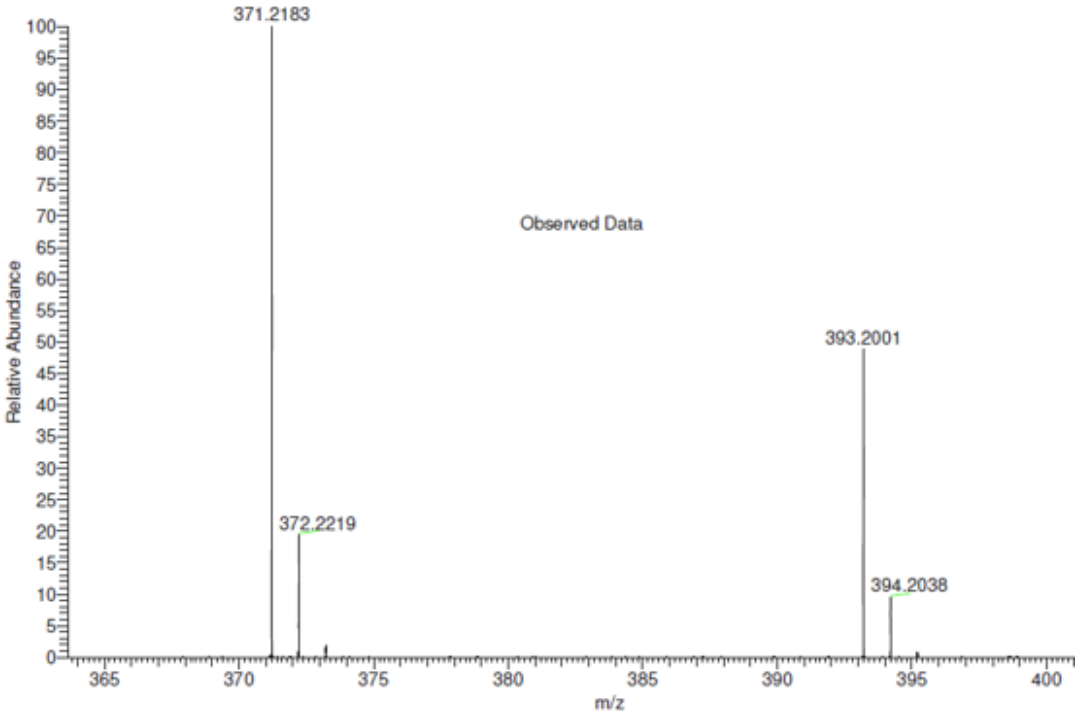

Isotope:	Min. .. Max.
14 N	0....15
16 O	0....15
12 C	0....80
1 H	0....100
23 Na	0....1
Tolerance Window:	+- 5.00 ppm
Db/Ring Equiv:	-3.. 100
Fits:	300

N-Rule:	Do not use
Charge:	1

Mass	Theoretical Mass	Delta [ppm]	RDB	Composition
371.2183	371.2182	0.4	-2.5	$C_{9}H_{31}O_{7}N_{14}$
	371.2177	1.7	4.5	$C_{18}H_{31}C_{4}N_{7}$
	371.2177	1.7	10.0	$C_{17}H_{25}C_{1}N_{9}$
	371.2190	-1.9	9.5	$C_{19}H_{27}C_{2}N_{6}$
	371.2195	-3.3	-3.0	$C_{5}H_{29}O_{8}N_{11}$
393.2001	393.2001	-0.0	-2.0	$C_{3}H_{26}O_{7}N_{14}Na_{1}$
	393.1996	1.3	5.0	$C_{18}H_{30}C_{6}N_{2}Na_{1}$
	393.1996	1.3	10.5	$C_{17}H_{24}C_{1}N_{8}Na_{1}$
	393.2007	-1.4	13.5	$C_{17}H_{27}N_{13}$
	393.2007	-1.5	8.0	$C_{18}H_{27}C_{4}N_{5}$
	393.1993	2.0	3.0	$C_{17}H_{31}C_{8}N_{1}$
	393.1993	2.0	8.5	$C_{16}H_{25}C_{4}N_{8}$
	393.2009	-2.1	10.0	$C_{18}H_{26}C_{2}N_{6}Na_{1}$
	393.2015	-3.4	-2.5	$C_{5}H_{28}O_{8}N_{11}Na_{1}$
	393.1983	4.7	5.5	$C_{16}H_{28}C_{5}N_{5}Na_{1}$
	393.1983	4.7	11.0	$C_{15}H_{27}N_{13}Na_{1}$
	393.2020	-4.9	13.0	$C_{19}H_{29}C_{1}N_{6}$
	393.2020	-4.9	7.5	$C_{20}H_{29}C_{6}N_{2}$

Figure 3.23. Representative LC-MS spectra for mask 7a of ions in peak at 20.16 mins and potentially matching elemental formulae for sodiated adducts.

It would seem from the data that if Azo dyes or similar species are present in these samples, they are below the detection limits of these techniques. For future experiments, the analysis

might benefit from a pre-concentration step. Due to the previously commented fact that any azo dye that has the chemical ability to transform into aromatic amine compounds can be dangerous to humans, further investigation is required to identify the ions representing this peak.

Olomoucine II like compounds were also detected in samples from masks 6 and 7a (*mz* = 371.2184 and 393.2003). A representative chromatogram of these peaks and the compounds associated are shown in Figure 3.24. Olomoucine II, the most recent roscovitine derivative, is a very powerful pharmacological inhibitor of the activities of cyclin-dependent kinases. Multiple wild-type human viruses, such as the human adenovirus type 4 and human cytomegalovirus, were suppressed by olomoucine II. Mutants of the herpes simplex and vaccinia viruses that are resistant to standard acyclovir treatment were likewise inhibited from replicating when in contact with this compound. A remarkable finding was the nearly total eradication of the transmission of infectious adenovirus type-4 progeny from infected cells when olomoucine II was combined with the DNA polymerase inhibitor cidofovir[261]. Considering this fact, it bears asking whether the same approach have been followed to give DPFMs the same properties. However, to the best knowledge of the author of this thesis, no studies have been published regarding the use of olomoucine II in the production of DPFMs or textiles in order to provide resistance to viruses.

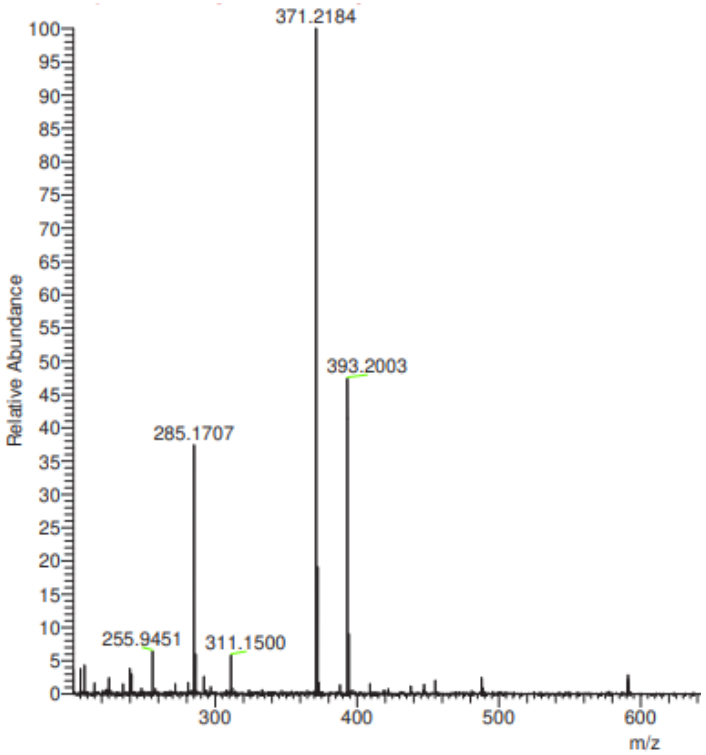

Isotope:	Min. .. Max.		
14 N	0....15		
16 O	0....15		
12 C	0....80		
1 H	0....100		
23 Na	0....1		
Tolerance Window:	+- 5.00 ppm		
Db/Ring Equiv:	-3.. 100	N-Rule:	Do not use
Fits:	300	Charge:	1

Mass	Theoretical Mass	Delta [ppm]	RDB	Composition
285.1707	285.1704	1.0	-1.5	$C_1 H_{20} O_3 N_{13} Na_1$
	285.1710	-1.0	8.5	$C_{16} H_{21} O_1 N_4$
	285.1699	2.7	5.5	$C_{16} H_{24} O_2 N_1 Na_1$
	285.1697	3.7	3.5	$C_{15} H_{25} O_5$
	285.1696	3.7	9.0	$C_{14} H_{19} N_7$
	285.1718	-3.8	-2.0	$C_3 H_{22} O_4 N_{10} Na_1$
371.2184	371.2182	0.6	-2.5	$C_3 H_{27} O_7 N_{14}$
	371.2190	-1.6	9.5	$C_{19} H_{27} O_2 N_6$
	371.2177	2.0	4.5	$C_{18} H_{31} O_6 N_2$
	371.2177	2.0	10.0	$C_{17} H_{25} O_1 N_9$
	371.2195	-3.0	-3.0	$C_5 H_{29} O_8 N_{11}$
393.2003	393.2001	0.5	-2.0	$C_3 H_{26} O_7 N_{14} Na_1$
	393.2007	-0.9	13.5	$C_{17} H_{21} N_{12}$
	393.2007	-0.9	8.0	$C_{18} H_{27} O_5 N_5$
	393.2009	-1.6	10.0	$C_{19} H_{26} O_2 N_6 Na_1$
	393.1996	1.8	5.0	$C_{18} H_{30} O_6 N_2 Na_1$
	393.1996	1.8	10.5	$C_{17} H_{24} O_1 N_9 Na_1$

Figure 3.24. Representative LC-MS spectra for mask 5 of ions with mz 371.2484 and mz 393.2003 tentatively identified as olomoucine II like compounds and potentially matching elemental formulae.

Of other compounds found, N-Undecyl-1-undecanamine was also a likely candidate found in Mask 5, which is a primary long chain surfactant type molecule, likely used in softening of PP during manufacture. MS/MS fragmentation data confirms N-Undecyl-1-undecanamine (*mz* = 326.3775) as a likely candidate (Figure 3.25), as it shows a loss of the decyl group a through probable homolytic cleavage, leaving a charged residing around a methyl-1-undecanamine fragment ion (*mz* = 186.2214). No more dye compounds were detected in the other samples, and it is likely that if any dye compounds were present in the leachate, then they were at significantly low levels and this methodology would need further optimization in order to identify them, such as preconcentration and instrument parameter optimization.

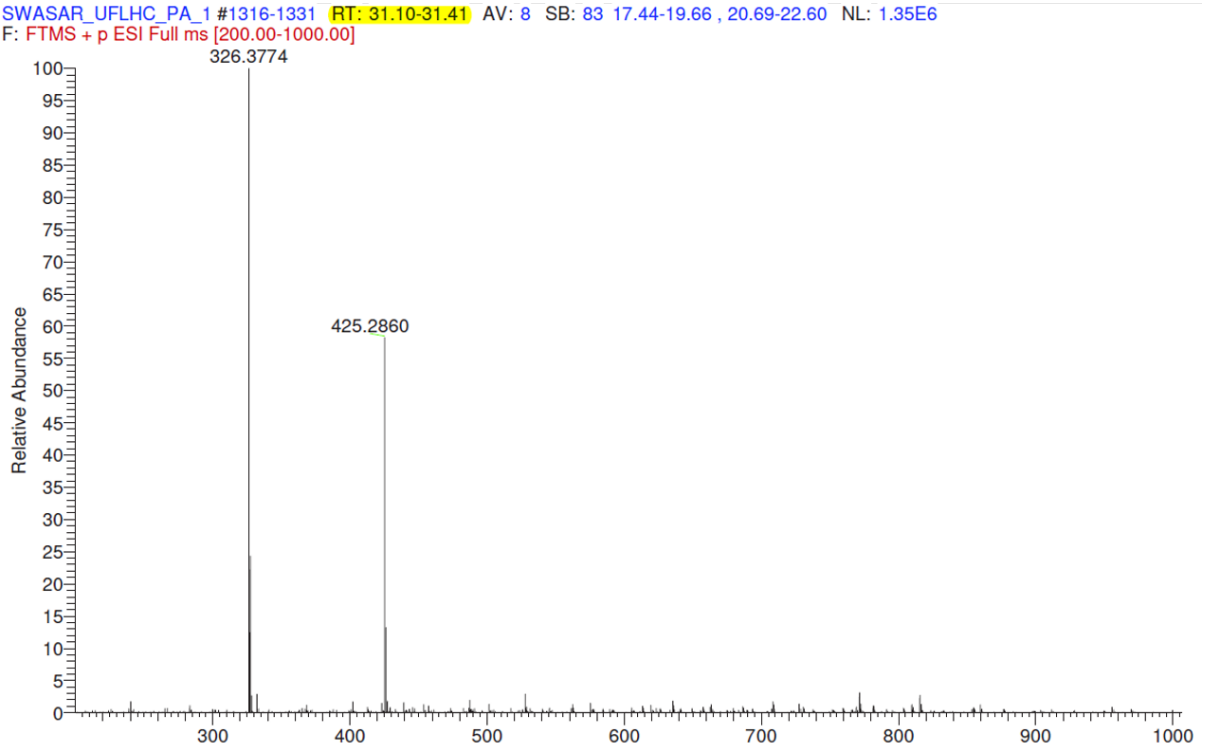

Figure 3.25. Representative LC-MS spectra for mask 5 of ions with mz 371.2484 and mz 393.2003 tentatively identified as N-Undecyl-1-undecanamine.

Table 3.5. LC-MS ions and their tentatively identified compound, preformed on the DPFMs leachates. Elemental formula takes into account of [$M+H]^+$ or [$M+Na]^+$ ion formation. Adapted from Sullivan et al., 2021.

Accurate mass ions identified	**Possible Elemental formula [M+H]$^+$ or [M+Na]$^+$**	**Tentatively identified contaminates**	**Present in samples**
227.1754	$C_{12}H_{23}O_2N_2$	Caprolactam (PA66 monomer)	Masks
249.157	$C_{12}H_{22}O_2N_2Na$	P66 [M+Na]$^+$	4, 6, 7 a,b,c
322.2485	$C_{18}H_{32}O_2N_3$	Unknown	
340.2590	$C_{18}H_{34}O_3N_3$	PA6 trimer	
362.2407	$C_{18}H_{33}O_3N_3Na$	PA6 trimer [M+Na]$^+$	
424.2111	$C_{17}H_{35}O_5N_4$	Unknown	
453.3421	$C_{24}H_{45}O_2N_4$	PA66 dimer or PA6 tetramer	
475.3237	$C_{24}H_{44}O_4N_4Na$	PA66 dimer or PA6 tetramer [M+Na]$^+$	
588.4082	$C_{30}H_{55}O_5N_5Na$	PA6 Pentamer	
285.1707	$C_{16}H_{21}ON_4$	Aromatic pyrrole like compound	Mask 6 7a
311.149	$C_{17}H_{19}O_2N_4$	Azo like compound refer to LC-UV	
371.2184	$C_{19}H_{26}O_2N_6$	olomoucine II like compound	
393.2002	$C_{19}H_{26}O_2N_6Na$	olomoucine II like compound [M+Na]$^+$	
534-987	$C_{2n}H_{4n+2}O_{n+1}$	PEG like derivatives	Mask 2, 5, 7a,b,c
701.493	$C_{36}H_{66}O_6N_6Na$	PA 66 adducts or PA6 Hexamer adducts [M+Na]$^+$	Mask 6
311.115	$C_{2n}H_{4n+2}O_{n+1}$	PEG derivative	
355.1784	$C_{2n}H_{4n+2}O_{n+1}$	PEG derivative	
377.1692	$C_{2n}H_{4n+2}O_{n+1}$	PEG derivative	
326.3775	$C_{21}H_{46}N_2$	N-Undecyl-1-undecanamine	Mask 5
455.3327	$C_{21}H_{47}N_2O_8$	N1-(2,5,8,11,14,17,20-Heptaoxadocosan-22-yl)-N1-(2-methoxyethyl)-N2-methylethane-1,2-diamine	
527.3892	$C_{25}H_{52}O_5N_6Na$	N-(7-Aminoheptyl)glycyl-N-[(2S)-6-amino-1-(carboxyoxy)-2-hexanyl]-N^2-(7-aminoheptyl)glycinamide* [M+Na]$^+$	

The main composition of the DPFMs, mostly synthetic material, was previously published[225,227] and some authors had appointed to the emission of other secondary pollutants, like dyes, surfactants and glues[225,226] as well as micro silica particles (SiMP)[239,240] and some metals typically used in the textile industry[169,171] and thus, the discovery of these

substances was expected.

The detection high of heavy metals like lead (Pb) or some organic compounds like polyamide-66 was, on the contrary, unanticipated and reinforced the initial hypothesis of DPFMs posing a threat to the environment not only with the expelling of MPs, NPs and chemicals, but also releasing organic compounds and heavy metals that could be detected not only on samples taken from the masks, but also from the leachates after filtration.

Further exploratory tests are required for more accurate identification, of components emitted from DPFMs such as GCMS for volatiles analysis, LCMS/MS and NMR for structural elucidation of unknowns, but it is striking from preliminary data that these masks are emitting organic compounds that may have adverse environmental fate and possibly have bioaccumulation properties[169].

Looking at the wider picture, the vast amount of DPFMs generated due to the COVID-19 pandemic could easily see the cumulative release of these elements breaching current guideline limits, addition to this, there is a clear worry for the mask wearers, who are potentially being exposed to heavy metals with no time dependant exposure data available.

3.4. Highlights

Chapter 3 outlines the current environmental issue caused by an increase in the usage and disposal of disposable plastic face masks (DPFMs) into the environment as a result of the SARS CoV-2 global pandemic. It demonstrates how, from various mask types, chemical pollutants are also released from DPFMs in addition to micro- and nanoparticles during physical degradation.

- The evidence suggests that DPFMs waste, possess serious environmental risk through the emission of different pollutant streams by the simple mechanism of water exposure. DPFMs release small physical pollutants such as micro and nano size particles; mainly consistent with plastic fibres and silicate grains and is well documented to have adverse effects on the environment and public health.
- With addition to physical particles pollution, harmful chemicals such as heavy metals (Pb and Sb), and organic pollutants are also readily released. Many of these toxic pollutants have bio-accumulative

properties when released into the environment and this research shows that DPFMs are a potential source of these environmental contaminants.

- It is, therefore, imperative that stricter regulations need to be enforced regarding the manufacture and disposal/recycling of DPFMs to minimise pollution release, the European regulation 14683:2019 seems not restrictive enough. Further to this DPFMs need to be fully investigated to de-risk the potential exposure of the public to these potential harmful pollutants.
- There is currently little data into the wearing of DPFMs on the human body, and the question needs to be raised, what is the level of exposure to the public to from these fibres/particles, heavy metals and organic compounds from wearing these masks on a day to day basis.

Most of the contents of this chapter were published by ScienceDirect/Elsevier in February 2021 in the article 'An investigation into the leaching of micro and nano particles and chemical pollutants from disposable face masks - linked to the COVID-19 pandemic' 199 of which the author of this thesis is co-first author. The preparation of the samples was fully conducted by the author of this thesis. Microscopy and FTIR analyses were carried out by the author of this thesis and Dr. Geraint Sullivan. IPC-MS analyses were carried out at Tata Steel (Port Talbot) and LC-MS analyses were carried out at the National Mass Spectrometry Facility (Swansea University).

Chapter 4: Disposable FFP2 and Type II Medical grade Face Masks - An exhaustive analysis into the leaching of micro and nanoparticles and chemical pollutants. Linked to the COVID-19 pandemic.

4.1. Introduction

As it was shown in the previous chapter, the Covid-19 pandemic has resulted in an increase in the use of disposable plastic face masks (DPFMs) all over the world as a means of preserving the health of citizens by limiting the virus' transmission. In order to safeguard the public's health, face coverings have been made compulsory in a number of situations[262]. The UK has expanded its mask production rates by establishing a number of new or improved manufacturing facilities as a result of the subsequent rise in demand[263,264]. Similarly, production capacity for masks has expanded to 1.5 billion per month in Europe alone, a 20-fold increase over pre-pandemic levels[265]. The increase in face mask usage has led to a surge in the number of such masks entering the marine environment, contributing to greater pollution of these bodies of water[224] in the form of macro and microplastics.

There are a variety of types of disposable masks which differ based on their use and classification under the relevant standards. Two such types designed for medical use are FFP2 and Type II, which are classified as a respirator mask and as a surgical mask under the British Standards BS EN 149:2001+A1:2009 and European regulation 14683:2019 respectively. Different forms of protection are provided by these two categories; FFP2 shields the user from infection, while Type II is meant to shield the wearer's surroundings[266]. As they offer greater protection, FFP2 masks are recommended for use within high-risk areas, such as in hospitals[267], whilst Type II, although is still used in medical applications, are the more common of the two types used within the general population[268]. Additionally, both mask designs would typically need to obtain CE certification before being sold in the UK and the European Economic Area to prove that they are both safe and compliant[269]. Some products, however, have been authorised for sale without this assessment and labelling in order to prevent delays in the entry of new products to the market during the pandemic[270]. Different brands of masks of the same design may display different CE numbers depending on which notification body is used for the assessment of the masks[271].

Both Type II and FFP2 mask are designed for single use and can be made from a variety of plastics, depending on the manufacturer, including polypropylene (the most common), polyethylene, polystyrene, and polyester[225,272,273]. Regardless of the design and the plastic used, if masks are incorrectly disposed of, either by littering or by the general mismanagement of waste, they may be transported into bodies of water adding to plastic pollution[68]. Even when business and organisations usually have a standard procedure for disposal of DPFMs, a great amount of them are disposed incorrectly by the general public. Aside from the shorter-term issues these masks may have on the environment, such as visual pollution on beaches and wildlife entanglement, they are potentially a source of MPs and NPs as well as other secondary contaminants[274]. The secondary pollutants which may be released include compounds such as fillers used within the plastics or dyes used to obtain certain colours[55]. These additives are of particular concern as the compounds used can pose significant risks to the environment and public health[69].

Among other components, the non-ionic surfactant Triton X was detected. In 2012, this detergent was included in the 'List of substances of very high concern' of the Registration, Evaluation, Authorisation and Restriction of Chemicals (REACH) by the European Chemicals Agency (ECHA). This organisation mandated industries, including pharmaceuticals, its replacement by January 2021, involving EU and non-EU manufacturers and importers[275]. One of the products resulting from degradation of Triton X has been demonstrated to have hormone-like properties that might affect organisms in the environment, and thus, is a cause of concern[276].

Other compounds like polyethylene glycol (PEG) were present after LC-MS analysis. Although PEG is considered biologically inert, approximately 72% of the population has been proved to have PEG antibodies[277]. Because of this, and due to the presence of PEG in a large amount of products, allergies and hypersensitive reactions are an increasing concern[278,279].

Traces of several heavy metals were found using SEM technologies. Concerning elements like arsenic, lead, mercury and antimony, among others, were found as part of the particles released into water by the DPFMs selected in this study. These heavy metals can have several different effects, depending on the exact metal and the concentration, including neurological disorders and muscular diseases[280]. In addition, some masks have Titanium dioxide nanoparticles bound within the fibres, as this compound exhibits antimicrobial properties[281,282]. Research has shown that such nanoparticles can cause oxidative stress and

have a genotoxic effect[283].

MPs and NPs formed from single use plastic products, like disposable face masks, (referred to as secondary MPs) are primarily formed from the degradation of the original source within the body of water by UV light or mechanical means[2], although the emission of this pollutants have also been observed from brand-new masks[207]. In addition, there is also the potential for particles to be released directly, without the need for material breakdown, as research has shown that masks can have significant loosely attached plastic particles[284]. Research has shown that both MPs and NPs can have toxic effects if they are ingested, including inflammation and oxidative stress due to interactions with biological membranes and organelles[61]. These particles can be transferred along the food chains by ingestion and bio-accumulation and have effects on the development and reproduction of the organisms by interfering with their metabolism[285]. Furthermore, these particles can adsorb contaminants already present in the water and transport them, if they are ingested, into marine animals leading to an increased build-up of harmful compounds within the animals[286]. The amount of pollutant that is adsorbed onto the particles is dependent on both the contaminant and the type of plastic[287,288]. In addition, the expel of previously adsorbed pollutants and additives into the cells and bodies presents a higher threat to organisms than nanoplastics themselves[285].

Determining which plastics and other pollutants that are released from these FFP2 and Type II masks when they are submerged in water, can then help establishing the wider impact their use will have on the environment. The current studies found on this topic used Fourier transform infrared (FTIR) spectroscopy to determine the plastics used within respirator and/or surgical masks. These studies revealed plastics that are known to form nanoparticles, but the research did not generate or analyse any nanoplastics or other contaminants released from the masks[225,226,289].

In addition to previous membranes, inorganic membranes with a pore size of 20 nm are added in this part of the project, as well as the use of field emission gun-scanning electron microscopy (FEG-SEM) to hold and analyse particles smaller than the commonly accepted limit of the nanoscale, which is 100 nm. The study is specifically focused on medical DPFMs produced in a number of nations (the UK, the EU, and non-EU), including a Type IIR brand that was utilised by the UK National Health Service (NHS)

Using the method outlined in Chapter 4, the leaching of masks was conducted such that nanoplastics and other pollutants were released from the masks into deionised water[207]. The

solution containing the contaminants was then filtered using a membrane and the particulate material analysed using light microscopy (LM). Further analysis was then conducted to determine the make-up of the filtered particles using FTIR, SEM, EDS, LC-MS and ICP-MS. Sub-samples of leachates were also analysed using mass spectroscopy to detect and characterise organic and inorganic pollutants[207]. Figure 4.1 summarises this approach.

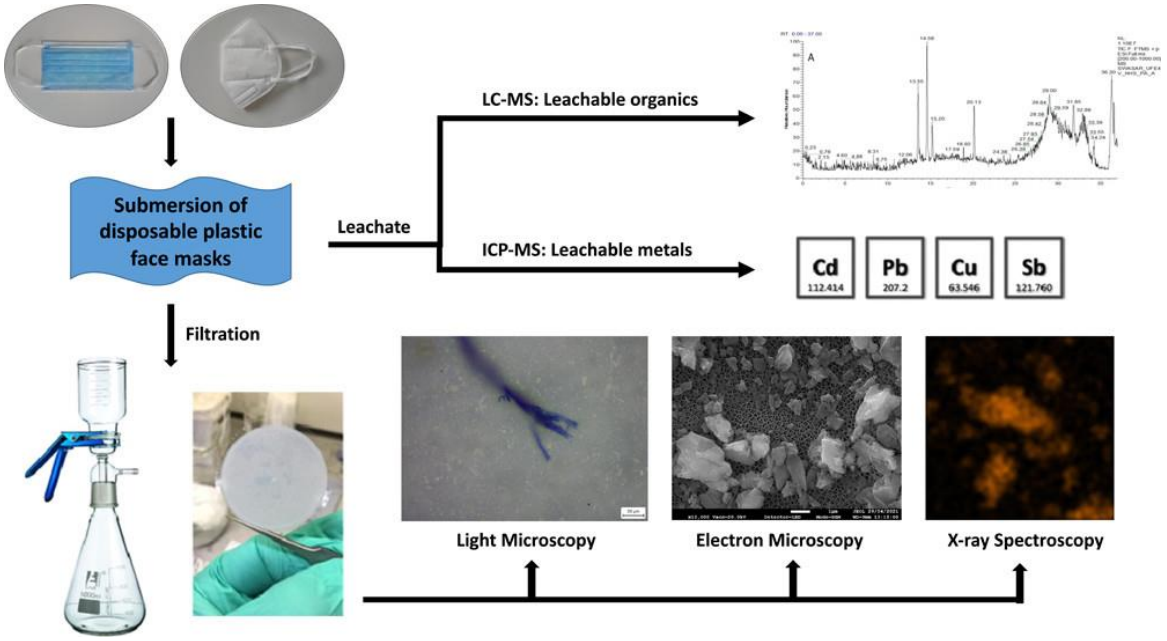

Figure 4.1. Diagram of the approach followed for this investigation. Following the approach on Chapter 3, the different DPFMs are submerged in deionised water to create two different types of samples: the leachates for ICP-MS and LC-MS analysis and the membranes with the deposited particles for microscopy analysis.

4.2. Materials and methods.

For this chapter, a selection of six different brands of DPFMs, three FFP2 and three Type IIR (Figure 4.2), from different manufacturers (Table 4.1), were acquired on Amazon. The FFP2 type masks used were sold under the brands Baltic, Soyes Geji (referred to as Geji within this chapter), and Soyes. Whilst the Type IIR brands were Omnitex, Duronic, and ones certified for use in COVID-19 test centres, and other environments, by the NHS. All the masks used were confirmed to conform to the relevant British Standard.

Figure 4.2. Images of masks used for this investigation. (A) Omnitex (showed as an example of all three Type IIR DPFMs), (B) Baltic (same features as Soyes), and (C) Geji (both FFP2 type).

Table 4.1. Manufacturer information for DPFMs used in the experiment, including type of masks and the number of masks used for each sampling approach. Adapted from Delgado-Gallardo et al., 2022.

Brand	**Type**	**Manufacturer**	**Masks used for the filtration of fibres and particles**	**Masks used for analysis of leachate (IPC-MS and LC-MS)**
Baltic	FFP2	InSpe (LT)	3 batches of 3 masks (total of 3 samples per membrane type (100 and 20 nm pore size)	3 masks per sample (total of 3 samples)
Duronic	II-R	Wujiang Kangjie Medical Co., Ltd. (CN)	3 batches of 3 masks (total of 3 samples per membrane type (100 and 20 nm pore size)	3 masks per sample (total of 3 samples)
Geji	FFP2	Guangzhou Dingdun Technology Co., Ltd. (CN)	3 batches of 3 masks (total of 3 samples per membrane type (100 and 20 nm pore size)	3 masks per sample (total of 3 samples)
NHS	II-R	Anhui JBH Medical Apparatus Co., Ltd. (CN)	3 batches of 3 masks (total of 3 samples per membrane type (100 and 20 nm pore size)	3 masks per sample (total of 3 samples)
Omnitex	II-R	Sharon Services (UK) Ltd.	3 batches of 3 masks (total of 3 samples per membrane type (100 and 20 nm pore size)	3 masks per sample (total of 3 samples)
Soyes	FFP2	Zhangzhou Anyue Sanitation Supplies Co., Ltd. (CN)	3 batches of 3 masks (total of 3 samples per membrane type (100 and 20 nm pore size)	3 masks per sample (total of 3 samples)

Deionised water was dispensed from Milli Q® type 1 dispenser, procedural blanks were also prepared using the same deionised water source. As in the previous chapter, the term 'reagent blank' relates to the blank samples composed of deionised water only, directly obtained from the Milli Q® type 1 dispenser. The term 'procedural blank' relates to samples of deionised water that has been filtered through a membrane and analysed as the rest of samples to identify any compound released from the membrane into the filtered water. For the leachates (ICP-MS and LC-MS samples) the term 'procedural blank' relates to samples of deionised water only that has been left in brand new beakers for 24 hours, as done with the samples, to analyse the release of any compounds from the beakers.

Whatman® Anodisc inorganic membranes of 0.1 and 0.02 µm pore size where purchased (Merck Group® UK) were used as membrane filters for particle deposition. A Glass vacuum manifold purchased from Sigma Aldrich®UK and vacuum pump Sparmax (The Airbrush Company Ltd, UK) was used to aid filtration of leachate. A brand new PURAIR P5-48 Nano (Air Science® Technologies Ltd) for particulates was employed to perform the filtering and overnight drying of the samples.

For microscopy analysis, a Zeiss Primotech light microscope (Carl Zeiss Ltd., Cambridge, UK) and TM3000 SEM electron microscope (Hitachi High-Technologies Corporation) was used for particle identification. High-resolution characterization was conducted using the Secondary Electron (SE) detector on a JEOL 7800F Field Emission Gun Scanning Electron Microscope (FEG-SEM) (JEOL, Tokyo, Japan)

A Perkin Elmer® ICP-MS NexIon 2000 metal leachate identification and quantification (Figure A1.3 of Appendix A-1). A Dionex ultimate® (UK) 3000 was used for LCMS analysis of organic contaminates, these were tentatively identified using identification using Thermo LTQ Orbitrap XL accurate Mass spectrometer. For chromatographic separation a reverse phase XBridge C18 column with dimensions: 3.5 µm x 2.1 mm x 150 mm and Guard column: XBridge C18 3.5 µm x 2.1 mm x 10 mm was used.

4.2.1. Leaching and Separation of Particles

Following a similar approach from previous chapter, for fibres and particle analysis, and in order to prepare three different samples for each brand, it was decided that three sets of three DPFMs of the same brand were sufficient to provide enough material for investigation and they were placed into beakers with 1L of deionised water, dispensed from a Milli Q® type 1 dispenser. Using a glass stirrer, the masks were gently stirred once every hour for four hours

while being submerged at room temperature. To conduct blank/control testing, the identical process was done with a beaker that only contained deionized water. The whole procedure was carried out under a fume hood to avoid external contamination of samples. As commented in the previous paragraph, this process what performed under a brand new PURAIR P5-48 Nano (Air Science® Technologies Ltd) for particulates.

When stirring wasn't occurring, the beakers were covered with aluminium foil that had been washed with ethanol and completely dried afterwards. After submersion, the eluent was filtered through either a 0.1 μm or a 0.02 μm Al_2O_3 Whatman® Anodisc membrane under vacuum using an Aldrich® glass funnel and receiving flask. A detail SEM image of 0.1 μm or a 0.02 μm membranes can be observed below (Figure 4.3). Each brand of DPFM was subjected to 3 repetitions employing each membrane pore size. After filtering all of the leachate, the membrane was put inside a brand new glass petri dish and left to dry at room temperature overnight under the fume hood. The identical filtration approach as described above was carried out on blank membranes using a beaker containing only deionized water.

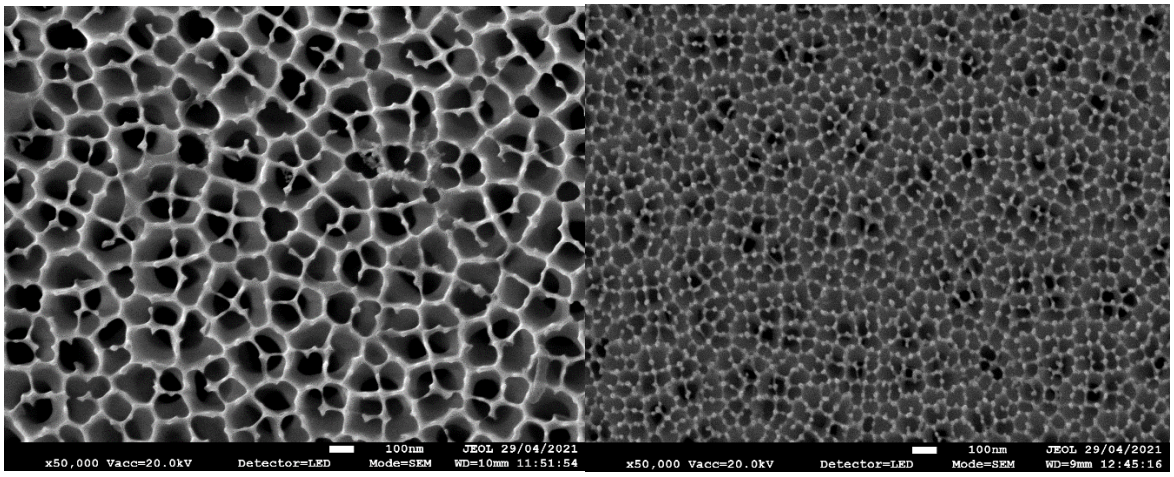

Figure 4.3. SEM images of blank membranes. 0.1 μm pore size (left) and 0.02 μm pore size (right).

To obtain the leachate samples for LC-MS and ICP-MS analysis, and in order to acquire enough compounds in the leachate to be analysed, three masks of each brand, instead of one in the previous chapter, were placed in brand new glass flasks containing 250 mL of deionised water and left submerged for 24 hours typical of leachate analysis in environmental laboratories. This approach was followed after running an experiment using only one mask (as in previous chapter) and observing that the levels of chemical pollutants were significantly lower than expected. For this reason, the medical DPFMs used in this chapter

are believed to have less chemicals and other components due to lack of different dyes compared to the DPFMs investigated in Chapter 3. The results of both analyses can be found in Table A-4.3 in Appendix A-4 for one mask experiment and Table 4.3 for the three masks experiment.

In order to avoid contamination from clothes or lab coats, nitrile gloves were placed covering the sleeves and elastic bands were used to make sure no fibres were released.

4.2.2. Microscopy of leached particles

The membranes were examined using light microscopy to assess the coverage of particle contamination, this was done using Zeiss Primotech microscope (Carl Zeiss Ltd., Cambridge, UK) at 50x and 500 overall magnifications.

For scanning electronic microscopy (SEM) and energy-dispersive X-ray spectroscopy (EDS) analysis, a Tabletop Microscope TM3000 was utilized (Hitachi High-Technologies Corporation), samples were mounted on carbon tape and placed in vacuum chamber.

A new technology was also put in place. Further high-resolution characterization was conducted using the Secondary Electron (SE) detector on a JEOL 7800F Field Emission Gun Scanning Electron Microscope (FEG-SEM) (JEOL, Tokyo, Japan). Prior to imaging, these samples were coated in 10nm of platinum.

4.2.3. ICP-MS elemental analysis for heavy metals in leachates

Three DPFMs from each brand (labelled; Baltic, Duronic, Geji, NHS, Omnitex and Soyes) were introduced in brand new glass flasks, submerged in 250 mL of deionised water, covered and left for 24 hours. Once the masks were removed, a 50 mL subsample of the solution obtained, referred as the "leachate", was then transferred into clean centrifuge tubes and acidified using 1 mL of 1 M nitric acid. The leachates were analysed for metal impurities using a Perkin Elmer ICP-MS NexIon 2000, a common method for elemental analysis in aqueous samples. A procedural blank (deionised water left in glass container for 24 hours) and reagent blank (deionised water only) were run with samples to check for background interference. The blanks were run after the highest calibration and after each sample to ensure there was no carryover. The supplementary documentation in Appendix A-4 contains calibration curves for each heavy metal tested (Figures A-4.46 to A-4.58). QC10, LOD, and procedure blank analyses are also supplied (Table 4.3).

Following the same approach showed in Chapter 3, a calibration standard, containing a

mixture of heavy metals (Ag, As, Cd, Cr, Co, Cu, Mo, Ni, Pb, Sb, Ti, V, and Hg) was acidified using 10% HNO_3 and diluted to a calibration range of 1 µg/L to 20 µg/L. The calibration standards were prepared from a 1000ppm mixed standard and were manufactured and tested under ISO 17034 and ISO 17025 guidelines. An external calibration curve was generated from injection of the diluted standards, and it required regression statistics above 0.9990 to be deemed acceptable. The calibration curves for each element can be found in Figures A-4.46 to Figure A-4.58 in Appendix A-4.

The samples that were concentrated above 20 µg/L were further diluted using acidified (10 %) deionised water to bring into dynamic range of the method. A number of quality control samples, prepared from a separate batch of multi-element standards and run at mid-range of the method (10 µg/L or 10ppb), were put in place to assess accuracy and precision of the analytical method and was required to be below 10% for both to be deemed acceptable. The instrument parameters were optimized prior to running samples and were set using the following conditions: plasma gas flow set at 18 L/minute of argon, auxiliary gas flow set at 1.8 L/minute and nebuliser flow rate of set at 0.98 L/minute. The sample uptake was set at 300 µL/minute with 3 replicates per sample. The RF voltage was applied at 1600W as determined by method optimization during method development.

4.2.4. LC-MS screen for organic compounds in leachates

For this experiment, no sample preparation, concentration or dilution was undertaken, all samples were analysed as submitted. The samples were kept in the freezer until time to be analysed, then defrosted and an aliquot pipetted into a glass autosampler vial for analysis. The LC/MS system was tuned, calibrated and a test sample analysed as per the SOP for this method prior to analyses of these samples. System blanks were run before each sample. The leachate was removed and analysed using reversed phases high-pressure liquid chromatography (RP-HPLC), with positive electrospray mass spectrometry (ESI-MS). 5 µL of sample was loop-injected into the pre-tuned and calibrated LC/MS system. Following the previous procedure, the reagent blanks and procedural blanks were run to identify the background ions and assess any potential carryover. The term ‘reagent blank’ relates to the blank samples composed of deionised water only and the term ‘procedural blank’ relates to samples of deionised water only that has been left in brand new beakers for 24 hours, as done with the samples, to analyse the release of any compounds from the beaker.

Organic contaminates were identified using Thermo LTQ Orbitrap XL accurate mass

spectrometer based on the empirical formula deduced from the accurate mass calculations and isotope patterns. For chromatographic separation, a reverse phase XBridge C18 column, with dimensions: 3.5 µm x 2.1 mm x 150 mm and Guard column: XBridge C18 3.5 µm x 2.1 mm x 10 mm, was used for analyte separation, with a flow rate of 150µl/min for LC/MS. The composition of the mobile phase A was 0.1% Formic acid; 2% (Acetonitrile) MeCN in H_2O and the mobile phase B was 0.1% Formic acid in MeCN. The elution gradient started at 2 % B and increased to 90 % at 32 minutes before returning to 2% B and ending with a total run time of 37 minutes. Following the same approach presented in Chapter 3, the gradient is standard for unknown samples, as it extends from low to high organic phase over a reasonably shallow linear gradient. The experiment was started at a low %B (2% in this case), hold it at this value for 2 mins so that all the salts and buffers in the samples that won't interact with the C_{18} stationary phase are eluted, then increase the organic solvent proportion over a period of 28 mins (2 - 30 mins) from 2 to 90% to elute the samples according to their partition with the stationary phase, with all being eluted by 90%B. This is then held at 90% for 2 mins to ensure elution of any particularly retentive components, then returned to 2% and allowed to equilibrate for a few minutes ready for the next run. The column was at RT (no column oven) and ramp rate just over 3.14^{o}C per minute.

A Dionex Ultimate 3000 HPLC system was connected in series to a Thermo LTQ Orbitrap XL accurate mass spectrometer, with API ion spray source. The MS parameters were optimized for a typical screening method. The following conditions were used: sheath gas flow was set to 15 L/minute, auxiliary gas flow set at 2 L per minute, the probe voltage was set at 4.3 kV with capillary and tube lens voltage of 43 and 150 V respectively. The MS scan conditions were full mass profile mode *m/z* 200-1000 with resolution of 60,000 and mass error of 0.5 ppm. For these analyses, HPLC-DAD analyses were not carried out due to lack of UV-Vis absorption inherent to polymeric species like PEG, Triton and polycaprolactam. The analysis conditions for HPLC and MS can be observed in tables A-4.1 and A-4.2 in the Appendix A-2.

4.3. Results and discussion

4.3.1. Optical microscopy of membranes[5]

Six batches of different brands of medical grade face masks, both FFP2 and Type II designs,

[5] Additional OM information can be found in Appendix A-4.

were tested to determine their potential to release plastic fibres and particles into water. As pointed out before, the samples from each batch were filtered using either a $0.1\ \mu m$ or a $0.02\ \mu m$ membrane and then analysed using LM to get an initial indication of particulate emission. This microscopic analysis revealed that all the masks tested emitted fibres visible at 50x magnification. The colour of the fibres seen were in line with the visual appearance of the masks they originated from, namely white and blue fibres from the Type II masks, white from the Baltic and Geji masks, and black from the Soyes masks. Figures 4.4 to 4.10 show the microscope images of both membranes for each of the mask brands and the blank sample at 50x magnification.

All three of the FFP2 masks emitted significantly greater amounts of MP fibres and particles than all Type IIR masks. Optical microscope images counting of areas of 3 μm^2 gave 4 to 6 times higher particles amounts released from FFP2 masks than Type IIR masks. This result contravenes the findings of previous research on the inhalation of MPs in air which found that N95 masks, which are approximately equivalent to FFP2 masks, emitted lower amounts of fibres than Type IIR masks[290]. The difference found in this work may be due to the fact that the fibre structure of melt-blown fabrics, which make-up the inner layers of both designs of masks as stated in the information provided by the manufacturers, is known to be damaged during washing with water[290]. As FFP2 masks have three inner layers[291], compared to the single layer in Type II masks[226], there is a larger amount of fabric to be damaged in this design of mask, potentially leading to the greater number of emitted fibres.

These results confirm the fourth hypothesis regarding the use of ceramic membranes as a valid support for the samples analysed and are also linked to the third objective of this thesis corroborating the release of different synthetic particles from DPFMs.

Figure 4.4. LM Images of 0.1 µm pore size membrane (left) and 0.02 µm pore size membrane (right) after the filtrations of Baltic DPFMs leachates at 50x magnification.

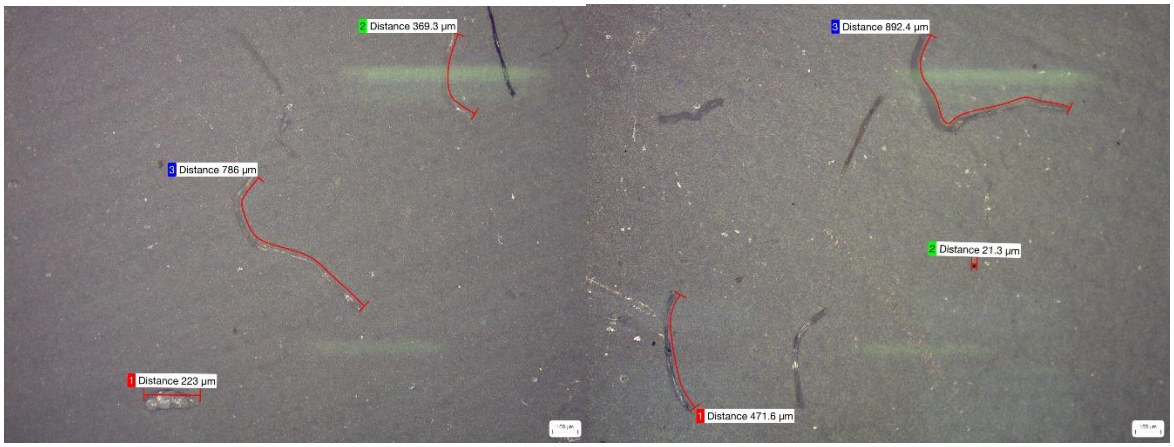

Figure 4.5. LM Images of 0.1 µm pore size membrane (left) and 0.02 µm pore size membrane (right) after the filtrations of Duronic DPFMs leachates at 50x magnification.

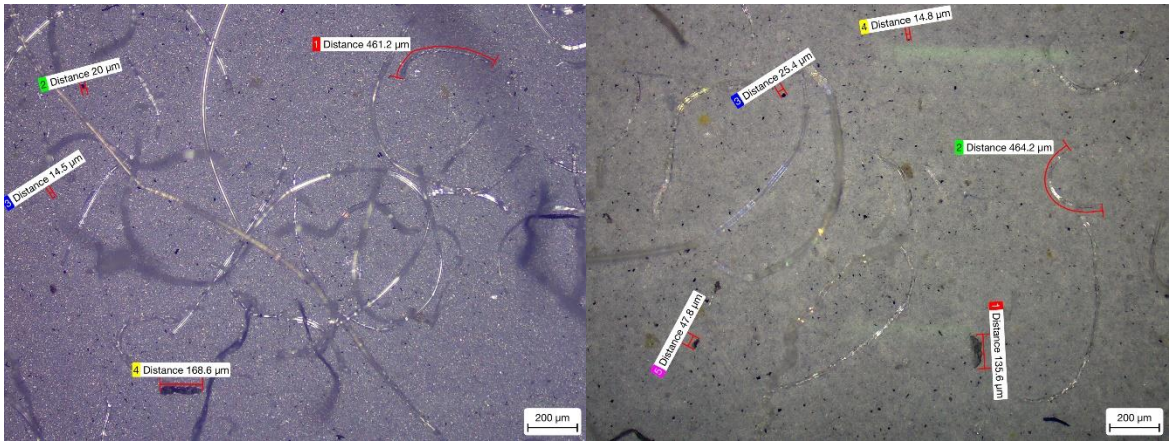

Figure 4.6. LM Images of 0.1 µm pore size membrane (left) and 0.02 µm pore size membrane (right) after the filtrations of Geji DPFMs leachates at 50x magnification.

Figure 4.7. LM Images of 0.1 µm pore size membrane (left) and 0.02 µm pore size membrane (right) after the filtrations of NHS DPFMs leachates at 50x magnification.

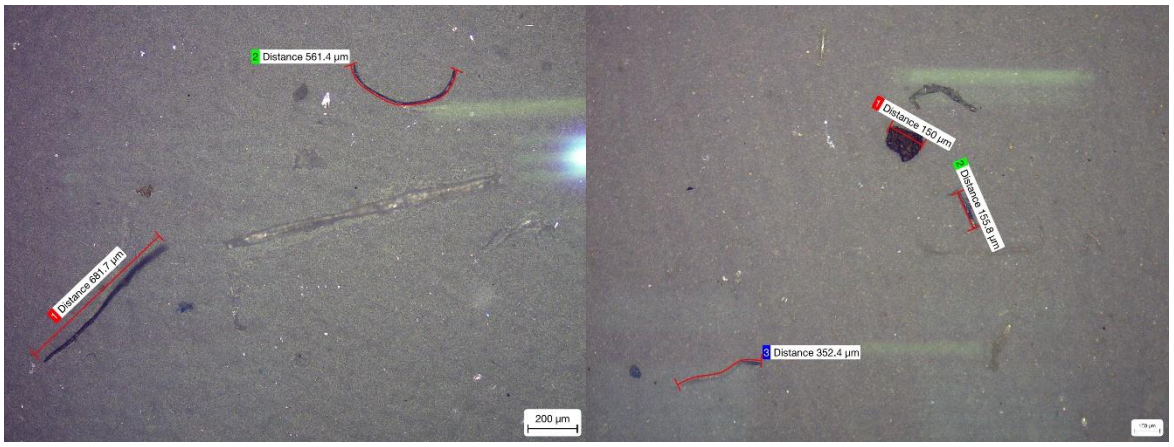

Figure 4.8. LM Images of 0.1 µm pore size membrane (left) and 0.02 µm pore size membrane (right) after the filtrations of Omnitex DPFMs leachates at 50x magnification.

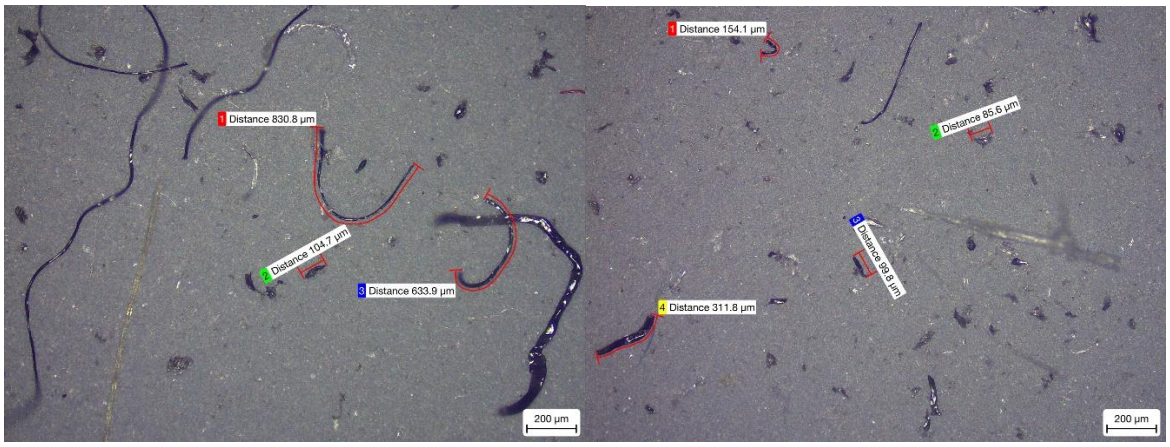

Figure 4.9. LM Images of 0.1 µm pore size membrane (left) and 0.02 µm pore size membrane (right) after the filtrations of Soyes DPFMs leachates at 50x magnification.

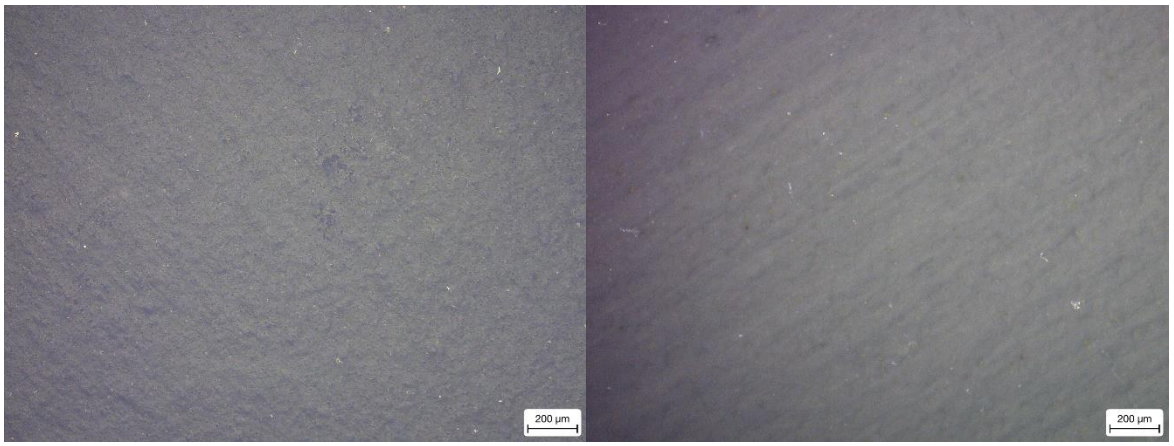

Figure 4.10. LM Images of 0.1 µm pore size membrane (left) and 0.02 µm pore size membrane (right) after the filtrations of Blank DPFMs leachates at 50x magnification.

In addition to the fibres, all the mask brands also emitted smaller fragments that were retained by the membranes, some of which required 500x magnification. These particles ranged in size from around 100 μm to approximately 1.5 μm, which aligns with the size of MP particles ($< 1\ mm$)[292]. The number of these fragments detected was limited for all brands, except for the membranes used to filter the Geji mask leachates. This can be seen in Figures 4.11 to 4.17 which shows the microscope images from both membranes taken at 500x magnification for each brand and the blank sample.

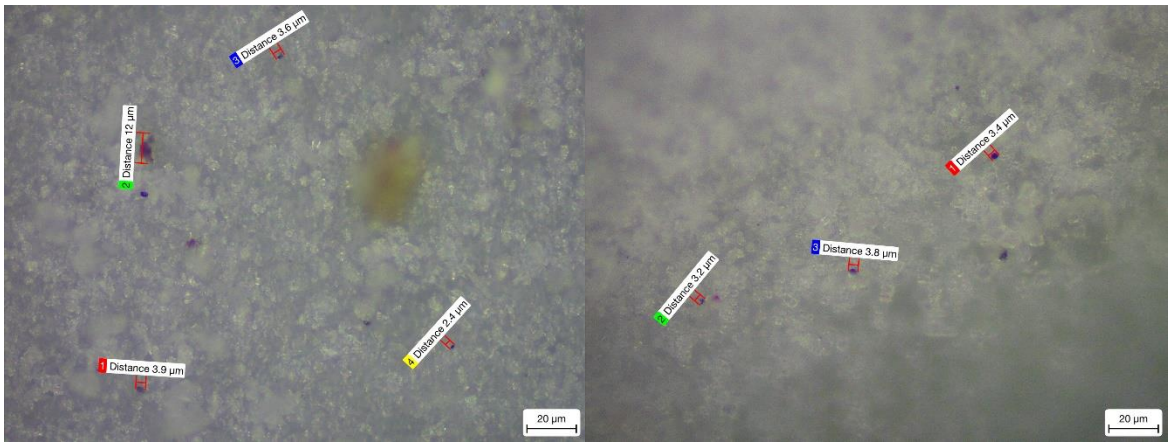

Figure 4.11. LM Images of 0.1 µm pore size membrane (left) and 0.02 µm pore size membrane (right) after the filtrations of Baltic DPFMs leachates at 500x magnification.

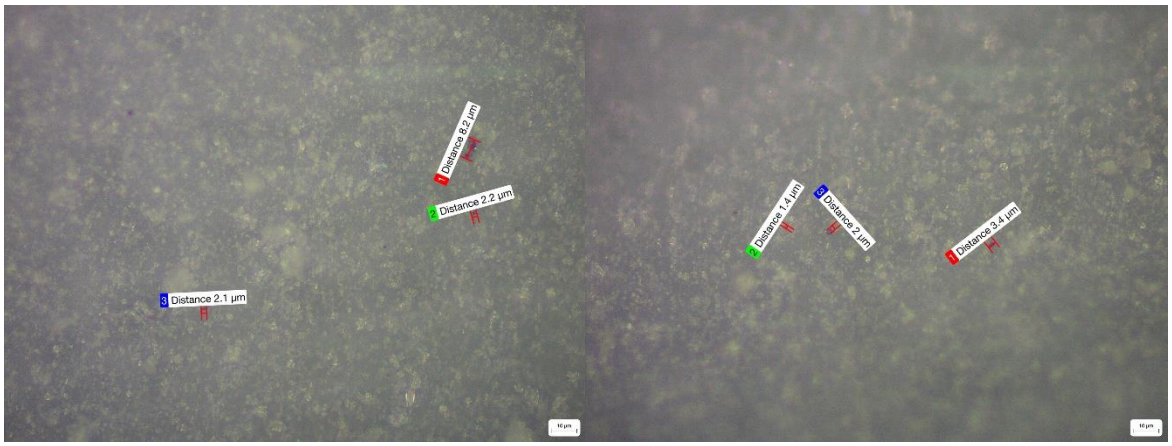

Figure 4.12. LM Images of 0.1 µm pore size membrane (left) and 0.02 µm pore size membrane (right) after the filtrations of Duronic DPFMs leachates at 500x magnification.

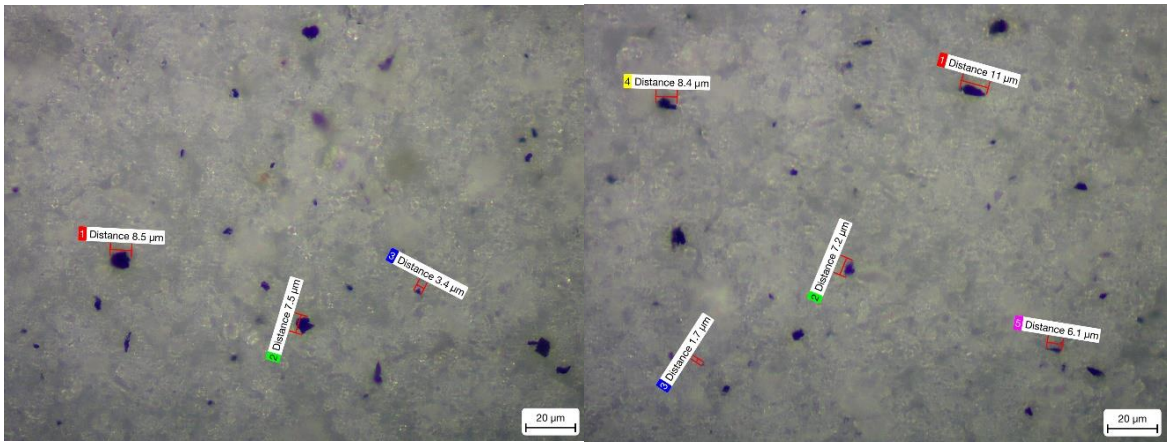

Figure 4.13. LM Images of 0.1 µm pore size membrane (left) and 0.02 µm pore size membrane (right) after the filtrations of Geji DPFMs leachates at 500x magnification.

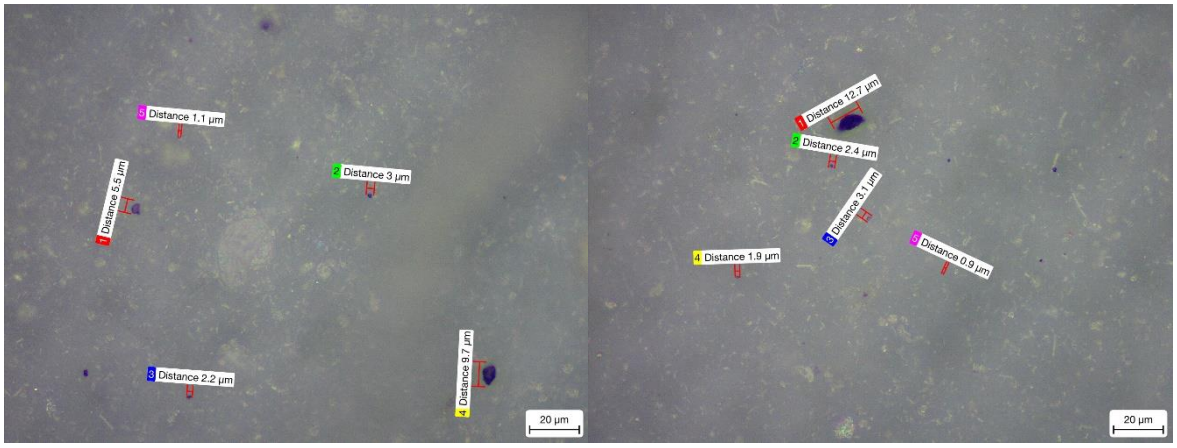

Figure 4.14. LM Images of 0.1 µm pore size membrane (left) and 0.02 µm pore size membrane (right) after the filtrations of NHS DPFMs leachates at 500x magnification.

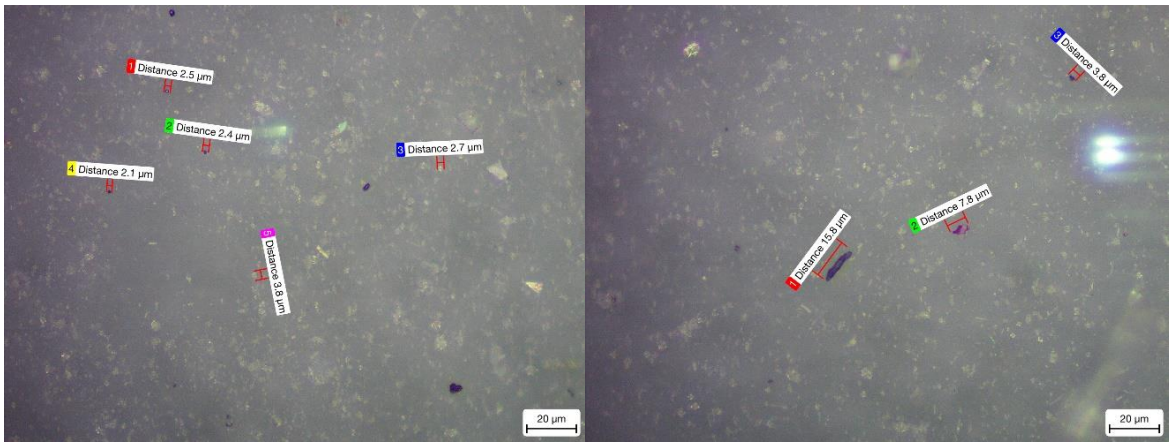

Figure 4.15. LM Images of 0.1 µm pore size membrane (left) and 0.02 µm pore size membrane (right) after the filtrations of Omnitex DPFMs leachates at 500x magnification.

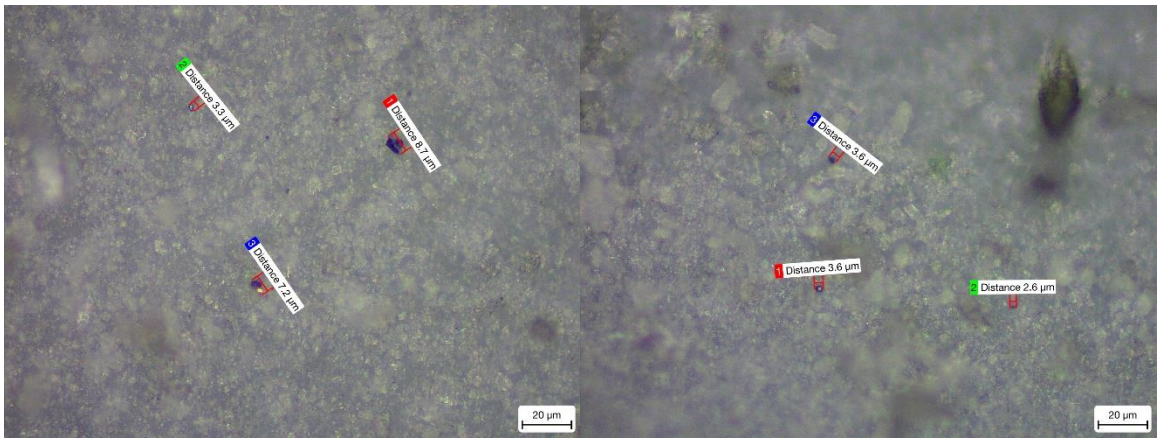

Figure 4.16. LM Images of 0.1 µm pore size membrane (left) and 0.02 µm pore size membrane (right) after the filtrations of Soyes DPFMs leachates at 500x magnification.

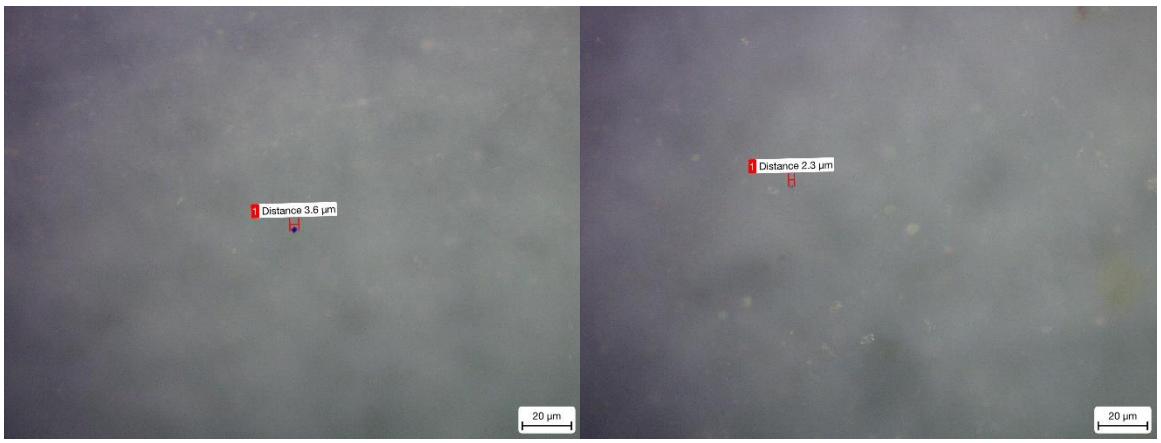

Figure 4.17. LM Images of 0.1 µm pore size membrane (left) and 0.02 µm pore size membrane (right) after the filtrations of Blank DPFMs leachates at 500x magnification.

As the number of fragments emitted from the other FFP2 masks were similar to the amounts released by the Type II masks, the large number of fragments from the Geji masks were thought to be likely due to the foam nose cushions which were only present on this brand of

mask. Foams of this type in MP form are known to have effects on microbial ecosystems in marine sediment[293] as well as leach harmful additives[294]. As such, these fragments pose a similar risk to the environment as the other fragments and fibres released by the masks, however some strains of bacteria and fungi have been reported as being able to efficiently degrade the foams[295].

Following the results in the previous chapter, the release of fibres and particles was anticipated. Nevertheless, the considerable amount of discharged debris coming from some of the masks (such as brand Geji) was unexpected and it supports the hypothesis that DPFMs are a potential new source of MPs that was put fifth in the introduction, and also the third objective presented. And again, the author of this thesis claims for more research to be done in order to measure and estimate the amount of fibres and particles produced from each mask. More images of light microscopy technology for both types of membranes (0.02 and 0.1 μm pore size) for all brands can be found in Appendix A-4, Figures A-4.1 to A-4.31.

4.3.2. Analysis of micro and nanoparticles with SEM[6]

The images taken using SEM techniques show the deposition of fibres and particles in all membranes. The particles with lighter colours usually contain heavier elements. It is noticeable the difference between the membranes with fibres and particles deposited (from the samples that were prepared submerging 3 masks in 1 L of deionised water and were gently stirred once every hour for four hours) and the blank membranes (which were filtered with deionized water, left for 4 hours and stirred the same as the other samples) as the number of particles is clearly much lower on the blanks. Apart from that, the NHS brand was the one with the lower number of particles on the surface (Figure 4.18 (a to g)).

[6] Additional SEM information can be found in Appendix A-4.

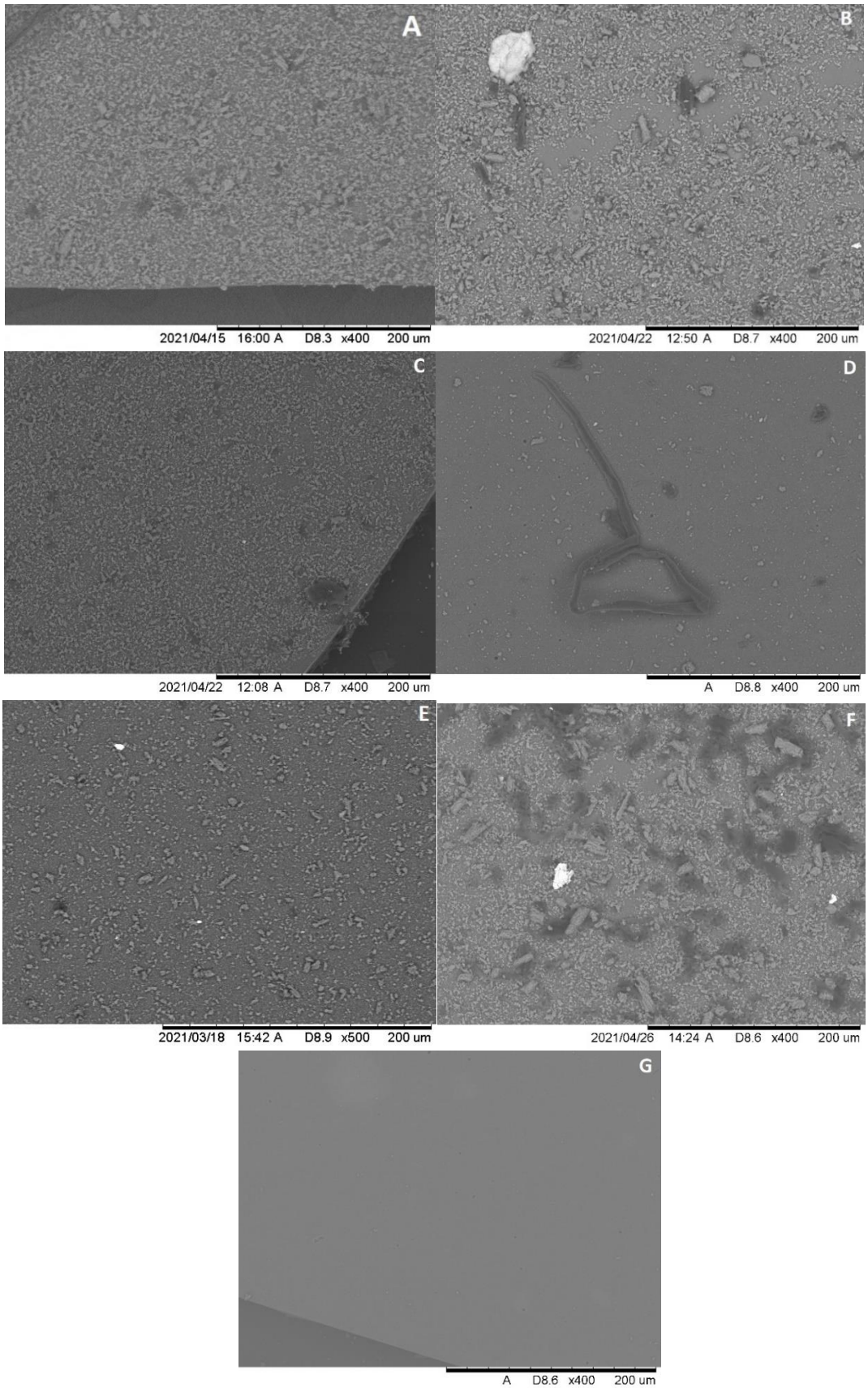

Figure 4.18. SEM images at x400 for all membranes after filtration. (A) Baltic, (B) Duronic, (C) Geji, (D) NHS, (E) Omnitex, (F) Soyes and (G) Blank. The difference in particle deposition can be observed.

This difference in the number of particles deposited between blank membranes and the rest was confirmed by the second SEM microscope utilized for this study. Figure 4.19 show results for Baltic, Figure 4.20 for Duronic, Figure 4.21 for Geji, Figure 4.22 for NHS, Figure 4.23 for Omnitex, Figure 4.24 for Soyes and Figure 4.25 for the blank membrane. More images obtained using SEM/TEM technology for both types of membranes (0.02 and 0.1 μm pore size) for all brands can be found in Appendix A-4, Figures A-4.32 to A-4.45.

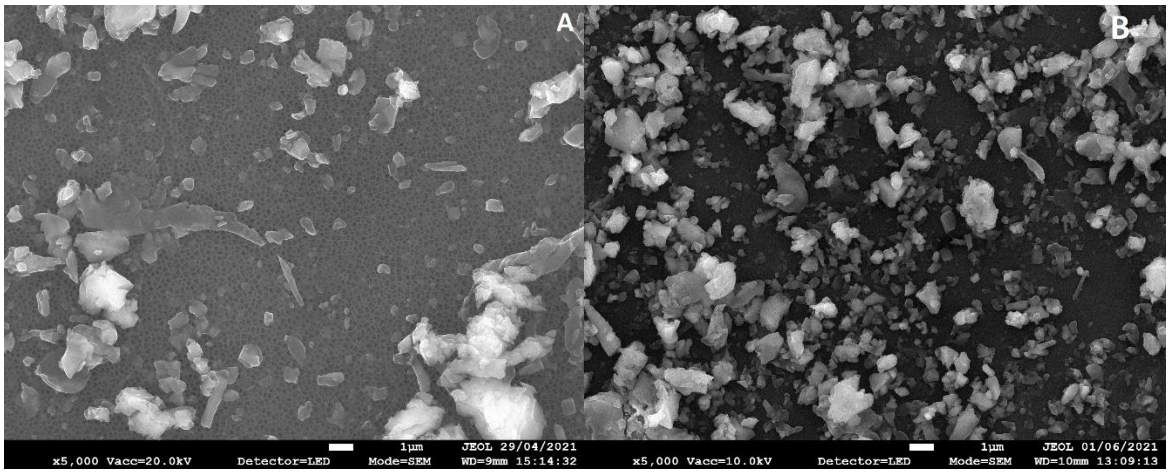

Figure 4.19. EDS images for brand Baltic at x5000. (A) 0.1 μm pore size and (B) 0.02 μm.

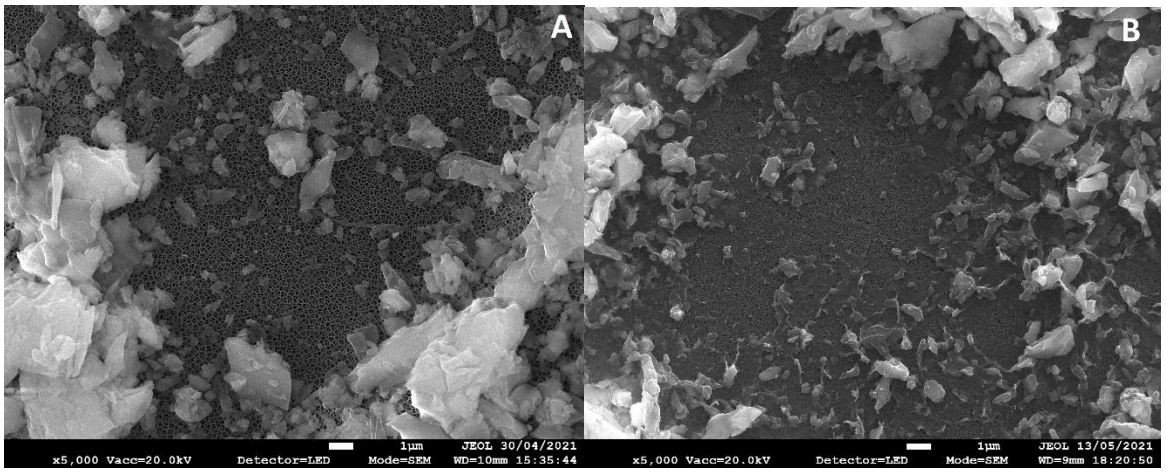

Figure 4.20. EDS images for brand Duronic at x5000. (A) 0.1 μm pore size and (B) 0.02 μm.

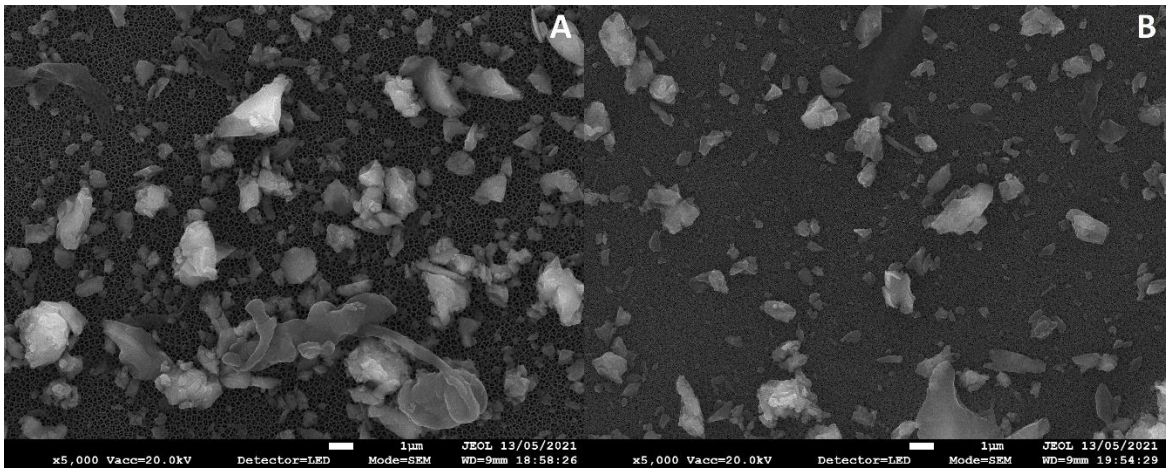

Figure 4.21. EDS images for brand Geji at x5000. (A) 0.1 µm pore size and (B) 0.02 µm.

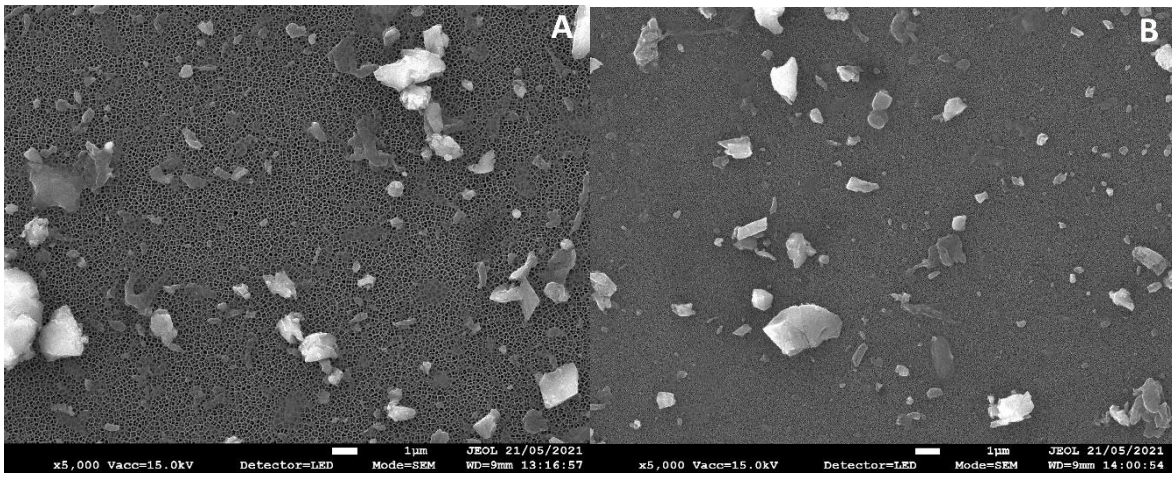

Figure 4.22. EDS images for brand NHS at x5000. (A) 0.1 µm pore size and (B) 0.02 µm.

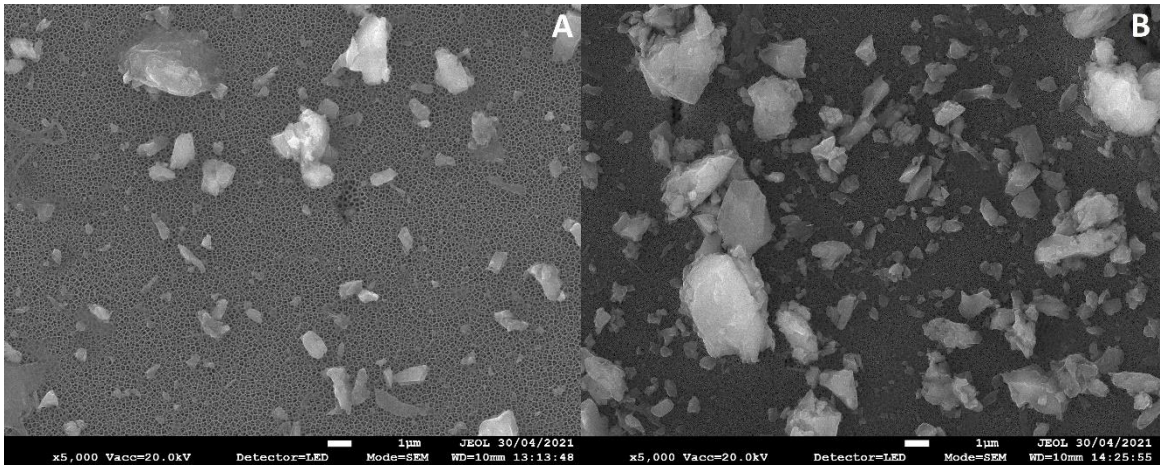

Figure 4.23. EDS images for brand Omnitex at x5000. (A) 0.1 µm pore size and (B) 0.02 µm.

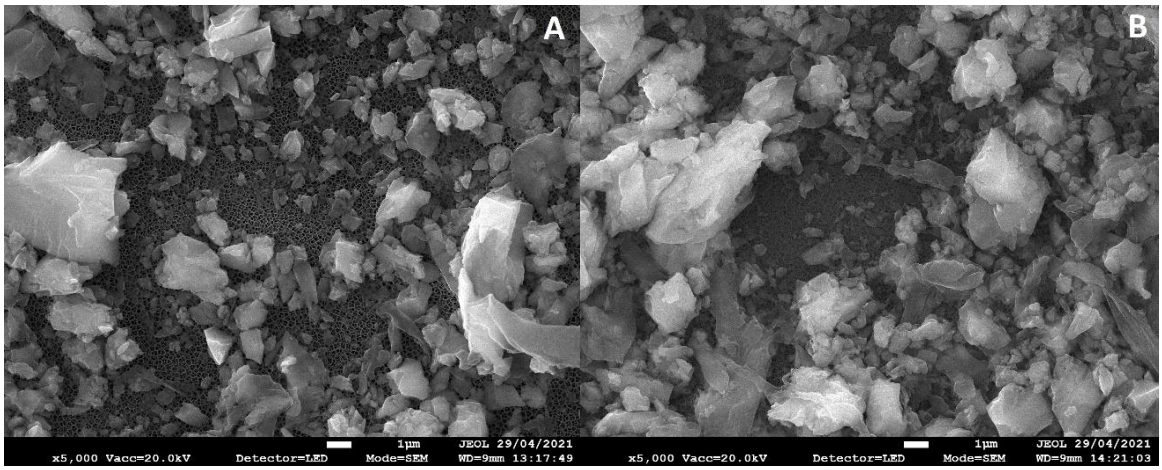

Figure 4.24. EDS images for brand Soyes at x5000. (A) 0.1 µm pore size and (B) 0.02 µm.

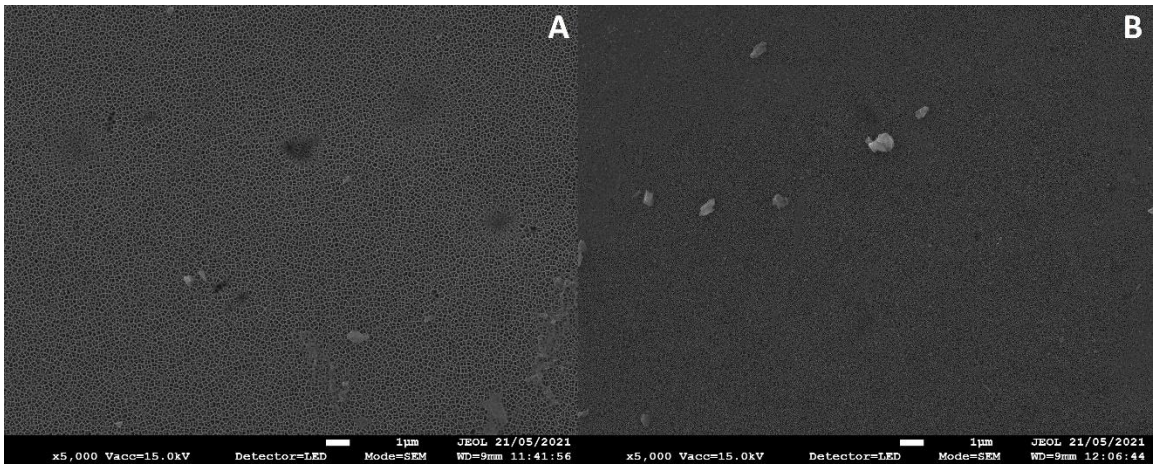

Figure 4.25. EDS images for blank at x5000. (A) 0.1 µm pore size and (B) 0.02 µm.

The presence of nanoparticles (> 100 nm) was also confirmed in all brands (Figure 4.26). These nanoparticles are most likely composed of silica and silica compounds, as most of the particles founds are of this origin, but the possibility of these SiNPs having traces of heavy metals cannot be omitted and it requires further analysis. As it was explained in the introduction of this chapter, SiMPs and SINPs are frequently employed in the production of plastics. The incorporation of silica into the fibre matrix during the stage of fibre formation have been proven to reduce the flammability of the final product. In addition, the formation of aluminium silicate can improve wash permanency and thus, avoiding unwanted leaching during washing procedures[296]. Textiles coated with a layer of SiNPs have been shown to improve the properties of treated fabrics. The UV protection factor of the treated textiles was significantly enhanced, along with the antibacterial and hydrophobic attributes[297].

However, as discussed in the introduction of this chapter, they may pose a risk to human health[239,240]. The interaction of spherical SiO_2 NPs with HaCaT cells has been investigated using particles with a diameter of 50 nm. It was discovered that SiO_2 nanoparticles were easily absorbed by HaCaT cells, where they accumulated in the cytoplasm, lysosomes, and autophagosomes. The cytotoxicity of these grains was demonstrated due to decreased cell viability and compromised cell membrane integrity. The primary cause of the cytotoxicity brought on by SiO2 NPs could be the significant glutathione depletion and reactive oxygen species production that decreased the quantity of cellular antioxidants[298].

This fact directly connects with the fifth objective of this thesis, regarding the evaluation of medical DPFMs as a source of MPs and NPs it also connects with the sixth hypothesis of this thesis that contemplates the potential risks these items pose for both the environment and human health.

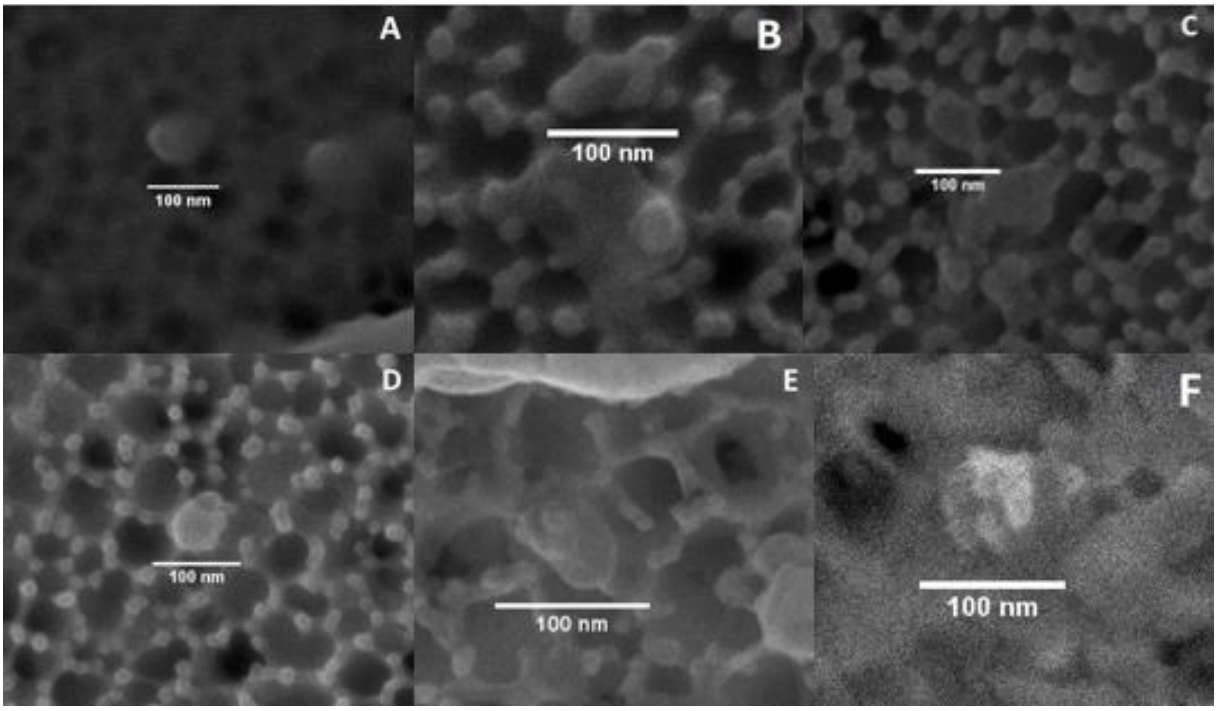

Figure 4.26. Nanoparticles found in all brands and thought to be compounds of silica as the larger particles and fibres found in the same samples. (A) Baltic, (B) Duronic, (C) Geji, (D) NHS, (E) Omnitex and (F) Soyes.

4.3.3. EDS elemental characterization of particles[7]

The composition of the particles and element traces found in all brands and blanks are detailed

[7] Additional EDS information can be found in Appendix A-4.

as follows and the presence of these traces is shown in Table 4.2. Traces of diverse elements and heavy metals like antimony, arsenic, cadmium, chlorine, iron, lead, mercury, nickel, platinum, silicon, tin, titanium, and zinc were found in all brands of this study to a greater or lesser extent.

Particles containing high percentages of iron (Fe) have been observed as part of bigger particles (Figure 4.27) and as part of fibres (Figure 4.28). Fibres also contained Si on their structure (Figure 4.28(d)). DPFMs usually have a nose strip that may be made of steel, and possibly PVC/PE.

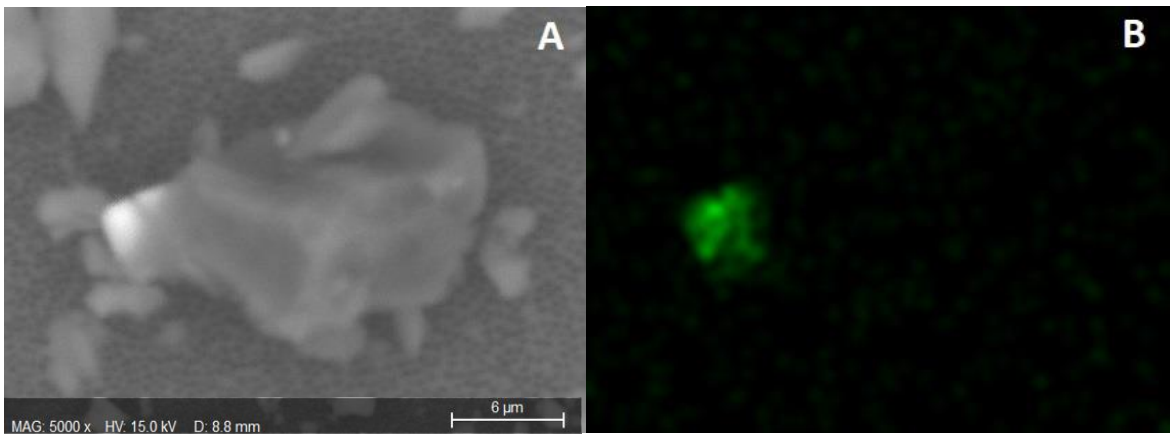

Figure 4.27. SEM image of a particle containing iron (Fe). This metal can be observed as part of the larger particle. (A) SEM generated image, (B) is a false colour map for elemental Fe.

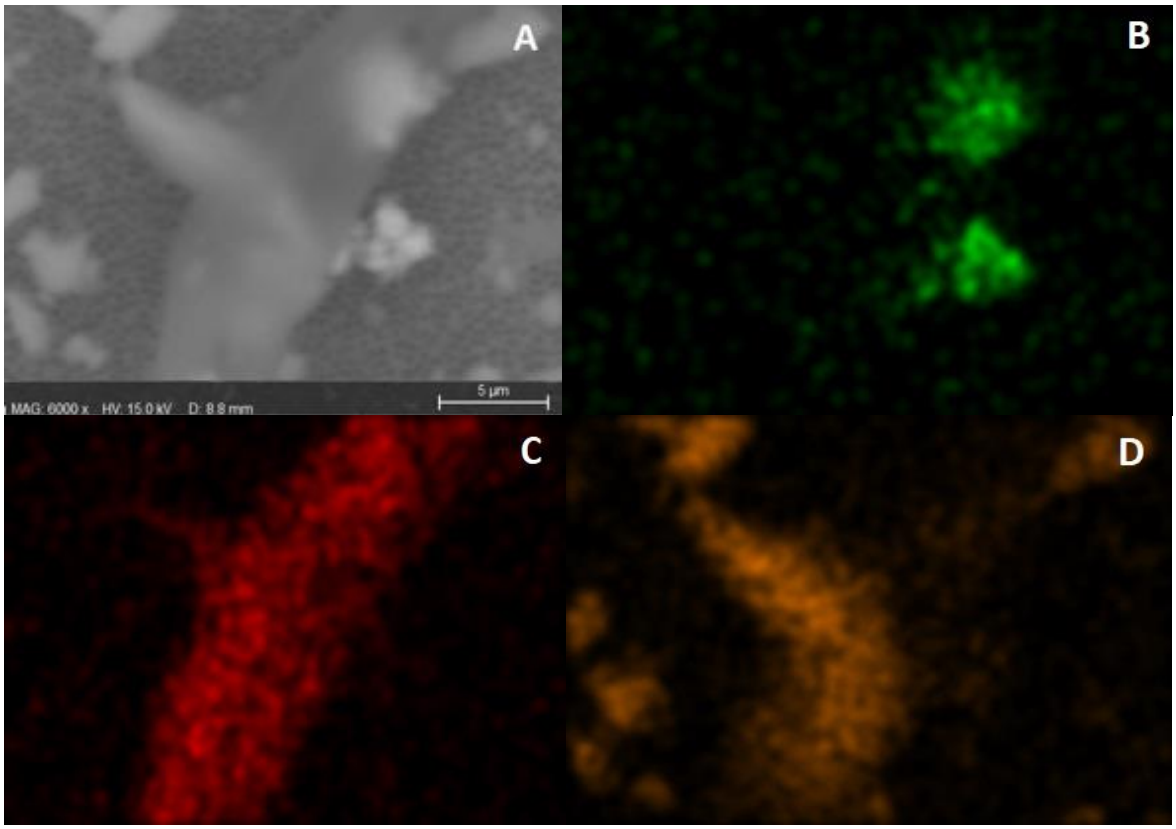

Figure 4.28. SEM image of a fibre with composed of mostly silicon and oxygen but also presenting iron. (A) is the image generated by the SEM, (B) is a false colour map for elemental Fe. (C) is a false colour map for elemental C and (D) is a false colour map for elemental Si.

Complex particles with high percentages of Fe and traces of many different heavy metals were found in NHS samples. Among the heavy metals found were Hg, Sb, Pb, As and Cd (Figure 4.29). The risks that these metals pose for the environment and human health have been detailed in chapter 3. The detection of Hg traces was totally unexpected. Not just because they were not found in the experiments carried out in Chapter 3 for non-medical DPFMs, but also because, as discussed in the introduction, the Information on fibre composition must be disclosed in accordance with European Regulation 1007/2011, and specific levels of metals cannot be contained in textile products sold in Europe. The legal limit in textiles for Hg is 0.02 µg/g. Nevertheless, a study of different textiles showed that Hg was found in samples analysed with concentrations between 0.0818 and 0.375 µg/g and thus, some of the textile items that were sold commercially in Europe and were part of this study did not adhere to European Regulation[182]. Hg is a global pollutant that affects human and ecosystem health. It is well documented that prenatal or postnatal exposure have negative neurological effects on both adults and children[299]. According to previous studies, prenatal

exposure to Hg is associated with a low birth weight, delayed neurodevelopment, and poor child growth and development. Mercury is a neurodevelopmental toxin, which puts the developing foetus and small children at particular risk. High methylmercury exposure during pregnancy has been linked to neurocognitive impairments, infantile cerebral palsy, and severe congenital malformations. Adults who have been exposed may experience neurological symptoms such ataxia, tremor, and issues with coordination[300]. For these reasons, the author of this thesis considers necessary to continue this investigation with further analysis in order to clarify the significant of the potential direct exposure to Hg and other metals that DPFMs pose.

B

Spectrum: Point

Element	AN	Series	Net	unn. C [wt.%]	norm. C [wt.%]	Atom. C [at.%]
Iron	26	K-series	591	104.19	57.07	64.03
Chromium	24	K-series	81	8.57	4.69	5.65
Selenium	34	L-series	84	8.41	4.61	3.66
Lead	82	M-series	61	5.65	3.09	0.94
Antimony	51	L-series	54	4.92	2.69	1.39
Mercury	80	M-series	52	4.71	2.58	0.81
Platinum	78	M-series	50	4.60	2.52	0.81
Cobalt	27	K-series	18	4.24	2.32	2.47
Nickel	28	K-series	14	3.96	2.17	2.31
Copper	29	K-series	9	3.73	2.04	2.01
Arsenic	33	L-series	31	3.65	2.00	1.67
Cadmium	48	L-series	43	3.47	1.90	1.06
Chlorine	17	K-series	63	3.06	1.67	2.96
Tellurium	52	L-series	29	2.82	1.54	0.76
Silicon	14	K-series	48	2.58	1.41	3.15
Tin	50	L-series	26	2.26	1.24	0.65
Palladium	46	L-series	24	1.81	0.99	0.58
Ruthenium	44	L-series	23	1.70	0.93	0.58
Manganese	25	K-series	11	1.53	0.84	0.95
Vanadium	23	K-series	16	1.52	0.83	1.02
Silver	47	L-series	19	1.48	0.81	0.47
Zinc	30	K-series	2	1.32	0.72	0.69
Titanium	22	K-series	13	1.11	0.61	0.80

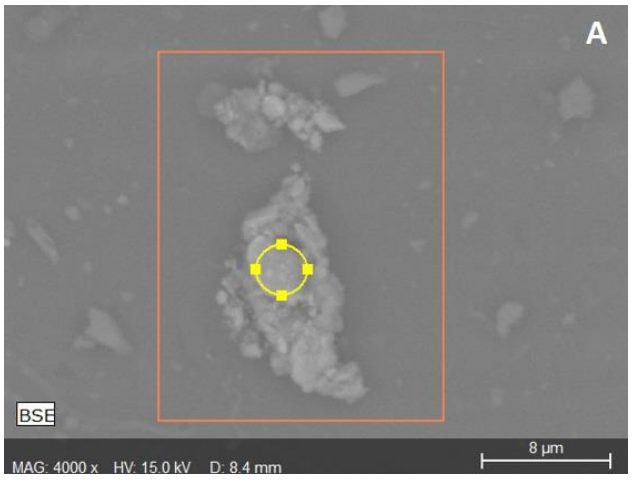

B

Spectrum: Point

Element	AN	Series	Net	unn. C [wt.%]	norm. C [wt.%]	Atom. C [at.%]
Iron	26	K-series	269	108.67	77.09	84.38
Titanium	22	K-series	15	3.98	2.83	3.61
Selenium	34	L-series	11	3.81	2.71	2.09
Platinum	78	M-series	10	3.07	2.18	0.68
Antimony	51	L-series	11	3.05	2.16	1.09
Bismuth	83	M-series	10	3.00	2.13	0.62
Ruthenium	44	L-series	10	2.41	1.71	1.04
Cadmium	48	L-series	9	2.21	1.57	0.85
Mercury	80	M-series	7	2.03	1.44	0.44
Zinc	30	K-series	2	2.03	1.44	1.35
Palladium	46	L-series	8	1.83	1.30	0.74
Manganese	25	K-series	5	1.61	1.14	1.27
Tellurium	52	L-series	5	1.57	1.11	0.53
Vanadium	23	K-series	3	0.83	0.59	0.71
Chromium	24	K-series	2	0.40	0.29	0.34
Tin	50	L-series	1	0.32	0.23	0.12
Silicon	14	K-series	0	0.06	0.04	0.09
Arsenic	33	L-series	0	0.05	0.03	0.03
Chlorine	17	K-series	0	0.02	0.01	0.02
Cobalt	27	K-series	0	0.00	0.00	0.00

Figure 4.29. EDS data referring to the composition of complex particles from NHS face mask. (A) are the images generated by the SEM at x4000 and (B) are the tabulated elemental composition data. It can be observed that concerning heavy metals like lead, antimony and mercury are amongst the elements detected. The complexity of this particles is noticeable.

A complete summary of the various chemical components found in this part of the investigation can be observed in Table 4.2.

Table 4.2. The different chemical elements found in particles deposited on the inorganic membranes after filtration. √ refers to presence of the element. Adapted from Delgado-Gallardo et al., 2022.

Suspected compound	**Procedural Blank**	**Baltic**	**Geji**	**Soyes**	**Duronic**	**NHS**	**Omnitex**
		FFP2			**Type IIR**		
Antimony	ND	√	ND	ND	√	√	ND
Arsenic	ND	√	√	√	√	√	√
Cadmium	ND	√	ND	ND	√	√	√
Iron	ND	√	√	√	√	√	√
Lead	ND	√	ND	ND	√	√	√
Mercury	ND	ND	ND	ND	√	√	√
Nickel	ND	√	√	√	√	√	√
Platinum	ND	√	√	√	√	√	√
Silicon	√	√	√	√	√	√	√
Tin	ND	ND	ND	ND	√	√	√
Tellurium	ND	√	√	√	√	√	√
Titanium	ND	√	√	√	√	√	√
Zinc	ND	ND	√	√	√	ND	ND

The particles found after filtration of the blank samples were mostly composed of silica in high percentage with low traces of other elements (like chlorine and platinum). Nevertheless, there particles were not as complex as the ones found with the submersion of DPFMs and no heavy metals were detected (Figure 4.30). The amount of particles found was significantly lower compared with the leachates that had DPFMs submerged.

B

Spectrum: Point

Element	AN	Series	Net	unn. C [wt.%]	norm. C [wt.%]	Atom. C [at.%]
Silicon	14	K-series	753	13.07	96.77	98.09
Chlorine	17	K-series	8	0.29	2.14	1.72
Platinum	78	M-series	2	0.12	0.92	0.13
Titanium	22	K-series	0	0.00	0.01	0.00
Vanadium	23	K-series	0	0.00	0.01	0.00
Chromium	24	K-series	0	0.00	0.01	0.00
Manganese	25	K-series	0	0.00	0.01	0.00
Iron	26	K-series	0	0.00	0.01	0.00
Cobalt	27	K-series	0	0.00	0.01	0.00
Nickel	28	K-series	0	0.00	0.01	0.00
Copper	29	K-series	0	0.00	0.01	0.00
Zinc	30	K-series	0	0.00	0.01	0.00
Cadmium	48	L-series	0	0.00	0.01	0.00
Rhodium	45	L-series	0	0.00	0.01	0.00
Palladium	46	L-series	0	0.00	0.01	0.00
Silver	47	L-series	0	0.00	0.01	0.00

Figure 4.30. EDS data referring to the composition of a particle found in Blank sample. (A) is the image generated by the SEM at x5000, (B) is the tabulated elemental composition data.

The release of synthetic fibres, particles and heavy metals proven in this paragraph and the previous one connects with the third objective of this thesis, regarding the ascertain of the potential risk for ecosystems and human health and it also connects with the fifth hypothesis of this thesis regarding DPFMs to be proven as a new source of MPs and NPs, chemicals and other pollutants.

More examples of the different particles found in this study and their composition can be observed in Appendix A-4, Figures A-4.59 to A-4.61.

4.3.4. ICP-MS results[8]

Following the methodology employed in the previous chapter, in order to determine the analyte concentration for ICP-MS analysis of samples, a complete external calibration was performed. Additionally, reagent and procedural blanks were performed before and after sample analysis to evaluate any potential carryover. All QC determinants for Ag, As, Cd, Co, Cr, Cu, Mo, Ni Pb, Sb, Ti, V, and Hg passed acceptance criteria. For blank samples, all values possessing concentration values below the analytical detection limits, except for Cu, Mo, Pb and V, subsequently any positives in samples were blank subtracted and corrected.

As commented on paragraph 4.2.1, three masks of each brand, as opposed to one as in the previous chapter, were placed in brand-new glass flasks holding 250 mL of deionized water and remained immersed for the 24-hour period typical of leachate analysis in environmental laboratories. This strategy was adopted following an experiment in which only one mask was

[8] Additional ICP-MS information can be found in Appendix A-4.

used (after experiments carried out in previous chapter), which revealed that the levels of chemical pollutants were significantly lower than anticipated. The results of this first study can be observed in Table A-4.3 of Appendix A-4. As a result, it is assumed that the medical DPFMs used in this chapter contain fewer chemicals and other components because they do not contain as many different dyes as the DPFMs examined in Chapter 3.

As in the previous chapter, a table is provided to show the leachable heavy metals from the medical DPFMs determined by ICP-MS analysis of the sub sampled water (Table 4.3). Again, these given values in Table 4.3 are the averages of the triplicates examined for each sample as provided by the technicians at Tata Steel (Port Talbot). Following the same previous approach, and to facilitate a better comprehension of the data collected, the table included the LOD values from the data supplied in Figures A-4.46 to A-4.58 in Appendix A-4. Also, the average, standard deviation and RSD have been calculated from the three quality control measurements provided and included in the table. RSD results for all metal elements are below 5% and thus, all of them are considered optimal.

Also as in Chapter 3, the different graphs representing each examined mask and the analysed concentration of the metals selected for this part of the investigation can be observed in Figures 4.31 to 4.36. To provide a graphical representation of the data variability and the validation of the results, the error bars for each element related to each of the standard deviations calculated from the QC data are also provided. The negative values, which are assumed as indicators of that element being absent in the sample, are also represented in order to give a better visualisation of those elements not detected. The values given are expressed in ppb. Table 4.4 shows the highlighted results for the main heavy metals found and calculated to µg/L.

Table 4.3. Raw data containing the averages of the triplicates examined for each sample as provided by the technicians at Tata Steel (Port Talbot), along with the limit of detection (LOD), quality controls (QC), QC averages, QC standard deviation and QC relative standard deviation (RSD). These results are for samples prepared submerging 3 medical DPFMs in 250 ml of deionized water as explained above.

Sample Id	Ag (ppb)	As (ppb)	Cd (ppb)	Co (ppb)	Cr (ppb)	Cu (ppb)	Mo (ppb)	Ni (ppb)	Pb (ppb)	Sb (ppb)	Ti (ppb)	V (ppb)	Hg (ppb)
Reagent blank	0.00	0.00	0.00	-0.01	0.21	0.17	-0.20	0.03	0.09	0.07	0.01	0.01	-0.194
Procedure blank	0.00	-0.02	-0.03	-0.01	0.21	0.17	0.31	0.61	-0.02	0.31	-0.26	0.02	-0.228
Baltic	0.01	0.03	-0.03	0.04	0.56	1.28	0.03	0.05	0.01	29.27	0.00	0.01	-0.239
Duronic	-0.01	-0.02	0.01	-0.01	0.01	2.59	0.08	0.18	0.01	0.13	-0.21	0.02	-0.232
Geji	0.00	0.02	-0.01	-0.01	0.18	2.57	0.23	0.83	0.06	4.06	-0.26	0.01	-0.224
NHS	0.00	-0.02	-0.02	-0.01	0.01	0.95	-0.01	0.08	0.00	0.10	-0.16	0.01	-0.228
Omnitex	-0.01	0.01	0.01	-0.01	0.02	56.29	0.00	0.30	0.63	4.79	0.05	0.02	-0.227
Soyes	-0.01	-0.03	-0.01	-0.01	0.03	0.57	-0.04	0.07	-0.01	2.10	-0.21	0.01	-0.207
LOD (ppb)	>0.01	>0.13	>0.01	>0.01	>0.03	>0.10	>0.03	>0.07	>0.01	>0.10	>1.0	>0.01	>0.05
QC 10	10.04	10.19	9.91	10.09	10.08	10.10	9.65	10.43	10.18	10.19	9.89	10.03	5.13 (QC 5)
QC 10	9.91	10.14	10.00	9.99	10.22	9.87	10.42	10.31	9.97	10.35	10.17	9.70	5.02 (QC 5)
QC 10	9.98	9.52	9.79	9.94	9.90	9.82	9.96	9.94	10.22	9.70	10.30	9.89	5.41 (QC 5)
Average QC	9.98	9.95	9.90	10.01	10.07	9.93	10.01	10.23	10.13	10.08	10.12	9.87	5.22
QC Standard Dev (±)	0.05	0.30	0.09	0.06	0.13	0.12	0.32	0.21	0.11	0.28	0.17	0.13	0.19
RSD (%)	0.54	3.06	0.90	0.59	1.30	1.25	3.19	2.03	1.08	2.76	1.68	1.36	3.72

In line with the results provided in chapter 3, all medical DPFMs in this experiment showed some level of Cu. Nevertheless, these are lower concentrations and only the brand Omnitex presented a significant outcome (average of 56.29 ppb). As mentioned in the previous chapter, Cu compounds are used in textile industry due to its antibacterial properties and are also used as catalysts[177].

The only other remarkable concentration found was that of Sb on Baltic brand DPFMs, of 29.27 ppb. As Cu, Sb is commonly found in polyester fibres due to its application as a catalyst in the manufacturing of polyethylene terephthalate and as a flame retardant synergist[256].

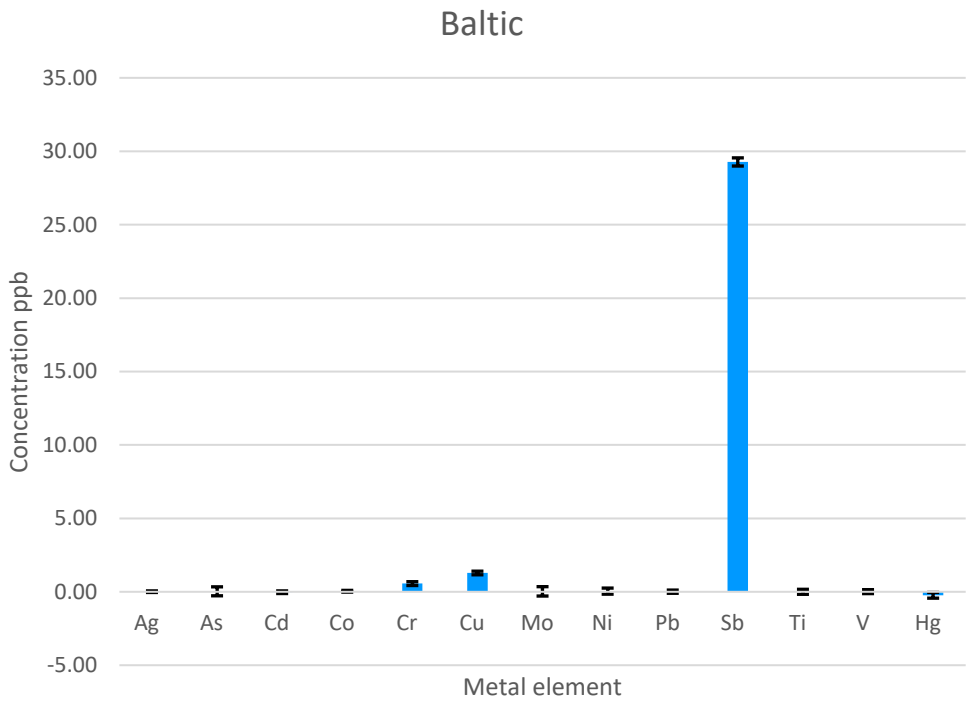

Figure 4.31. EDS data graph with error bars for DPFM brand Baltic representing the analysed concentration (ppb) of each of the metals selected. Sb is the metals with higher concentration.

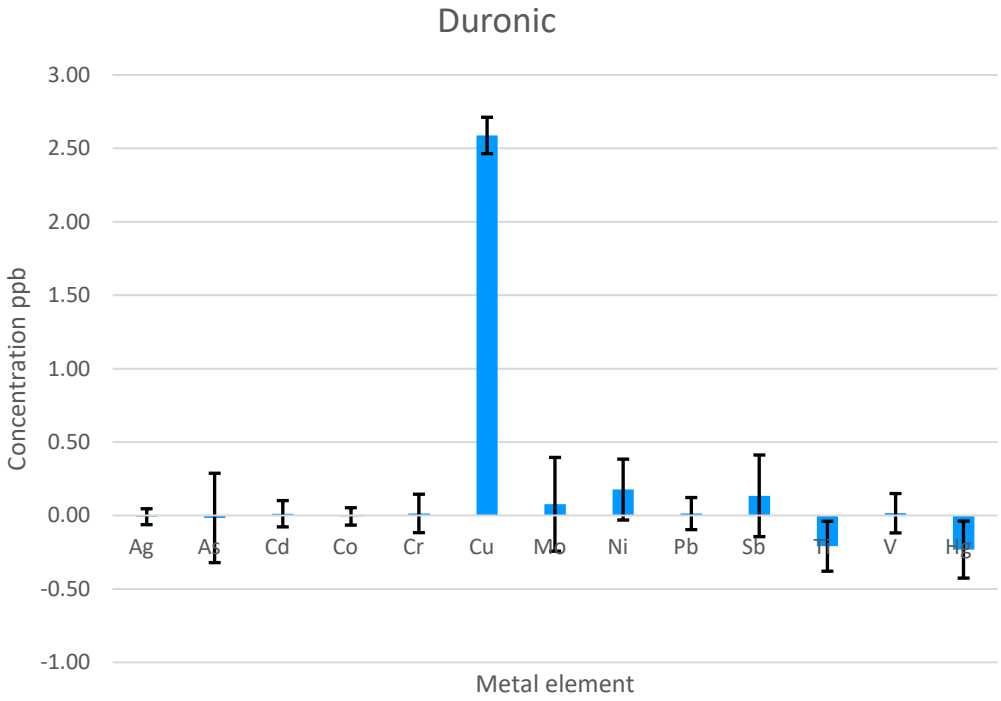

Figure 4.32. EDS data graph with error bars for DPFM brand Duronic representing the analysed concentration (ppb) of each of the metals selected. Cu is the metals with higher concentration.

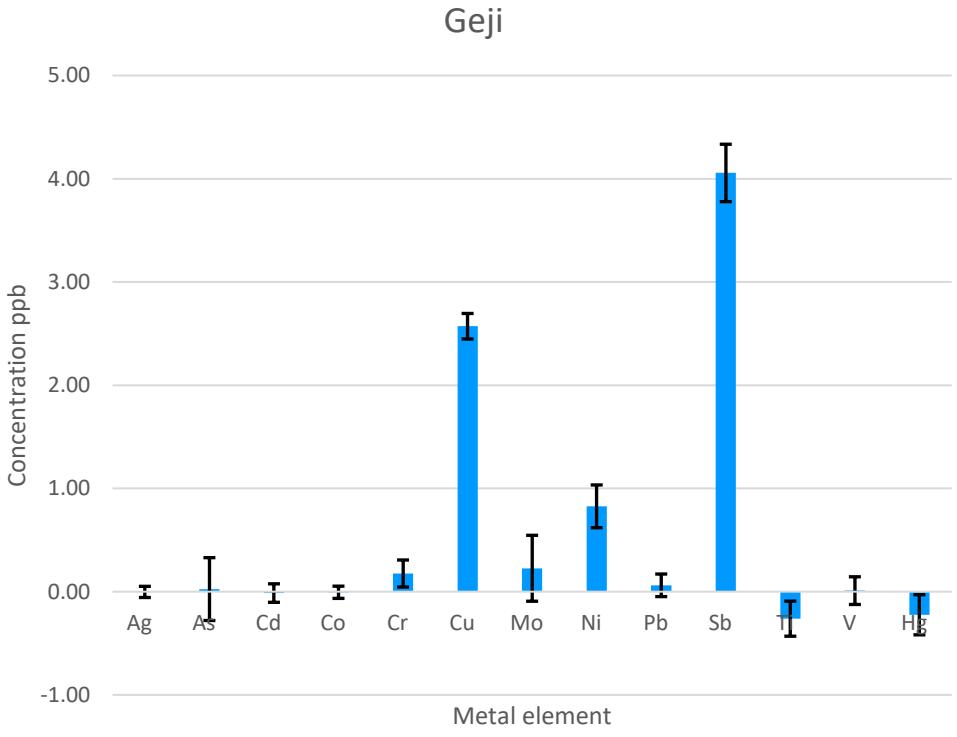

Figure 4.33. EDS data graph with error bars for DPFM brand Geji representing the analysed concentration (ppb) of each of the metals selected. Cu and Sb are the metals with higher concentrations.

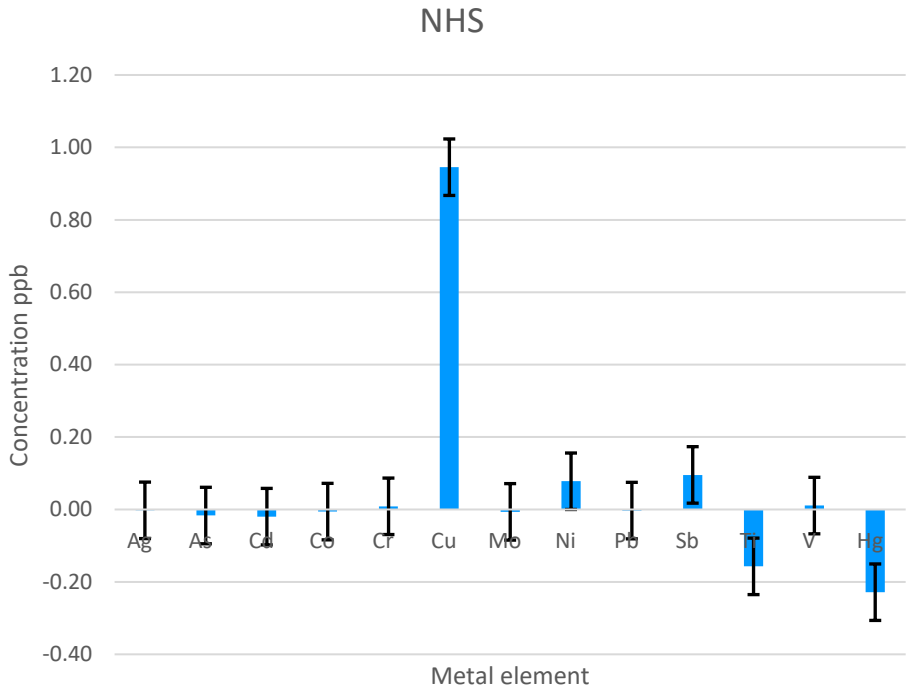

Figure 4.34. EDS data graph with error bars for DPFM brand NHS representing the analysed concentration (ppb) of each of the metals selected. Cu is the metals with higher concentration.

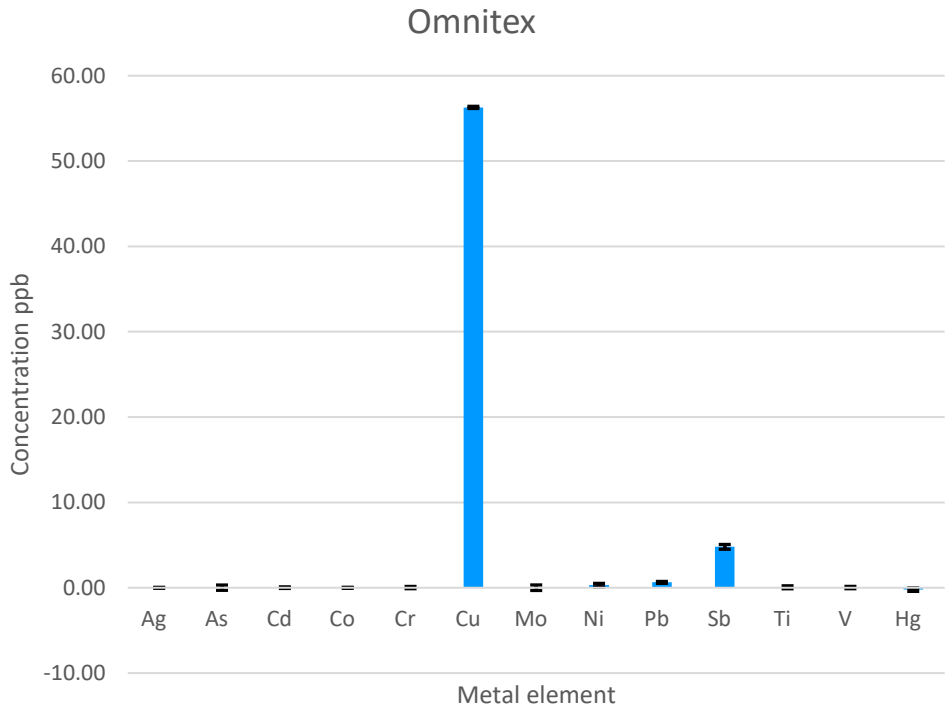

Figure 4.35. EDS data graph with error bars for DPFM brand Omnitex representing the analysed concentration (ppb) of each of the metals selected. Cu is the metals with higher concentration.

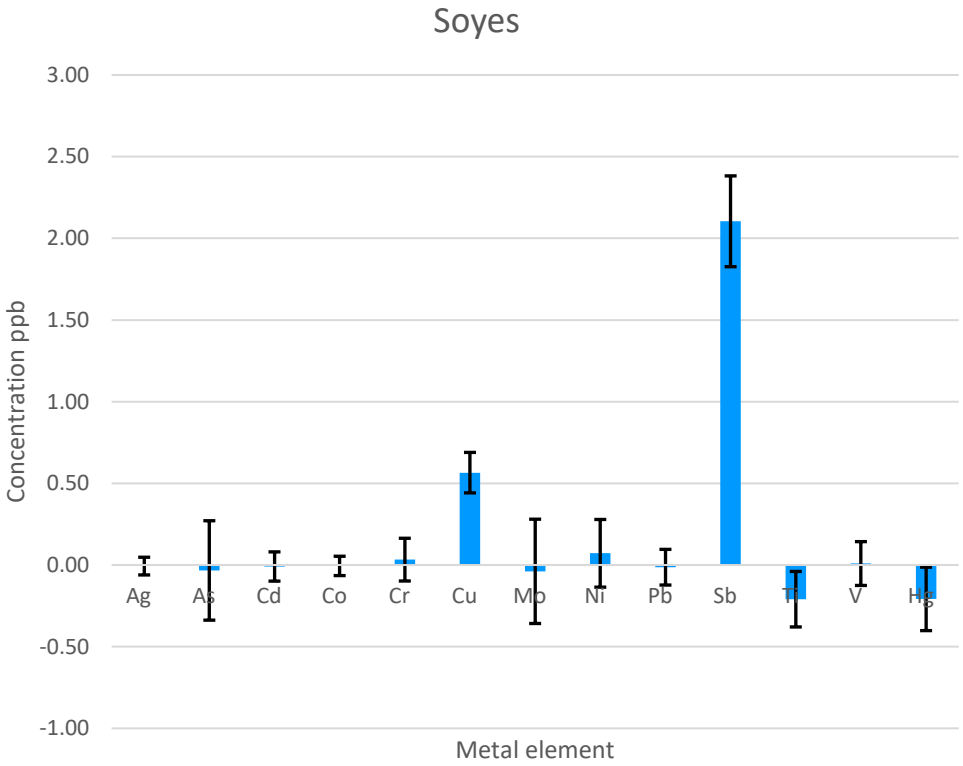

Figure 4.36. EDS data graph with error bars for DPFM brand Soyes representing the analysed concentration (ppb) of each of the metals selected. Sb is the metals with higher concentration.

Table 4.4 shows the concentrations of leachable heavy metals from the medical DPFMs converted to µg/L. Following the same procedure shown in Chapter 3, the ppb results from Table 4.3 were divided by 4 as the DPFMs were submerged in 250ml of deionised water and further divided by 3 as three DPFMs from each brand were submerged for this experiment instead of one, as explained in paragraph 4.2.1.

The metal levels found in medical DPFMs leachate were all typically low levels, with majority being sub parts per billion (ppb) level, and some not detected altogether (As and Hg). As previously commented, the highest concentrations of metals were found to be Cu for Omnitex mask leachate at 4.68 ug/L and Sb in the Baltic mask leachate at 2.41 µg/L.

Overall, medical masks appear to have significantly lower levels of trace metals than previously analysed ones in Chapter 3. Upon the comparison of Sb and Pb levels present in medical mask leachates analysed in this chapter and mask 5 (Type II R) of Chapter 3, Sb in medical DPFMs ranged from 0.01-2.41 µg/L and Pb >0.001-0.005 µg/L, whereas in mask 5 had higher levels of Sb ca. 3 µg/L, and Pb values up to 0.75 µg/L indicating a significant increase in emission in type II masks (Table 3.4).

Again, analysis for the toxic metals Cd, Ni and Cr emission proved negligible in medical masks. Cd was found at very low concentration levels in Duronic and Omnitex mask leachates, with a slight elevation of Chromium detected in Geji, Soyes and Baltic samples (0.015-0.033 µg/L). Nickel was found in all masks apart from Baltic, likely to arise from the metal wiring parts if the mask, but this was still at very low levels (0.006 - 0.025 µg/L) (See Table 4.3).

These results are linked to the fourth and fifth objectives of this thesis and also confirm the fifth hypothesis of this thesis regarding DPFMs to be proven as a new source of MPs and NPs, chemicals and other pollutants.

Further analyses are recommended in order to elucidate the discrepancy in the results and to corroborate the potential risks that DPFMs pose due to containing heavy metals.

Table 4.4. Results of metals leached from medical DPFMs converted to µg/L. To calculate the values to 1 mask per L, the ppb concentrations obtained during the experiment (see Table 4.3) were blank corrected and then divided by a factor of 12. Adapted from Delgado-Gallardo et al., 2022.

Sample Identity	**As**	**Cd**	**Co**	**Cr**	**Cu**	**Mo**	**Ni**	**Pb**	**Sb**	**Ti**
	µg/L									
Baltic	ND	ND	0.003	0.029	0.093	0.003	ND	ND	2.413	0.001
Duronic	ND	0.001	ND	ND	0.201	0.006	0.015	0.001	0.011	0.001
Geji	ND	ND	ND	0.015	0.2	0.083	0.018	0.005	0.312	0.001
NHS	ND	ND	ND	ND	0.065	>0.03	0.007	ND	ND	0.001
Omnitex	ND	0.001	ND	ND	4.676	>0.03	0.025	0.005	0.373	0.002
Soyes	ND	ND	ND	0.033	0.033	>0.03	0.006	ND	0.149	ND

4.3.5. LC-MS results

Based on precise mass measurements, ms/ms fragmentation information and analyst discrimination, the organic contaminants found in the leachate were identified. Polymeric species of caprolactam, $-(C_6H_{11}NO)_n-$, a precursor for Nylon 6 or 66 with peaks at between

7.5 – 9.5 mins [m/z 209, 227, 249] 13.5 mins [m/z 322, 340 and 362], 14.6 mins [m/z 435, 453 and 475], 15.3 mins [m/z 548, 566, and 588] and 15.7 [m/z 679, 701] was found in samples, SOYES, NHS, Duronic, and Geji. Figure 4.37 shows an example of these peaks for brand Geji and their composition can be observed in Figure 4.38. These peaks were not identified in Baltic, Omnitex samples and both system and procedural blank samples (Table 4.5). As documented in Chapter 3, nylon is typically used in the elasticized portions of DPFMs and may be woven into multiple layers of the face covering[289] and these types of compounds were expected to be found in these samples as well. To illustrate these findings, Figure 4.37 represents the total ion chromatogram (TIC) and the mass spectrums for the associated peaks of the TIC for one of the brands (Geji) tentatively identified as Caprolactam and oligomers of this organic compound.

As in Chapter 3, the formation of sodiated adducts was also recorded. Following the same approach and in order to evaluate any potential background and carryover, a procedural blank was injected in between samples. The blanks verified there was no sample carryover, and the background was clear of any ions from the samples. Of the compounds identified in the leachates, none of these species were identified in the procedural blank (Figure 4.38).

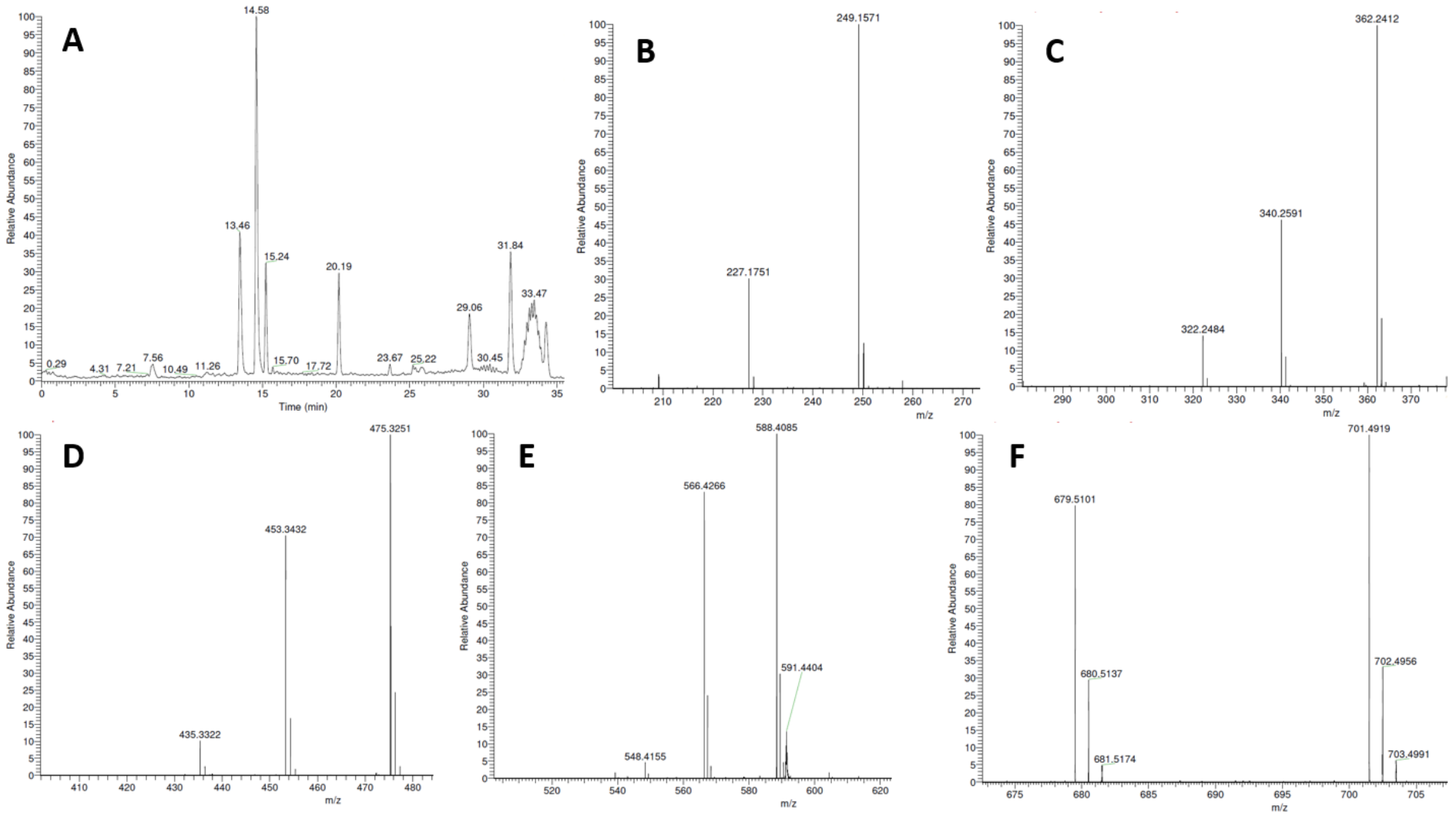

Figure 4.37. LC-MS representative spectra obtained from Leachate sample from brand Geji. Top A is the total ion chromatogram (TIC) and B-F are mass spectrums for the associated peaks of the TIC. Peak at Rt 7.73 has a mz of 249.1572 (B) was tentatively identified as Caprolactam. Mass spectrums C, D, E and F are therefore, likely to be oligomers of Caprolactam. More information regarding peak identity can be found in Figure 4.38..

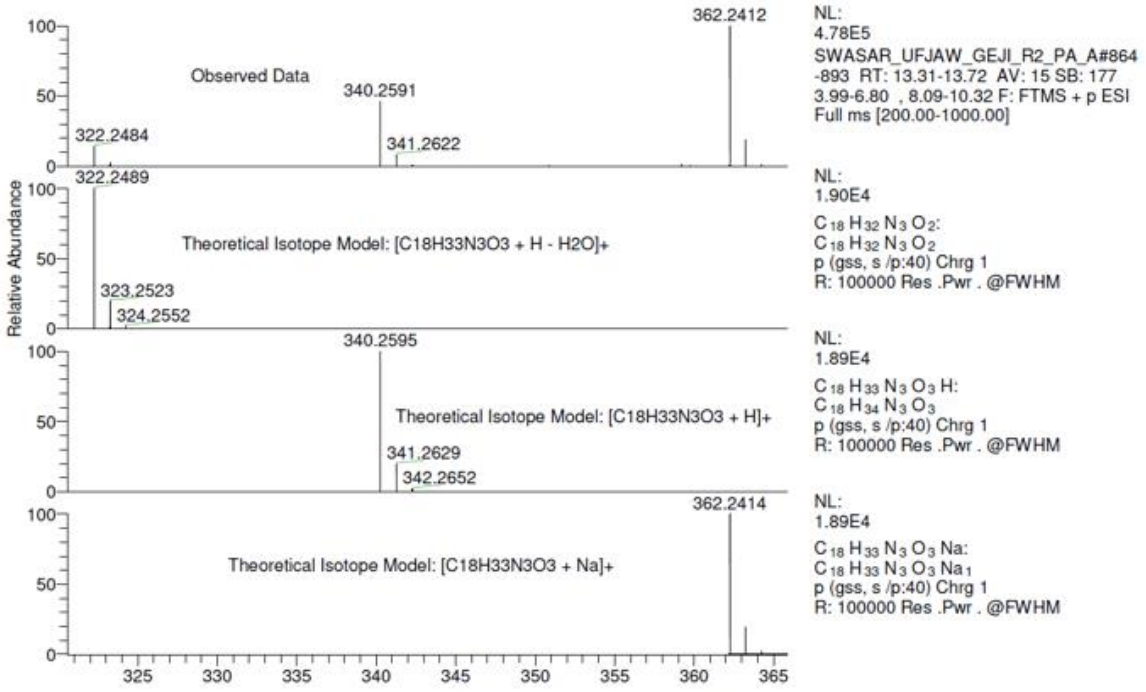

Isotope:	Min. .. Max.
14 N	0....15
16 O	0....25
12 C	0....80
1 H	0....100
23 Na	0....1
Tolerance Window:	+- 5.00 ppm
Db/Ring Equiv:	-3.. 100
Fits:	300

N-Rule:	Do not use
Charge:	1

Mass	Theoretical Mass	Delta [ppm]	RDB	Composition
322.2484	322.2489	-1.6	4.5	$C_{18} H_{32} O_2 N_3$
	322.2476	2.6	5.0	$C_{16} H_{30} O_1 N_6$
	322.2494	-3.1	-2.5	$C_3 H_{28} O_3 N_{15}$
340.2591	340.2595	-1.1	3.5	$C_{18} H_{34} O_3 N_3$
	340.2581	2.9	4.0	$C_{16} H_{32} O_2 N_6$
362.2412	362.2411	0.2	2.0	$C_{17} H_{34} O_6 N_2$
	362.2411	0.2	7.5	$C_{16} H_{28} O_1 N_9$
	362.2414	-0.6	3.5	$C_{18} H_{33} O_3 N_3 Na_1$
	362.2401	3.1	4.0	$C_{16} H_{31} O_2 N_6 Na_1$
	362.2425	-3.5	7.0	$C_{18} H_{30} O_2 N_6$
	362.2398	3.9	2.5	$C_{15} H_{32} O_5 N_5$
	362.2398	3.9	8.0	$C_{14} H_{26} N_{12}$
	362.2428	-4.3	3.0	$C_{20} H_{35} O_4 Na_1$

Figure 4.38. LC-MS representative spectra for peaks with mz 322, 340 and 362 in the data for brand Geji, associated to nylon-type ions (highlighted in yellow).

Ions consistent with polyethylene glycol polymers (homologues series separated by m/z 44) were observed in all sample leachates and not in the blanks, indicating evidence of organic substance release from the facemasks. Similar organic compounds were present in Type II medical masks analysed in previous study. PEG like and detergent compounds are likely to

be associated with plasticizers used in modifying the plastic properties during in manufacture of the DPFM plastic material[301,302]. PEG, as it was discussed in Chapter 1, is also added to the treated fabrics in order to increase their tensile strength, resistance to creases, water absorption, and abrasion resistance[188]. PEG is known for its antifouling qualities as well[189]. For these reasons, and because these contaminants were detected in the leachate samples in Chapter 3, it was expected that they would also be detected in these analyses.

Triton X, another organic compound, was found in all DPFMs brands, with peaks at 29.1 mins [m/z 383.2765], 31.9 mins m/z [455.3338] and 34.2 mins m/z [527.3910] (Figure 4.39) The detection of this substance was not expected, more even when they were not detected when running previous test for non-medical masks. The fact that both system and procedural blanks showed no trace of these compounds verify that no contamination of the samples took place, and that triton is indeed leaching from the analysed masks.

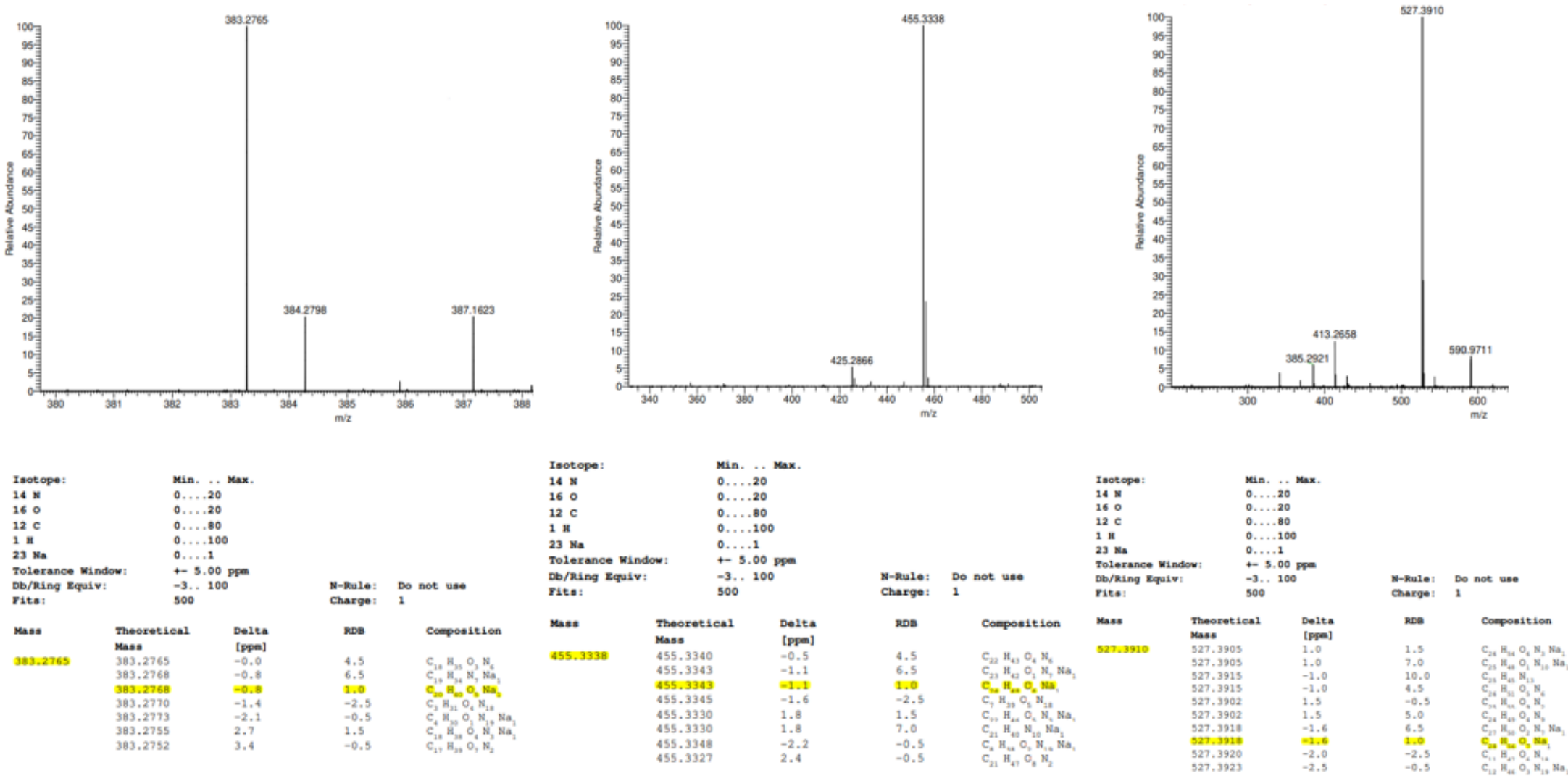

Isotope:	Min. .. Max.
14 N	0....20
16 O	0....20
12 C	0....80
1 H	0....100
23 Na	0....1
Tolerance Window:	+- 5.00 ppm
Db/Ring Equiv:	-3.. 100
Fits:	500

N-Rule:	Do not use
Charge:	1

Mass	Theoretical Mass	Delta [ppm]	RDB	Composition
383.2765	383.2765	-0.0	4.5	$C_{18}H_{35}O_3N_6$
	383.2768	-0.8	6.5	$C_{19}H_{34}N_3Na_3$
	383.2768	-0.8	1.0	$C_{20}H_{40}O_6Na_2$
	383.2770	-1.4	-2.5	$C_2H_{31}O_4N_{16}$
	383.2773	-2.1	-0.5	$C_4H_{30}O_2N_{13}Na_3$
	383.2755	2.7	1.5	$C_{16}H_{36}O_4N_3Na_3$
	383.2752	3.4	-0.5	$C_{17}H_{39}O_3N_2$

Isotope:	Min. .. Max.
14 N	0....20
16 O	0....20
12 C	0....80
1 H	0....100
23 Na	0....1
Tolerance Window:	+- 5.00 ppm
Db/Ring Equiv:	-3.. 100
Fits:	500

N-Rule:	Do not use
Charge:	1

Mass	Theoretical Mass	Delta [ppm]	RDB	Composition
455.3338	455.3340	-0.5	4.5	$C_{22}H_{43}O_4N_6$
	455.3343	-1.1	6.5	$C_{23}H_{42}O_3N_3Na_3$
	455.3343	-1.1	1.0	$C_{24}H_{48}O_6Na_2$
	455.3345	-1.6	-2.5	$C_7H_{39}O_5N_{18}$
	455.3330	1.8	1.5	$C_{10}H_{44}O_4N_{15}Na_3$
	455.3330	1.8	7.0	$C_{23}H_{40}N_{10}Na_2$
	455.3348	-2.2	-0.5	$C_8H_{46}O_7N_{14}Na_3$
	455.3327	2.4	-0.5	$C_{21}H_{47}O_8N_2$

Isotope:	Min. .. Max.
14 N	0....20
16 O	0....20
12 C	0....80
1 H	0....100
23 Na	0....1
Tolerance Window:	+- 5.00 ppm
Db/Ring Equiv:	-3.. 100
Fits:	500

N-Rule:	Do not use
Charge:	1

Mass	Theoretical Mass	Delta [ppm]	RDB	Composition
527.3910	527.3905	1.0	1.5	$C_{26}H_{54}O_6N_3Na_3$
	527.3905	1.0	7.0	$C_{25}H_{48}O_1N_{10}Na_3$
	527.3915	-1.0	10.0	$C_{25}H_{51}N_{13}$
	527.3915	-1.0	4.5	$C_{26}H_{51}O_3N_6$
	527.3902	1.5	-0.5	$C_{31}H_{51}O_4N_3$
	527.3902	1.5	5.0	$C_{24}H_{49}O_4N_9$
	527.3918	-1.6	6.5	$C_{27}H_{50}O_2N_9Na_3$
	527.3918	-1.6	1.0	$C_{28}H_{56}O_6Na_3$
	527.3920	-2.0	-2.5	$C_{11}H_{47}O_4N_{14}$
	527.3923	-2.5	-0.5	$C_{12}H_{44}O_3N_{19}Na_3$

Figure 4.39. LC-MS representative spectra obtained from Leachate sample from brand Omnitex for peaks at 29.1 mins [m/z 383.2765], 31.9 mins m/z [455.3338] and 34.2 mins m/z [527.3910] which are related to tentative identified Triton.

Triton X is one of the most popular non-ionic surfactants used to lyse cells and remove protein and other cellular organelles, as well as to permeabilize the living cell membranes for transfection[303]. For this reason, the origin this contamination is uncertain.

As previously commented, this compound was included in the "List of substances of very high concern of the REACH by the European Chemicals Agency, mandating all industries, its replacement by January 2021[275]. For this reason, it was not expected to find traces of it. Furthermore, it is believed this contaminant can affect organisms and the environment as one of the products resulting from the degradation of Triton X has been demonstrated to have hormone-like properties[276].

There are studies that have verified and increase in the fixation percentage and colour strength of fibres dyed in TX-100, specially for dyes including Reactive Blue 222, Reactive Red 195 and Reactive Yellow 145[304]. TX-100 and other surfactants have been applied to the synthesis of tin oxide nanoparticles ($SnO_{2)}$ and it was demonstrated that these SnO_2 nanoparticles presented positive antibacterial activities than that of pure SnO_2 nanoparticles against S. aureus and E. coli bacteria[305]. In light of these facts, it bears asking whether the same approach have been followed to give SiMPs and SiNPs used in textile industry the same antibacterial properties. However, no published studies have been found regarding this subject. It is recommended that additional experiments are executed in order to elucidate the origin of this contamination.

Table 4.5 below summarises the findings for LC-MS experiments carried out and Figures 4.40 and 4.41 present total ion chromatogram (TIC) from the LC-MS analysis of leachate of all samples including the blank.

Table 4.5. Leachable organic compounds from DPFMs identified by LC-MS accurate mass; ND refers to analyte not being detected, √ indicates its presence. All mask presented Triton compounds and most of them also presented Caprolactam and PEG-like-species compounds. Adapted from Delgado-Gallardo et al., 2022.

Suspected compound/ species	*m/z* of detected ion	System Blank	Procedural Blank	Baltic	Duronic	Geji	NHS	Omnitex	Soyes
Caprolactam	209/227/219	ND*	ND	ND	√	√	√	ND	√
Caprolactam oligomers	322/340/362 435/453/475 548/566/588 679/701	ND	ND	ND	√	√	√	ND	√
PEG-Like-species	373/417/461/ 505/549	ND	ND	ND	√	√	ND	√	√
PEG-Like-species	665/709/753/797	ND	ND	ND	ND	√	√	ND	ND
PEG-Like-species	459/503/547/ 591/635	ND	ND	ND	ND	√	√	ND	ND
PEG-Like-species	487/431/575/ 619/663	ND	ND	ND	√	ND	ND	ND	ND
PEG-Like-species	473/561/605/ 649/693	ND	ND	√	√	√	ND	ND	√
Triton	383	ND	ND	√	ND	√	√	√	√
Triton	455	ND	ND	√	√	√	√	√	√
Triton	527	ND	ND	√	√	√	√	√	√

*ND: Not detected

The detection of some heavy metals and organic compounds was, again, unexpected and reinforced the initial hypothesis of medical DPFMs also posing a threat to the environment. All these organic leachable compounds commonly found in textile industry have known environmental and health hazards associated with them, and release from DPFMs is an additional cause for concern[306,307]. Nevertheless, comparing medical DPFMs to previously examined ones, the amounts of trace metals in medical masks appear to be much lower. Again, these results prove right the fifth hypothesis of this thesis regarding DPFMs to be proven as a new source of MPs and NPs, chemicals and other pollutants and are also connected to the fourth and fifth objectives of this thesis and also confirm

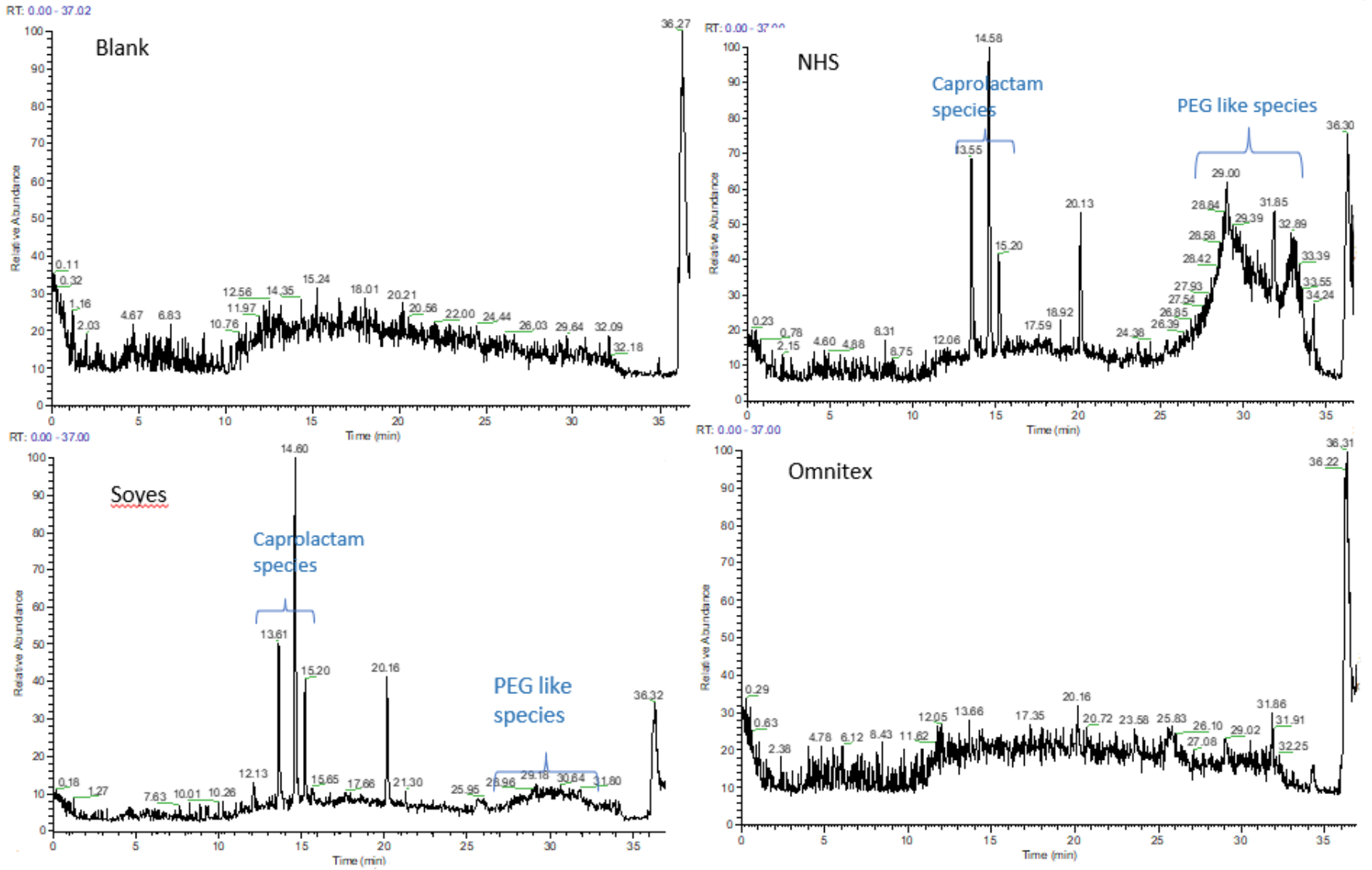

Figure 4.40. Total ion chromatogram (TIC) from the LC-MS analysis of leachate of all samples and blank. Omnitex appears to release the least number of organic species and its TIC has a similar appearance to that of the blank sample. Caprolactam polymeric species, Polyethylene glycol polymers and detergent molecules have been labelled on associated chromatograms.

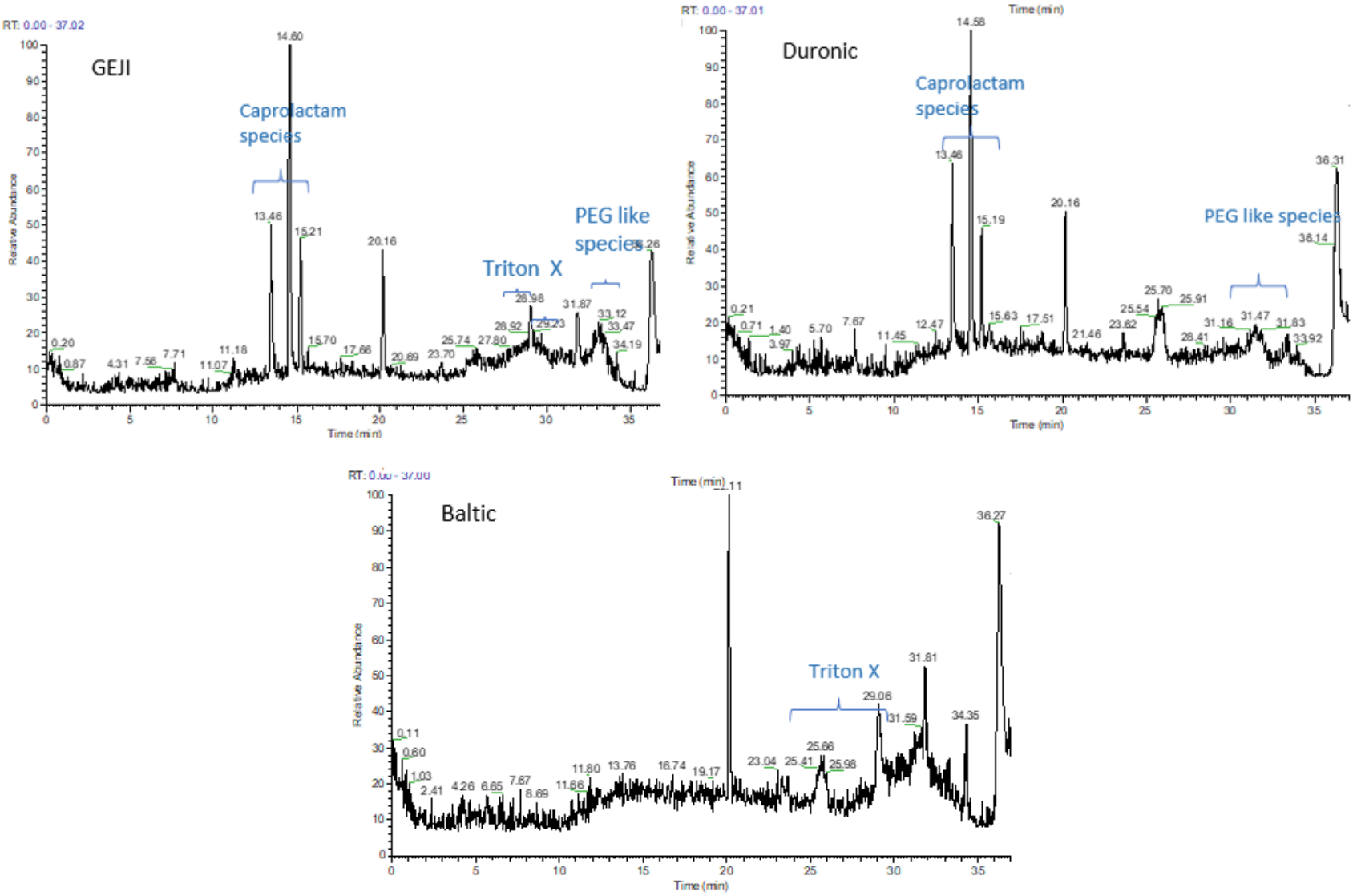

Figure 4.41. Total ion chromatogram (TIC) from the LCMS analysis of leachate of all samples and blank. Caprolactam polymeric species, Polyethylene glycol polymers and detergent molecules have been labelled on associated chromatograms.

4.4. Highlights

Chapter 4 specifically analyses medical plastic face masks of type II and FFP2 and builds on the conclusions of chapter 4's findings. New microscopical methods and the usage of filtration membranes with pore sizes of 20 nanometres are both included with the aim of providing additional and more detailed results.

- FFP2 and Type II Medical grade DPFMs have been showed to release micro and nanoplastic particles and fibres when submerged in water.
- FFP2 masks were found to emit more fibres than Type II masks of the two types of masks studied, and considerable levels of extra MP particles were emitted from foam nose cushions on one of the FFP2 brand masks.
- These DPFMs have been observed to also release heavy metals (such as arsenic, antimony, mercury, lead, tin, titanium, and zinc) in addition to plastic particles and fibres. This indicates their potential as a severe contamination source.
- Medical DPFMs should provide less of a risk because the amounts of these pollutants are lower than those previously reported for non-medical DPFMs. Nevertheless, more research should be conducted in order to determine the source of these substances and whether the fabrication method has to change.

Most of the contents of this chapter were published by ScienceDirect/Elsevier in March 2022 in the article 'Disposable FFP2 and Type IIR Medical-Grade Face Masks: An Exhaustive Analysis into the Leaching of Micro- and Nanoparticles and Chemical Pollutants Linked to the COVID-19 Pandemic' 200 of which the author of this thesis is first author. Microscopy analyses were carried out by the author of this thesis. IPC-MS analyses were carried out at Tata Steel (Port Talbot) and LC-MS analyses were carried out at the National Mass Spectrometry Facility (Swansea University).

Chapter 5: Conclusions and future work

5.1. Conclusions

Depending on the technique employed for the final analysis, the process for identifying MPs and NPs in samples from aquatic settings can involve a number of distinct processes. Depending on the environment being sampled, the sample collecting process may be laborious and usually requires specific equipment. Apart from MPs and NPs being found in all environments (air, water, soil, etc.), the fact that tools and apparatuses utilised worldwide in the labs are totally or partially made of plastics can lead to a high risk of external contamination of the samples. In order to avoid this, several measures have been put in place during this investigation, like the use of a particulate fume hood for handling and processing the samples, the application of brand new glassware with no parts made of plastics or the utilisation of elastic bands to fix gloves (when gloves were used) to the sleeves so there were no fibres coming from the lab coats.

For the majority of analytical procedures, the separation and purification (either physical, chemical, or biological) are essential and crucial steps that entail the removal of both inorganic and organic matter adhering to the surface of the plastic pollutants, in order to enable accurate identification. However, these are highly time consuming and current research using more advanced analytical techniques has demonstrated that this phase can be avoided.

Microscopy, spectroscopy, and thermal analysis are the three most often utilised tools for MP identification. Although the use of microscopy alone has its limitations, it has been widely employed in studies where the nature of the plastic particles is already known. In order to identify unknown types of polymers, spectroscopy and microscopy are typically combined. The reviewed literature shows that the identification of the polymeric composition of MPs is broadly performed using IR and Raman spectroscopy. It should be noted that Raman spectroscopy and FTIR are complementary. Raman spectroscopy can detect some molecular vibrations, which are IR inactive, and vice versa. However, an important limitation to IR is the presence of water in the samples as it also strongly absorbs infrared light and may interfere with the analysis of dissolved, suspended particles. Therefore, wet samples are needed to be dried as best as possible to remove its water content and prevent analysis errors. In addition, the composition of the sample is also important as it has been demonstrated that the presence of pigments or fillers (such as TiO_2, $BaSO_4$ etc.) can interfere with the analysis. More recent studies are showing that a significant number of the limitations shown in

previous analytical technologies are being overcome with the use of thermal techniques coupled to GC-MS, which are proving to be more suitable regarding identification of MPs and NPs due to its robustness, reliability and applicability for the analysis of even complex aqueous matrix samples. This technology has shown ground-breaking low detection levels and high repeatability, paving the way for a fast, cheap, and standardised procedure in the detection of these micropollutants.

A new approach for the identification of MPs and NPs is presented in Chapter 2. The first step involves separation and deposition of submicron particles with a cross sectional area down to 0.1 µm is achieved by means of filtering the aqueous samples through PTFE membranes that present different pore sizes (from 0.45 to 0.1 µm) in order to obtain a solid sample. The membranes are introduced in a glass filtration system, and it has been proven that this technique facilitates the concentration of a larger amount of material to be analysed, overcoming one of the main issues previously discussed regarding the low amount of material that is usually found in aqueous samples. This way, larger volumes of liquid samples can be analysed and the deposition and analysis of MPs and NPs on PTFE membranes has also shown to be a robust and reliable approach. MPs and NPs can be detected in complex aqueous samples at concentrations as low as 50 parts per billion thanks to the Py-GCToFMS exceptional sensitivity, which was used as the analytical tool in this research. While PTFE contributes to part of the ions in the baseline (at 500 °C), the MPs and NPs contribute to peaks that have a higher signal to noise ratio and can be distinguished as a result. The selection of PTFE membranes is due to the material's features, including its wide availability, low cost, and significant thermal resistance, which allow it to apply this technology without time-consuming procedures and with sample sizes volumes under 500 ml. In less than an hour, the membranes holding the micropollutants can be prepared. It is possible to identify PS, PP, and PVC even when they are present in a mixture thanks to the employment of certain differential markers ions for plastics. It was also possible to quantify the markers present on the filters by the addition of a known compound as an internal standard. The summation of these values gave an indicator to the amount of MPs present on the filter. The repeatability of this analytical method was good with a RSD <20 % for the PVC and PS, which also indicates that the MPs have been laid down on the membranes homogenously. The ability to detect PS on a membrane filtered with water from a nearby river proves that this technology is appropriate for the investigation of samples of a complex matrix nature. The results indicated the existence of PS with a semi-quantifiable result of 241.8 g/L.

The usage of PTFE filters does have some limitations though; the background material they

emit increases the theoretical analytical detection threshold due to an enhanced noise region, which might prove it challenging to analyse plastics that could emit comparable breakdown products to the filters. In order to detect and quantify additional types of plastics and remove the ion background connected to the usage of PTFE membranes, a new approach involving the use of inorganic membranes is proposed.

Chapters 3 and 4 part of this thesis focus on the issue that disposable plastic face masks (DPFMs) pose for the environment and potentially for human health. There is worrying evidence that DPFM waste could release harmful contaminants into the environment by being exposed to water, which could have a significant negative impact in nature. Microparticles and microfibers are released into the air, water, and soil when textiles are produced, when clothing is worn, and when end-of-life disposal occurs. According to the International Union for Conservation of Nature (IUCN), washing a single piece of clothing causes the release of roughly 1900 microfibres and a single wash cycle can remove over 700,000 microfibres. The most common polymeric additives in the plastic synthesis and textile industries are bleaching agents, which are also extremely persistent and have recently been discovered in freshwater, marine, and terrestrial environments. The most typical additives also include dyes, flame retardants, plasticizers, antibacterial, antistatic, and antioxidant compounds. Due to the introduction of more and more innovative chemicals, the majority of additives have not been sufficiently monitored or evaluated. Additives are frequently attached to the plastic polymer physically rather than chemically. Therefore, throughout the processes of washing, abrasion, and transportation, MPs can easily leak additives into the environment. Dyeing involves the largest range of chemicals with an estimated 800 dyes currently in use. Some chemicals discovered in textiles are a result of processes that happen between the time of manufacture and the time of purchase, including packaging, transit, and storage, and even the presence of heavy metals in synthetic textile fibres has been documented**.**

This thesis has shown that DPFMs release microscopic physical pollutants, primarily plastic fibres and silicate grains, in the form of micro- and nanosized particles, and that their release is rather simple (gentle agitation in water). But not only MPs and NPs are expelled; traces of concerning heavy metals, such as lead in concentrations up to 6.79 g/L, were identified as part of these silicon-containing particles. Other leachable metals like cadmium (up to 1.92 g/L), antimony (up to 393 g/L), and copper (up to 4.17 g/L) were also detected by ICP-MS. Polyamide-66 monomer and oligomers (nylon-66 synthesis), surfactant molecules, dye-like

molecules, and polyethylene glycol were all tentatively found in the prepared leachates; these polar leachable organic species were associated to plastic additives and pollutants.
The negative effects that silicates and microplastics have on the environment and public health are well documented in the field of micro and nanoparticle research. In addition to the problem of physical pollution, there is also the issue of known harmful chemicals being released, such as the emission of heavy metals (especially Pb and Sb) and the leakage of organic pollutants. When released into the environment, many of these harmful contaminants exhibit bio-accumulative characteristics, and DPFMs have been shown to be a possible source of these pollutants. Therefore, in order to minimise pollution emission, tougher restrictions must be put into place for the production, disposal, and recycle of DPFMs. Additionally, in order to reduce the risk to the general population being exposed to these potentially harmful substances, DPFMs must be thoroughly investigated. There is currently little information about the effects of wearing DPFMs on the human body, so it is important to examine what amount of exposure to fibres, particles, heavy metals, and organic compounds the general public is exposed to when wearing these masks on a daily basis.

The analysis in Chapter 4 focuses on FFP2 and Type II Medical grade DPFMs and shows the release of micro and nanoplastic particles and fibres when submerged in water. The masks' characteristics revealed that these fibres and particles were almost certainly comprised of polypropylene. Of the two designs of masks researched, FFP2 masks were found to emit more fibres than Type II masks with significant amounts of additional MP particles being released from foam nose cushions present on one of the FFP2 brand masks.
The masks have been observed to release heavy metals (such as arsenic, antimony, mercury, lead, tin, titanium, and zinc) in addition to plastic fibres and particles, indicating their potential as a severe contamination source due to their extensive use as a result of the COVID-19 pandemic. ICP-MS results also confirmed traces of heavy metals (antimony up to 2.41 µg/L and copper up to 4.68 µg/L). Also, the non-ionic surfactant Triton X was detected, a compound that that is considered of very high concern by the ECHA, and all industries must have replaced its use by January 2021.
Medical DPFMs should present less of a risk as these pollutants are present at lower levels than previously disclosed for non-medical DPFMs. However, more research should be conducted to determine the source of these substances and whether the fabrication process has to be altered. While some of these substances are believed to be production waste, others, including metals like titanium and zinc, are thought to have been added by manufacturers on

purpose in the form of nanoparticles to give the masks antibacterial qualities.
As it is uncertain how firmly they are attached to the mask fibres, the presence of particles containing heavy metals in the masks is of particular concern. All of the elements found are also known to be toxic and can have detrimental effects on humans if they are ingested in high enough concentrations. As a result, significant problems could arise from the leaching of these particles when wearing the masks or while they are in contact with the environment. Given the prolonged use by the general public and healthcare professionals, as well as the substantial amount of medicinal DPFMs that are disposed of in the environment, the bio-accumulation characteristics of the discovered heavy metals are a subject of concern. Based on these findings, and as stated before, it is recommended that DPFM manufacturing and disposal should be subject to stricter regulations. A thorough investigation must also be conducted to determine the full scope of dangers and potential effects of the fibres and particles released during use of these objects and when they enter the environment.

This thesis concludes having reached its goals regarding the development of a reliable, straightforward and fast method to detect, identify, and semi quantify MPs and NPs in water sources and the study and analysis of medical and non-medical DPFMs in order to elucidate the potential hazard they pose to the environment due to their chemical and physical characteristics. In addition, all the objectives related with these aims have been fulfilled and all the contemplated hypotheses have been also proven true and correct.

5.2. Future work

The achievements of this thesis can be applied to many different areas of investigation and some of the approaches followed can be improved. Although this study has explored some possibilities for the application of ceramic/inorganic membranes, there are still opportunities for future work:

- The use of inorganic membranes is highly recommended for the study of MPs and NPs using PY-GC/MS. Even when this material is more expensive than PTFE membranes, the ion contribution would be avoided. Ceramic membranes are not affected by high temperatures as PTFE.

- This type of membranes facilitates the use of SEM technology as they do not react and charge as much as PTFE membranes.

Even when this thesis has provided in Chapter 2 with a method for the semi-quantification of MPs and NPs present in water samples, it is recommended that further investigation is done in order to obtain a quantification approach more reliable and precise.

The methodology developed in Chapter 2 could also be applied to many other areas of investigation. An example could be the analysis of MPs and NPs in sludge from WWTPs. The need for effective microplastics mitigation in sewage sludge is critical since it is a significant source of microplastics entering the environment[308]. In the treatment of sludge with pyrolysis, it has been demonstrated that when the temperature of the pyrolysis process was raised to 500 °C, the microplastics contents in the sludge residues considerably decreased from 550.8 to 960.9 particles/g to 1.4−2.3 particles/g. Nevertheless, MPs and NPs and organic compounds in sludge may react to form new polymers, and heavy metals in sludge may also be combined[308]. The approach showed in Chapter 2 employs the same temperature and could be combined in order to identify and quantify the amount of MPs and NPs coming from a sludge sample as well as being a method to identify new compounds that could be form during the pyrolysis process. The same principle could be applied to soil samples in order to identify and quantify the amount of MPs and NPs in the soil samples as it has been previously tested[309]. Some pre-treatment of the samples may be necessary as the synthetic particles could be heavily contaminated with organic materials and other chemicals.

It could also be employed to anticipate the kind of bacteria that will form a biofilm in a water body. As seen before, plastic debris comprises different polymers and it has been demonstrated that this fact may influence microbial colonisation[310]. By quantifying the biofilm formed by six marine bacterial strains (Vibrio, Pseudoalteromonas, Phaeobacter) on polyethylene (PE), polypropylene (PP), or polystyrene (PS) pellets, it was observed that each strain had a distinct colonization behaviour, either favouring PS or PP over the other polymer types or having no preference at all. Using free-living or complete communities as inoculum, PE, PP, and PS pellets were exposed to the natural seawater microbiota. Both the initial inoculum's composition and the type of plastic utilised had an impact on the microbial assembly. The plastic biofilms contained known hydrocarbon and polymer degraders such Hydrogenophaga, Paraglaciecola, and Oleibacter. Hence, both the microorganisms and the kind of polymer have an impact on bacterial colonisation on plastic at the community level, and certain strains can display polymer-specific colonisation[310]. Based on this, and the fact that the approach presented on this thesis can be used not only to identify the type of

polymers but it could even be used to ascertain the source of that contamination by upstream monitoring of the river catchment (as explained in 2.3.9), it could be possible to predict the type of bacteria that will colonise MPs and NPs and will be present in that water body. This is important not only for biological reasons but also because it is believed that biofilms may contain antibiotic resistance genes (ARGs) as, according to the results of a study on samples from a river estuary, polypropylene (PP) and polyethylene (PE) with visible biofilms were highly abundant, and the average absolute abundance of the majority of the tested ARGs in the biofilms was higher than that in the sediment and water, suggesting that biofilms on plastics can serve as a reservoir for ARGs[311].

With regards to the study of DPFMs and the potential inhalation of fibres and particles while using them, it was the aim of this project to continue the investigation using manikins that would simulate human respiration in order to simulate real conditions of DPFMs usage by individuals. Due to the high demand because of the COVID-19 pandemic, all respirators, even those used by veterinary surgeons, were unavailable as they were needed in hospitals for patients.

Even when the use of DPFMs is not mandatory anymore in many countries by the time this thesis was written, the production and usage worldwide continue to be high. Furthermore, every individual working in medical, care and related environments will continue using them every day regardless of the pandemic. For this reason, and to also elucidate the environmental fate of DPFMs, it is necessary to continue with this investigation to clarify:

- The real risk that DPFMs pose for human when inhaling fibres and particles while using these items and any other risks derived (i.e. skin contact), by quantifying the amount of MPs, NPs, heavy metals and other potential pollutants found in this thesis.

- In the same vein, to quantify the amount of DPFMs that have been littered into the environment to attain an idea of the amount of micro- and nanopollutants that have been released since the beginning of the pandemic and make an attempt on quantifying the amount of synthetic fibres and particles that are released from a single mask to have a better understanding of the extent of this issue.

The use of more sensitive liquid chromatography techniques is also recommended. Approaches like liquid chromatography-electrospray ionization-tandem mass spectrometry (LC/ESI-MS/MS) could be applied in order to perform a structural elucidation of components of interest using appropriate software such as Compound Discoverer or

mzCloud. This could allow to obtain results that fully characterise all components in leachate samples[312].

Also, as previously commented, the use of SP-ICP-MS apparatuses is highly advise, particularly for the fast characterisation of NPs. This method has spread widely in recent years and is close to becoming a standard practise for nanoparticle analysis as it can provide data on particle size distribution, particle number concentration, and mass concentration in diluted samples with little to no sample preparation.

The last few months of this project it was decided to include the investigation of the release of MPs, NPs, chemicals and other organic compounds from textile samples and water samples obtained after the wash of different textile materials. As mentioned before, laundering synthetic textiles and clothes has been investigated and proven as a source MPs and NPs emissions into the environment and there is still research to be done. This analysis is being carried out using a new technology, gas chromatography–vacuum ultraviolet spectroscopy (GC-VUV) that provides both qualitative and quantitative spectral information. Unfortunately, the results for this part of the study were not completely ready by the time this thesis was written and presented. However, some preliminary results are presented in Table 5.1, where it can be observed that some concerning compounds (like chlorophenyls compounds) have been tentatively identified.

Table 5.1. Preliminary results obtained during the analysis of different aqueous textile samples where different compounds have been tentatively identified, including chlorophenyl compounds. Further analysis is recommended.

Sample	RT	filter (nm)	Proposed ID R2	Match Factor	%cont	ID
870959	26.198	200-240	0.9951	0.9899	100	2,3-dimethylfuran
			0.9904	0.9778	100	2,3,3',5,5'-Pentachlorobiphenyl
	28.677	200-240	0.9775	0.9319	100	3,3',4,5,5'-Pentachlorobiphenyl
	29.34	170-205	0.9934	0.9865	63.6	Fluorobenzene
	33.5024	200-240	0.9802	0.9356	100	3,3',4,4',5,5'-Hexachlorobiphenyl
870553	34.719	125-160	0.9966	0.9855	100	2-Ethylbicyclo[2.2.1]heptane
			0.996	0.9831	100	Dieldrin
x60571	29.315	170-205	0.9987	0.9856	74.4	Diphenyl ether
				0.9593	25.6	3-methylthiophene
57714	29.289	170-205	0.9945	0.9809	100	4-Chlorophenyl phenyl ether
870305	29.277	170-205	0.9961	0.983	100	4-Chlorophenyl phenyl ether

The investigation of this type of contamination is highly recommended, especially now that new regulations are being proposed, like the new bill recently presented in the UK which aim is to require manufacturers to fit microplastic-catching filters to new domestic and commercial washing machines. This has been proposed to raise awareness about the consequences of microplastics from washing machines for pollution in rivers and seas and to make provision about the promotion of the use of microplastic-catching filters in washing machines.

References

1. da Costa, J. P., Santos, P. S. M., Duarte, A. C. & Rocha-Santos, T. (Nano)plastics in the environment - Sources, fates and effects. *Sci. Total Environ.* **566**–**567**, 15–26 (2016).
2. Andrady A. L. *Persistence of Plastic Litter in the Oceans*. *Marine Anthropogenic Litter* (2015). doi:10.1007/978-3-319-16510-3.
3. Arthur, C., Baker, J. & Bamford, H. Proceedings of the International Research Workshop on the Occurrence , Effects , and Fate of Microplastic Marine Debris. *Group* 530 (2009).
4. Lambert, S. & Wagner, M. Characterisation of nanoplastics during the degradation of polystyrene. *Chemosphere* **145**, 265–268 (2016).
5. Klaine, S. J. *et al.* Nanomaterials in the environment: Behavior, fate, bioavailability, and effects. *Environmental Toxicology and Chemistry* at https://doi.org/10.1897/08-090.1 (2008).
6. Gigault, J. *et al.* Nanoplastics are neither microplastics nor engineered nanoparticles. *Nature Nanotechnology* at https://doi.org/10.1038/s41565-021-00886-4 (2021).
7. Ivleva, N. P., Wiesheu, A. C. & Niessner, R. Microplastic in Aquatic Ecosystems. *Angew. Chemie - Int. Ed.* **56**, 1720–1739 (2017).
8. Hurley, R., Woodward, J. & Rothwell, J. J. Microplastic contamination of river beds significantly reduced by catchment-wide flooding. *Nat. Geosci.* (2018) doi:10.1038/s41561-018-0080-1.
9. Horton, A. A., Svendsen, C., Williams, R. J., Spurgeon, D. J. & Lahive, E. Large microplastic particles in sediments of tributaries of the River Thames, UK – Abundance, sources and methods for effective quantification. *Mar. Pollut. Bull.* **114**, 218–226 (2017).
10. Vaughan, R., Turner, S. D. & Rose, N. L. Microplastics in the sediments of a UK urban lake. *Environ. Pollut.* **229**, 10–18 (2017).
11. Vogelsang, C. *et al. Microplastics in road dust – characteristics, pathways and measures*. (Norwegian Institute for Water Research (NIVA), 2018).
12. Herath, S., Hagare, D., Siddiqui, Z. & Maheshwari, B. Microplastics in urban stormwater—developing a methodology for its monitoring. *Environ. Monit. Assess.* (2022) doi:10.1007/s10661-022-09849-1.
13. Xiong, X., Xie, S., Feng, K. & Wang, Q. Occurrence of microplastics in a pond-river-lake connection water system: How does the aquaculture process affect microplastics in natural water bodies. *J. Clean. Prod.* **352**, 131632 (2022).
14. Panno, S. V. *et al.* Microplastic Contamination in Karst GK, M. B., Natesan, U., R, V., R, P. K., R, R., & S, S. (2021). Spatial distribution of microplastic concentration around landfill sites and its potential risk on groundwater. Chemosphere. https://doi.org/10.1016/j.chem. *Groundwater* (2019) doi:10.1111/gwat.12862.
15. K, M. B. *et al.* Spatial distribution of microplastic concentration around landfill sites and its potential risk on groundwater. *Chemosphere* (2021) doi:10.1016/j.chemosphere.2021.130263.
16. Kooi, M., Besseling, E., Kroeze, C., Van Wezel, A. P. & Koelmans, A. A. Modeling the fate and transport of plastic debris in freshwaters: Review and Guidance. in *Handbook of Environmental Chemistry* (2018). doi:10.1007/978-3-319-61615-5_7.
17. Duan, J. *et al.* Weathering of microplastics and interaction with other coexisting constituents in terrestrial and aquatic environments. *Water Research* at https://doi.org/10.1016/j.watres.2021.117011 (2021).
18. Alimi, O. S., Farner Budarz, J., Hernandez, L. M. & Tufenkji, N. Microplastics and Nanoplastics in Aquatic Environments: Aggregation, Deposition, and Enhanced Contaminant Transport. *Environmental Science and Technology* at https://doi.org/10.1021/acs.est.7b05559 (2018).
19. Wang, X. *et al.* A review of microplastics aggregation in aquatic environment: Influence factors, analytical methods, and environmental implications. *J. Hazard. Mater.* (2021) doi:10.1016/j.jhazmat.2020.123496.
20. Sharma, V. K., Ma, X., Guo, B. & Zhang, K. Environmental factors-mediated behavior of microplastics and nanoplastics in water: A review. *Chemosphere* at

https://doi.org/10.1016/j.chemosphere.2021.129597 (2021).
21. Wu, J., Jiang, R., Lin, W. & Ouyang, G. Effect of salinity and humic acid on the aggregation and toxicity of polystyrene nanoplastics with different functional groups and charges. *Environ. Pollut.* (2019) doi:10.1016/j.envpol.2018.11.055.
22. Li, L., Sillanpää, M. & Risto, M. Influences of water properties on the aggregation and deposition of engineered titanium dioxide nanoparticles in natural waters. *Environ. Pollut.* (2016) doi:10.1016/j.envpol.2016.09.080.
23. Zhang, B. *et al.* Research progress of nanoplastics in freshwater. *Sci. Total Environ.* **757**, 143791 (2021).
24. Dris, R., Gasperi, J., Saad, M., Mirande, C. & Tassin, B. Synthetic fibers in atmospheric fallout: A source of microplastics in the environment? *Mar. Pollut. Bull.* **104**, 290–293 (2016).
25. Wetherbee, G., Baldwin, A. & Ranville, J. It Is Raining. *USGS Numbered Ser.* **Open-File**, (2019).
26. Allen, S. *et al.* Atmospheric transport and deposition of microplastics in a remote mountain catchment. *Nat. Geosci.* (2019) doi:10.1038/s41561-019-0335-5.
27. Wang, X. *et al.* Exponential decrease of airborne microplastics: From megacity to open ocean. *Sci. Total Environ.* **849**, 157702 (2022).
28. Dris, R. *et al.* A first overview of textile fibers, including microplastics, in indoor and outdoor environments. *Environ. Pollut.* **221**, 453–458 (2017).
29. Zhang, J., Wang, L. & Kannan, K. Microplastics in house dust from 12 countries and associated human exposure. *Environ. Int.* (2020) doi:10.1016/j.envint.2019.105314.
30. O'Brien, S. *et al.* Airborne emissions of microplastic fibres from domestic laundry dryers. *Sci. Total Environ.* (2020) doi:10.1016/j.scitotenv.2020.141175.
31. Gasperi, J. *et al.* Microplastics in air: Are we breathing it in? *Curr. Opin. Environ. Sci. Heal.* **1**, 1–5 (2018).
32. Vianello, A., Jensen, R. L., Liu, L. & Vollertsen, J. Simulating human exposure to indoor airborne microplastics using a Breathing Thermal Manikin. *Sci. Rep.* (2019) doi:10.1038/s41598-019-45054-w.
33. Baeza-Martínez, C. *et al.* First evidence of microplastics isolated in European citizens' lower airway. *J. Hazard. Mater.* **438**, 129439 (2022).
34. Morales, A. C. *et al.* Atmospheric emission of nanoplastics from sewer pipe repairs. *Nat. Nanotechnol. 2022* 1–7 (2022) doi:10.1038/s41565-022-01219-9.
35. Hurley, R. R. & Nizzetto, L. Fate and occurrence of micro(nano)plastics in soils: Knowledge gaps and possible risks. *Curr. Opin. Environ. Sci. Heal.* **1**, 6–11 (2018).
36. Chia, R. W., Lee, J. Y., Jang, J., Kim, H. & Kwon, K. D. Soil health and microplastics: a review of the impacts of microplastic contamination on soil properties. *J. Soils Sediments 2022* 1–16 (2022) doi:10.1007/S11368-022-03254-4.
37. Nizzetto, L., Futter, M. & Langaas, S. Are Agricultural Soils Dumps for Microplastics of Urban Origin? *Environmental Science and Technology* at https://doi.org/10.1021/acs.est.6b04140 (2016).
38. Rillig, M. C., Ingraffia, R. & De Souza Machado, A. A. Microplastic incorporation into soil in agroecosystems. *Front. Plant Sci.* **8**, 8–11 (2017).
39. DEFRA. Department for Environment, Food and Rural Affairs Annual Report and Accounts 2012-13. (2013).
40. Zhang, J. *et al.* Effects of plastic residues and microplastics on soil ecosystems: A global meta-analysis. *J. Hazard. Mater.* **435**, 129065 (2022).
41. Ren, X., Tang, J., Wang, L. & Liu, Q. Microplastics in soil-plant system: effects of nano/microplastics on plant photosynthesis, rhizosphere microbes and soil properties in soil with different residues. *Plant Soil* (2021) doi:10.1007/s11104-021-04869-1.
42. Bläsing, M. & Amelung, W. Plastics in soil: Analytical methods and possible sources. *Science of the Total Environment* at https://doi.org/10.1016/j.scitotenv.2017.08.086 (2018).
43. Da Costa, J. P., Paço, A., Santos, P. S. M., Duarte, A. C. & Rocha-Santos, T. Microplastics in soils: Assessment, analytics and risks. *Environ. Chem.* (2019) doi:10.1071/EN18150.
44. Wahl, A. *et al.* Nanoplastic occurrence in a soil amended with plastic debris. *Chemosphere* (2021) doi:10.1016/j.chemosphere.2020.127784.

45. Jin, M., Wang, X., Ren, T., Wang, J. & Shan, J. Microplastics contamination in food and beverages: Direct exposure to humans. *Journal of Food Science* at https://doi.org/10.1111/1750-3841.15802 (2021).
46. Liebezeit, G. & Liebezeit, E. Non-pollen particulates in honey and sugar. *Food Addit. Contam. - Part A Chem. Anal. Control. Expo. Risk Assess.* (2013) doi:10.1080/19440049.2013.843025.
47. Liebezeit, G. & Liebezeit, E. Synthetic particles as contaminants in German beers. *Food Addit. Contam. - Part A Chem. Anal. Control. Expo. Risk Assess.* (2014) doi:10.1080/19440049.2014.945099.
48. Karami, A. *et al.* The presence of microplastics in commercial salts from different countries. *Sci. Rep.* **7**, 1–11 (2017).
49. Van Cauwenberghe, L. & Janssen, C. R. Microplastics in bivalves cultured for human consumption. *Environ. Pollut.* (2014) doi:10.1016/j.envpol.2014.06.010.
50. Mason, S. A., Welch, V. & Neratko, J. Synthetic Polymer Contamination in Global Drinking Water. *Fredonia* (2017).
51. Fadare, O. O., Wan, B., Guo, L. H. & Zhao, L. Microplastics from consumer plastic food containers: Are we consuming it? *Chemosphere* (2020) doi:10.1016/j.chemosphere.2020.126787.
52. Deng, J. *et al.* Microplastics released from food containers can suppress lysosomal activity in mouse macrophages. *J. Hazard. Mater.* **435**, 128980 (2022).
53. Barboza, L. G. A. *et al.* Microplastics cause neurotoxicity, oxidative damage and energy-related changes and interact with the bioaccumulation of mercury in the European seabass, Dicentrarchus labrax (Linnaeus, 1758). *Aquat. Toxicol.* **195**, 49–57 (2018).
54. Ragusa, A. *et al.* Plasticenta: First evidence of microplastics in human placenta. *Environment International* at https://doi.org/10.1016/j.envint.2020.106274 (2021).
55. Galloway, T. S. Micro- and nano-plastics and human health. in *Marine Anthropogenic Litter* (2015). doi:10.1007/978-3-319-16510-3_13.
56. Latini, G. *et al.* In utero exposure to di-(2-ethylhexyl)phthalate and duration of human pregnancy. *Environ. Health Perspect.* (2003) doi:10.1289/ehp.6202.
57. Ait Bamai, Y. *et al.* Exposure to house dust phthalates in relation to asthma and allergies in both children and adults. *Sci. Total Environ.* (2014) doi:10.1016/j.scitotenv.2014.03.059.
58. Vaughn, B. C. *Bisphenol A and phthalates: Uses, health effects and environmental risks*. *Bisphenol A and Phthalates: Uses, Health Effects and Environmental Risks* (2010).
59. Xing, J., Zhang, S., Zhang, M. & Hou, J. A critical review of presence, removal and potential impacts of endocrine disruptors bisphenol A. *Comparative Biochemistry and Physiology Part - C: Toxicology and Pharmacology* at https://doi.org/10.1016/j.cbpc.2022.109275 (2022).
60. Revel, M., Châtel, A. & Mouneyrac, C. Micro(nano)plastics: A threat to human health? *Curr. Opin. Environ. Sci. Heal.* **1**, 17–23 (2018).
61. de Souza Machado, A. A., Kloas, W., Zarfl, C., Hempel, S. & Rillig, M. C. Microplastics as an emerging threat to terrestrial ecosystems. *Glob. Chang. Biol.* **24**, 1405–1416 (2018).
62. Schirinzi, G. F. *et al.* Cytotoxic effects of commonly used nanomaterials and microplastics on cerebral and epithelial human cells. *Environ. Res.* **159**, 579–587 (2017).
63. Qin, J., Xia, P. F., Yuan, X. Z. & Wang, S. G. Chlorine disinfection elevates the toxicity of polystyrene microplastics to human cells by inducing mitochondria-dependent apoptosis. *J. Hazard. Mater.* (2022) doi:10.1016/j.jhazmat.2021.127842.
64. Blackburn, K. & Green, D. The potential effects of microplastics on human health: What is known and what is unknown. *Ambio 2021 513* **51**, 518–530 (2021).
65. Schwarz, A. E., Ligthart, T. N., Boukris, E. & van Harmelen, T. Sources, transport, and accumulation of different types of plastic litter in aquatic environments: A review study. *Mar. Pollut. Bull.* (2019) doi:10.1016/j.marpolbul.2019.04.029.
66. Ceccarini, A. *et al.* The Hidden Microplastics: New Insights and Figures from the Thorough Separation and Characterization of Microplastics and of Their Degradation Byproducts in Coastal Sediments. *Environ. Sci. Technol.* (2018) doi:10.1021/acs.est.8b01487.
67. Ostle, C. *et al.* The rise in ocean plastics evidenced from a 60-year time series. *Nat. Commun.* (2019) doi:10.1038/s41467-019-09506-1.

68. Horton, A. A., Walton, A., Spurgeon, D. J., Lahive, E. & Svendsen, C. Microplastics in freshwater and terrestrial environments: Evaluating the current understanding to identify the knowledge gaps and future research priorities. *Sci. Total Environ.* **586**, 127–141 (2017).
69. Lusher, A. L., Welden, N. A., Sobral, P. & Cole, M. Sampling, isolating and identifying microplastics ingested by fish and invertebrates. *Anal. Methods* **9**, 1346–1360 (2017).
70. Song, Y. K. *et al.* A comparison of microscopic and spectroscopic identification methods for analysis of microplastics in environmental samples. *Mar. Pollut. Bull.* **93**, 202–209 (2015).
71. Fischer, M. & Scholz-Böttcher, B. M. Simultaneous Trace Identification and Quantification of Common Types of Microplastics in Environmental Samples by Pyrolysis-Gas Chromatography-Mass Spectrometry. *Environ. Sci. Technol.* (2017) doi:10.1021/acs.est.6b06362.
72. Bitter, H. & Lackner, S. Fast and easy quantification of semi-crystalline microplastics in exemplary environmental matrices by differential scanning calorimetry (DSC). *Chem. Eng. J.* (2021) doi:10.1016/j.cej.2021.129941.
73. Ter Halle, A. *et al.* Nanoplastic in the North Atlantic Subtropical Gyre. *Environ. Sci. Technol.* **51**, 13689–13697 (2017).
74. Löder, M. G. J. & Gerdts, G. Methodology used for the detection and identification of microplastics - A critical Appraisal. *Mar. Anthropog. Litter* 9–14 (2015) doi:10.1007/978-3-319-16510-3_8.
75. Takasuka, A., Nyuji, M., Kuroda, H. & Oozeki, Y. Variability of swept area by sea-surface tows of a neuston net: Balance of resistance, clogging, and over-inflow effects. *Fish. Res.* (2019) doi:10.1016/j.fishres.2018.10.021.
76. Setälä, O., Magnusson, K., Lehtiniemi, M. & Norén, F. Distribution and abundance of surface water microlitter in the Baltic Sea: A comparison of two sampling methods. *Mar. Pollut. Bull.* (2016) doi:10.1016/j.marpolbul.2016.06.065.
77. Prata, J. C. *et al.* A new approach for routine quantification of microplastics using Nile Red and automated software (MP-VAT). *Sci. Total Environ.* **690**, 1277–1283 (2019).
78. Li, J., Liu, H. & Paul Chen, J. Microplastics in freshwater systems: A review on occurrence, environmental effects, and methods for microplastics detection. *Water Res.* **137**, 362–374 (2018).
79. Ziajahromi, S., Neale, P. A., Rintoul, L. & Leusch, F. D. L. Wastewater treatment plants as a pathway for microplastics: Development of a new approach to sample wastewater-based microplastics. *Water Res.* **112**, 93–99 (2017).
80. Magnusson, K. & Norén, F. Screening of microplastic particles in and down-stream a wastewater treatment plant. *IVL Swedish Environ. Res. Inst.* (2014) doi:naturvardsverket-2226.
81. Julia Talvitie; Mari Heinonen. Preliminary study on synthetic microfibers and particles at a municipal waste water treatment plant. *Balt. Mar. Environ. Prot. Comm. HELCOM* (2014) doi:10.1055/s-2003-38830.
82. Talvitie, J. *et al.* Do wastewater treatment plants act as a potential point source of microplastics? Preliminary study in the coastal Gulf of Finland, Baltic Sea. *Water Sci. Technol.* **72**, 1495–1504 (2015).
83. Talvitie, J., Mikola, A., Koistinen, A. & Setälä, O. Solutions to microplastic pollution – Removal of microplastics from wastewater effluent with advanced wastewater treatment technologies. *Water Res.* **123**, 401–407 (2017).
84. Mintenig, S. M., Int-Veen, I., Löder, M. G. J., Primpke, S. & Gerdts, G. Identification of microplastic in effluents of waste water treatment plants using focal plane array-based micro-Fourier-transform infrared imaging. *Water Res.* **108**, 365–372 (2017).
85. Boyle, K. & Örmeci, B. Microplastics and nanoplastics in the freshwater and terrestrial environment: A review. *Water (Switzerland)* at https://doi.org/10.3390/w12092633 (2020).
86. Nguyen, B. *et al.* Separation and Analysis of Microplastics and Nanoplastics in Complex Environmental Samples. *Acc. Chem. Res.* **52**, 858–866 (2019).
87. Hildebrandt, L., Mitrano, D. M., Zimmermann, T. & Pröfrock, D. A Nanoplastic Sampling and Enrichment Approach by Continuous Flow Centrifugation. *Front. Environ. Sci.* (2020) doi:10.3389/fenvs.2020.00089.
88. Delgado-Gallardo, J. *et al.* From Sampling to Analysis: A Critical Review of Techniques

Used in the Detection of Micro- and Nanoplastics in Aquatic Environments. *ACS ES&T Water* (2021) doi:10.1021/acsestwater.0c00228.

89. Browne, M. A., Galloway, T. S. & Thompson, R. C. Spatial patterns of plastic debris along estuarine shorelines. *Environ. Sci. Technol.* (2010) doi:10.1021/es903784e.
90. Nuelle, M. T., Dekiff, J. H., Remy, D. & Fries, E. A new analytical approach for monitoring microplastics in marine sediments. *Environ. Pollut.* (2014) doi:10.1016/j.envpol.2013.07.027.
91. Imhof, H. K., Ivleva, N. P., Schmid, J., Niessner, R. & Laforsch, C. Contamination of beach sediments of a subalpine lake with microplastic particles. *Current Biology* at https://doi.org/10.1016/j.cub.2013.09.001 (2013).
92. Imhof, H. K. *et al.* Pigments and plastic in limnetic ecosystems: A qualitative and quantitative study on microparticles of different size classes. *Water Res.* (2016) doi:10.1016/j.watres.2016.03.015.
93. Corcoran, P. L., Biesinger, M. C. & Grifi, M. Plastics and beaches: A degrading relationship. *Mar. Pollut. Bull.* (2009) doi:10.1016/j.marpolbul.2008.08.022.
94. Fuller, S. & Gautam, A. A Procedure for Measuring Microplastics using Pressurized Fluid Extraction. *Environ. Sci. Technol.* (2016) doi:10.1021/acs.est.6b00816.
95. Hanke, G. *Guidance on Monitoring of Marine Litter in European Seas Contact information*. *Joint Research Centre* (2013).
96. Cole, M. *et al.* Isolation of microplastics in biota-rich seawater samples and marine organisms. *Sci. Rep.* (2014) doi:10.1038/srep04528.
97. Enders, K., Lenz, R., Stedmon, C. A. & Nielsen, T. G. Abundance, size and polymer composition of marine microplastics ≥10 μm in the Atlantic Ocean and their modelled vertical distribution. *Mar. Pollut. Bull.* (2015) doi:10.1016/j.marpolbul.2015.09.027.
98. Löder, M. G. J. *et al.* Enzymatic Purification of Microplastics in Environmental Samples. *Environ. Sci. Technol.* (2017) doi:10.1021/acs.est.7b03055.
99. Qiu, Q. *et al.* Extraction, enumeration and identification methods for monitoring microplastics in the environment. *Estuarine, Coastal and Shelf Science* at https://doi.org/10.1016/j.ecss.2016.04.012 (2016).
100. Shim, W. J., Hong, S. H. & Eo, S. E. Identification methods in microplastic analysis: A review. *Analytical Methods* at https://doi.org/10.1039/c6ay02558g (2017).
101. Li, J., Green, C., Reynolds, A., Shi, H. & Rotchell, J. M. Microplastics in mussels sampled from coastal waters and supermarkets in the United Kingdom. *Environ. Pollut.* (2018) doi:10.1016/j.envpol.2018.05.038.
102. Von Moos, N., Burkhardt-Holm, P. & Köhler, A. Uptake and effects of microplastics on cells and tissue of the blue mussel Mytilus edulis L. after an experimental exposure. *Environ. Sci. Technol.* (2012) doi:10.1021/es302332w.
103. Dazzi, A. *et al.* AFM-IR: Combining atomic force microscopy and infrared spectroscopy for nanoscale chemical characterization. *Appl. Spectrosc.* (2012) doi:10.1366/12-06804.
104. Fries, E. *et al.* Identification of polymer types and additives in marine microplastic particles using pyrolysis-GC/MS and scanning electron microscopy. *Environ. Sci. Process. Impacts* (2013) doi:10.1039/c3em00214d.
105. Gniadek, M. & Dąbrowska, A. The marine nano- and microplastics characterisation by SEM-EDX: The potential of the method in comparison with various physical and chemical approaches. *Mar. Pollut. Bull.* (2019) doi:10.1016/j.marpolbul.2019.07.067.
106. Gigault, J., Pedrono, B., Maxit, B. & Ter Halle, A. Marine plastic litter: The unanalyzed nano-fraction. *Environ. Sci. Nano* (2016) doi:10.1039/c6en00008h.
107. Awet, T. T. *et al.* Effects of polystyrene nanoparticles on the microbiota and functional diversity of enzymes in soil. *Environ. Sci. Eur.* (2018) doi:10.1186/s12302-018-0140-6.
108. Grasseschi, D., Lima, F. S., Nakamura, M. & Toma, H. E. Hyperspectral dark-field microscopy of gold nanodisks. *Micron* (2015) doi:10.1016/j.micron.2014.10.007.
109. Mattsson, K. *et al.* Brain damage and behavioural disorders in fish induced by plastic nanoparticles delivered through the food chain. *Sci. Rep.* (2017) doi:10.1038/s41598-017-10813-0.
110. Fournier, S., D'Errico, J. & Stapleton, P. Translocation of Engineered Nanomaterials from the Maternal Lungs to the Fetal Compartment After Instillation. *FASEB J.* (2018).

111. Shim, W. J., Song, Y. K., Hong, S. H. & Jang, M. Identification and quantification of microplastics using Nile Red staining. *Mar. Pollut. Bull.* (2016) doi:10.1016/j.marpolbul.2016.10.049.
112. Greenspan, P. & Fowler, S. D. Spectrofluorometric studies of the lipid probe, nile red. *J. Lipid Res.* (1985) doi:10.1016/s0022-2275(20)34307-8.
113. Erni-Cassola, G., Gibson, M. I., Thompson, R. C. & Christie-Oleza, J. A. Lost, but Found with Nile Red: A Novel Method for Detecting and Quantifying Small Microplastics (1 mm to 20 μm) in Environmental Samples. *Environ. Sci. Technol.* (2017) doi:10.1021/acs.est.7b04512.
114. Andrady, A. L. Microplastics in the marine environment. *Marine Pollution Bulletin* at https://doi.org/10.1016/j.marpolbul.2011.05.030 (2011).
115. Lv, L. *et al.* A simple method for detecting and quantifying microplastics utilizing fluorescent dyes - Safranine T, fluorescein isophosphate, Nile red based on thermal expansion and contraction property. *Environ. Pollut.* (2019) doi:10.1016/j.envpol.2019.113283.
116. Chae, Y., Kim, D., Kim, S. W. & An, Y. J. Trophic transfer and individual impact of nano-sized polystyrene in a four-species freshwater food chain. *Sci. Rep.* (2018) doi:10.1038/s41598-017-18849-y.
117. Ruozi, B. *et al.* AFM, ESEM, TEM, and CLSM in liposomal characterization: a comparative study. *Int. J. Nanomedicine* (2011) doi:10.2147/ijn.s14615.
118. Wang, Y. N., Wei, J., She, Q., Pacheco, F. & Tang, C. Y. Microscopic characterization of FO/PRO membranes - A comparative study of CLSM, TEM and SEM. *Environ. Sci. Technol.* (2012) doi:10.1021/es301885m.
119. Li, L. *et al.* Confocal measurement of microplastics uptake by plants. *MethodsX* (2020) doi:10.1016/j.mex.2019.11.023.
120. Razanajatovo, R. M., Ding, J., Zhang, S., Jiang, H. & Zou, H. Sorption and desorption of selected pharmaceuticals by polyethylene microplastics. *Mar. Pollut. Bull.* (2018) doi:10.1016/j.marpolbul.2018.09.048.
121. Yin, L., Chen, B., Xia, B., Shi, X. & Qu, K. Polystyrene microplastics alter the behavior, energy reserve and nutritional composition of marine jacopever (Sebastes schlegelii). *J. Hazard. Mater.* (2018) doi:10.1016/j.jhazmat.2018.07.110.
122. Zubris, K. A. V. & Richards, B. K. Synthetic fibers as an indicator of land application of sludge. *Environ. Pollut.* **138**, 201–211 (2005).
123. Mallard, F., Le Bourlot, V. & Tully, T. An Automated Image Analysis System to Measure and Count Organisms in Laboratory Microcosms. *PLoS One* (2013) doi:10.1371/journal.pone.0064387.
124. Karathanasis, C., Fricke, F., Hummer, G. & Heilemann, M. Molecule Counts in Localization Microscopy with Organic Fluorophores. *ChemPhysChem* (2017) doi:10.1002/cphc.201601425.
125. Li, L., Zhou, Q., Yin, N., Tu, C. & Luo, Y. Uptake and accumulation of microplastics in an edible plant. *Kexue Tongbao/Chinese Sci. Bull.* (2019) doi:10.1360/N972018-00845.
126. Shan, J. *et al.* Simple and rapid detection of microplastics in seawater using hyperspectral imaging technology. *Anal. Chim. Acta* **1050**, 161–168 (2019).
127. Silva, A. B. *et al.* Microplastics in the environment: Challenges in analytical chemistry - A review. *Analytica Chimica Acta* at https://doi.org/10.1016/j.aca.2018.02.043 (2018).
128. Capillo, G. *et al.* Quali-quantitative analysis of plastics and synthetic microfibers found in demersal species from Southern Tyrrhenian Sea (Central Mediterranean). *Mar. Pollut. Bull.* (2020) doi:10.1016/j.marpolbul.2019.110596.
129. Cincinelli, A. *et al.* Microplastic in the surface waters of the Ross Sea (Antarctica): Occurrence, distribution and characterization by FTIR. *Chemosphere* (2017) doi:10.1016/j.chemosphere.2017.02.024.
130. Harrison, J. P., Ojeda, J. J. & Romero-González, M. E. The applicability of reflectance micro-Fourier-transform infrared spectroscopy for the detection of synthetic microplastics in marine sediments. *Sci. Total Environ.* (2012) doi:10.1016/j.scitotenv.2011.11.078.
131. Levin, I. W. & Bhargava, R. FOURIER TRANSFORM INFRARED VIBRATIONAL SPECTROSCOPIC IMAGING: Integrating Microscopy and Molecular Recognition. *Annu.*

Rev. Phys. Chem. (2005) doi:10.1146/annurev.physchem.56.092503.141205.
132. Löder, M. G. J., Kuczera, M., Mintenig, S., Lorenz, C. & Gerdts, G. Focal plane array detector-based micro-Fourier-transform infrared imaging for the analysis of microplastics in environmental samples. *Environ. Chem.* (2015) doi:10.1071/EN14205.
133. Sun, D. W. *Infrared Spectroscopy for Food Quality Analysis and Control*. *Infrared Spectroscopy for Food Quality Analysis and Control* (2009). doi:10.1016/B978-0-12-374136-3.X0001-6.
134. Schymanski, D., Goldbeck, C., Humpf, H. U. & Fürst, P. Analysis of microplastics in water by micro-Raman spectroscopy: Release of plastic particles from different packaging into mineral water. *Water Res.* **129**, 154–162 (2018).
135. Gillibert, R. *et al.* Raman tweezers for small microplastics and nanoplastics identification in seawater. *Environ. Sci. Technol.* (2019) doi:10.1021/acs.est.9b03105.
136. Lenz, R., Enders, K., Stedmon, C. A., MacKenzie, D. M. A. & Nielsen, T. G. A critical assessment of visual identification of marine microplastic using Raman spectroscopy for analysis improvement. *Mar. Pollut. Bull.* (2015) doi:10.1016/j.marpolbul.2015.09.026.
137. Claessens, M., Meester, S. De, Landuyt, L. Van, Clerck, K. De & Janssen, C. R. Occurrence and distribution of microplastics in marine sediments along the Belgian coast. *Mar. Pollut. Bull.* (2011) doi:10.1016/j.marpolbul.2011.06.030.
138. Vianello, A. *et al.* Microplastic particles in sediments of Lagoon of Venice, Italy: First observations on occurrence, spatial patterns and identification. *Estuar. Coast. Shelf Sci.* (2013) doi:10.1016/j.ecss.2013.03.022.
139. Martins, J. & Sobral, P. Plastic marine debris on the Portuguese coastline: A matter of size? *Mar. Pollut. Bull.* (2011) doi:10.1016/j.marpolbul.2011.09.028.
140. Wang, J. *et al.* Microplastics in the surface sediments from the Beijiang River littoral zone: Composition, abundance, surface textures and interaction with heavy metals. *Chemosphere* (2017) doi:10.1016/j.chemosphere.2016.12.074.
141. Frei, S. *et al.* Occurence of microplastics in the hyporheic zone of rivers. *Sci. Rep.* (2019) doi:10.1038/s41598-019-51741-5.
142. Carr, S. A., Liu, J. & Tesoro, A. G. Transport and fate of microplastic particles in wastewater treatment plants. *Water Res.* (2016) doi:10.1016/j.watres.2016.01.002.
143. Gips, J. P. Shale Characterization Using TGA, Py-GC-MS, and NMR APPROVED BY SUPERVISING COMMITTEE. (2014).
144. McNeill, I. C., Memetea, L. & Cole, W. J. A study of the products of PVC thermal degradation. *Polym. Degrad. Stab.* **49**, 181–191 (1995).
145. Bockhorn, H., Hornung, A., Hornung, U. & Schawaller, D. Kinetic study on the thermal degradation of polypropylene and polyethylene. *J. Anal. Appl. Pyrolysis* **48**, 93–109 (1999).
146. Faravelli, T. *et al.* Thermal Degradation of Polystyrene. *J. Anal. Appl. Pyrolysis* **6060**, 103–121 (2001).
147. Halász, L., Belina, K. & Szucs, A. Thermal degradation of poly(olefin-α olefin) copolymers. in *AIP Conference Proceedings* (2014). doi:10.1063/1.4873768.
148. Duemichen, E., Braun, U., Senz, R., Fabian, G. & Sturm, H. Assessment of a new method for the analysis of decomposition gases of polymers by a combining thermogravimetric solid-phase extraction and thermal desorption gas chromatography mass spectrometry. *J. Chromatogr. A* **1354**, 117–128 (2014).
149. Majewsky, M., Bitter, H., Eiche, E. & Horn, H. Determination of microplastic polyethylene (PE) and polypropylene (PP) in environmental samples using thermal analysis (TGA-DSC). *Sci. Total Environ.* **568**, 507–511 (2016).
150. Dümichen, E. *et al.* Fast identification of microplastics in complex environmental samples by a thermal degradation method. *Chemosphere* **174**, 572–584 (2017).
151. Rocha-Santos, T. & Duarte, A. C. A critical overview of the analytical approaches to the occurrence, the fate and the behavior of microplastics in the environment. *TrAC - Trends in Analytical Chemistry* at https://doi.org/10.1016/j.trac.2014.10.011 (2015).
152. Kusch, P. *et al.* Application of pyrolysis-gas chromatography/mass spectrometry for the identification of polymeric materials in failure analysis in the automotive industry. *Eng. Fail. Anal.* **35**, 114–124 (2013).
153. Hermabessiere, L. *et al.* Optimization, performance, and application of a pyrolysis-GC/MS

method for the identification of microplastics. *Anal. Bioanal. Chem.* **410**, 6663–6676 (2018).
154. El-Aneed, A., Cohen, A. & Banoub, J. Mass spectrometry, review of the basics: Electrospray, MALDI, and commonly used mass analyzers. *Appl. Spectrosc. Rev.* **44**, 210–230 (2009).
155. Choi, B. K., Hercules, D. M. & Zhang, T. Comparison of Quadrupole, Time-of-Flight, and Fourier Transform Mass Analyzers for LC-MS Applications. *Curr. Trends Mass Spectrom.* **18(5S)**, 24–31 (2003).
156. Fries, E. *et al.* Identification of polymer types and additives in marine microplastic particles using pyrolysis-GC/MS and scanning electron microscopy. *Environ. Sci. Process. Impacts* **15**, 1949–1956 (2013).
157. Murphy, F., Ewins, C., Carbonnier, F. & Quinn, B. Wastewater Treatment Works (WwTW) as a Source of Microplastics in the Aquatic Environment. *Environ. Sci. Technol.* (2016) doi:10.1021/acs.est.5b05416.
158. Periyasamy, A. P. & Tehrani-Bagha, A. A review on microplastic emission from textile materials and its reduction techniques. *Polymer Degradation and Stability* at https://doi.org/10.1016/j.polymdegradstab.2022.109901 (2022).
159. Šaravanja, A., Pušić, T. & Dekanić, T. Microplastics in Wastewater by Washing Polyester Fabrics. *Materials (Basel).* **15**, (2022).
160. Henry, B., Laitala, K. & Klepp, I. G. Microfibres from apparel and home textiles: Prospects for including microplastics in environmental sustainability assessment. *Sci. Total Environ.* (2019) doi:10.1016/j.scitotenv.2018.10.166.
161. Kiran, B. R., Kopperi, H. & Venkata Mohan, S. Micro/nano-plastics occurrence, identification, risk analysis and mitigation: challenges and perspectives. *Reviews in Environmental Science and Biotechnology* at https://doi.org/10.1007/s11157-021-09609-6 (2022).
162. Singh, R. P., Mishra, S. & Das, A. P. Synthetic microfibers: Pollution toxicity and remediation. *Chemosphere* at https://doi.org/10.1016/j.chemosphere.2020.127199 (2020).
163. Dehghani, S., Moore, F. & Akhbarizadeh, R. Microplastic pollution in deposited urban dust, Tehran metropolis, Iran. *Environ. Sci. Pollut. Res.* (2017) doi:10.1007/s11356-017-9674-1.
164. Amobonye, A., Bhagwat, P., Raveendran, S., Singh, S. & Pillai, S. Environmental Impacts of Microplastics and Nanoplastics: A Current Overview. *Frontiers in Microbiology* at https://doi.org/10.3389/fmicb.2021.768297 (2021).
165. Athey, S. N. *et al.* The Widespread Environmental Footprint of Indigo Denim Microfibers from Blue Jeans. *Environ. Sci. Technol. Lett.* (2020) doi:10.1021/acs.estlett.0c00498.
166. Rovira, J. & Domingo, J. L. Human health risks due to exposure to inorganic and organic chemicals from textiles: A review. *Environmental Research* at https://doi.org/10.1016/j.envres.2018.09.027 (2019).
167. Chen, Y., Chen, Q., Zhang, Q., Zuo, C. & Shi, H. An Overview of Chemical Additives on (Micro)Plastic Fibers: Occurrence, Release, and Health Risks. *Rev. Environ. Contam. Toxicol. 2022 2601* **260**, 1–25 (2022).
168. Schäfer, T. & Herter, M. Input-Oriented Chemicals Management Along the Textile Supply Chain. in *Sustainable Textile and Fashion Value Chains* (2021). doi:10.1007/978-3-030-22018-1_7.
169. Hahladakis, J. N., Velis, C. A., Weber, R., Iacovidou, E. & Purnell, P. An overview of chemical additives present in plastics: Migration, release, fate and environmental impact during their use, disposal and recycling. *J. Hazard. Mater.* **344**, 179–199 (2018).
170. Akhbarizadeh, R. *et al.* Suspended fine particulate matter (PM2.5), microplastics (MPs), and polycyclic aromatic hydrocarbons (PAHs) in air: Their possible relationships and health implications. *Environ. Res.* **192**, 110339 (2021).
171. Sungur, Ş. & Gülmez, F. Determination of metal contents of various fibers used in textile industry by MP-AES. *J. Spectrosc.* (2015) doi:10.1155/2015/640271.
172. Yetisen, A. K. *et al.* Nanotechnology in Textiles. *ACS Nano* at https://doi.org/10.1021/acsnano.5b08176 (2016).
173. Montazer, M. & Harifi, T. Introduction: Textile finishing. in *Nanofinishing of Textile Materials* (2018). doi:10.1016/b978-0-08-101214-7.00001-7.

174. Tung, W. S. & Daoud, W. A. Self-cleaning fibers via nanotechnology: A virtual reality. *Journal of Materials Chemistry* at https://doi.org/10.1039/c0jm03856c (2011).
175. Montazer, M. & Harifi, T. Nanofinishes for protective textiles. in *Nanofinishing of Textile Materials* (2018). doi:10.1016/b978-0-08-101214-7.00018-2.
176. Zhang, Y. Y., Xu, Q. B., Fu, F. Y. & Liu, X. D. Durable antimicrobial cotton textiles modified with inorganic nanoparticles. *Cellulose* at https://doi.org/10.1007/s10570-016-1012-0 (2016).
177. Rivero, P. J., Urrutia, A., Goicoechea, J. & Arregui, F. J. Nanomaterials for Functional Textiles and Fibers. *Nanoscale Research Letters* at https://doi.org/10.1186/s11671-015-1195-6 (2015).
178. Licina, D., Morrison, G. C., Bekö, G., Weschler, C. J. & Nazaroff, W. W. Clothing-Mediated Exposures to Chemicals and Particles. *Environmental Science and Technology* at https://doi.org/10.1021/acs.est.9b00272 (2019).
179. Turner, A. & Filella, M. Hazardous metal additives in plastics and their environmental impacts. *Environment International* at https://doi.org/10.1016/j.envint.2021.106622 (2021).
180. Tolinski, M. *Additives for Polyolefins*. *Additives for Polyolefins* (2009). doi:10.1201/9780203908716.ch20.
181. Rovira, J., Nadal, M., Schuhmacher, M. & Domingo, J. L. Trace elements in skin-contact clothes and migration to artificial sweat: Risk assessment of human dermal exposure. *Text. Res. J.* (2017) doi:10.1177/0040517516639816.
182. Rujido-Santos, I., Herbello-Hermelo, P., Barciela-Alonso, M. C., Bermejo-Barrera, P. & Moreda-Piñeiro, A. Metal Content in Textile and (Nano)Textile Products. *Int. J. Environ. Res. Public Health* (2022) doi:10.3390/ijerph19020944.
183. Imtiazuddin, S. M. & Tiki, A. Textile Azo Dyes; Significance, Ecological, Health, and Safety issues. *Pakistan J. Chem.* (2021) doi:10.15228/2020.v10.i01-4.p05.
184. Engel, E. *et al.* Azo pigments and a basal cell carcinoma at the thumb. *Dermatology* (2007) doi:10.1159/000109363.
185. KAWAKAMI, T., ISAMA, K. & NISHIMURA, T. Survey of Primary Aromatic Amines Originating from Azo Dyes in Commercial Textile Products in Direct Contact with Skin and in Commercial Leather Products in Japan. *J. Environ. Chem.* (2012) doi:10.5985/jec.22.197.
186. Talouizte, H., Merzouki, M., Benlemlih, M. & Bendriss Amraoui, M. Chemical Characterization of Specific Micropollutants from Textile Industry Effluents in Fez City, Morocco. *J. Chem.* (2020) doi:10.1155/2020/3268241.
187. Castillo, M. & Barceló, D. Characterisation of organic pollutants in textile wastewaters and landfill leachate by using toxicity-based fractionation methods followed by liquid and gas chromatography coupled to mass spectrometric detection. in *Analytica Chimica Acta* (2001). doi:10.1016/S0003-2670(00)00828-X.
188. Afshari, M., Tavakoli, M., Norouzifar, M. & Masoumi, Z. Effect of polyethylene glycol on physical properties of durable press finished cotton fabric. *Indian J. Fibre Text. Res.* (2006).
189. Amri, A. *et al.* Polyethylene terephthalate textile heart valve: How poly(ethylene glycol) grafting limits fibrosis. (2022) doi:10.1002/jbm.b.35065.
190. Lakhouit, A. Practical recommendations for temporary storage of medical wastes during the COVID-19 pandemic. *Indoor and Built Environment* at https://doi.org/10.1177/1420326X20950432 (2020).
191. Patrício Silva, A. L. *et al.* Increased plastic pollution due to COVID-19 pandemic: Challenges and recommendations. *Chemical Engineering Journal* at https://doi.org/10.1016/j.cej.2020.126683 (2021).
192. Adyel, T. M. Accumulation of plastic waste during COVID-19. *Science (80-.).* **369**, 1314–1315 (2020).
193. Freeman, C. *et al.* Preliminary evaluation of filtration efficiency and differential pressure astm f3502 testing methods of non-medical masks using a face filtration mount. *Int. J. Environ. Res. Public Health* (2021) doi:10.3390/ijerph18084124.
194. Anastopoulos, I. & Pashalidis, I. Single-use surgical face masks, as a potential source of microplastics: Do they act as pollutant carriers? *J. Mol. Liq.* (2021) doi:10.1016/j.molliq.2020.115247.
195. Pranaityte, B., Padarauskas, A. & Naujalis, E. Application of ICP-MS for the determination

of trace metals in textiles. *Chemija* (2007).
196. Thomas, R. *Practical Guide to ICP-MS A Tutorial for Beginners*. *PRACTICAL SPECTROSCOPY A SERIES* (2003).
197. Dussubieux, L. & Ballard, M. W. Using ICP-MS to detect inorganic elements in organic materials: A new tool to identify mordants or dyes on ancient textiles. in *Materials Research Society Symposium Proceedings* (2005). doi:10.1557/proc-852-oo4.1.
198. Mackevica, A., Olsson, M. E. & Hansen, S. F. Quantitative characterization of TiO2 nanoparticle release from textiles by conventional and single particle ICP-MS. *J. Nanoparticle Res.* (2018) doi:10.1007/s11051-017-4113-2.
199. Bolea-Fernandez, E., Rua-Ibarz, A., Velimirovic, M., Tirez, K. & Vanhaecke, F. Detection of microplastics using inductively coupled plasma-mass spectrometry (ICP-MS) operated in single-event mode. *J. Anal. At. Spectrom.* (2020) doi:10.1039/c9ja00379g.
200. Niessen, W. M. A. & Tinke, A. P. Liquid chromatography-mass spectrometry General principles and instrumentation. *Journal of Chromatography A* at https://doi.org/10.1016/0021-9673(94)01198-N (1995).
201. Editorial Team. High Performance Liquid Chromatography (HPLC) : Principle, Types, Instrumentation and Applications | LaboratoryInfo.com. *Laboratory Info* (2020).
202. Sutthivaiyakit, P. *et al.* LC-MS/MS method for the confirmatory determination of aromatic amines and its application in textile analysis. *Anal. Bioanal. Chem.* (2005) doi:10.1007/s00216-004-2852-2.
203. Tölgyesi, Á. & Sharma, V. K. Quantification of aromatic amines derived from azo colorants in textile by ion-pairing liquid chromatography tandem mass spectrometry. *J. Chromatogr. B Anal. Technol. Biomed. Life Sci.* (2020) doi:10.1016/j.jchromb.2019.121957.
204. Weschenfelder, S. E., Jos, H. J., Gebhardt, W. & Schröder, H. F. Monitoring the physicochemical and chemical treatment of textile wastewater using GC/MS, LC/MS and -MS/MS techniques. in *Separation Science and Technology* (2007). doi:10.1080/01496390701290193.
205. Zhang, X. & Laursen, R. Application of LC-MS to the analysis of dyes in objects of historical interest. *Int. J. Mass Spectrom.* (2009) doi:10.1016/j.ijms.2008.07.014.
206. Sullivan, G. L. *et al.* Detection of trace sub-micron (nano) plastics in water samples using pyrolysis-gas chromatography time of flight mass spectrometry (PY-GCToF). *Chemosphere* **249**, (2020).
207. Sullivan, G. L., Delgado-Gallardo, J., Watson, T. M. & Sarp, S. An investigation into the leaching of micro and nano particles and chemical pollutants from disposable face masks - linked to the COVID-19 pandemic. *Water Res.* (2021) doi:10.1016/j.watres.2021.117033.
208. Delgado-Gallardo, J. *et al.* Disposable FFP2 and Type IIR Medical-Grade Face Masks: An Exhaustive Analysis into the Leaching of Micro- and Nanoparticles and Chemical Pollutants Linked to the COVID-19 Pandemic. *ACS Environ. Sci. Technol. Water* **2**, 527–538 (2022).
209. Lehner, R., Weder, C., Petri-Fink, A. & Rothen-Rutishauser, B. Emergence of Nanoplastic in the Environment and Possible Impact on Human Health. *Environ. Sci. Technol.* **53**, 1748–1765 (2019).
210. Lusher, A. L., Welden, N. A., Sobral, P. & Cole, M. Sampling, isolating and identifying microplastics ingested by fish and invertebrates. *Analytical Methods* at https://doi.org/10.1039/c6ay02415g (2017).
211. Odochian, L., Moldoveanu, C. & Maftei, D. TG-FTIR study on thermal degradation mechanism of PTFE under nitrogen atmosphere and in air. Influence of the grain size. *Thermochim. Acta* **598**, 28–35 (2014).
212. Steyaert, S. M. J. G. *et al.* Faecal spectroscopy: a practical tool to assess diet quality in an opportunistic omnivore. *Wildlife Biol.* **18**, 431–438 (2012).
213. Watson, J. T. & Sparkman, O. D. *Electron Ionization*. *Introduction to Mass Spectrometry* (2008). doi:10.1002/9780470516898.ch6.
214. Crouch, S., Holker, J. & Skoog, F. *Principles of Instrumental Analysis : Introduction*. *Thomson Brooks/Cole* (2007).
215. Matsuzawa, Y., Ayabe, M., Nishino, J., Kubota, N. & Motegi, M. Evaluation of char fuel ratio in municipal pyrolysis waste. in *Fuel* (2004). doi:10.1016/j.fuel.2004.02.006.
216. Yu, J., Sun, L., Ma, C., Qiao, Y. & Yao, H. Thermal degradation of PVC: A review. *Waste*

Manag. **48**, 300–314 (2016).
217. Sin, M. C., Tan, I. K. P., Annuar, M. S. M. & Gan, S. N. Thermal behaviour and thermodegradation kinetics of poly(vinyl chloride) plasticized with polymeric and oligomeric medium-chain-length poly(3-hydroxyalkanoates). *Polym. Degrad. Stab.* **97**, 2118–2127 (2012).
218. De Amorim, M. T. S. P., Comel, C. & Vermande, P. Pyrolysis of polypropylene. I. Identification of compounds and degradation reactions. *J. Anal. Appl. Pyrolysis* (1982) doi:10.1016/0165-2370(82)80028-4.
219. Bortoluzzi, J. H., Pinheiro, E. A., Carasek, E. & Soldi, V. Solid phase microextraction to concentrate volatile products from thermal degradation of polymers. *Polym. Degrad. Stab.* (2005) doi:10.1016/j.polymdegradstab.2004.12.021.
220. Kim, Y. S. *et al.* Pyrolysis of polystyrene in a batch-type stirred vessel. *Korean J. Chem. Eng.* (1999) doi:10.1007/BF02706830.
221. Springall, A. & Romano, A. Applied Statistics for Science and Industry. *Appl. Stat.* (1979) doi:10.2307/2346746.
222. Nugnes, R., Lavorgna, M., Orlo, E., Russo, C. & Isidori, M. Toxic impact of polystyrene microplastic particles in freshwater organisms. *Chemosphere* (2022) doi:10.1016/j.chemosphere.2022.134373.
223. Wilson, N., Corbett, S. & Tovey, E. Airborne transmission of covid-19. *BMJ* **370**, 10–11 (2020).
224. Adyel, T. M. Accumulation of plastic waste during COVID-19. *Science (New York, N.Y.)* at https://doi.org/10.1126/science.abd9925 (2020).
225. Aragaw, T. A. Surgical face masks as a potential source for microplastic pollution in the COVID-19 scenario. *Mar. Pollut. Bull.* (2020) doi:10.1016/j.marpolbul.2020.111517.
226. Fadare, O. O. & Okoffo, E. D. Covid-19 face masks: A potential source of microplastic fibers in the environment. *Sci. Total Environ.* (2020) doi:10.1016/j.scitotenv.2020.140279.
227. Jung, S., Lee, S., Dou, X. & Kwon, E. E. Valorization of disposable COVID-19 mask through the thermo-chemical process. *Chem. Eng. J.* **126658**, (2021).
228. Wu, C. L., Zhang, M. Q., Rong, M. Z. & Friedrich, K. Silica nanoparticles filled polypropylene: Effects of particle surface treatment, matrix ductility and particle species on mechanical performance of the composites. *Compos. Sci. Technol.* **65**, 635–645 (2005).
229. Skorodumova, O., Tarakhno, O., Chebotaryova, O., Hapon, Y. & Emen, F. M. Formation of fire retardant properties in elastic silica coatings for textile materials. in *Materials Science Forum* (2020). doi:10.4028/www.scientific.net/MSF.1006.25.
230. Nischala, K., Rao, T. N. & Hebalkar, N. Silica-silver core-shell particles for antibacterial textile application. *Colloids Surfaces B Biointerfaces* (2011) doi:10.1016/j.colsurfb.2010.08.039.
231. Tchounwou, P. B., Yedjou, C. G., Patlolla, A. K. & Sutton, D. J. *Molecular, Clinical and Environmental Toxicology*. *Molecular, Clinical and Environmental Toxicology* vol. 101 (Springer Basel, 2012).
232. Lellis, B., Fávaro-Polonio, C. Z., Pamphile, J. A. & Polonio, J. C. Effects of textile dyes on health and the environment and bioremediation potential of living organisms. *Biotechnol. Res. Innov.* **3**, 275–290 (2019).
233. Bianco, A. & Passananti, M. Atmospheric micro and nanoplastics: An enormous microscopic problem. *Sustain.* **12**, (2020).
234. Paul, M. B. *et al.* Micro- And nanoplastics-current state of knowledge with the focus on oral uptake and toxicity. *Nanoscale Adv.* **2**, 4350–4367 (2020).
235. Toussaint, B. *et al.* Review of micro- and nanoplastic contamination in the food chain. *Food Addit. Contam. - Part A Chem. Anal. Control. Expo. Risk Assess.* **36**, 639–673 (2019).
236. Kögel, T., Bjorøy, Ø., Toto, B., Bienfait, A. M. & Sanden, M. Micro- and nanoplastic toxicity on aquatic life: Determining factors. *Science of the Total Environment* at https://doi.org/10.1016/j.scitotenv.2019.136050 (2020).
237. Prüst, M., Meijer, J. & Westerink, R. H. S. The plastic brain: Neurotoxicity of micro- And nanoplastics. *Part. Fibre Toxicol.* **17**, 1–16 (2020).
238. Bhagat, J., Zang, L., Nishimura, N. & Shimada, Y. Zebrafish: An emerging model to study microplastic and nanoplastic toxicity. *Sci. Total Environ.* **728**, 138707 (2020).

239. Masuki, H. *et al.* Acute cytotoxic effects of silica microparticles used for coating of plastic blood-collection tubes on human periosteal cells. *Odontology* **108**, 545–552 (2020).
240. Murugadoss, S. *et al.* Toxicology of silica nanoparticles: an update. *Arch. Toxicol.* **91**, 2967–3010 (2017).
241. Lin, W., Huang, Y. wern, Zhou, X. D. & Ma, Y. In vitro toxicity of silica nanoparticles in human lung cancer cells. *Toxicol. Appl. Pharmacol.* **217**, 252–259 (2006).
242. You, R. *et al.* Silica nanoparticles induce neurodegeneration-like changes in behavior, neuropathology, and affect synapse through MAPK activation. *Part. Fibre Toxicol.* **15**, 1–18 (2018).
243. Fruijtier-Pölloth, C. The toxicological mode of action and the safety of synthetic amorphous silica-A nanostructured material. *Toxicology* **294**, 61–79 (2012).
244. Grahn, H. F. & Geladi, P. *Techniques and Applications of Hyperspectral Image Analysis*. *Techniques and Applications of Hyperspectral Image Analysis* (2007). doi:10.1002/9780470010884.
245. Hudecová, J. *et al.* CH stretching region: Computational modeling of vibrational optical activity. *J. Chem. Theory Comput.* (2013) doi:10.1021/ct400285n.
246. Coates, J. Interpretation of Infrared Spectra, A Practical Approach. *Encycl. Anal. Chem.* 1–23 (2006) doi:10.1002/9780470027318.a5606.
247. Charles, J., Ramkumaar, G. R., Azhagiri, S. & Gunasekaran, S. FTIR and thermal studies on nylon-66 and 30% glass fibre reinforced nylon-66. *E-Journal Chem.* **6**, 23–33 (2009).
248. Jung, M. R. *et al.* Validation of ATR FT-IR to identify polymers of plastic marine debris, including those ingested by marine organisms. *Mar. Pollut. Bull.* **127**, 704–716 (2018).
249. Bartošová, A., Blinová, L., Sirotiak, M. & Michalíková, A. Usage of FTIR-ATR as non-destructive analysis of selected toxic dyes. **25**, 103–111 (2017).
250. A.K., S. A review on copper pollution. *Indian J. Environmental Protection* vol. 29 552–560 at (2009).
251. Keller, A. A. *et al.* Comparative environmental fate and toxicity of copper nanomaterials. *NanoImpact* **7**, 28–40 (2017).
252. Freedman, R., Olson, L. & Hoffer, B. J. Toxic effects of lead on neuronal development and function. *Environ. Health Perspect.* **89**, 27–33 (1990).
253. Gundacker, C. & Hengstschläger, M. The role of the placenta in fetal exposure to heavy metals. *Wiener Medizinische Wochenschrift* **162**, 201–206 (2012).
254. Zhang, X. *et al.* Impacts of lead/zinc mining and smelting on the environment and human health in China. *Environmental Monitoring and Assessment* at https://doi.org/10.1007/s10661-011-2115-6 (2012).
255. Burke, F. *et al.* Impact of Cadmium Polluted Groundwater on Human Health: Winder, Balochistan. *SAGE Open* (2016) doi:10.1177/2158244016634409.
256. Biver, M., Turner, A. & Filella, M. Antimony release from polyester textiles by artificial sweat solutions: A call for a standardized procedure. *Regul. Toxicol. Pharmacol.* (2021) doi:10.1016/j.yrtph.2020.104824.
257. Boreiko, C. J. & Rossman, T. G. Antimony and its compounds: Health impacts related to pulmonary toxicity, cancer, and genotoxicity. *Toxicology and Applied Pharmacology* at https://doi.org/10.1016/j.taap.2020.115156 (2020).
258. Tran, J. C. & Doucette, A. A. Cyclic Polyamide Oligomers Extracted from Nylon 66 Membrane Filter Disks as a Source of Contamination in Liquid Chromatography/Mass Spectrometry. *J. Am. Soc. Mass Spectrom.* **17**, 652–656 (2006).
259. Kruve, A., Kaupmees, K., Liigand, J., Oss, M. & Leito, I. Sodium adduct formation efficiency in ESI source. *J. Mass Spectrom.* (2013) doi:10.1002/jms.3218.
260. Wilm, M. Principles of electrospray ionization. *Molecular and Cellular Proteomics* at https://doi.org/10.1074/mcp.M111.009407 (2011).
261. Holcakova, J. *et al.* The inhibitor of cyclin-dependent kinases, olomoucine II, exhibits potent antiviral properties. *Antivir. Chem. Chemother.* (2010) doi:10.3851/IMP1460.
262. Eikenberry, S. E. *et al.* To mask or not to mask: Modeling the potential for face mask use by the general public to curtail the COVID-19 pandemic. *Infect. Dis. Model.* (2020) doi:10.1016/j.idm.2020.04.001.
263. Gov.uk. 70 million face masks for NHS and care workers through new industry deal.

Financial Services Monitor Worldwide (2020).
264. Life Science Hub Wales. UK's first medical-grade face mask manufacturing facility set to open in Cardiff | Life Sciences. https://lshubwales.com/news/uks-first-medical-grade-face-mask-manufacturing-facility-set-open-cardiff (2020).
265. Nonwovens Industry. EU Set To Increase Face Mask Production 20-Fold By November - Nonwovens Industry Magazine - News, Markets & Analysis for the Nonwovens Industry. https://www.nonwovens-industry.com/contents/view_breaking-news/2020-06-23/eu-set-to-increase-face-mask-production-20-fold-by-november (2020).
266. Gawn, J., Clayton, M., Makison, C., Crook, B. & Hill, H. Evaluating the protection afforded by surgical masks against influenza bioaerosols. *Heal. Saf. Exec.* (2008).
267. World Health Organization. Advice on the use of masks in the context of COVID-19: Interim guidance. *WHO* (2020).
268. Cumbo, E. & Scardina, G. A. Management and use of filter masks in the "none-medical" population during the Covid-19 period. *Saf. Sci.* (2021) doi:10.1016/j.ssci.2020.104997.
269. Inspec International. INSPEC International - CE marking. https://www.inspec-international.com/certification/ce-marking.
270. Gov.uk. *Essential technical requirements for new High-Volume Manufacture of Personal Protective Equipment (PPE) and Medical Devices (MD) during COVID-19*. https://www.gov.uk/government/publications/technical-specifications-for-personal-protective-equipment-ppe (2020).
271. European Commission. Internal Market, Industry, Entrepreneurship and SMEs. *Eur. Comm.* (2019).
272. Hardshell.co.uk. Surgical Face Masks- Type IIR Face Masks Made in the UK | Hardshell UK. https://hardshell.co.uk/product/surgical-face-masks-type-iir/.
273. Rodríguez, N. B., Formentini, G., Favi, C. & Marconi, M. Environmental implication of personal protection equipment in the pandemic era: LCA comparison of face masks typologies. in *Procedia CIRP* (2021). doi:10.1016/j.procir.2021.01.108.
274. Walker, T. R., Grant, J. & Archambault, M. C. Accumulation of marine debris on an intertidal beach in an urban park (Halifax Harbour, Nova Scotia). *Water Qual. Res. J. Canada* (2006) doi:10.2166/wqrj.2006.029.
275. ECHA. Candidate List of substances of very high concern for Authorisation - ECHA. *Eur. Chem. Agency* (2020).
276. White, R. Environmentally persistent alkylphenolic compounds are estrogenic. *Endocrinology* (1994) doi:10.1210/en.135.1.175.
277. Yang, Q. & Lai, S. K. Anti-PEG immunity: Emergence, characteristics, and unaddressed questions. *Wiley Interdiscip. Rev. Nanomedicine Nanobiotechnology* (2015) doi:10.1002/wnan.1339.
278. Stone, C. A. *et al.* Immediate Hypersensitivity to Polyethylene Glycols and Polysorbates: More Common Than We Have Recognized. *J. Allergy Clin. Immunol. Pract.* (2019) doi:10.1016/j.jaip.2018.12.003.
279. Wenande, E. & Garvey, L. H. Immediate-type hypersensitivity to polyethylene glycols: a review. *Clinical and Experimental Allergy* at https://doi.org/10.1111/cea.12760 (2016).
280. Swarnkumar Reddy & Osborne, W. J. Heavy metal determination and aquatic toxicity evaluation of textile dyes and effluents using Artemia salina. *Biocatal. Agric. Biotechnol.* (2020) doi:10.1016/j.bcab.2020.101574.
281. Li, Y., Leung, P., Yao, L., Song, Q. W. & Newton, E. Antimicrobial effect of surgical masks coated with nanoparticles. *J. Hosp. Infect.* (2006) doi:10.1016/j.jhin.2005.04.015.
282. Sciensano. Evaluation of the types, efficient use and health risks of application of silver-based biocides to provide antimicrobial properties to face masks applied during the COVID-19 crisis | sciensano.be. https://www.sciensano.be/en/projects/evaluation-types-efficient-use-and-health-risks-application-silver-based-biocides-provide.
283. Baranowska-Wójcik, E., Szwajgier, D., Oleszczuk, P. & Winiarska-Mieczan, A. Effects of Titanium Dioxide Nanoparticles Exposure on Human Health—a Review. *Biological Trace Element Research* at https://doi.org/10.1007/s12011-019-01706-6 (2020).
284. Han, J. & He, S. Need for assessing the inhalation of micro(nano)plastic debris shed from masks, respirators, and home-made face coverings during the COVID-19 pandemic.

Environmental Pollution at https://doi.org/10.1016/j.envpol.2020.115728 (2021).
285. Shen, M. *et al.* Recent advances in toxicological research of nanoplastics in the environment: A review. *Environmental Pollution* at https://doi.org/10.1016/j.envpol.2019.05.102 (2019).
286. Magrì, D. *et al.* PET nanoplastics interactions with water contaminants and their impact on human cells. *Environ. Pollut.* (2021) doi:10.1016/j.envpol.2020.116262.
287. Leggett, D. C. & Parker, L. V. Modeling the Equilibrium Partitioning of Organic Contaminants between PTFE, PVC, and Groundwater. *Environ. Sci. Technol.* (1994) doi:10.1021/es00056a008.
288. Teuten, E. L., Rowland, S. J., Galloway, T. S. & Thompson, R. C. Potential for plastics to transport hydrophobic contaminants. *Environ. Sci. Technol.* (2007) doi:10.1021/es071737s.
289. Benson, N. U., Fred-Ahmadu, O. H., Bassey, D. E. & Atayero, A. A. COVID-19 pandemic and emerging plastic-based personal protective equipment waste pollution and management in Africa. *J. Environ. Chem. Eng.* (2021) doi:10.1016/j.jece.2021.105222.
290. Li, L., Zhao, X., Li, Z. & Song, K. COVID-19: Performance study of microplastic inhalation risk posed by wearing masks. *J. Hazard. Mater.* (2021) doi:10.1016/j.jhazmat.2020.124955.
291. Connexions. Face Mask Manufacturer, Kn95 Mask Supplier, Disposable Face Mask Wholesale -Connexions. https://www.connexions-tech.com/.
292. Picó, Y. & Barceló, D. Analysis and prevention of microplastics pollution in water: Current perspectives and future directions. *ACS Omega* (2019) doi:10.1021/acsomega.9b00222.
293. Seeley, M. E., Song, B., Passie, R. & Hale, R. C. Microplastics affect sedimentary microbial communities and nitrogen cycling. *Nat. Commun.* (2020) doi:10.1038/s41467-020-16235-3.
294. Luo, H. *et al.* Leaching behavior of fluorescent additives from microplastics and the toxicity of leachate to Chlorella vulgaris. *Sci. Total Environ.* (2019) doi:10.1016/j.scitotenv.2019.04.401.
295. Islam, S., Apitius, L., Jakob, F. & Schwaneberg, U. Targeting microplastic particles in the void of diluted suspensions. *Environ. Int.* (2019) doi:10.1016/j.envint.2018.12.029.
296. Paul, B. *et al.* Silica incorporated cellulose fibres as green concept for textiles with reduced flammability. *Polym. Degrad. Stab.* (2022) doi:10.1016/j.polymdegradstab.2021.109808.
297. Attia, N. F., Moussa, M., Sheta, A. M. F., Taha, R. & Gamal, H. Synthesis of effective multifunctional textile based on silica nanoparticles. *Prog. Org. Coatings* (2017) doi:10.1016/j.porgcoat.2017.02.006.
298. Liang, H. *et al.* Cytotoxicity of silica nanoparticles on HaCaT cells. *J. Appl. Toxicol.* (2014) doi:10.1002/jat.2953.
299. Harada, M. Minamata disease: Methylmercury poisoning in Japan caused by environmental pollution. *Crit. Rev. Toxicol.* (1995) doi:10.3109/10408449509089885.
300. Ha, E. *et al.* Current progress on understanding the impact of mercury on human health. *Environ. Res.* (2017) doi:10.1016/j.envres.2016.06.042.
301. Jarray, A., Gerbaud, V. & Hemati, M. Polymer-plasticizer compatibility during coating formulation: A multi-scale investigation. *Prog. Org. Coatings* (2016) doi:10.1016/j.porgcoat.2016.08.008.
302. Vieira, M. G. A., Da Silva, M. A., Dos Santos, L. O. & Beppu, M. M. Natural-based plasticizers and biopolymer films: A review. *European Polymer Journal* at https://doi.org/10.1016/j.eurpolymj.2010.12.011 (2011).
303. Koley, D. & Bard, A. J. Triton X-100 concentration effects on membrane permeability of a single HeLa cell by scanning electrochemical microscopy (SECM). *Proc. Natl. Acad. Sci. U. S. A.* (2010) doi:10.1073/pnas.1011614107.
304. Yi, S., Deng, Y. & Sun, S. Adsorption and dyeing characteristics of reactive dyes onto cotton fiber in nonionic Triton X-100 reverse micelles. *Fibers Polym.* (2014) doi:10.1007/s12221-014-2131-6.
305. Karuppiah, S., Thangaraj, S., Palaniappan, S. A. & Lakshmanan, S. O. Influence of surfactants on structural, morphological, optical and antibacterial properties of SnO2 nanoparticles. *IET Nanobiotechnology* (2019) doi:10.1049/iet-nbt.2019.0095.
306. Hongthong, S., Leese, H. S., Allen, M. J. & Chuck, C. J. Assessing the conversion of various nylon polymers in the hydrothermal liquefaction of macroalgae. *Environ. - MDPI*

(2021) doi:10.3390/ENVIRONMENTS8040034.

307. Madhav, S., Ahamad, A., Singh, P. & Mishra, P. K. A review of textile industry: Wet processing, environmental impacts, and effluent treatment methods. *Environ. Qual. Manag.* (2018) doi:10.1002/tqem.21538.
308. Ni, B. J. *et al.* Microplastics Mitigation in Sewage Sludge through Pyrolysis: The Role of Pyrolysis Temperature. *Environ. Sci. Technol. Lett.* (2020) doi:10.1021/acs.estlett.0c00740.
309. Steinmetz, Z., Kintzi, A., Muñoz, K. & Schaumann, G. E. A simple method for the selective quantification of polyethylene, polypropylene, and polystyrene plastic debris in soil by pyrolysis-gas chromatography/mass spectrometry. *J. Anal. Appl. Pyrolysis* (2020) doi:10.1016/j.jaap.2020.104803.
310. Hansen, J., Melchiorsen, J., Ciacotich, N., Gram, L. & Sonnenschein, E. C. Effect of polymer type on the colonization of plastic pellets by marine bacteria. *FEMS Microbiol. Lett.* (2021) doi:10.1093/femsle/fnab026.
311. Guo, X. pan *et al.* Antibiotic resistance genes in biofilms on plastic wastes in an estuarine environment. *Sci. Total Environ.* (2020) doi:10.1016/j.scitotenv.2020.140916.
312. Khan, M. N., Ul Haq, F., Rahman, S., Ali, A. & Musharraf, S. G. Metabolite distribution and correlation studies of Ziziphus jujuba and Ziziphus nummularia using LC-ESI-MS/MS. *J. Pharm. Biomed. Anal.* (2020) doi:10.1016/j.jpba.2019.112918.

Appendices

Additional Tables, Figures Calibration curves of the analysis and photographs of the relevant equipment.

Appendix A-1

Figure A-1.1. Malvern ZetaSizer Nano setup.

Figure A-1.2. Perkin Elmer ATR-FTI.

Figure A-1.3. Liquid chromatography mass spectrometer (LC-MS).

Appendix A-2

Supplementary figures and tables for Chapter 2.

Table A-2.1. Concentration and relative standard deviation (RSD) for PVC on a river sample. Information regarding intensity (of both the sample and internal standard), concentrations, means, standard deviation and relative standard deviation is facilitated . The data shown demonstrate PVC was not detected in the samples.

PVC					
Ion Markers	**Mass-to-charge ratio (m/z)**	**Intensity sample 1**	**Intensity sample 2**	**Intensity sample 3**	**Mean intensity**
Toluene	91	-7.63E+08	-8.72E+08	1.32E+08	-5.01E+08
Naphthalene	128	-1.43E+08	2.37E+07	-1.64E+08	-9.44E+07
Indene	116	-1.65E+08	-1.02E+08	-1.67E+08	-1.45E+08
1-Methyl-naphthalene	142	-7.25E+07	-3.86E+07	-7.06E+07	-6.05E+07
Biphenyl	154	2.21E+09	2.98E+09	1.87E+09	2.35E+09
Ion Markers	**Mass-to-charge ratio (m/z)**	**St Dev (±)**	**Intensity internal standard 1**	**Intensity internal standard 2**	**Intensity internal standard 3**
Toluene	91	4.50E+08	2.30E+07	6.69E+07	1.04E+08
Naphthalene	128	8.39E+07	2.30E+07	6.69E+07	1.04E+08
Indene	116	3.02E+07	2.30E+07	6.69E+07	1.04E+08
1-Methyl-naphthalene	142	1.56E+07	2.30E+07	6.69E+07	1.04E+08
Biphenyl	154	4.64E+08	2.30E+07	6.69E+07	1.04E+08
Ion Markers	**Mass-to-charge ratio (m/z)**	**Concentration 1 (ng)**	**Concentration 2 (ng)**	**Concentration 3 (ng)**	
Toluene	91	-3.32E+01	-1.30E+01	1.27E+00	
Naphthalene	128	-6.23E+00	3.54E-01	-1.57E+00	
Indene	116	-7.19E+00	-1.53E+00	-1.61E+00	
1-Methyl-naphthalene	142	-3.15E+00	-5.77E-01	-6.79E-01	
Biphenyl	154	9.60E+01	4.46E+01	1.80E+01	
	Totals	**4.62E+01**	**2.98E+01**	**1.55E+01**	
Ion Markers	**Mass-to-charge ratio (m/z)**	**Mean Concentration**	**St Dev (±)**	**Relative St Dev (RSD) (%)**	
Toluene	91	-1.50E+01	14.15	-9.44E+01	
Naphthalene	128	-2.48E+00	2.76	-1.11E+02	
Indene	116	-3.44E+00	2.65	-7.70E+01	
1-Methyl-naphthalene	142	-1.47E+00	1.19	-8.11E+01	
Biphenyl	154	5.29E+01	32.35	6.12E+01	
	Totals	3.05E+01	12.55	4.12E+01	

Appendix A-3
Supplementary figures and tables for Chapter 3.

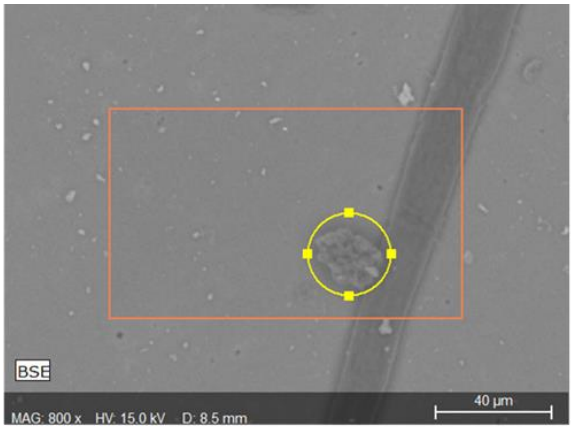

Spectrum: Point

Element	AN	Series	Net	unn. C [wt.%]	norm. C [wt.%]	Atom. C [at.%]	Error [%]
Oxygen	8	K-series	590	24.31	35.70	36.78	4.5
Carbon	6	K-series	263	22.03	32.35	44.40	4.9
Aluminium	13	K-series	2242	17.15	25.19	15.39	0.8
Silicon	14	K-series	375	3.53	5.18	3.04	0.2
Lead	82	M-series	24	0.44	0.65	0.05	0.0
Phosphorus	15	K-series	29	0.28	0.41	0.22	0.0
Selenium	34	L-series	24	0.26	0.39	0.08	0.0
Cobalt	27	K-series	1	0.04	0.06	0.02	0.0
Chromium	24	K-series	1	0.04	0.06	0.02	0.0
Scandium	21	K-series	0	0.00	0.00	0.00	0.0
Vanadium	23	K-series	0	0.00	0.00	0.00	0.0
Tin	50	L-series	0	0.00	0.00	0.00	0.0
Cadmium	48	L-series	0	0.00	0.00	0.00	0.0
Bismuth	83	M-series	0	0.00	0.00	0.00	0.0
Antimony	51	L-series	0	0.00	0.00	0.00	0.0
Arsenic	33	L-series	0	0.00	0.00	0.00	0.0
Copper	29	K-series	0	0.00	0.00	0.00	0.0
Total:				68.11	100.00	100.00	

Figure A-3.1. EDS of polymer fragments from mask 3.

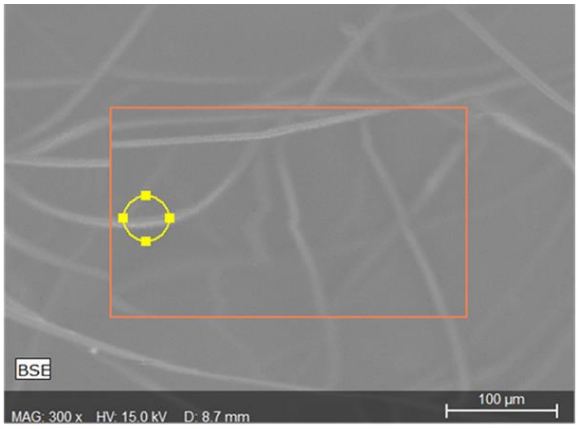

Spectrum: Point

Element	AN	Series	Net	unn. C [wt.%]	norm. C [wt.%]	Atom. C [at.%]	Error [%]
Oxygen	8	K-series	18	13.24	79.42	91.20	7.6
Silicon	14	K-series	3	1.11	6.63	4.34	0.1
Arsenic	33	L-series	2	1.49	8.95	2.20	0.1
Sulfur	16	K-series	2	0.59	3.52	2.02	0.0
Cadmium	48	L-series	1	0.24	1.44	0.24	0.0
Phosphorus	15	K-series	0	0.00	0.01	0.00	0.0
Titanium	22	K-series	0	0.00	0.01	0.00	0.0
Chromium	24	K-series	0	0.00	0.01	0.00	0.0
Copper	29	K-series	0	0.00	0.01	0.00	0.0
Zinc	30	K-series	0	0.00	0.01	0.00	0.0
Lead	82	M-series	0	0.00	0.01	0.00	0.0
Carbon	6	K-series	0	0.00	0.00	0.00	0.0
Total:				16.68	100.00	100.00	

Figure A-3.2. EDS results of Mask 4 coloured fibres (purple).

Spectrum: Point

Element	AN	Series	Net	unn. C [wt.%]	norm. C [wt.%]	Atom. C [at.%]	Error [%]
Aluminium	13	K-series	2954	46.40	51.01	41.60	2.2
Oxygen	8	K-series	588	35.40	38.91	53.51	6.5
Titanium	22	K-series	51	2.16	2.37	1.09	0.1
Phosphorus	15	K-series	83	1.84	2.02	1.44	0.1
Silicon	14	K-series	62	1.48	1.62	1.27	0.1
Antimony	51	L-series	27	1.12	1.23	0.22	0.1
Tin	50	L-series	11	0.44	0.49	0.09	0.0
Chromium	24	K-series	7	0.38	0.42	0.18	0.0
Selenium	34	L-series	16	0.37	0.41	0.11	0.0
Copper	29	K-series	2	0.31	0.34	0.12	0.0
Arsenic	33	L-series	12	0.30	0.33	0.10	0.0
Scandium	21	K-series	9	0.30	0.33	0.16	0.0
Bismuth	83	M-series	6	0.27	0.30	0.03	0.0
Vanadium	23	K-series	3	0.14	0.16	0.07	0.0
Cadmium	48	L-series	1	0.05	0.05	0.01	0.0
Cobalt	27	K-series	0	0.00	0.00	0.00	0.0
Lead	82	M-series	0	0.00	0.00	0.00	0.0
Carbon	6	K-series	0	0.00	0.00	0.00	0.0
			Total:	90.97	100.00	100.00	

Figure A-3.3. EDS results of Grain from Mask 6.

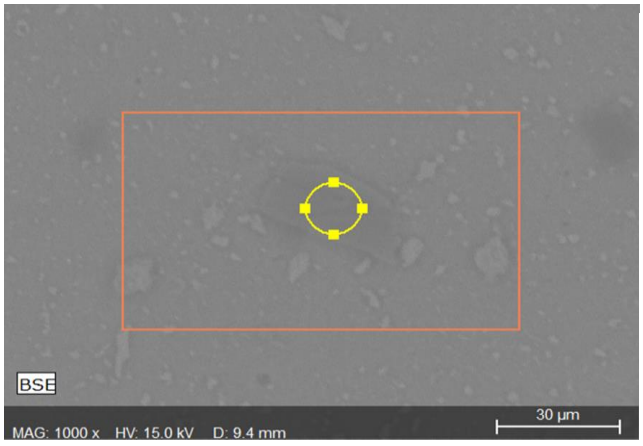

Spectrum: Point

Element	AN	Series	Net	unn. C [wt.%]	norm. C [wt.%]	Atom. C [at.%]	Error [%]
Oxygen	8	K-series	34	59.74	50.11	63.80	26.6
Aluminium	13	K-series	63	39.45	33.09	24.98	1.8
Silicon	14	K-series	11	8.83	7.40	5.37	0.4
Magnesium	12	K-series	4	2.71	2.27	1.91	0.2
Phosphorus	15	K-series	3	2.49	2.09	1.38	0.1
Sulfur	16	K-series	2	1.35	1.13	0.72	0.1
Chlorine	17	K-series	2	1.42	1.19	0.69	0.1
Sodium	11	K-series	1	0.82	0.68	0.61	0.1
Arsenic	33	L-series	2	2.41	2.02	0.55	0.2
Calcium	20	K-series	1	0.00	0.00	0.00	0.0
Titanium	22	K-series	0	0.00	0.00	0.00	0.0
Chromium	24	K-series	0	0.00	0.00	0.00	0.0
Cobalt	27	K-series	1	0.00	0.00	0.00	0.0
Copper	29	K-series	0	0.00	0.00	0.00	0.0
Cadmium	48	L-series	0	0.00	0.00	0.00	0.0
Lead	82	M-series	0	0.00	0.00	0.00	0.0
Carbon	6	K-series	0	0.00	0.00	0.00	0.0
			Total:	119.23	100.00	100.00	

Figure A-3.4. EDS results of Grain from Mask 7C.

Table A-3.1. Analysis conditions for HPLC in analysis carried out in Chapter 3.

Agilent 1100 for LC/UV and Dionex Ultimate 3000 for LC/MS	
Waters XBridge C18 column: 3.5 µm x 2.1 mm x 150 mm Guard column: XBridge C18 3.5 µm x 2.1 mm x 10 mm	
Flow rate 200µl/min for LC/UV; 150µl/min for LC/MS	
Mobile Phase A = 0.1% Formic acid; 2% MeCN in H_2O	
Mobile Phase B = 0.1% Formic acid in MeCN	
5µl full loop injection	
Mobile Phase Gradient:	
Time(mins)	**%B**
0-2	2
2-30	90
30-32	90
32-34	2
34-37	2

Table A-3.2. Analysis conditions for UV-Vis / Diode Array in analysis carried out in Chapter 3.

Agilent 1100 UV-Vis parameters:			
Wavelength (nm)	**Bandwidth**	**Reference**	**Bandwidth**
254	4	360	100
214	16	360	100
360	32	360	100
DAD Spectrum	190 – 700 nm	**Step**	2 nm

Table A-3.3. Analysis conditions for MS in analysis carried out in Chapter 3.

Thermo LTQ Orbitrap XL with API ion spray source	
Parameters	**+ve mode**
Sheath gas flow	15
Aux Gas	2
Probe kV	4.3
Capillary T (°C)	325
Capillary V	43
Tube Lens V	150
MS Scan	FT: Full MS Profile mode m/z 200-1000; Resolution 60,000

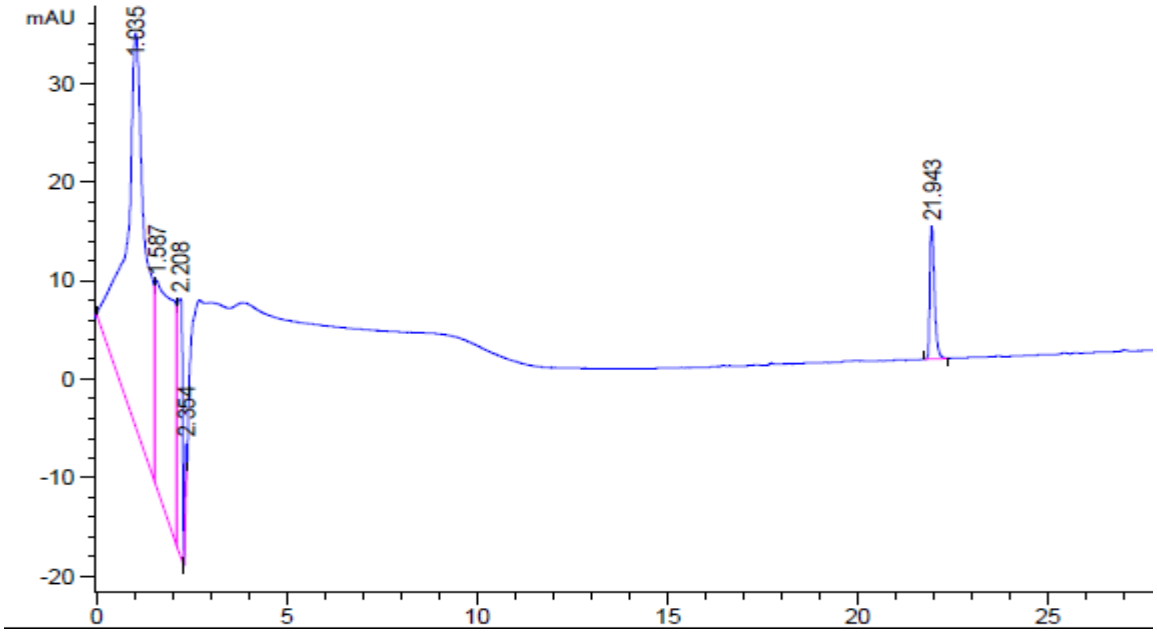

Figure A-3.5. LC-UV adsorption of Mask 2 absorbance peak 21.93 correlates with LCMS data for azo like compounds.

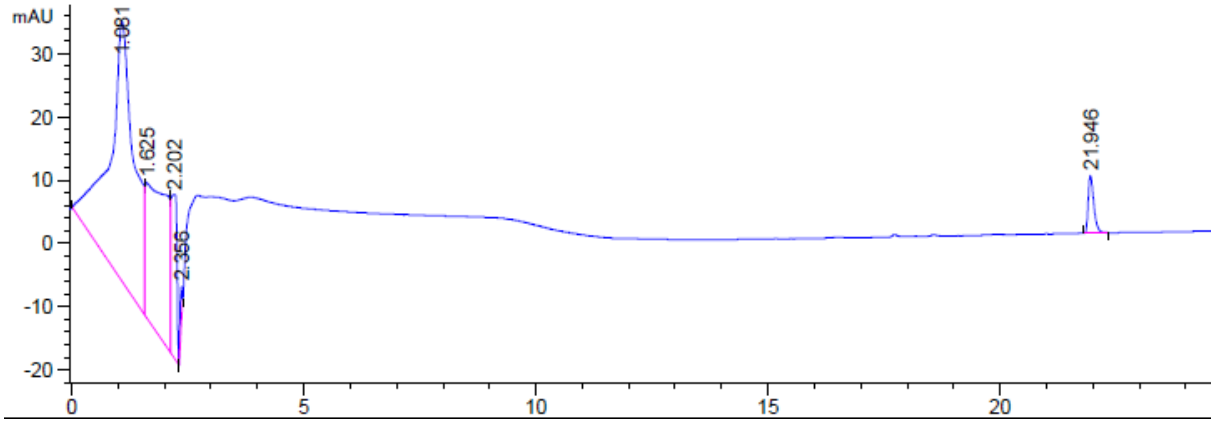

Figure A-3.6. LC-UV adsorption of Mask 5 absorbance peak 21.93 correlates with LCMS data for azo like compounds.

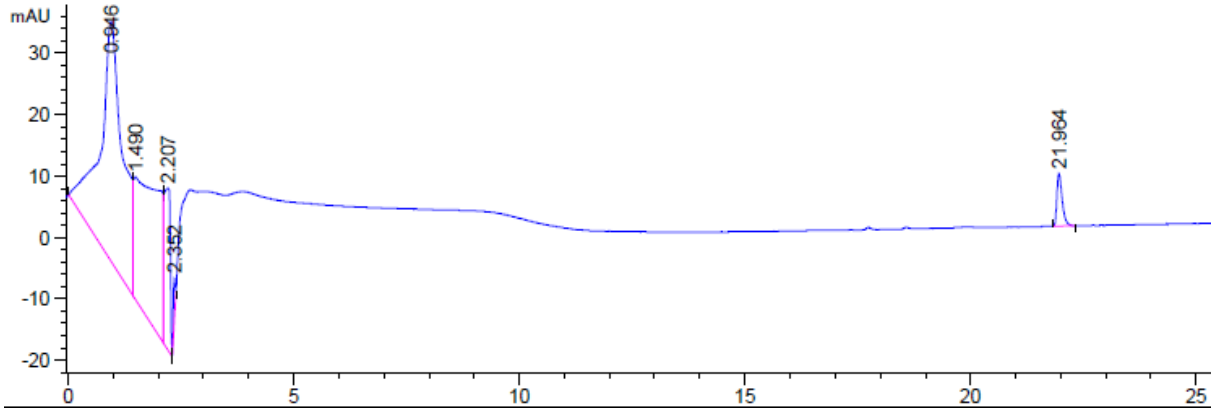

Figure A-3.7. LC-UV adsorption of Mask 7a absorbance peak 21.93 correlates with LCMS data for azo like compounds.

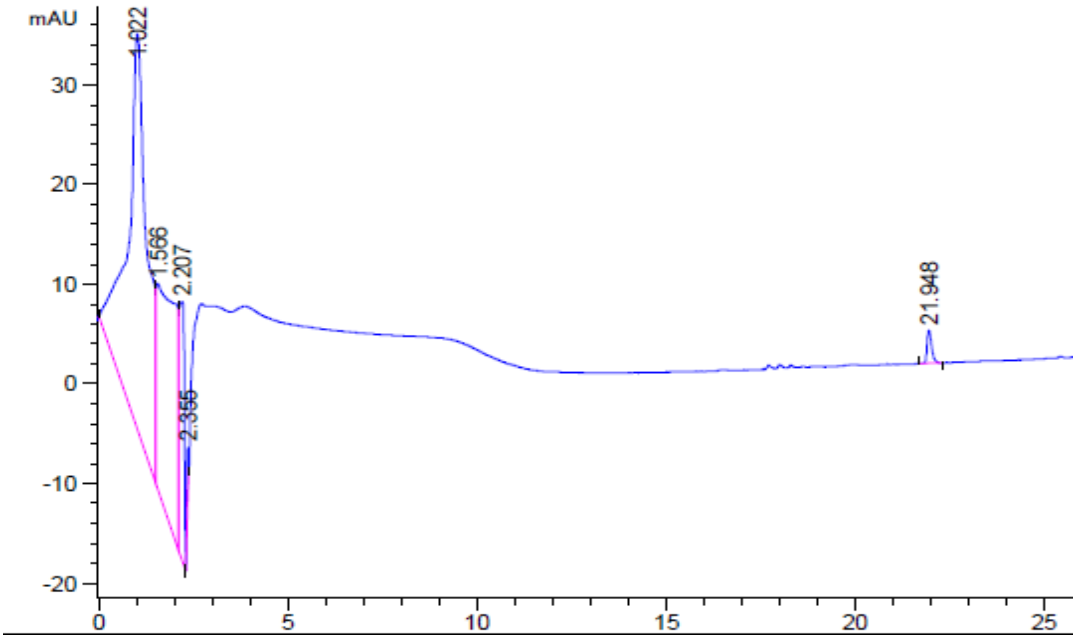

Figure A-3.8. LC-UV adsorption of Mask 7c absorbance peak 21.93 correlates with LCMS data for azo like compounds.

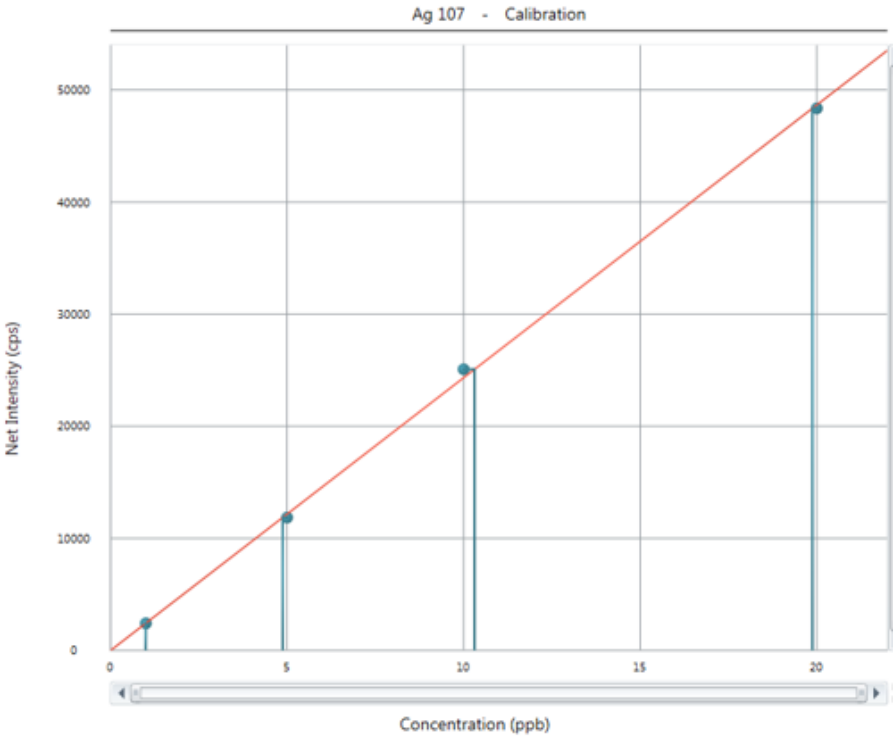

Figure A-3.9. Calibration curve of the ICP-MS analyses of the leachates for Ag element.

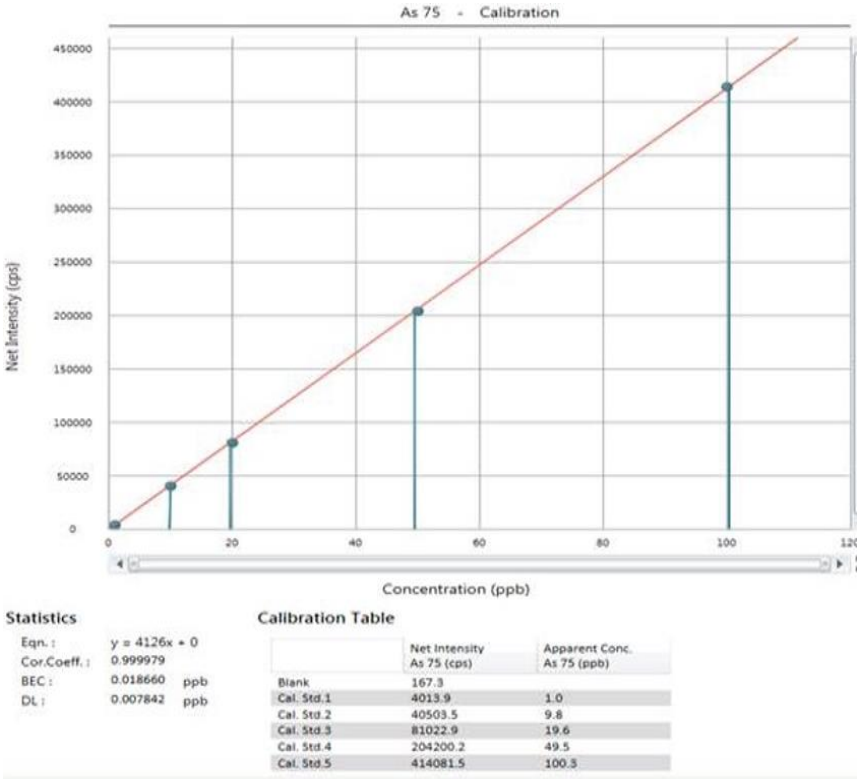

Figure A-3.10. Calibration curve of the ICP-MS analyses of the leachates for As element.

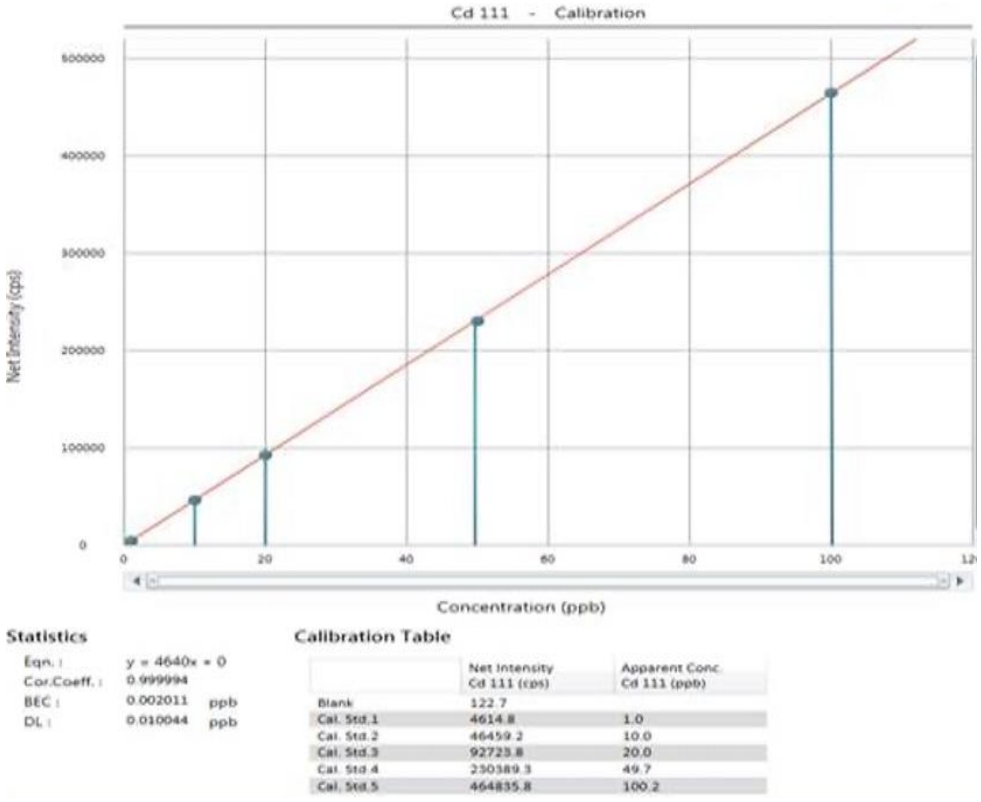

Figure A-3.11. Calibration curve of the ICP-MS analyses of the leachates for Cd element.

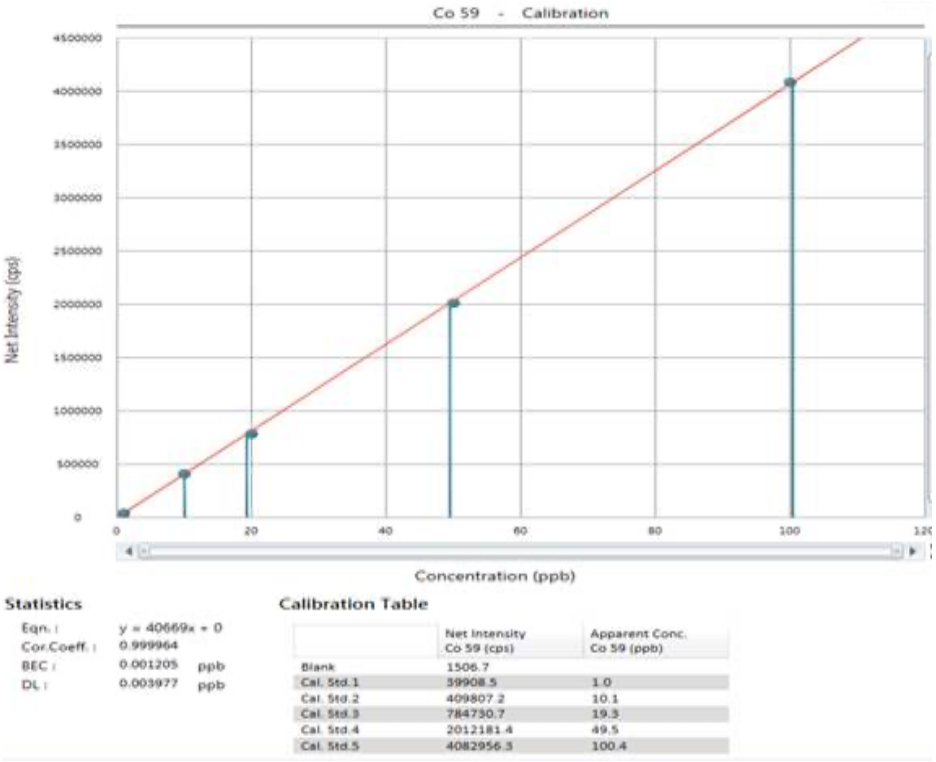

Figure A-3.12. Calibration curve of the ICP-MS analyses of the leachates for Co element.

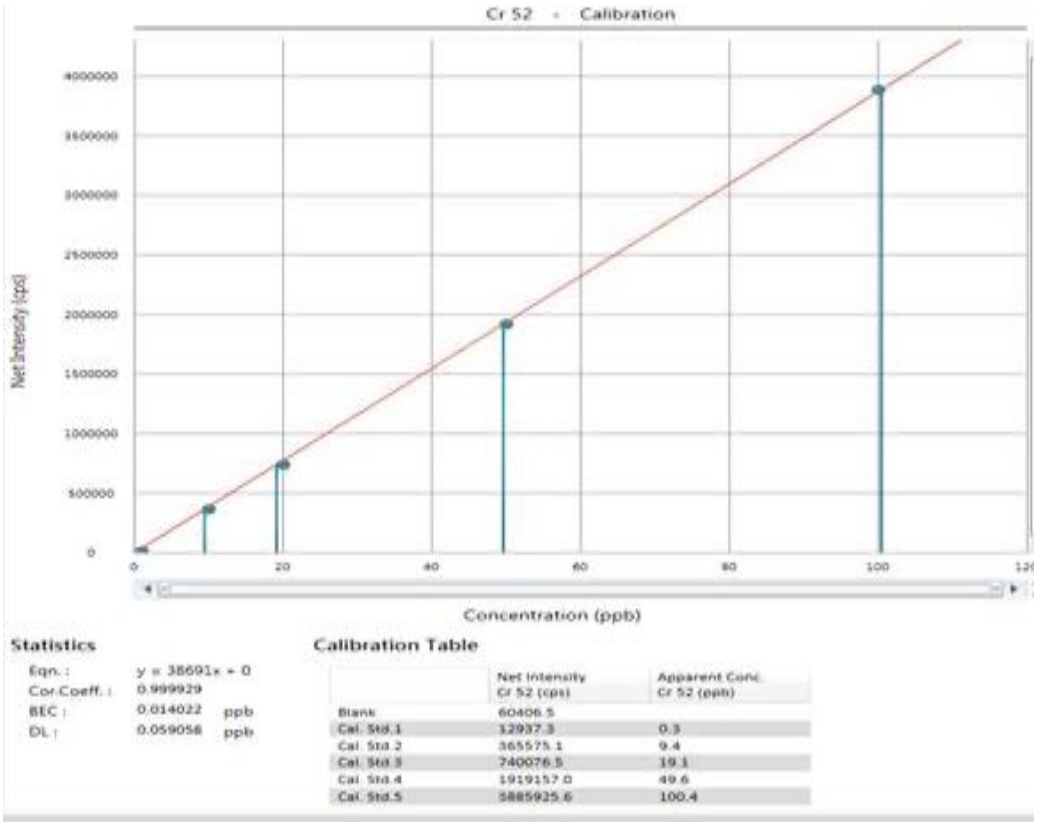

Figure A-3.13. Calibration curve of the ICP-MS analyses of the leachates for Cr element.

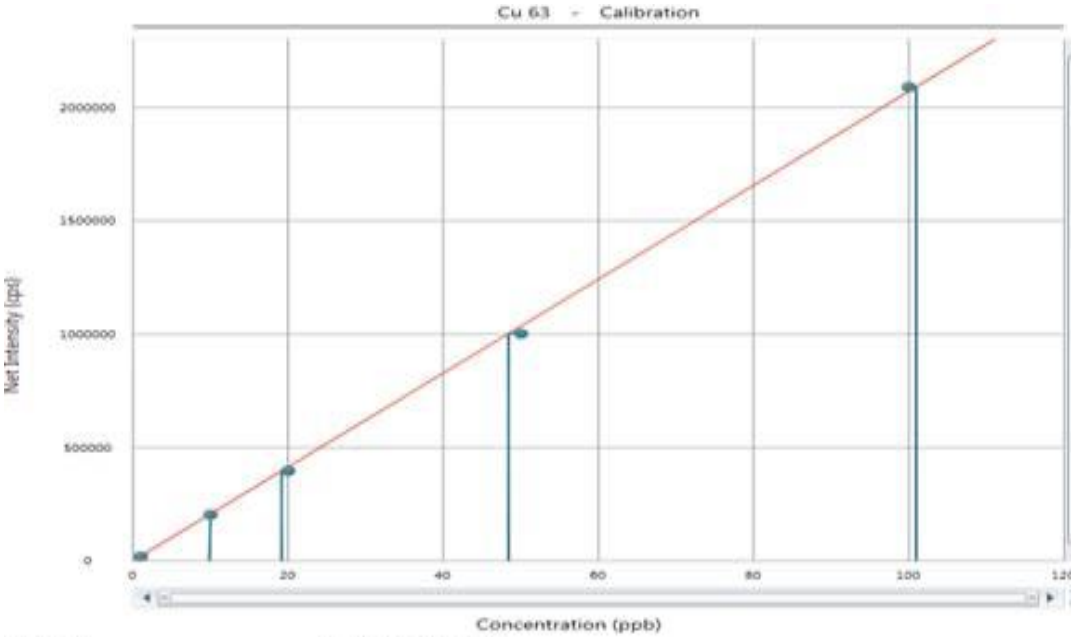

Figure A-3.14. Calibration curve of the ICP-MS analyses of the leachates for Cu element.

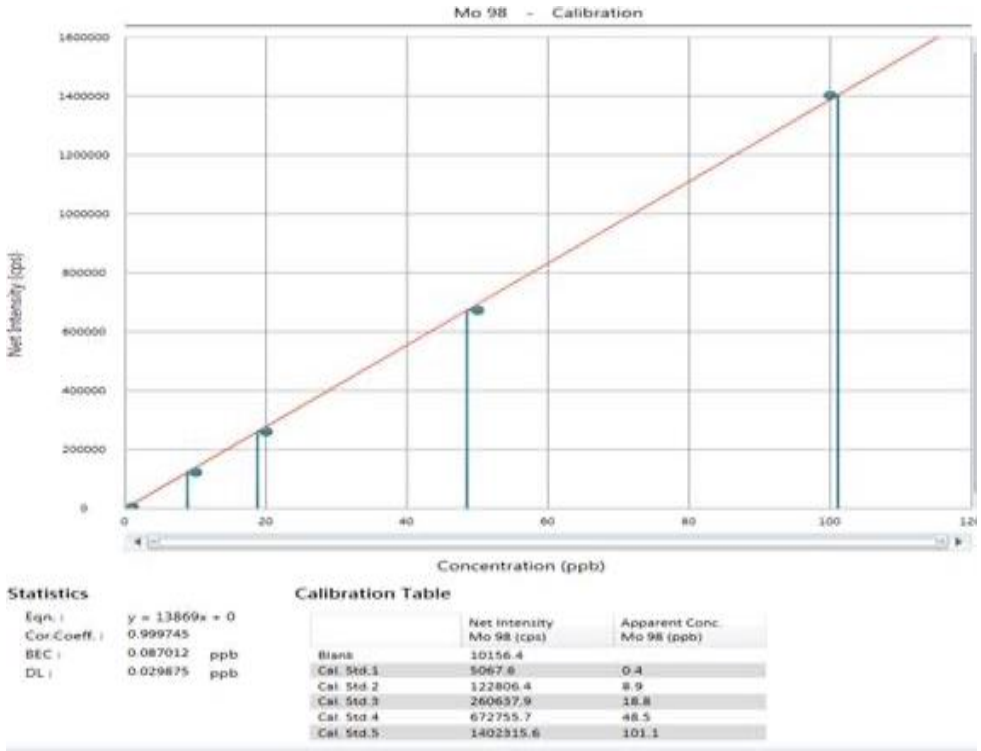

Figure A-3.15. Calibration curve of the ICP-MS analyses of the leachates for Mo element.

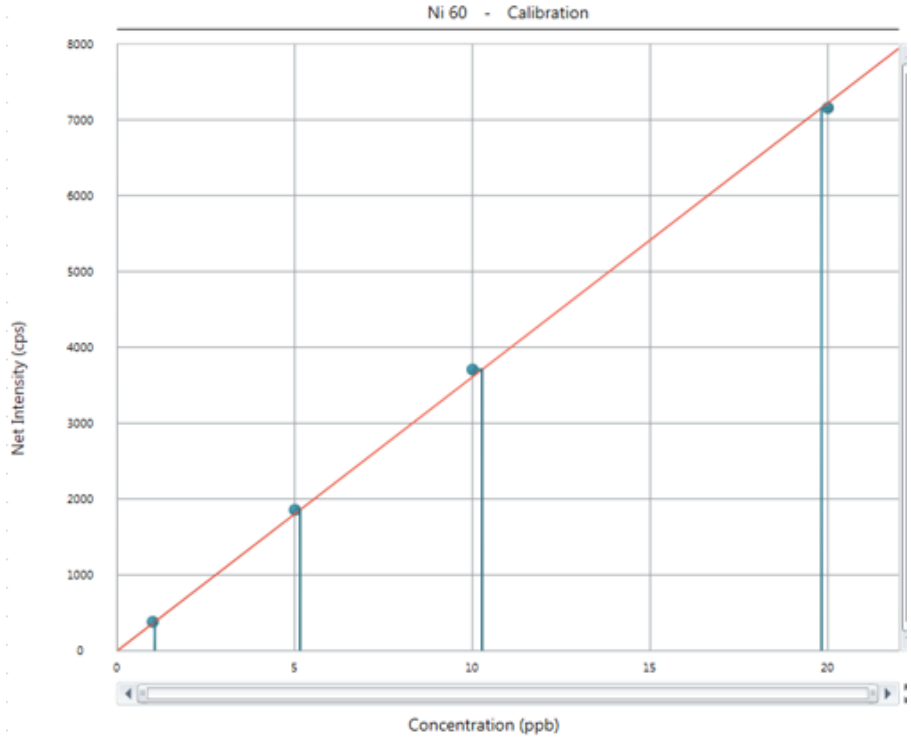

Statistics

Eqn. :	y = 361x + 0	
Cor.Coeff. :	0.999877	
BEC :	0.087725	ppb
DL :	0.026716	ppb

Calibration Table

	Net Intensity Ni 60 (cps)	Apparent Conc. Ni 60 (ppb)
Blank	31.7	
Cal. Std.1	383.0	1.1
Cal. Std.2	1858.5	5.1
Cal. Std.3	3707.5	10.3
Cal. Std.4	7156.1	19.8

Figure A-3.16. Calibration curve of the ICP-MS analyses of the leachates for Ni element.

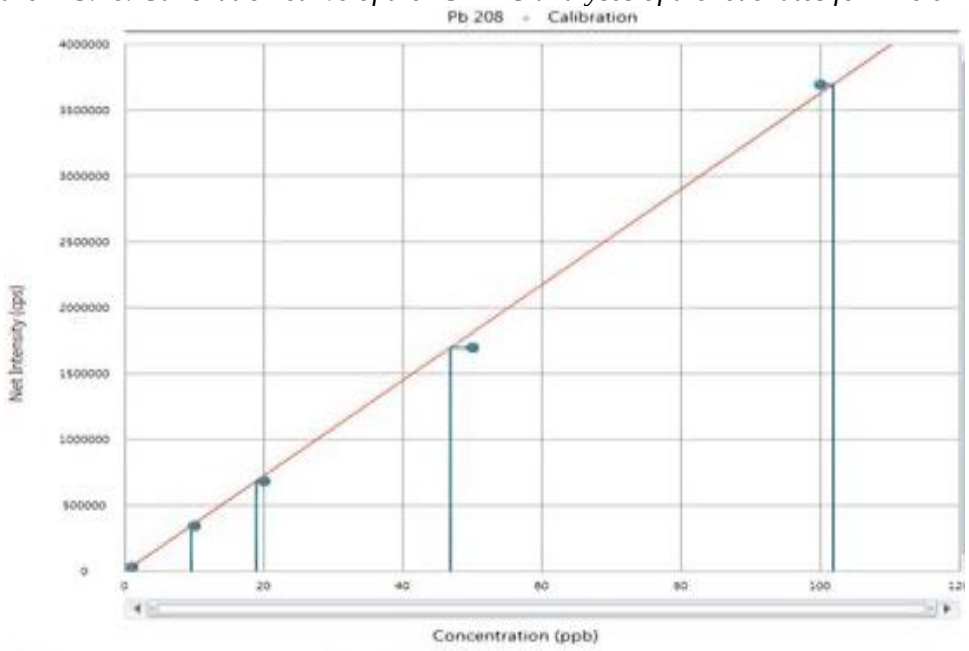

Statistics

Eqn. :	y = 36253x + 0	
Cor.Coeff. :	0.999425	
BEC :	0.000726	ppb
DL :	0.002321	ppb

Calibration Table

	Net Intensity Pb 208 (cps)	Apparent Conc. Pb 208 (ppb)
Blank	934.4	
Cal. Std.1	34272.0	0.9
Cal. Std.2	345858.2	9.5
Cal. Std.3	684925.4	18.9
Cal. Std.4	1697510.8	46.8
Cal. Std.5	3692632.9	101.9

Figure A-3.17. Calibration curve of the ICP-MS analyses of the leachates for Pb element.

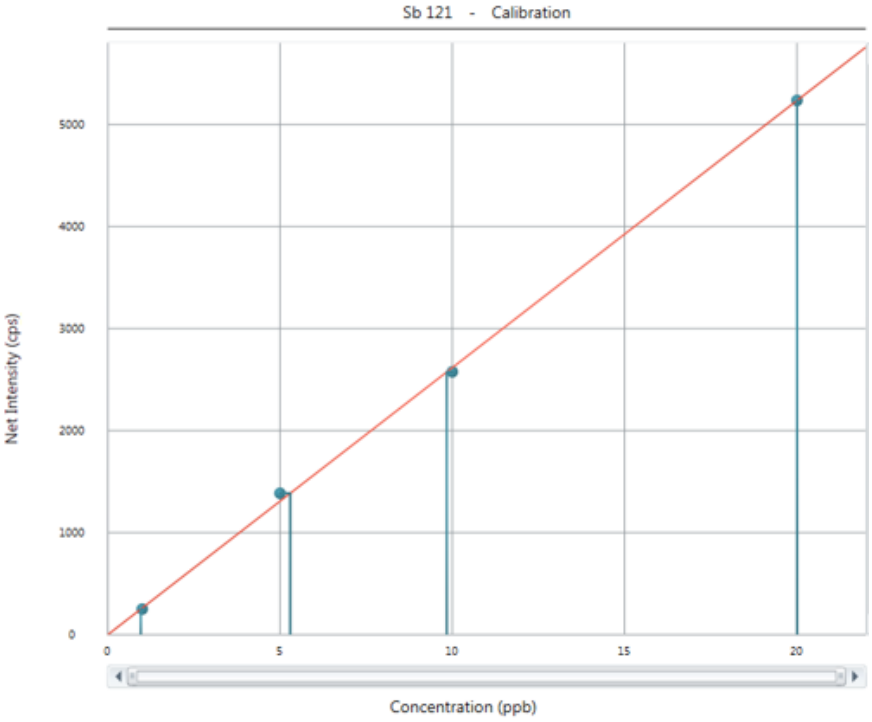

Statistics

Eqn. :	y = 262x + 0	
Cor.Coeff. :	0.999890	
BEC :	0.098052	ppb
DL :	0.047714	ppb

Calibration Table

	Net Intensity Sb 121 (cps)	Apparent Conc. Sb 121 (ppb)
Blank	25.7	
Cal. Std.1	252.0	1.0
Cal. Std.2	1387.1	5.3
Cal. Std.3	2576.2	9.8
Cal. Std.4	5237.0	20.0

Figure A-3.18. Calibration curve of the ICP-MS analyses of the leachates for Sb element.

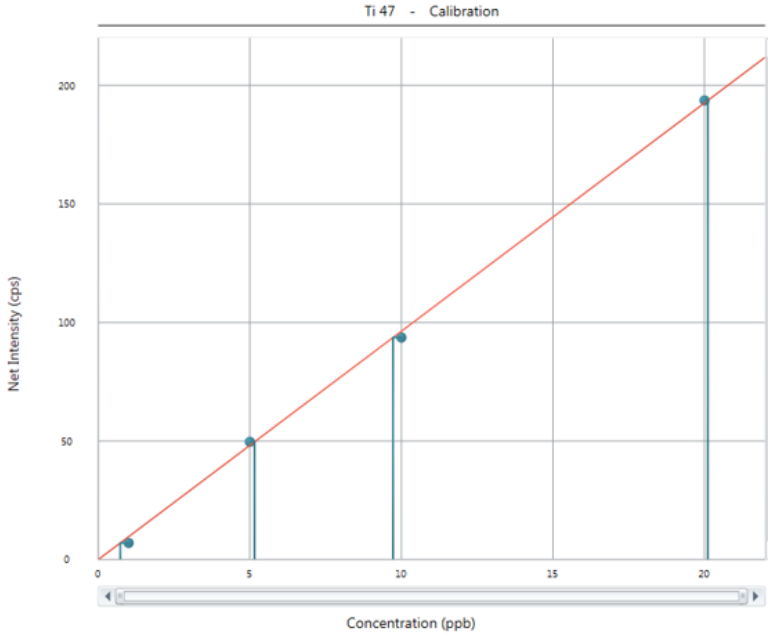

Statistics

Eqn. :	y = 10x + 0	
Cor.Coeff. :	0.999823	
BEC :	0.380756	ppb
DL :	0.179860	ppb

Calibration Table

	Net Intensity Ti 47 (cps)	Apparent Conc. Ti 47 (ppb)
Blank	3.7	
Cal. Std.1	7.0	0.7
Cal. Std.2	49.7	5.2
Cal. Std.3	93.7	9.7
Cal. Std.4	193.7	20.1

Figure A-3.19. Calibration curve of the ICP-MS analyses of the leachates for Ti element.

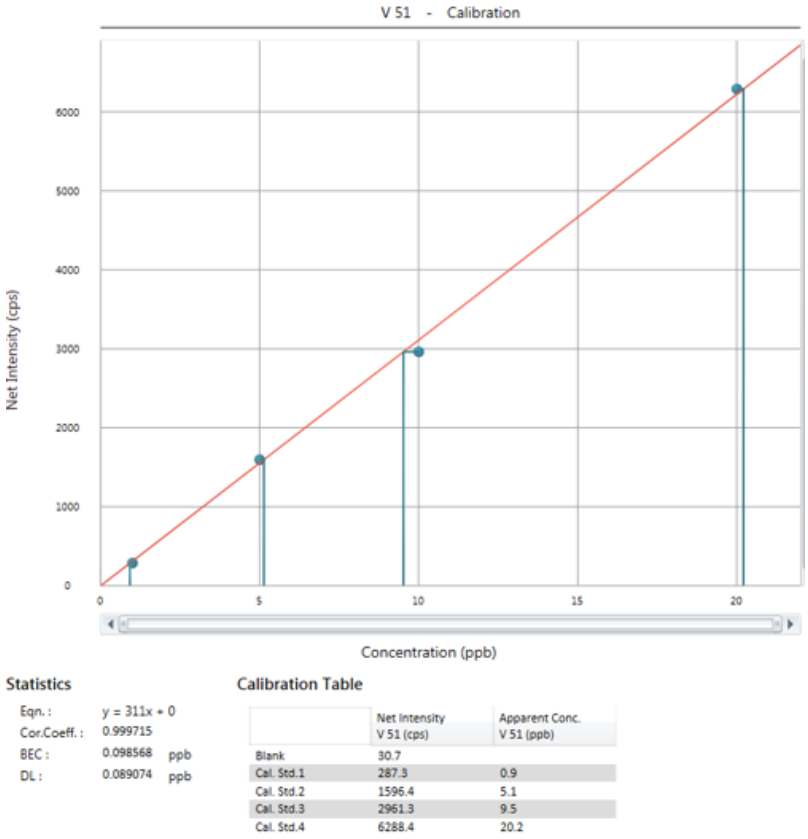

Figure A-3.20. Calibration curve of the ICP-MS analyses of the leachates for V element.

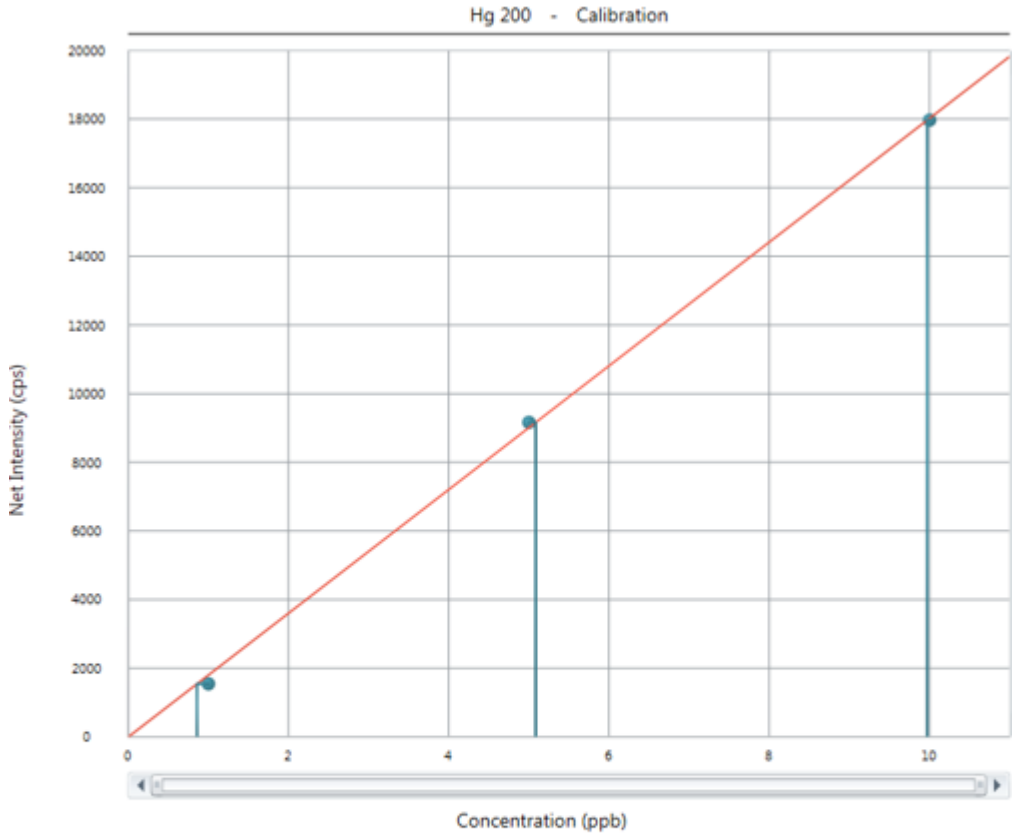

Statistics

Eqn. :	y = 1802x + 0	
Cor.Coeff. :	0.999889	
BEC :	0.030150	ppb
DL :	0.012605	ppb

Calibration Table

	Net Intensity Hg 200 (cps)	Apparent Conc. Hg 200 (ppb)
Blank	54.3	
Cal. Std.1	1548.1	0.9
Cal. Std.2	9164.3	5.1
Cal. Std.3	17969.4	10.0

Figure A-3.21. Calibration curve of the ICP-MS analyses of the leachates for Hg element.

Appendix A-4

Supplementary figures and tables for Chapter 4.

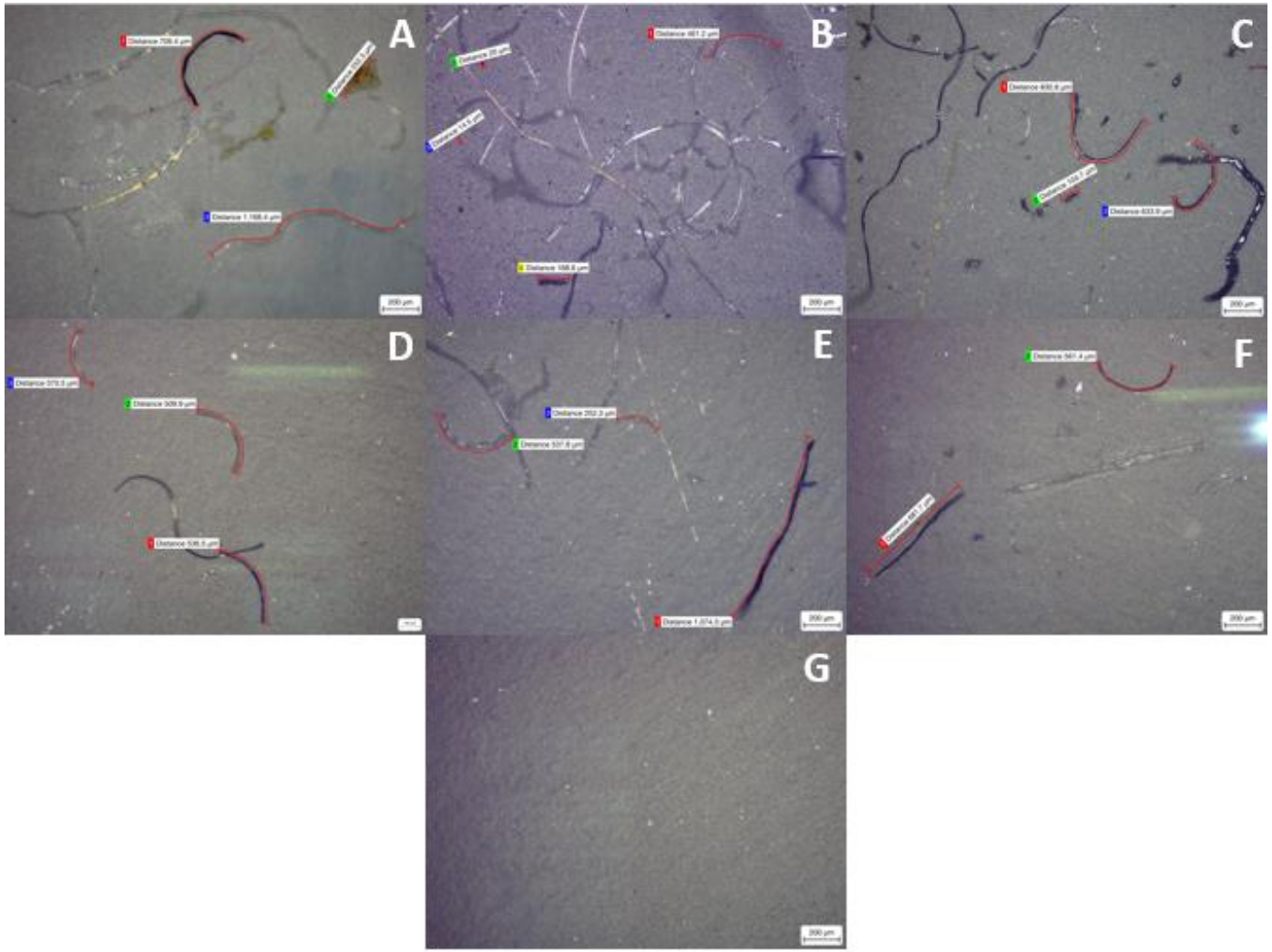

Figure A-4.1. Light microscope images at 50x overall magnification of 0.1 µm pore size membranes for all brands after filtration. (A) Baltic, (B) Geji, (C) Soyes (all FFP2), (D) Duronic, © NHS, (F) Omnitex (all Type IIR) and (G) Blank.

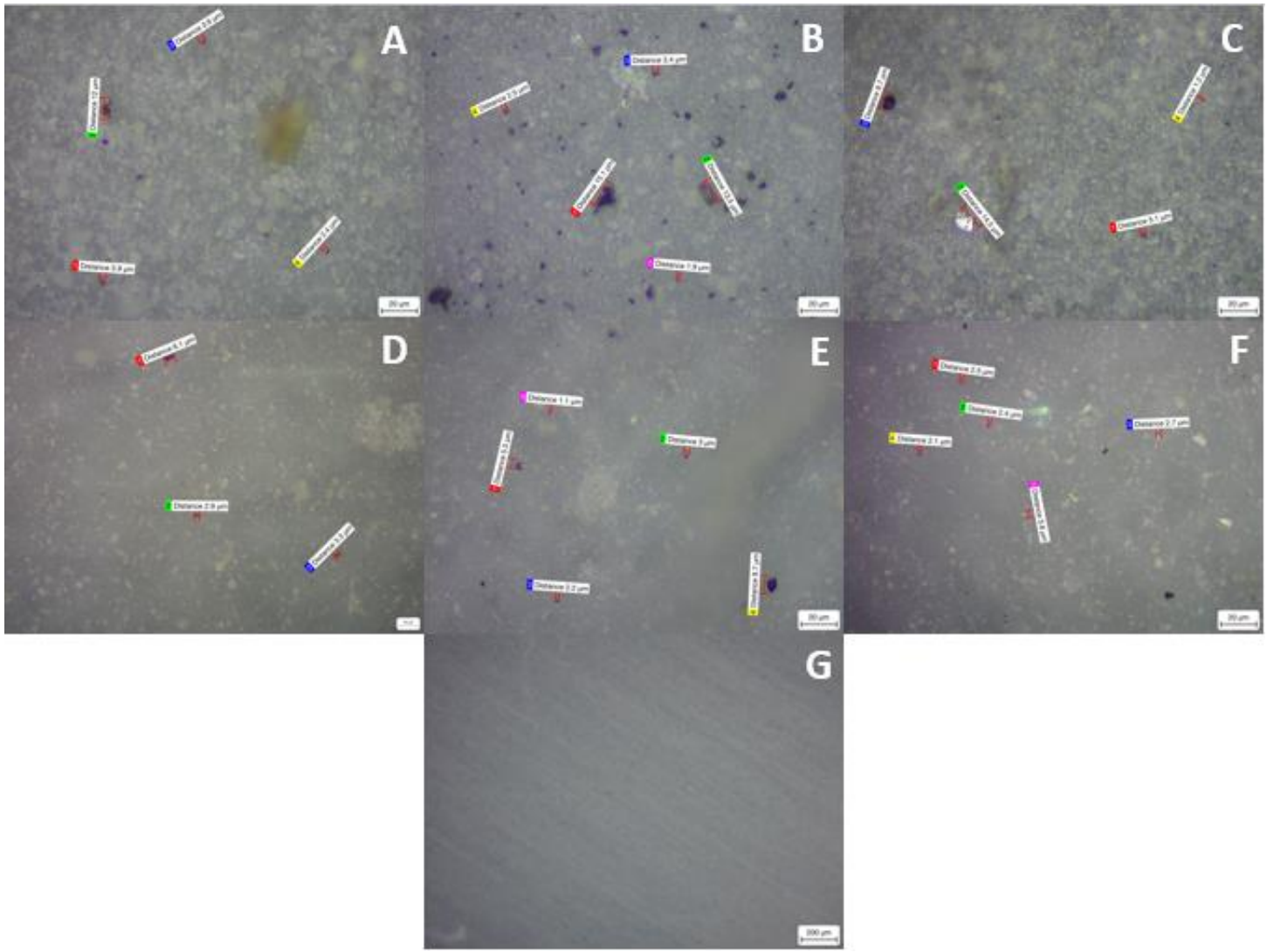

Figure A-4.2. Light microscope images at 500x overall magnification of 0.1 µm pore size membranes for all brands after filtration. (A) Baltic, (B) Geji, (C) Soyes (all FFP2), (D) Duronic, © NHS, (F) Omnitex (all Type IIR) and (G) Blank.

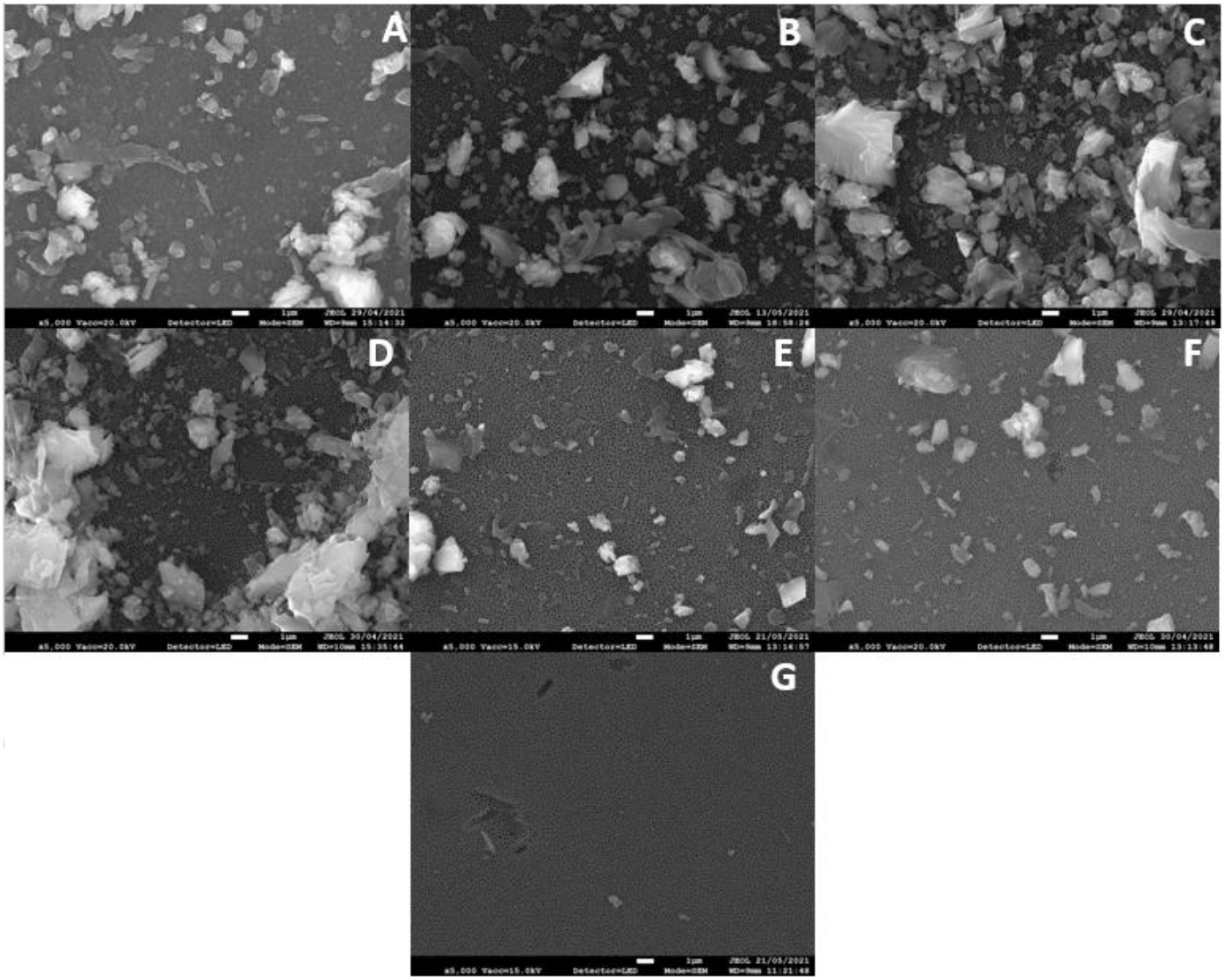

Figure A-4.3. FEG-SEM images of 0.1 µm pore size membranes for all brands at x5000. (A) Baltic, (B) Geji, (C) Soyes (all FFP2), (D) Duronic, © NHS, (F) Omnitex (all Type IIR) and (G) Blank.

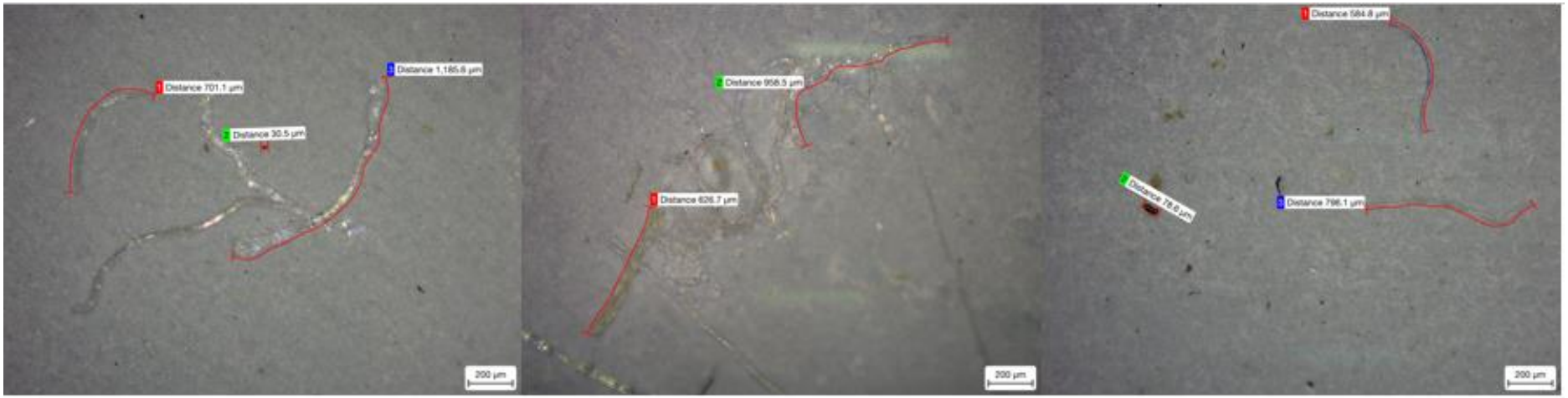

Figure A-4.4. Some replicates for light microscope images, at 50x overall magnification, of 0.02 µm pore size membranes. Baltic brand.

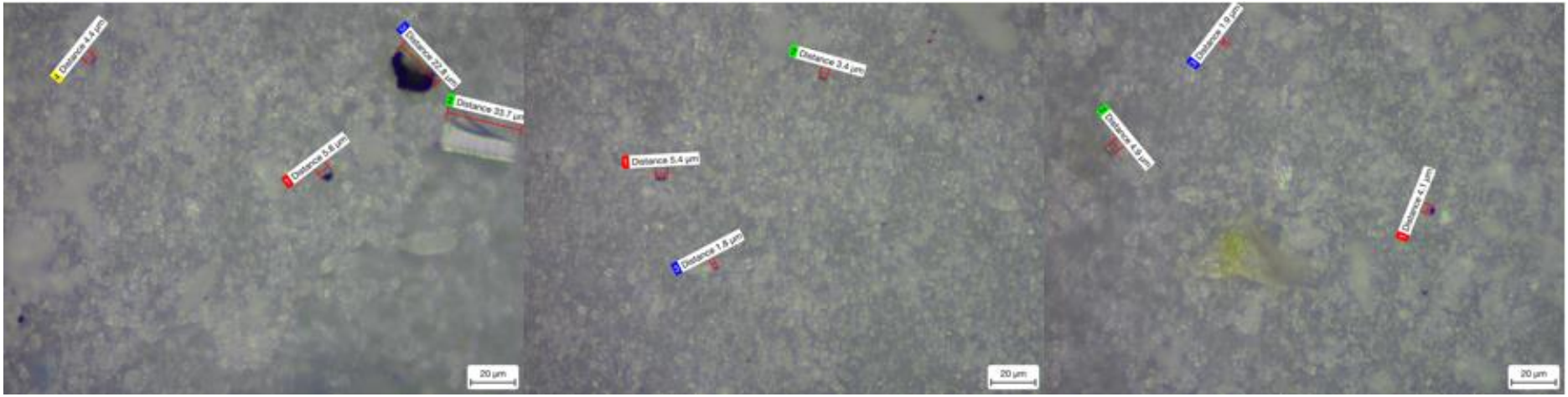

Figure A-4.5. Some replicates for light microscope images, at 500x overall magnification, of 0.02 µm pore size membranes. Baltic brand.

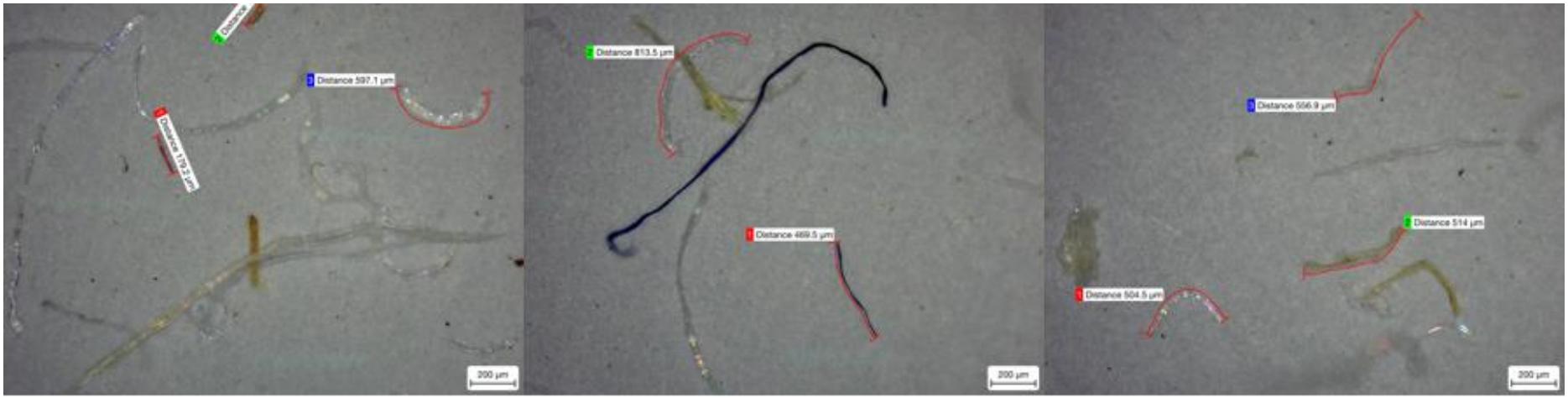

Figure A-4.6 Some replicates for light microscope images, at 50x overall magnification, of 0.1 µm pore size membranes. Baltic brand.

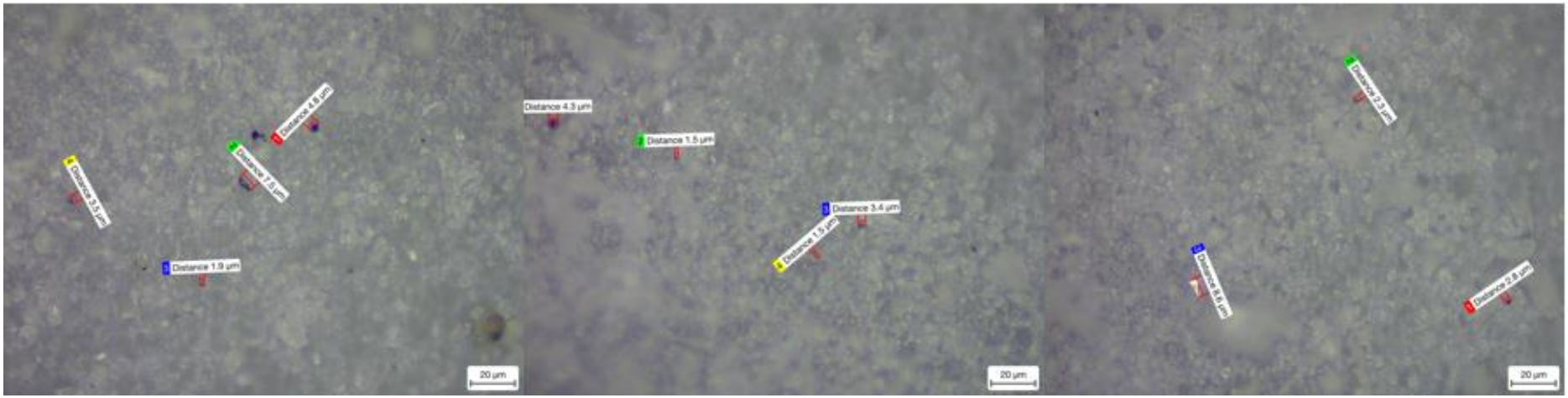

Figure A-4.7. Some replicates for light microscope images, at 500x overall magnification, of 0.1 µm pore size membranes. Baltic brand.

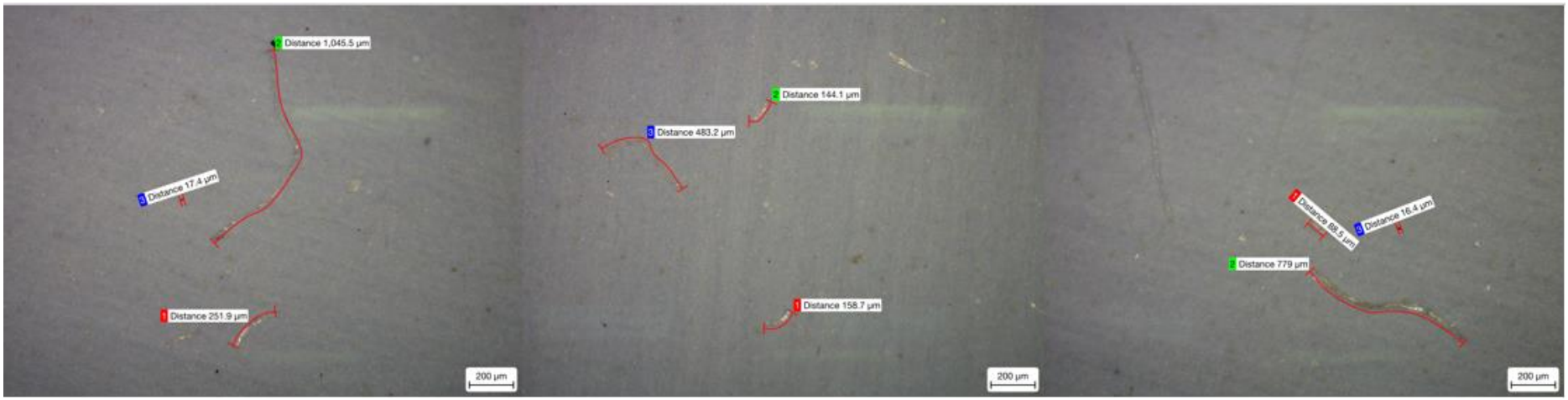

Figure A-4.8. Some replicates for light microscope images, at 50x overall magnification, of 0.02 µm pore size membranes. Duronic brand.

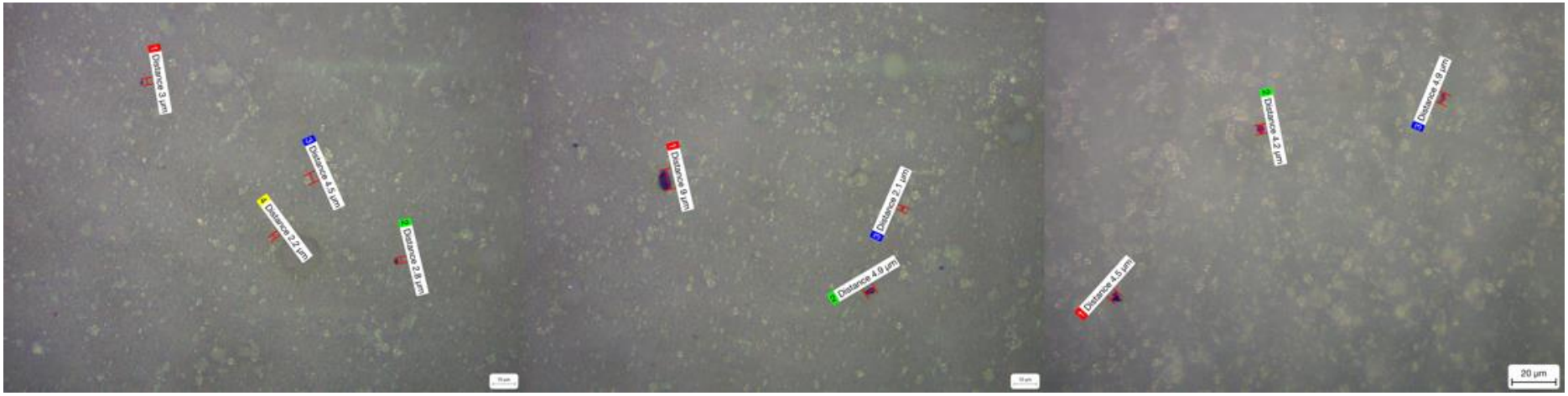

Figure A-4.9. Some replicates for light microscope images, at 500x overall magnification, of 0.02 µm pore size membranes. Duronic brand.

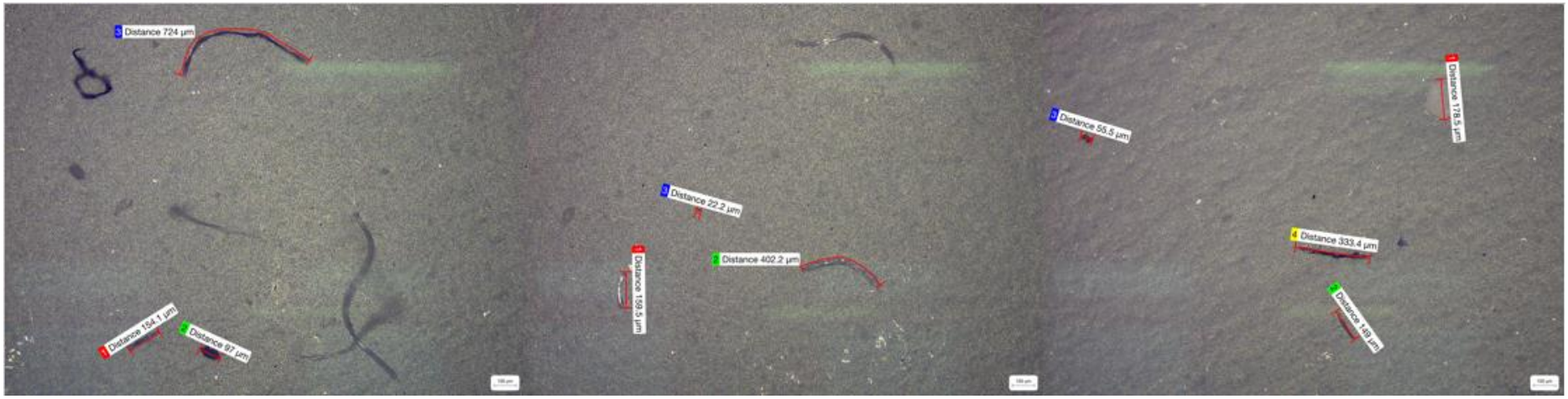

Figure A-4.10. Some replicates for light microscope images, at 50x overall magnification, of 0.1 µm pore size membranes. Duronic brand.

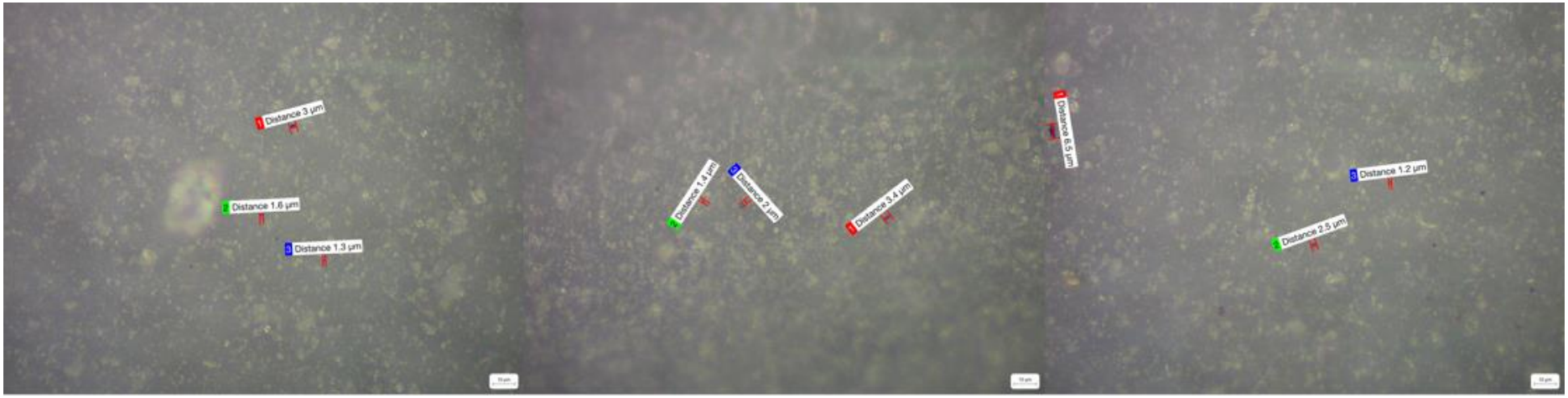

Figure A-4.11. Some replicates for light microscope images, at 500x overall magnification, of 0.1 µm pore size membranes. Duronic brand.

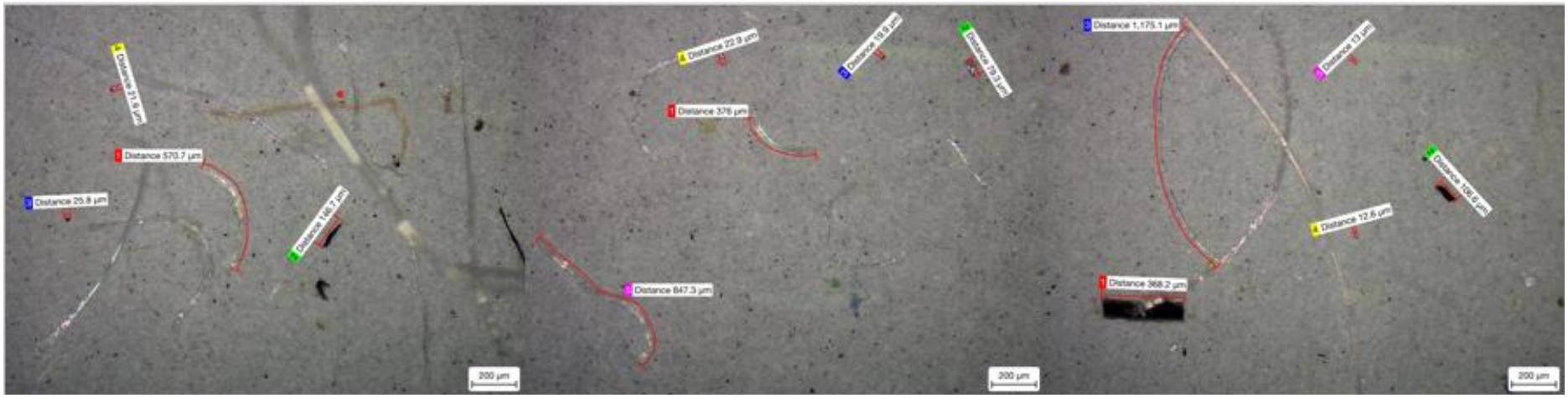

Figure A-4.12. Some replicates for light microscope images, at 50x overall magnification, of 0.02 µm pore size membranes. Geji brand.

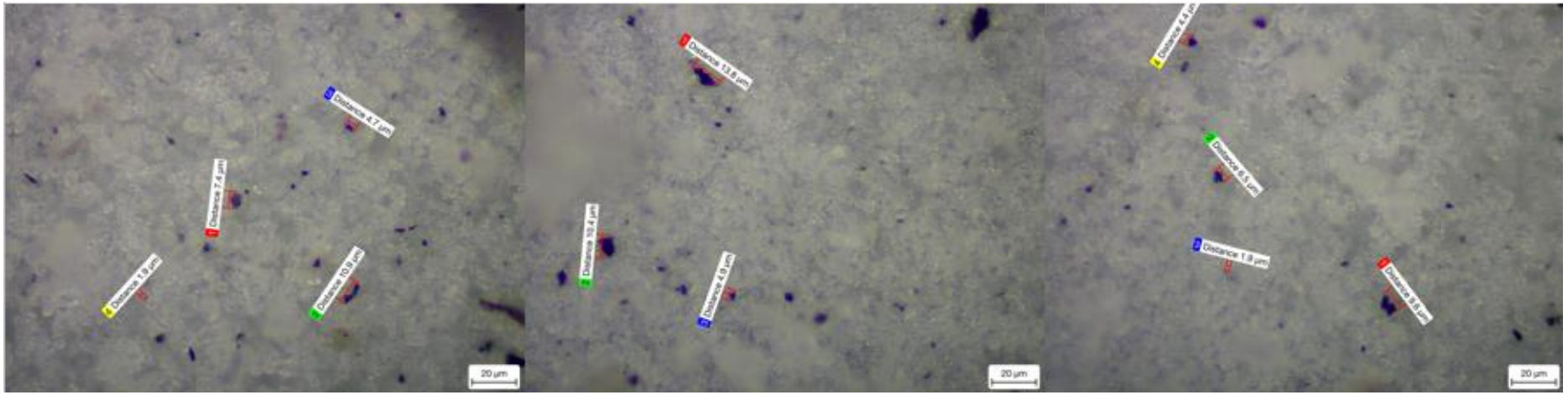

Figure A-4.13. Some replicates for light microscope images, at 500x overall magnification, of 0.02 µm pore size membranes. Geji brand.

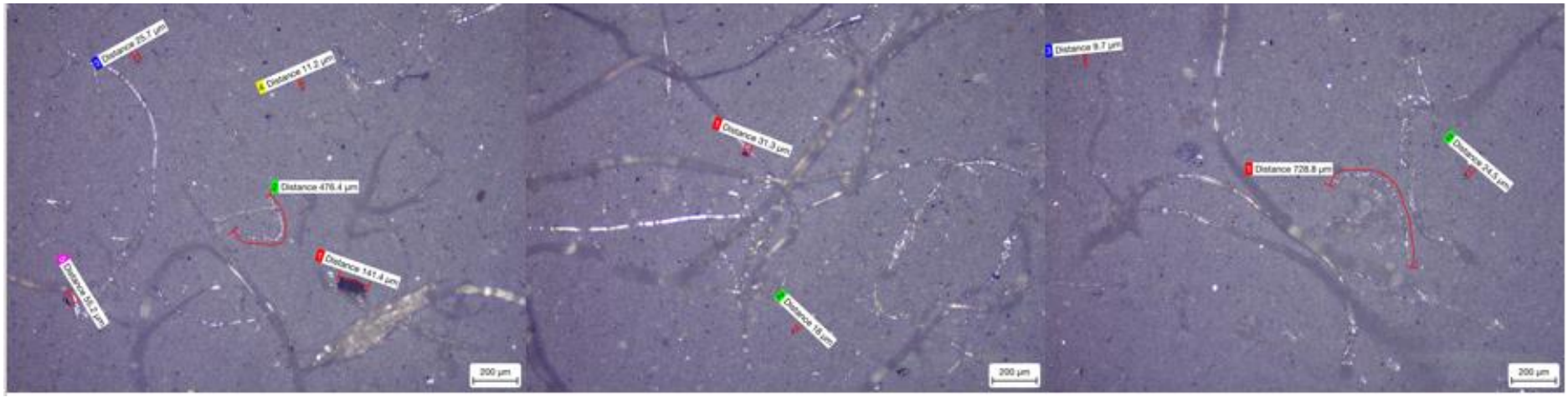

Figure A-4.14. Some replicates for light microscope images, at 50x overall magnification, of 0.1 µm pore size membranes. Geji brand.

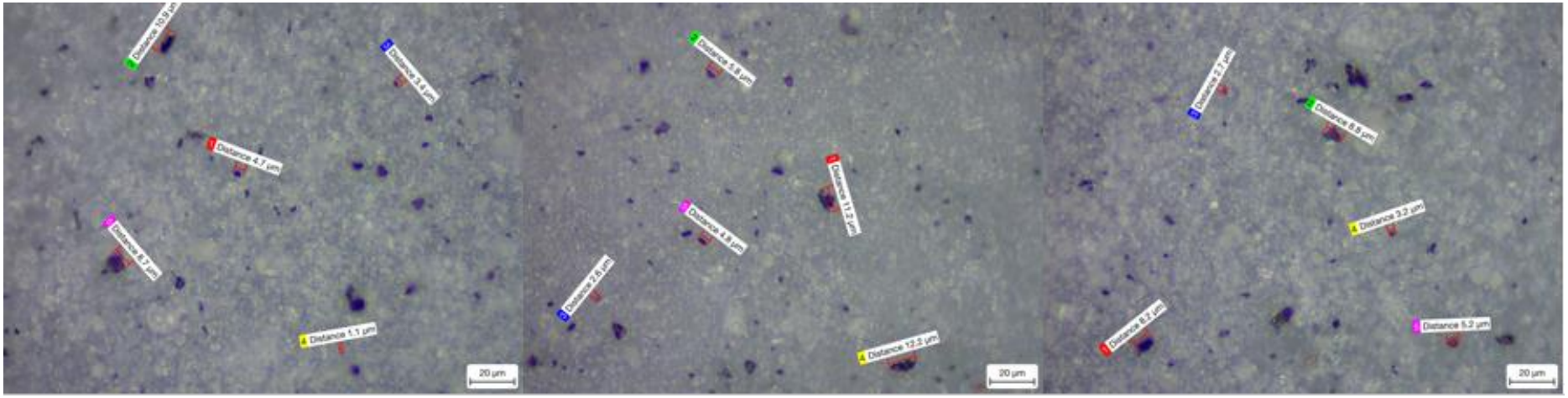

Figure A-4.15. Some replicates for light microscope images, at 500x overall magnification, of 0.1 µm pore size membranes. Geji brand.

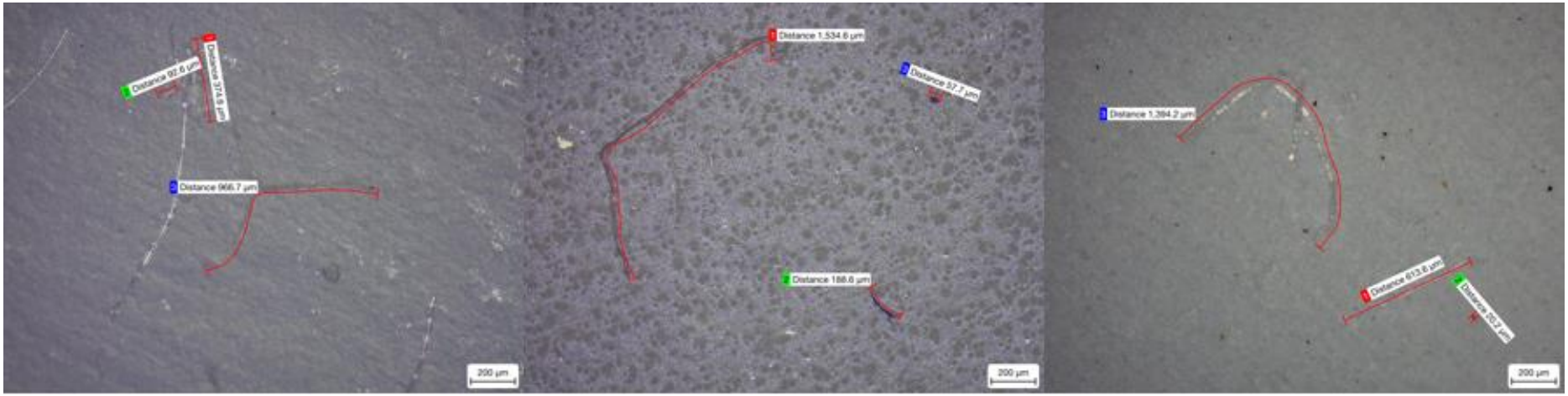

Figure A-4.16. Some replicates for light microscope images, at 50x overall magnification, of 0.02 µm pore size membranes. NHS brand.

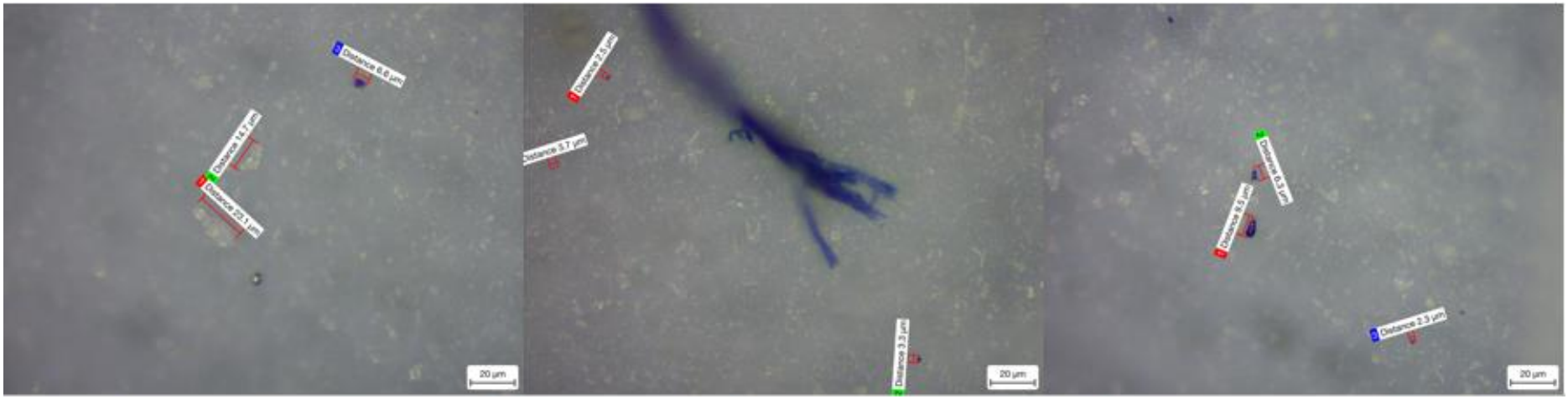

Figure A-4.17. Some replicates for light microscope images, at 500x overall magnification, of 0.02 µm pore size membranes. NHS brand.

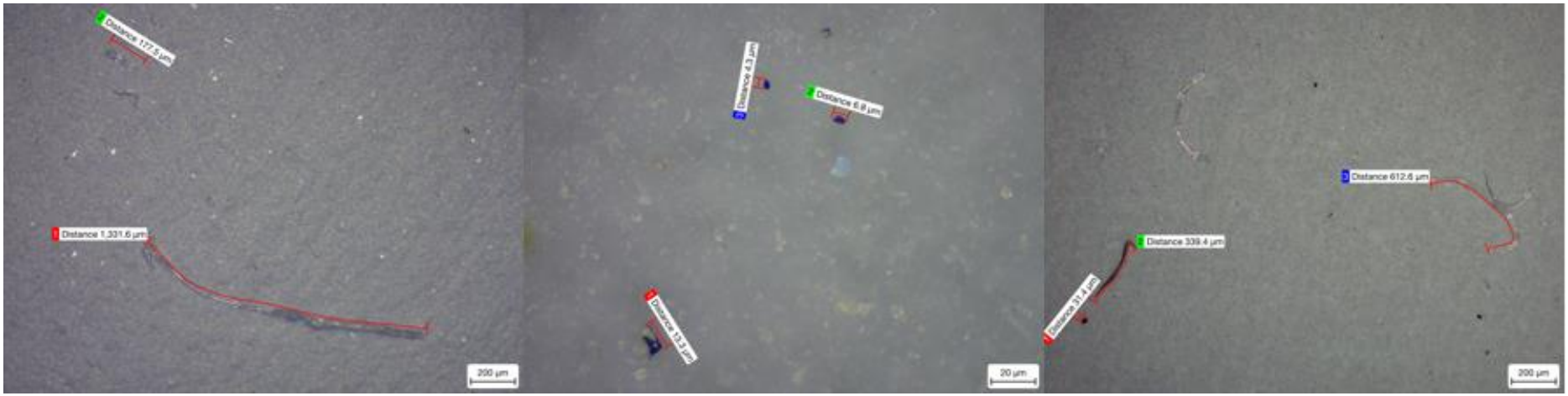

Figure A-4.18. Some replicates for light microscope images, at 50x overall magnification, of 0.1 µm pore size membranes. NHS brand.

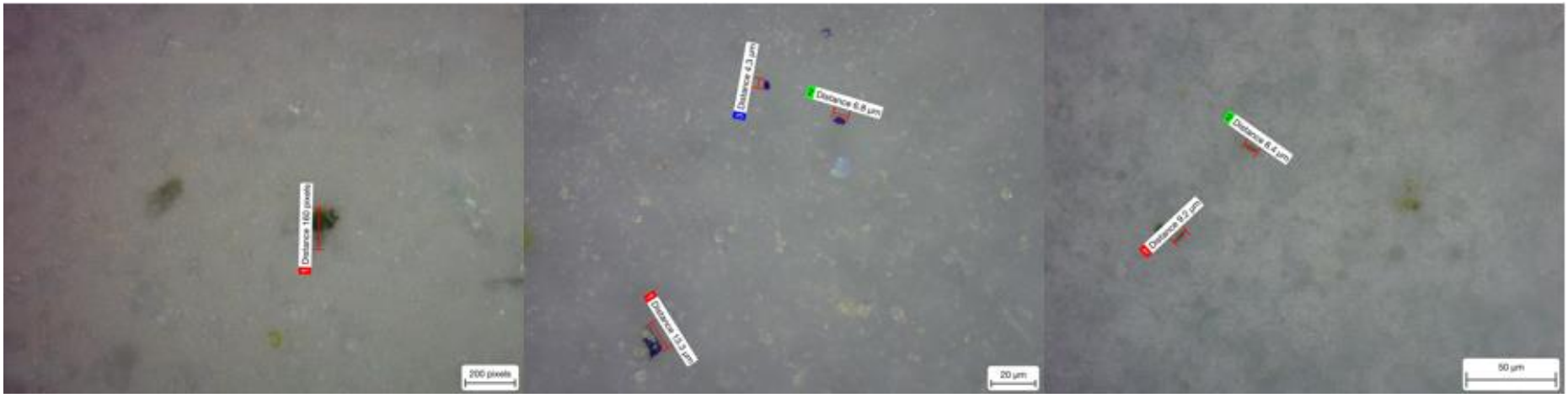

Figure A-4.19. Some replicates for light microscope images, at 500x overall magnification, of 0.1 µm pore size membranes. NHS brand.

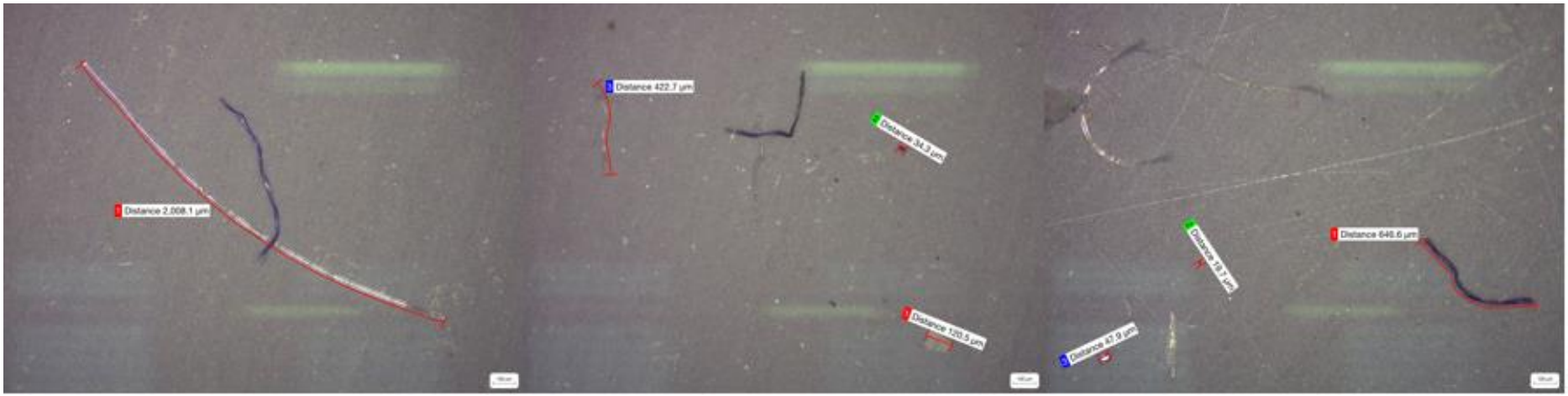

Figure A-4.20. Some replicates for light microscope images, at 50x overall magnification, of 0.02 µm pore size membranes. Omnitex brand.

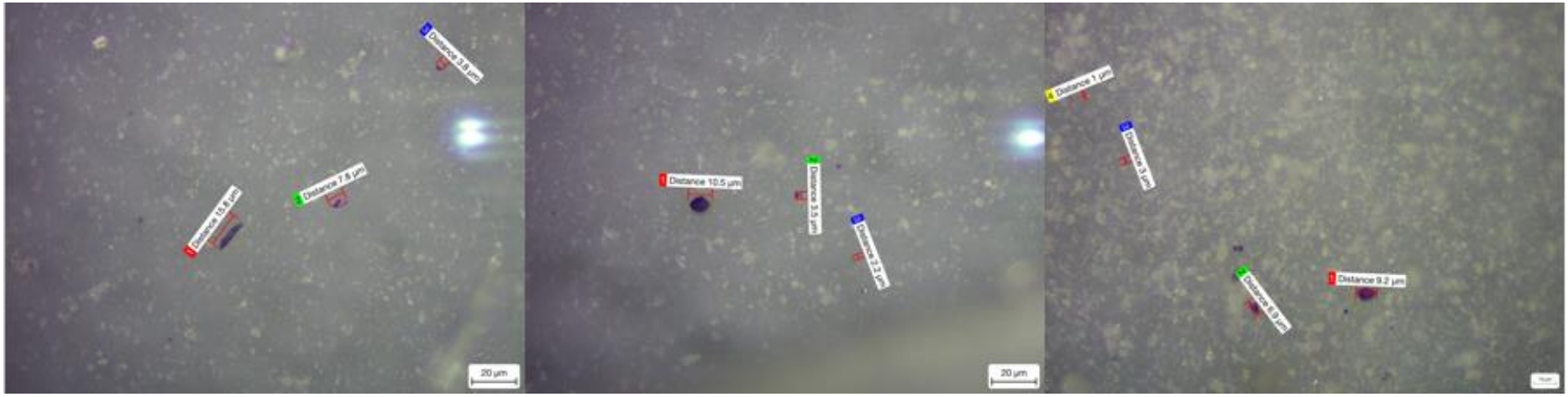

Figure A-4.21. Some replicates for light microscope images, at 500x overall magnification, of 0.02 µm pore size membranes. Omnitex brand.

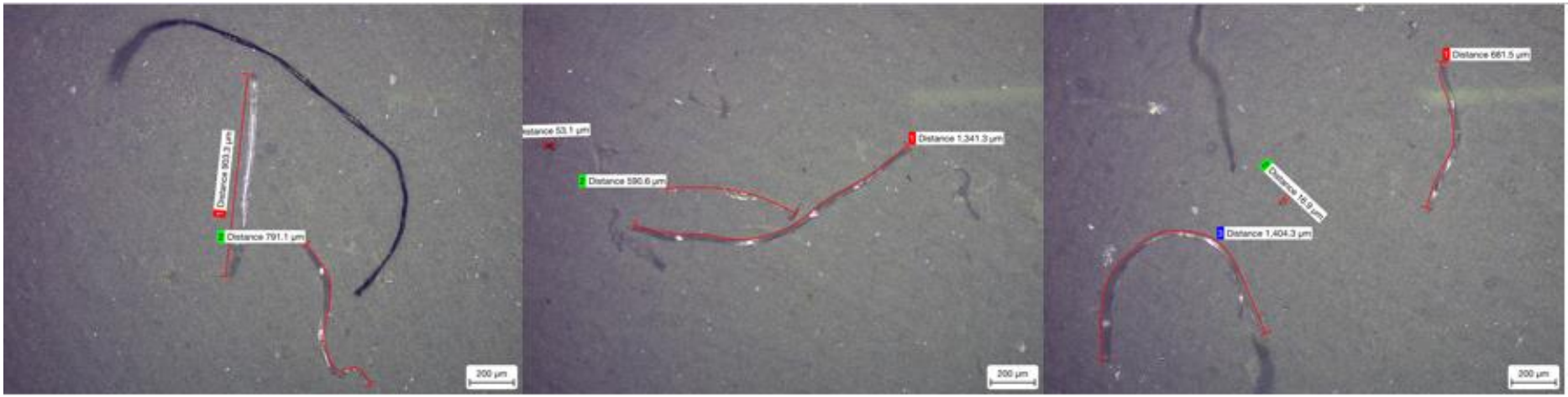

Figure A-4.22. Some replicates for light microscope images, at 50x overall magnification, of 0.1 µm pore size membranes. Omnitex brand.

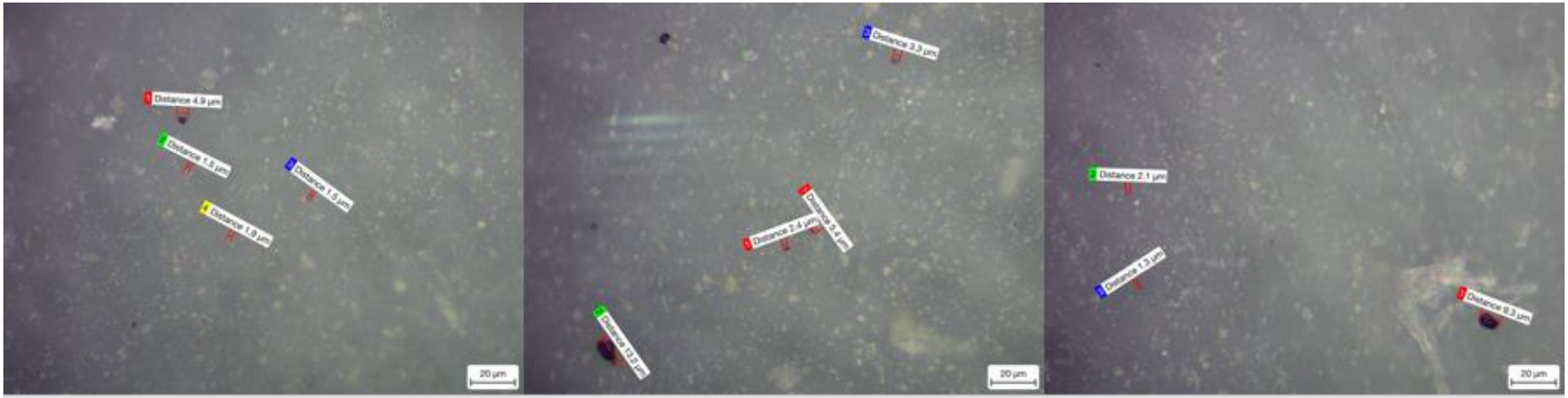

Figure A-4.23. Some replicates for light microscope images, at 500x overall magnification, of 0.1 µm pore size membranes. Omnitex brand.

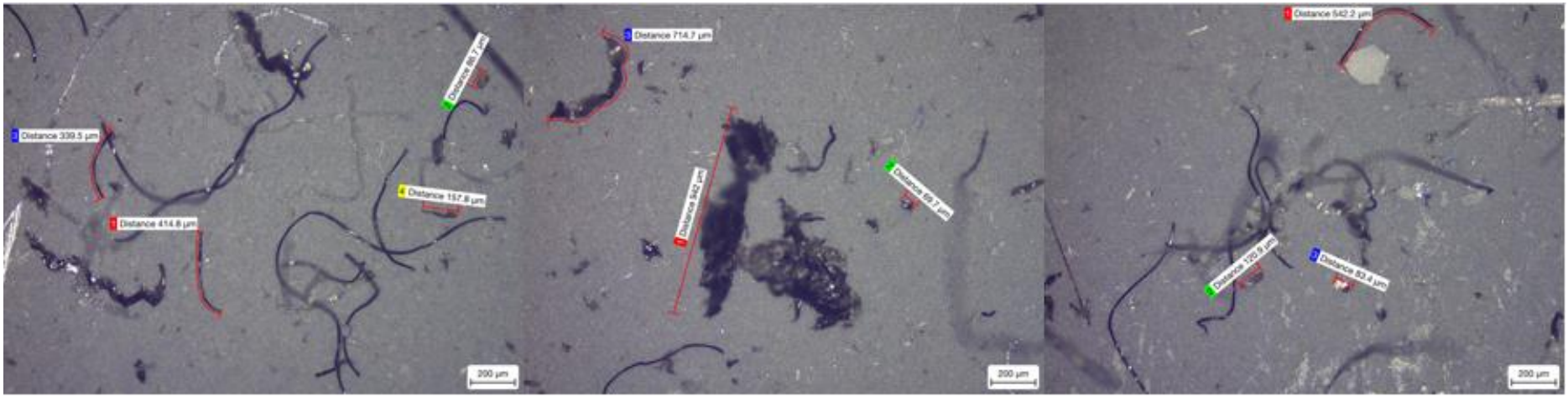

Figure A-4.24. Some replicates for light microscope images, at 50x overall magnification, of 0.02 µm pore size membranes. Soyes brand.

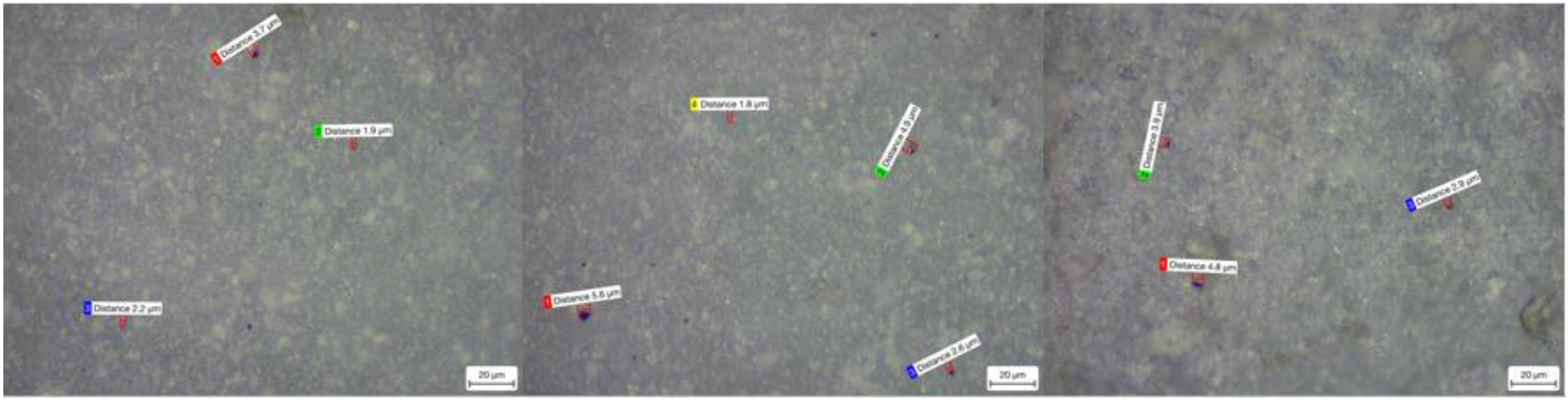

Figure A-4.25. Some replicates for light microscope images, at 500x overall magnification, of 0.02 µm pore size membranes. Soyes brand.

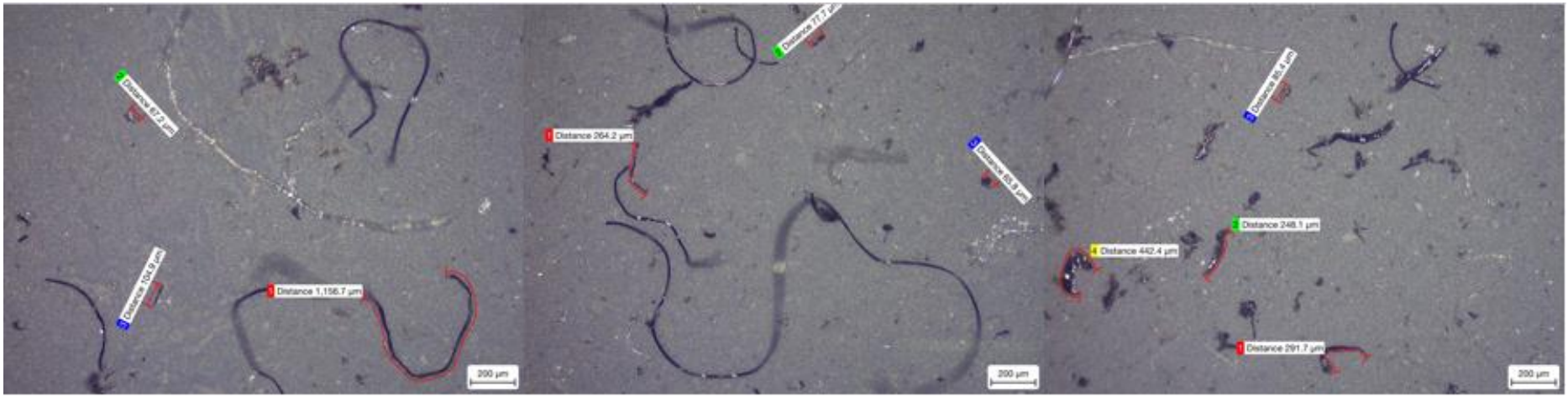

Figure A-4.26. Some replicates for light microscope images, at 50x overall magnification, of 0.1 µm pore size membranes. Soyes brand.

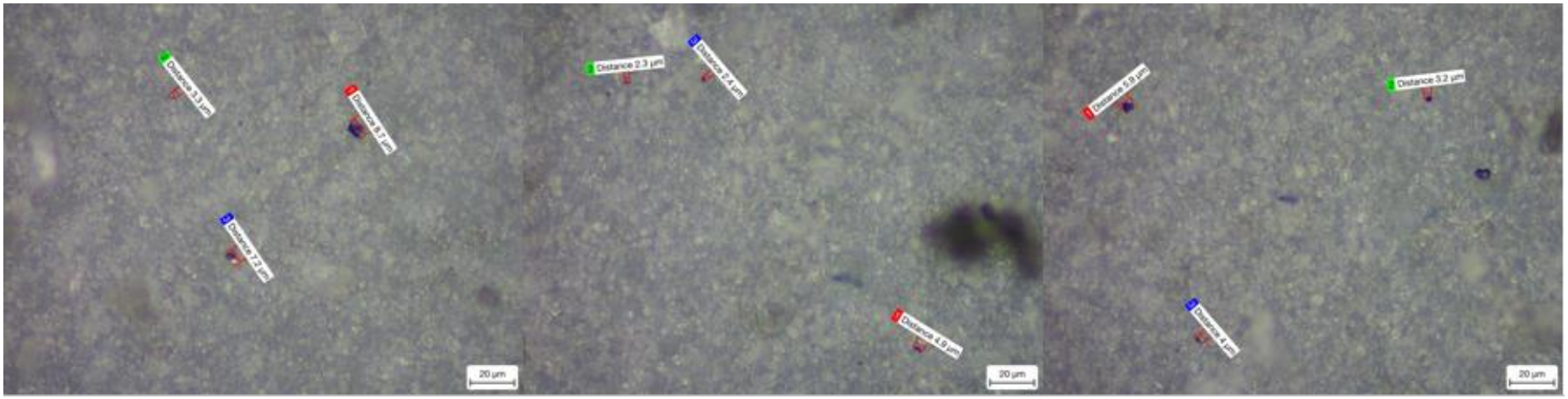

Figure A-4.27. Some replicates for light microscope images, at 500x overall magnification, of 0.1 µm pore size membranes. Soyes brand.

Figure A-4.28. Some replicates for light microscope images, at 50x overall magnification, of 0.02 µm pore size membranes. Blank.

Figure A-4.29. Some replicates for light microscope images, at 500x overall magnification, of 0.02 µm pore size membranes. Blank.

Figure A-4.30. Some replicates for light microscope images, at 50x overall magnification, of 0.1 µm pore size membranes. Blank.

Figure A-4.31 Some replicates for light microscope images, at 500x overall magnification, of 0.1 µm pore size membranes. Blank.

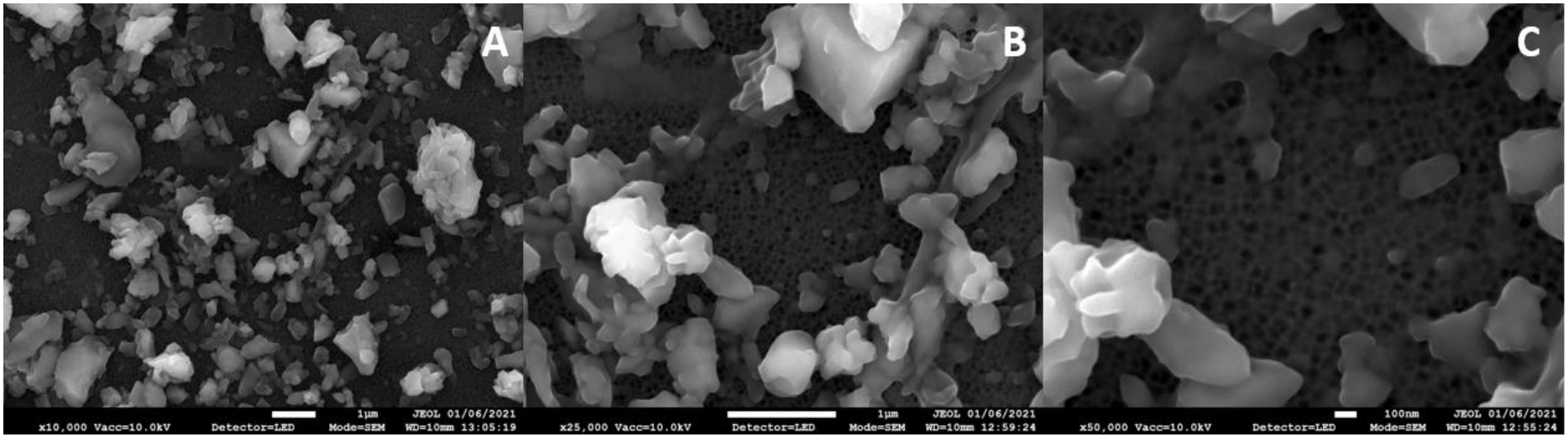

Figure A-4.32. FEG-SEM replicates of 0.02 µm pore size membranes for Brand Baltic (FFP2). (A) 10000x, (B) 25000x and (C) 50000x.

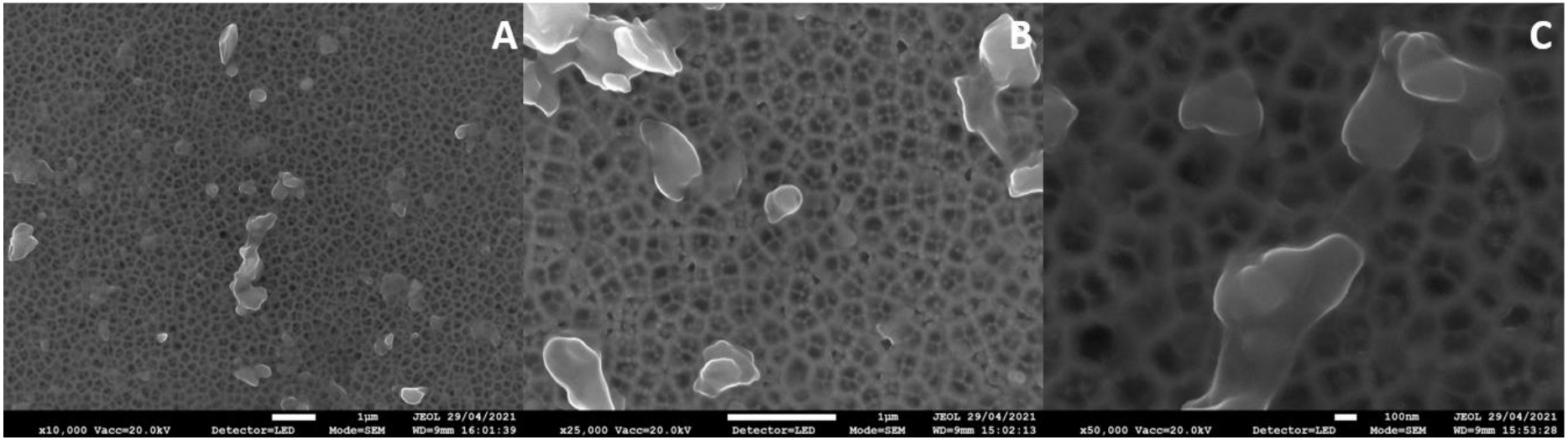

Figure A-4.33. FEG-SEM replicates of 0.1 µm pore size membranes for Brand Baltic (FFP2). (A) 10000x, (B) 25000x and (C) 50000x.

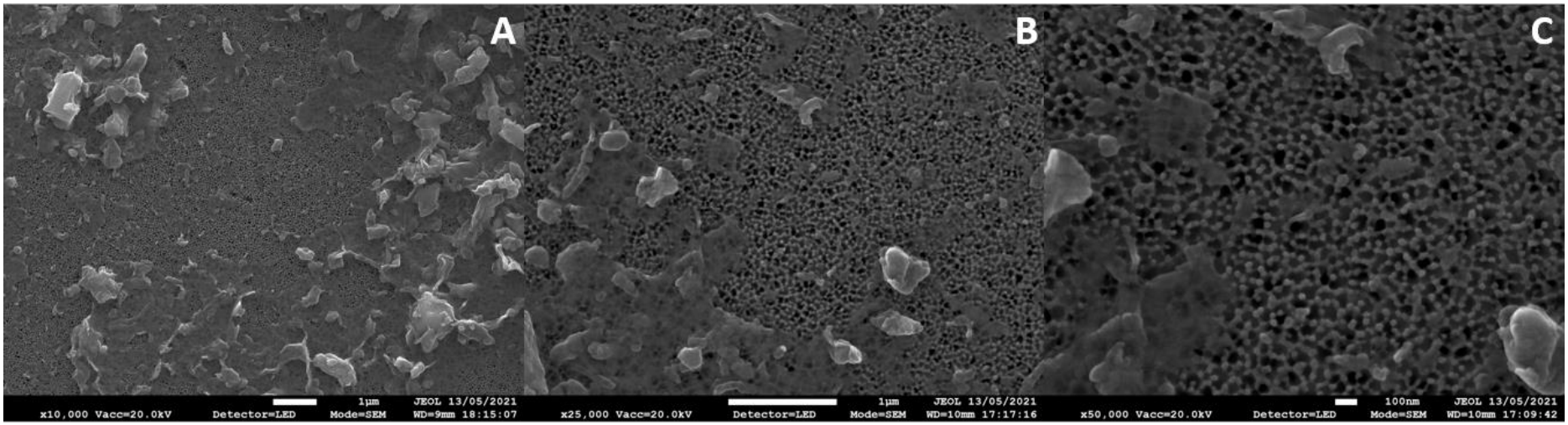

Figure A-4.34. FEG-SEM replicates of 0.02 µm pore size membranes for Brand Duronic (IIR). (A) 10000x, (B) 25000x and (C) 50000x.

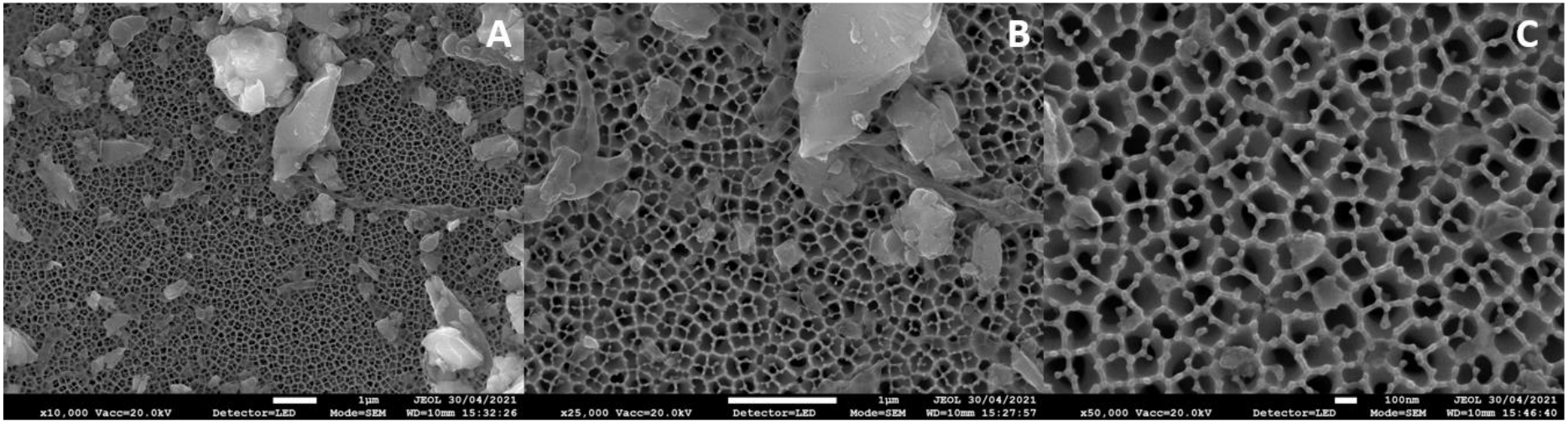

Figure A-4.35. FEG-SEM replicates of 0.1 µm pore size membranes for Brand Duronic (IIR). (A) 10000x, (B) 25000x and (C) 50000x.

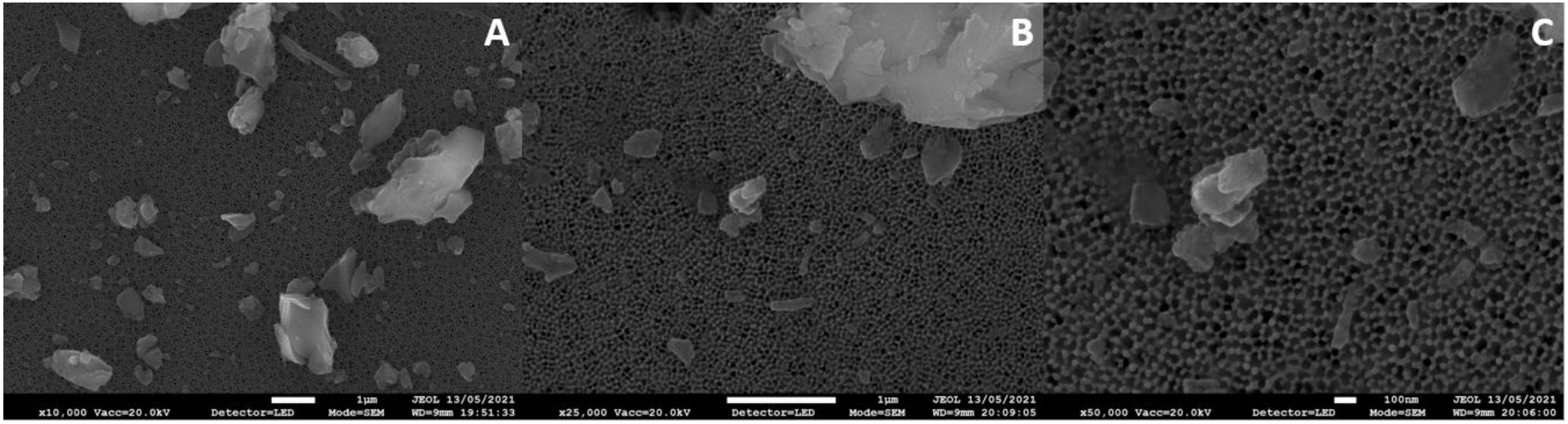

Figure A-4.36. FEG-SEM replicates of 0.02 µm pore size membranes for Brand Geji (FFP2). (A) 10000x, (B) 25000x and (C) 50000x.

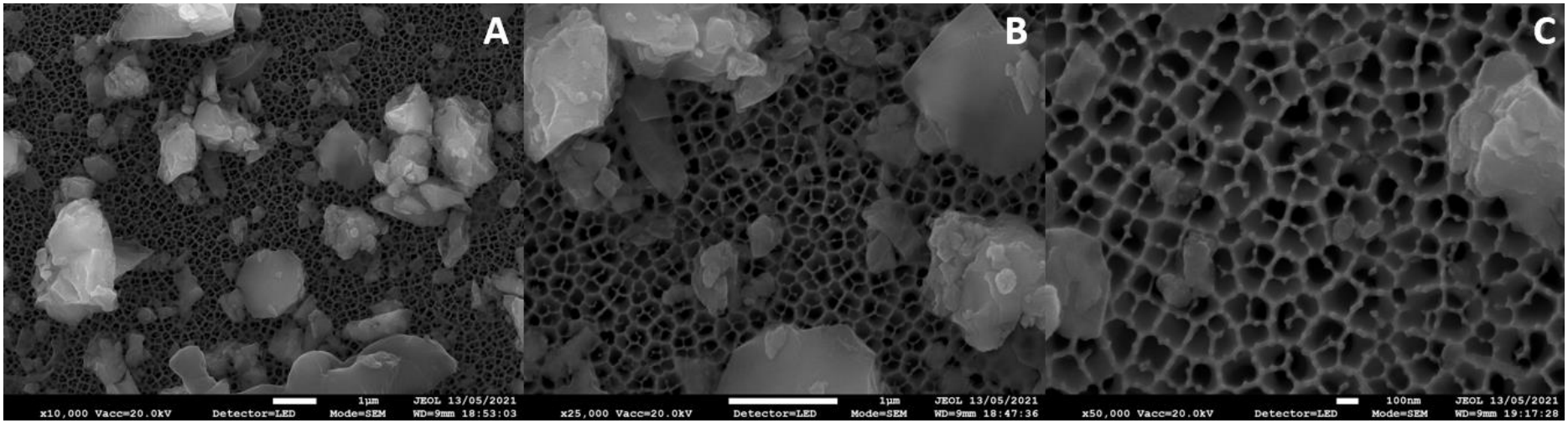

Figure A-4.37. FEG-SEM replicates of 0.1 µm pore size membranes for Brand Geji (FFP2). (A) 10000x, (B) 25000x and (C) 50000x.

Figure A-4.38. FEG-SEM replicates of 0.02 µm pore size membranes for Brand NHS (IIR). (A) 10000x, (B) 25000x and (C) 50000x.

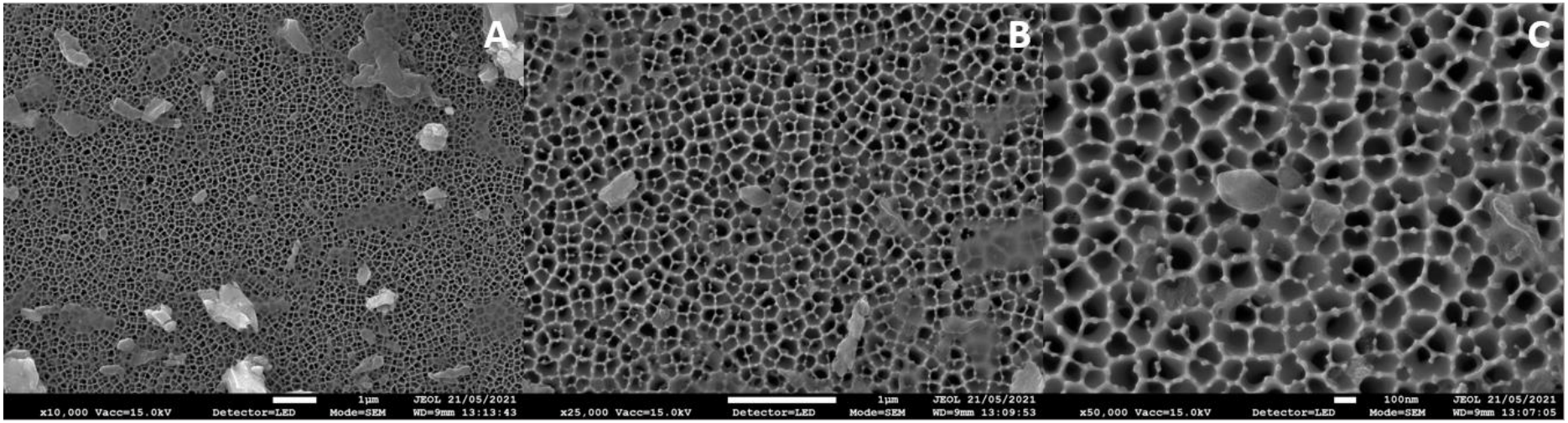

Figure A-4.39. FEG-SEM replicates of 0.1 µm pore size membranes for Brand NHS (IIR). (A) 10000x, (B) 25000x and (C) 50000x.

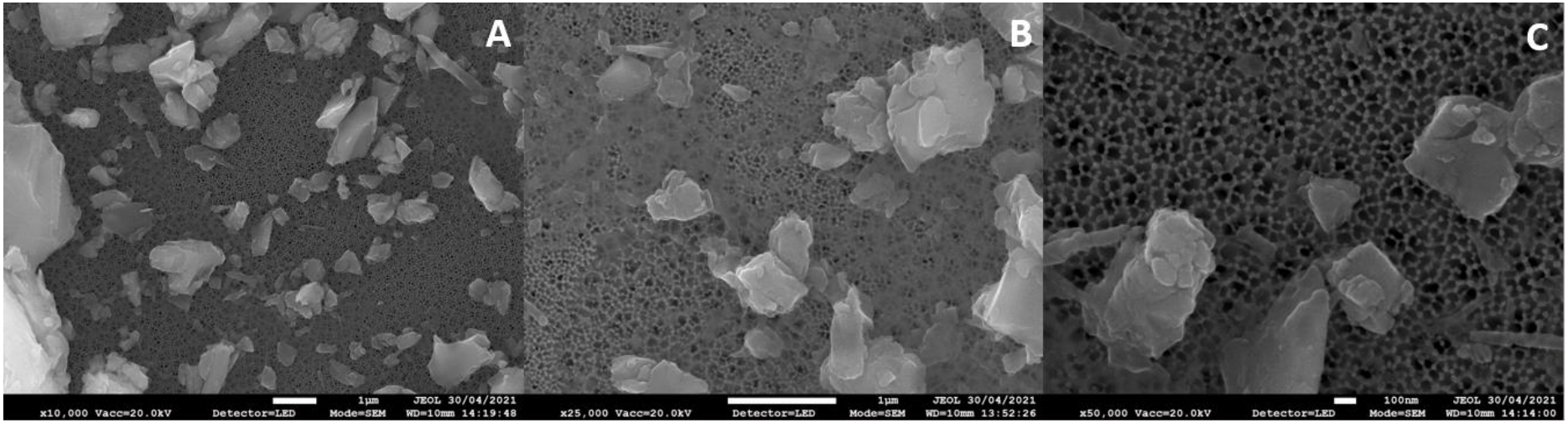

Figure A-4.40. FEG-SEM replicates of 0.02 µm pore size membranes for Brand Omnitex (IIR). (A) 10000x, (B) 25000x and (C) 50000x.

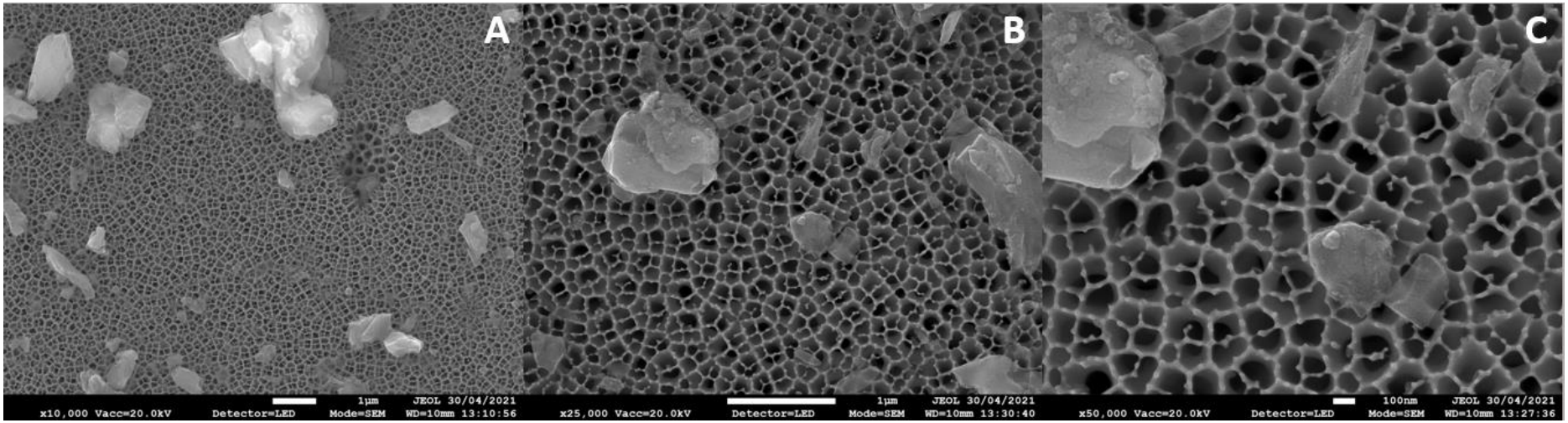

Figure A-4.41. FEG-SEM replicates of 0.1 µm pore size membranes for Brand Omnitex (IIR). (A) 10000x, (B) 25000x and (C) 50000x.

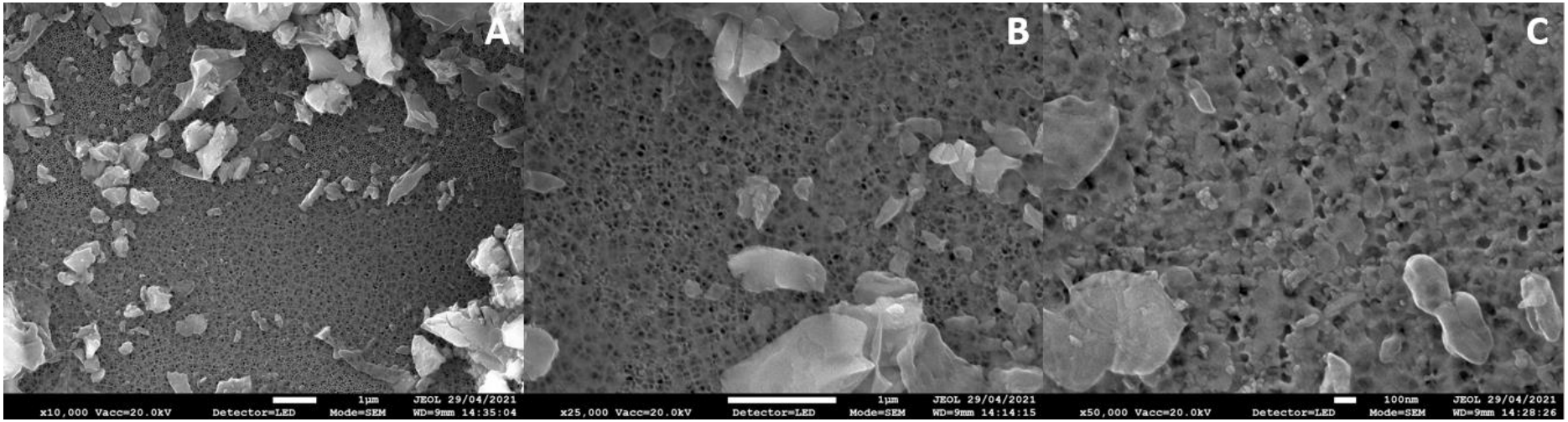

Figure A-4.42. FEG-SEM replicates of 0.02 µm pore size membranes for Brand Soyes (FFP2). (A) 10000x, (B) 25000x and (C) 50000x.

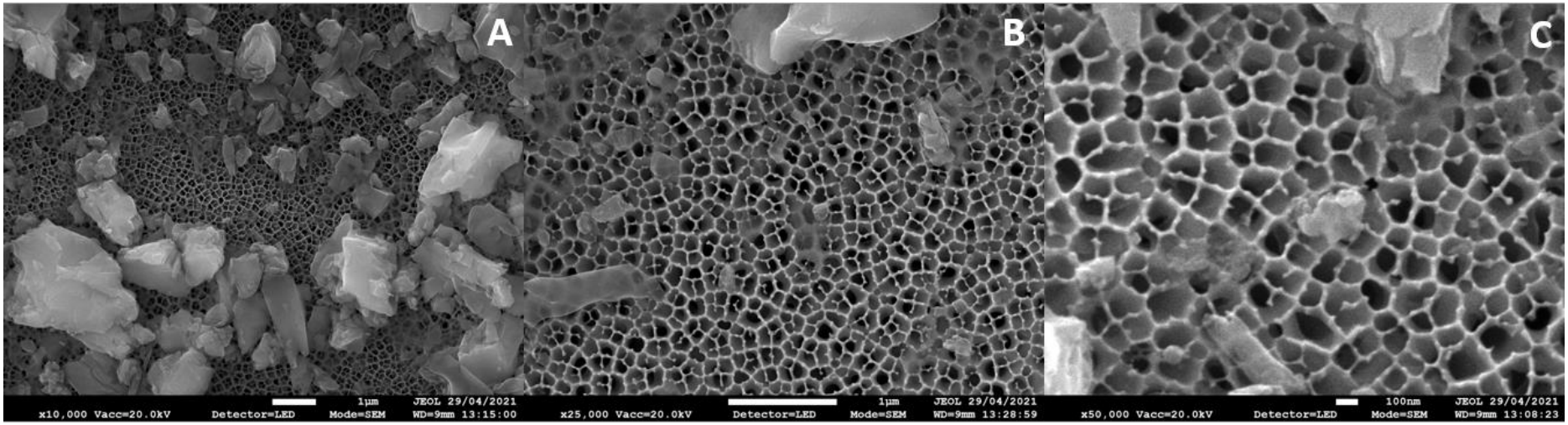

Figure A-4.43. FEG-SEM replicates of 0.1 µm pore size membranes for Brand Soyes (FFP2). (A) 10000x, (B) 25000x and (C) 50000x.

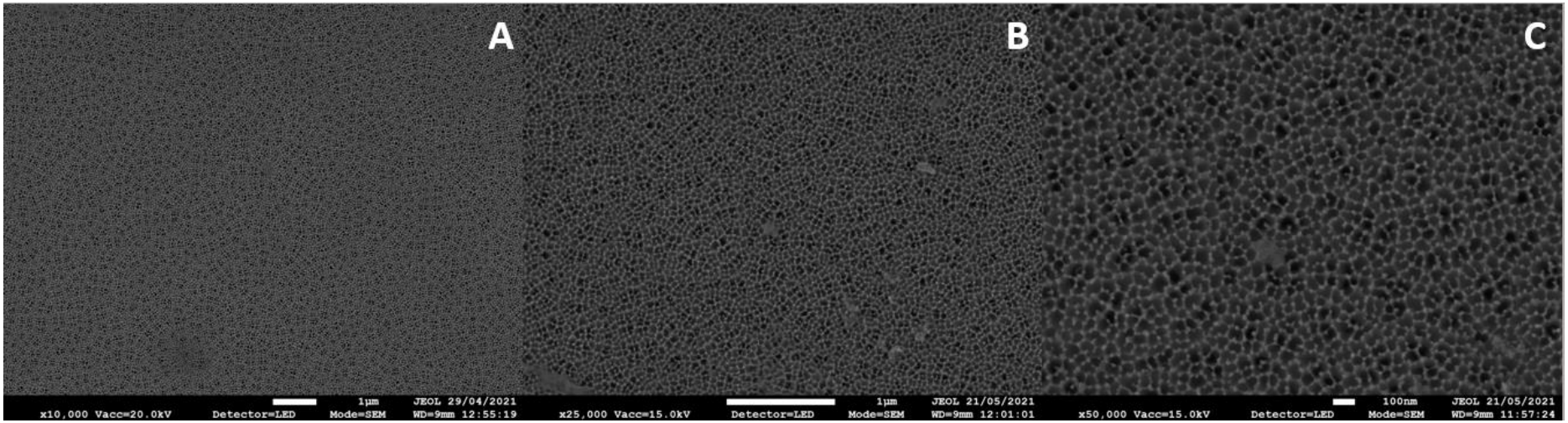

Figure A-4.44. FEG-SEM replicates of 0.02 µm pore size membranes Blank samples. (A) 10000x, (B) 25000x and (C) 50000x.

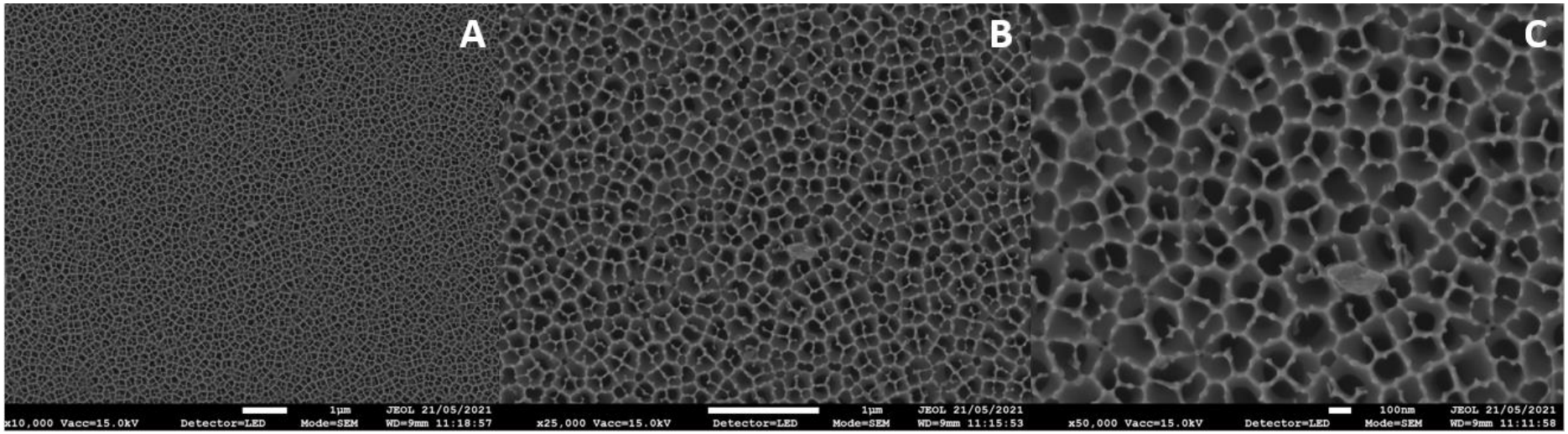

Figure A-4.45. FEG-SEM replicates of 0.1 µm pore size membranes Blank samples. (A) 10000x, (B) 25000x and (C) 50000x.

Table A-4.1. Analysis conditions for HPLC in analysis carried out in Chapter 4.

Dionex Ultimate 3000	
Waters XBridge C18 column: 3.5 µm x 2.1 mm x 150 mm Guard column: XBridge C18 3.5 µm x 2.1 mm x 10 mm	
Flow rate = 150µl/min	
Mobile Phase A = 0.1% Formic acid; 2% MeCN in H_2O	
Mobile Phase B = 0.1% Formic acid in MeCN	
5µl full loop injection	
Mobile Phase Gradient:	
Time(mins)	**%B**
0-2	2
2-30	90
30-32	90
32-34	2
34-37	2

Table A-4.2. Analysis conditions for MS in analysis carried out in Chapter 4.

Thermo LTQ Orbitrap XL with API ion spray source	
Parameters	**+ve mode**
Sheath gas flow	15
Aux Gas	2
Probe kV	4.3
Capillary T (°C)	325
Capillary V	43
Tube Lens V	150
MS Scan	FT: +ve ion profile mode m/z 200-1000; Resolution 60,000

Table A-4.3. Raw data containing the averages of the triplicates examined for each sample as provided by the technicians at Tata Steel (Port Talbot), along with the limit of detection (LOD), quality controls (QC), QC averages, QC standard deviation and QC relative standard deviation (RSD). These results are for samples prepared submerging 1 medical DPFM in 250 ml of deionized water.

Sample Id	**As (ppb)**	**Cd (ppb)**	**Co (ppb)**	**Cr (ppb)**	**Cu (ppb)**	**Mo (ppb)**
QC 10	9.08	9.82	9.53	9.88	9.84	9.80
sample blank	0.00	0.00	0.00	-0.01	0.21	0.17
Baltic	0.04	0.01	0.03	0.10	0.74	0.20
Duronic	0.03	0.00	0.00	0.01	2.22	0.17
Geji	0.02	0.01	0.00	0.00	0.93	0.14
NHS	0.00	0.00	-0.01	0.00	0.50	0.15
Omnitext	0.01	0.01	0.00	0.00	2.65	0.17
Soyes	0.04	0.02	0.00	1.21	1.53	0.16
QC10	9.62	9.89	9.94	10.06	9.87	9.46
Sample Id	**Ni (ppb)**	**Pb (ppb)**	**Sb (ppb)**	**Ti (ppb)**	**V (ppb)**	**Hg (ppb)**
QC 10	9.55	9.80	9.96	9.54	9.56	5.43 (QC 5)
sample blank	-0.20	0.03	0.09	0.07	0.01	<0.050
Baltic	0.04	0.27	4.93	0.14	0.03	<0.050
Duronic	0.07	0.02	0.41	0.00	0.00	<0.050
Geji	-0.10	0.14	0.61	0.48	0.01	<0.050
NHS	-0.15	0.05	0.21	0.14	0.01	<0.050
Omnitext	-0.08	0.02	2.10	0.00	0.03	<0.050
Soyes	0.11	0.03	1.65	0.14	0.00	<0.050
QC10	9.84	10.12	9.66	10.20	9.87	5.42 (QC 5)

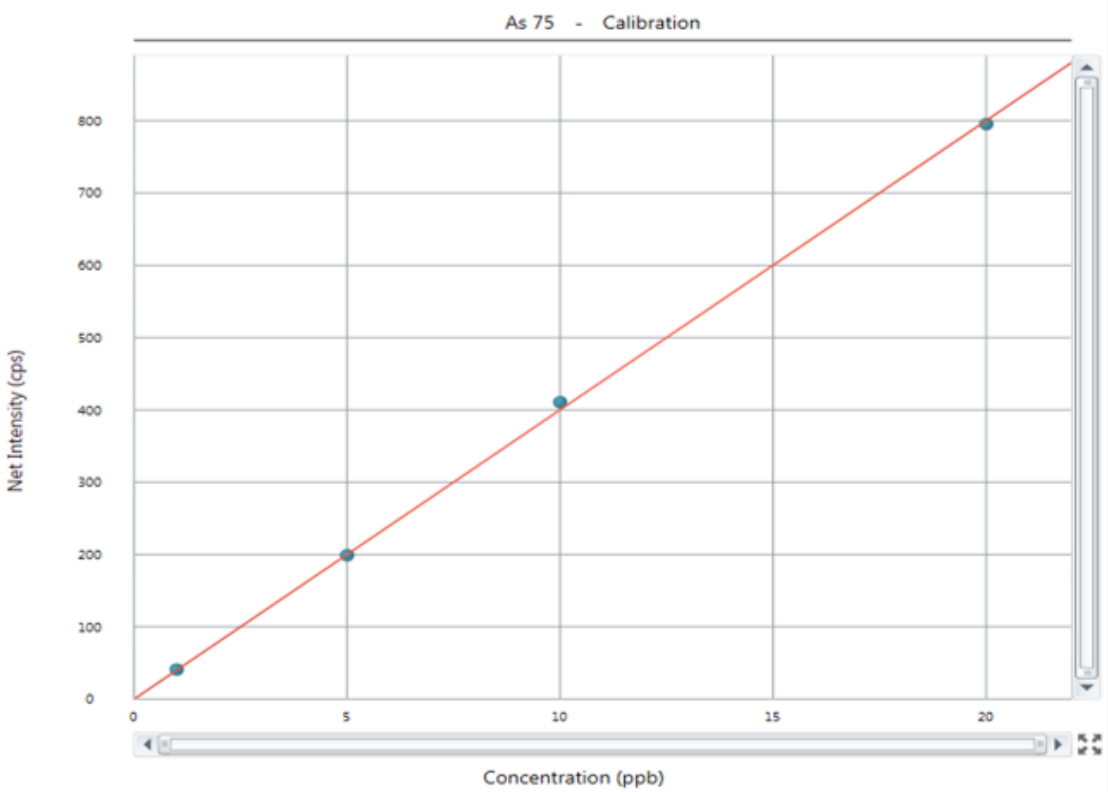

Statistics

Eqn. :	y = 40x + 0	
Cor.Coeff. :	0.999919	
BEC :	0.074965	ppb
DL :	0.129843	ppb

Calibration Table

	Net Intensity As 75 (cps)	Apparent Conc. As 75 (ppb)
Blank	3.0	
Cal. Std.1	41.0	1.0
Cal. Std.2	199.0	5.0
Cal. Std.3	410.7	10.3
Cal. Std.4	795.4	19.9

Figure A-4.46. Calibration curve of the ICP-MS analyses of the leachates for As element.

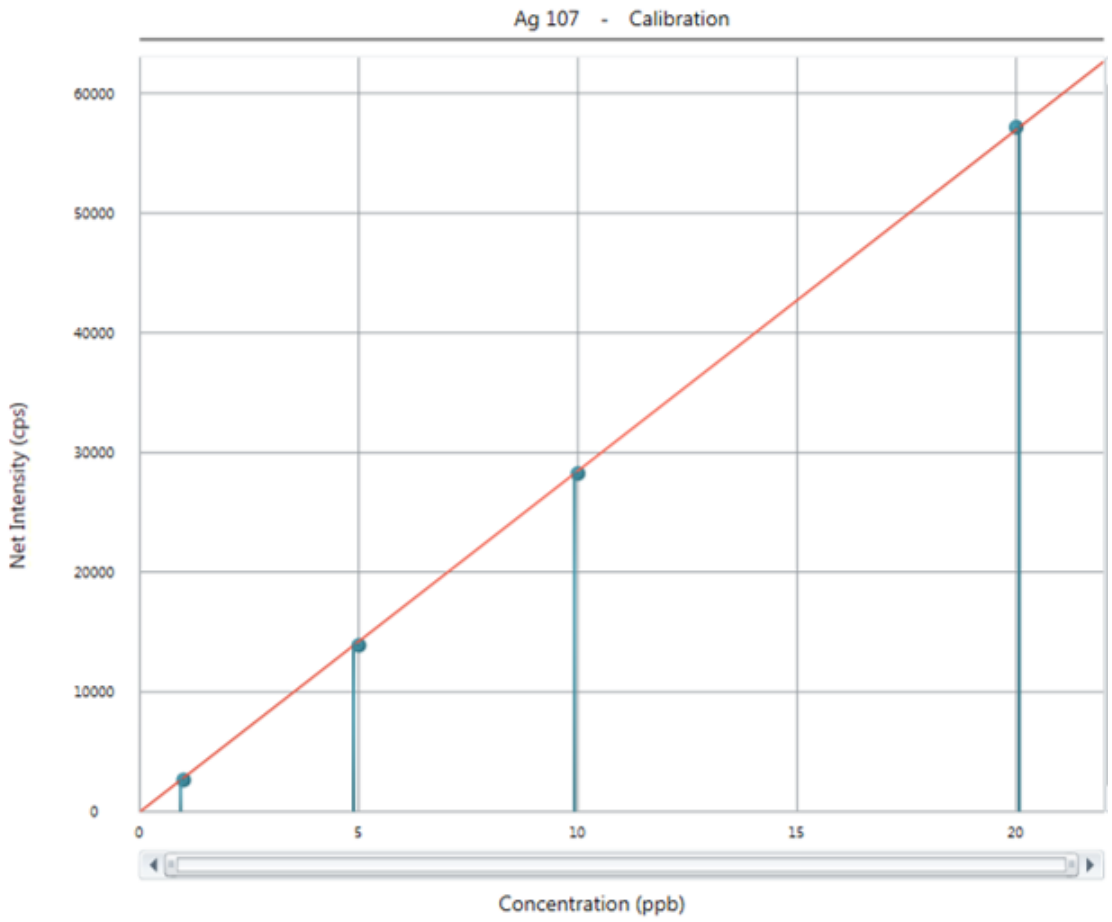

Statistics

Eqn. :	y = 2848x + 0	
Cor.Coeff. :	0.999971	
BEC :	0.012639	ppb
DL :	0.008999	ppb

Calibration Table

	Net Intensity Ag 107 (cps)	Apparent Conc. Ag 107 (ppb)
Blank	36.0	
Cal. Std.1	2654.9	0.9
Cal. Std.2	13902.5	4.9
Cal. Std.3	28255.0	9.9
Cal. Std.4	57173.7	20.1

Figure A-4.47. Calibration curve of the ICP-MS analyses of the leachates for Ag element.

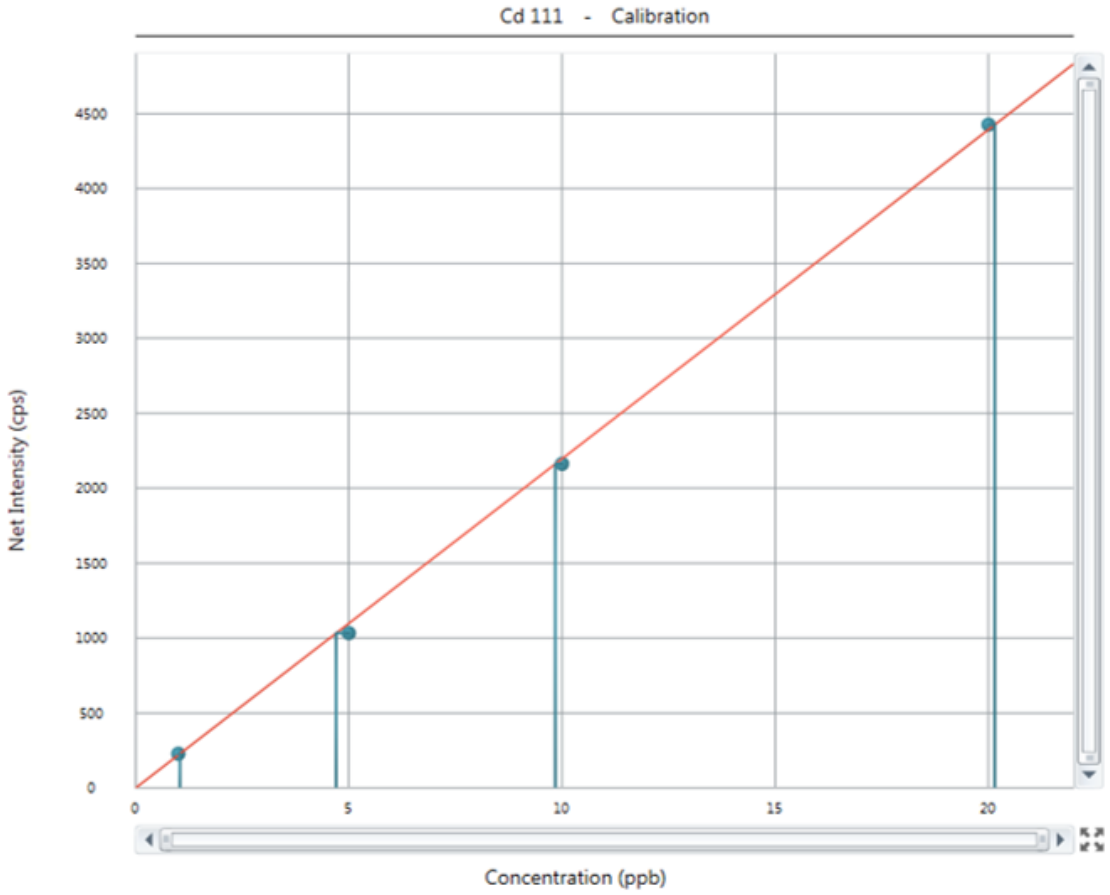

Statistics

Eqn. :	y = 220x + 0	
Cor.Coeff. :	0.999871	
BEC :	0.044004	ppb
DL :	0.007885	ppb

Calibration Table

	Net Intensity Cd 111 (cps)	Apparent Conc. Cd 111 (ppb)
Blank	9.7	
Cal. Std.1	228.3	1.0
Cal. Std.2	1033.0	4.7
Cal. Std.3	2162.8	9.8
Cal. Std.4	4426.4	20.1

Figure A-4.48. Calibration curve of the ICP-MS analyses of the leachates for Cd element.

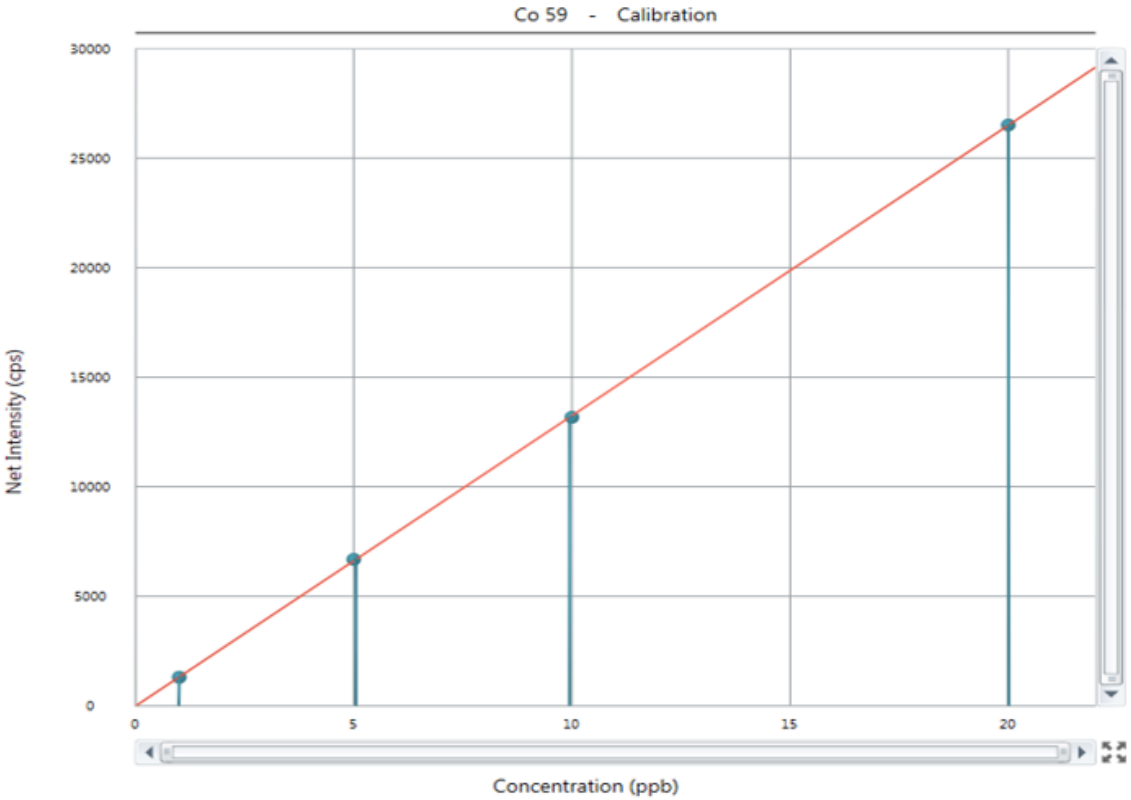

Statistics

Eqn. :	y = 1325x + 0	
Cor.Coeff. :	0.999995	
BEC :	0.013335	ppb
DL :	0.008573	ppb

Calibration Table

	Net Intensity Co 59 (cps)	Apparent Conc. Co 59 (ppb)
Blank	17.7	
Cal. Std.1	1313.7	1.0
Cal. Std.2	6693.2	5.1
Cal. Std.3	13178.1	9.9
Cal. Std.4	26514.3	20.0

Figure A-4.49. Calibration curve of the ICP-MS analyses of the leachates for Co element.

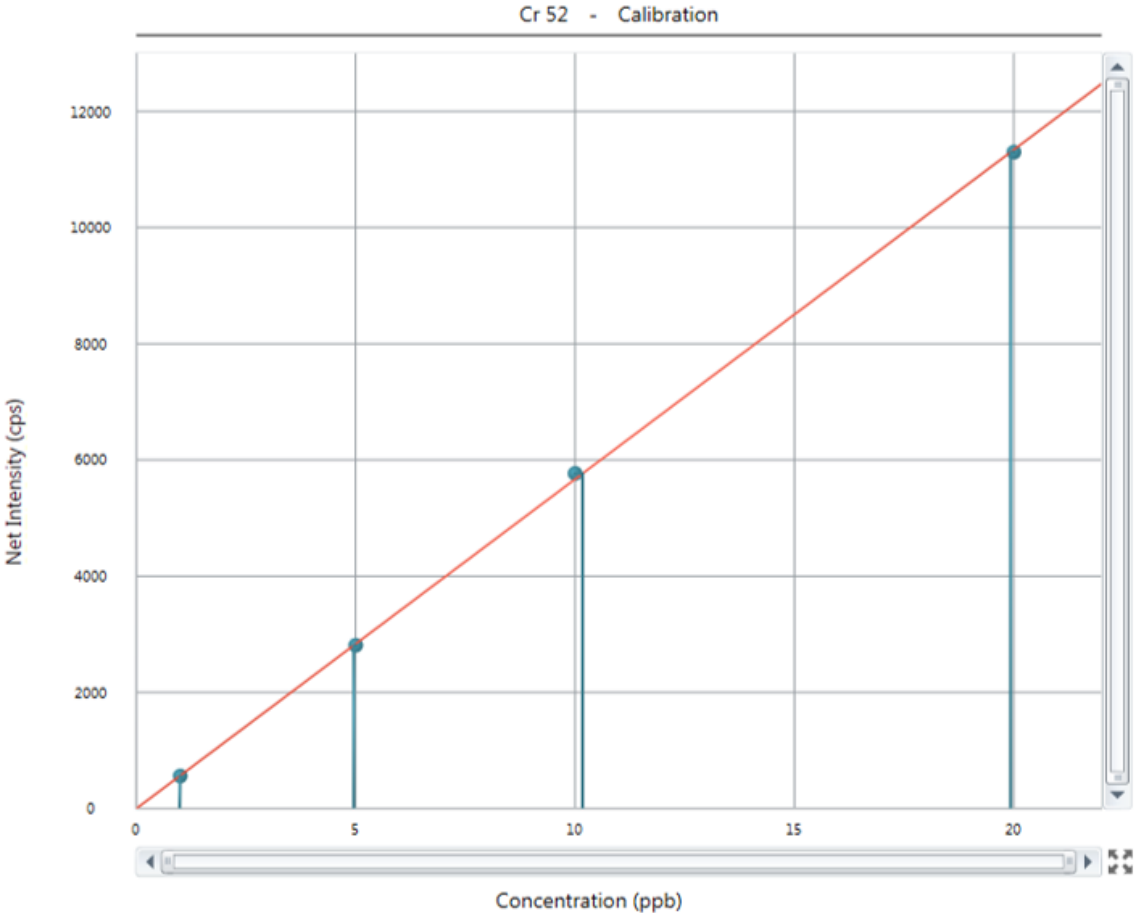

Statistics

Eqn. :	y = 567x + 0	
Cor.Coeff. :	0.999964	
BEC :	0.077601	ppb
DL :	0.027997	ppb

Calibration Table

	Net Intensity Cr 52 (cps)	Apparent Conc. Cr 52 (ppb)
Blank	44.0	
Cal. Std.1	561.0	1.0
Cal. Std.2	2810.6	5.0
Cal. Std.3	5767.8	10.2
Cal. Std.4	11297.5	19.9

Figure A-4.50. Calibration curve of the ICP-MS analyses of the leachates for Cr element.

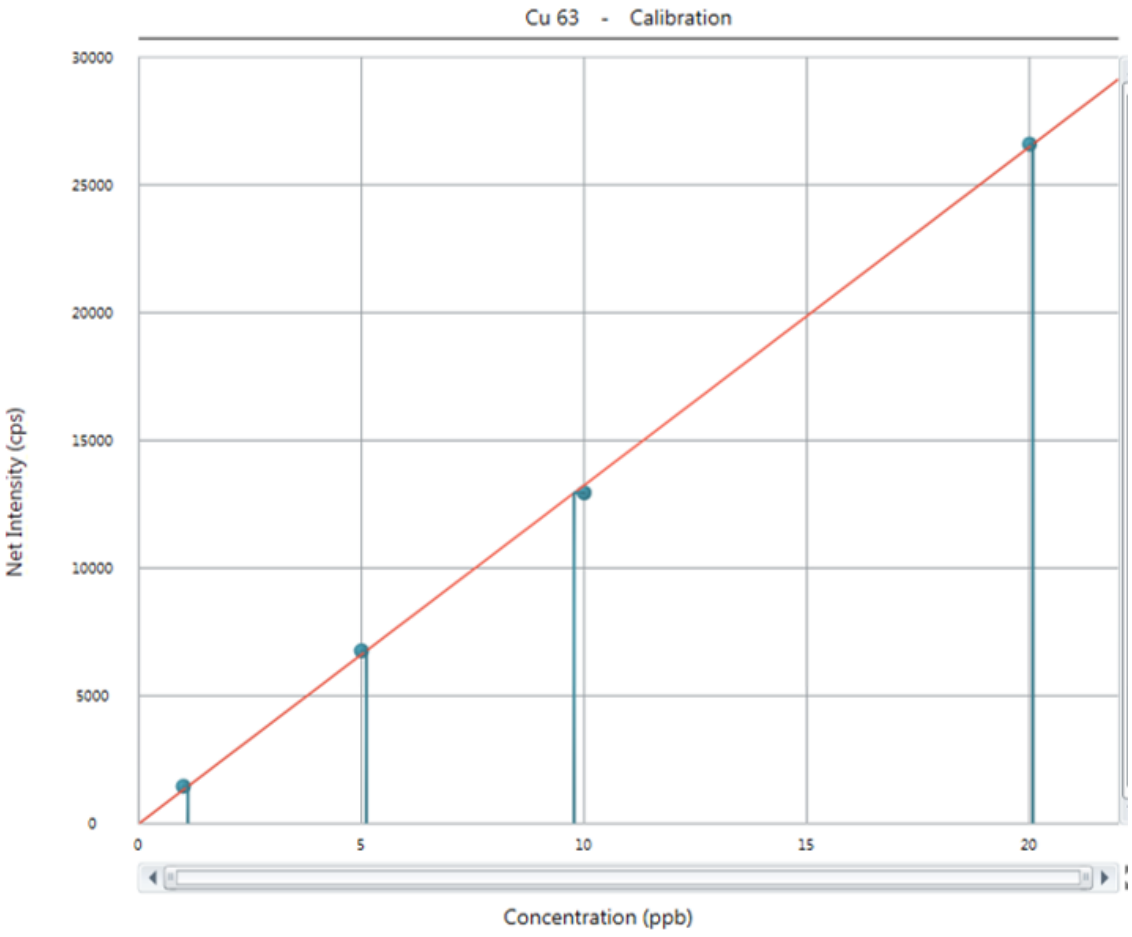

Statistics

Eqn. :	y = 1324x + 0	
Cor.Coeff. :	0.999924	
BEC :	0.233861	ppb
DL :	0.095300	ppb

Calibration Table

	Net Intensity Cu 63 (cps)	Apparent Conc. Cu 63 (ppb)
Blank	309.7	
Cal. Std.1	1461.8	1.1
Cal. Std.2	6764.7	5.1
Cal. Std.3	12943.8	9.8
Cal. Std.4	26589.4	20.1

Figure A-4.51. Calibration curve of the ICP-MS analyses of the leachates for Cu element.

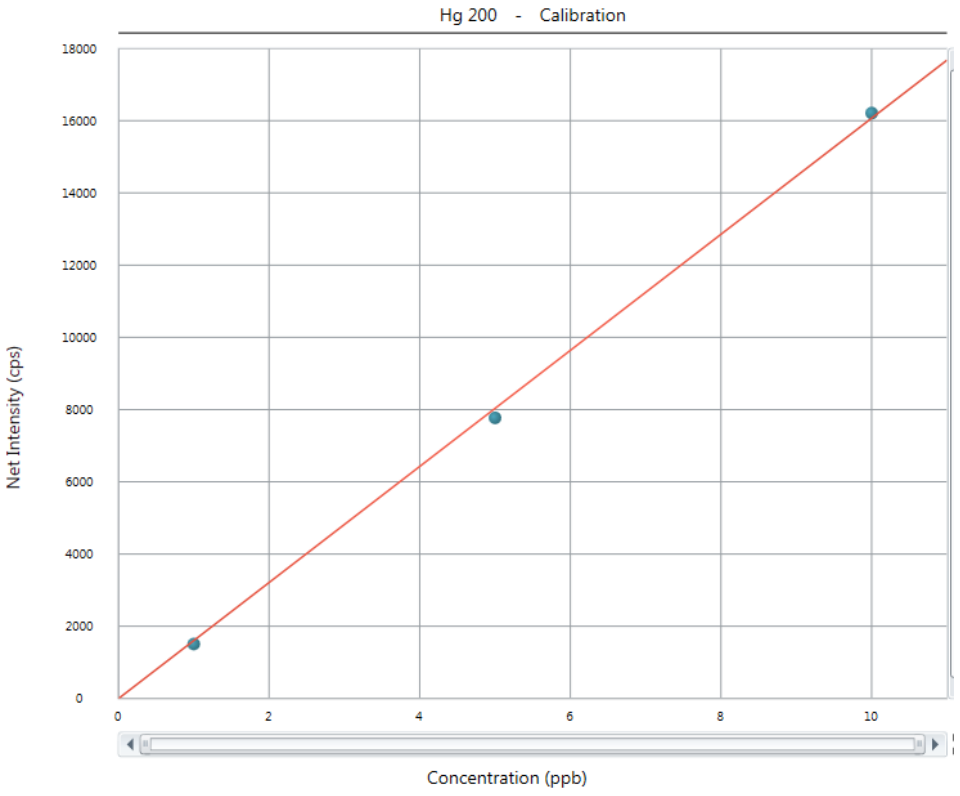

Statistics

Eqn. :	y = 1607x + 0	
Cor.Coeff. :	0.999850	
BEC :	0.165417	ppb
DL :	0.014135	ppb

Calibration Table

	Net Intensity Hg 200 (cps)	Apparent Conc. Hg 200 (ppb)
Blank	265.8	
Cal. Std.1	1511.1	0.9
Cal. Std.2	7773.3	4.8
Cal. Std.3	16211.3	10.1

Figure A-4.52. Calibration curve of the ICP-MS analyses of the leachates for Hg element.

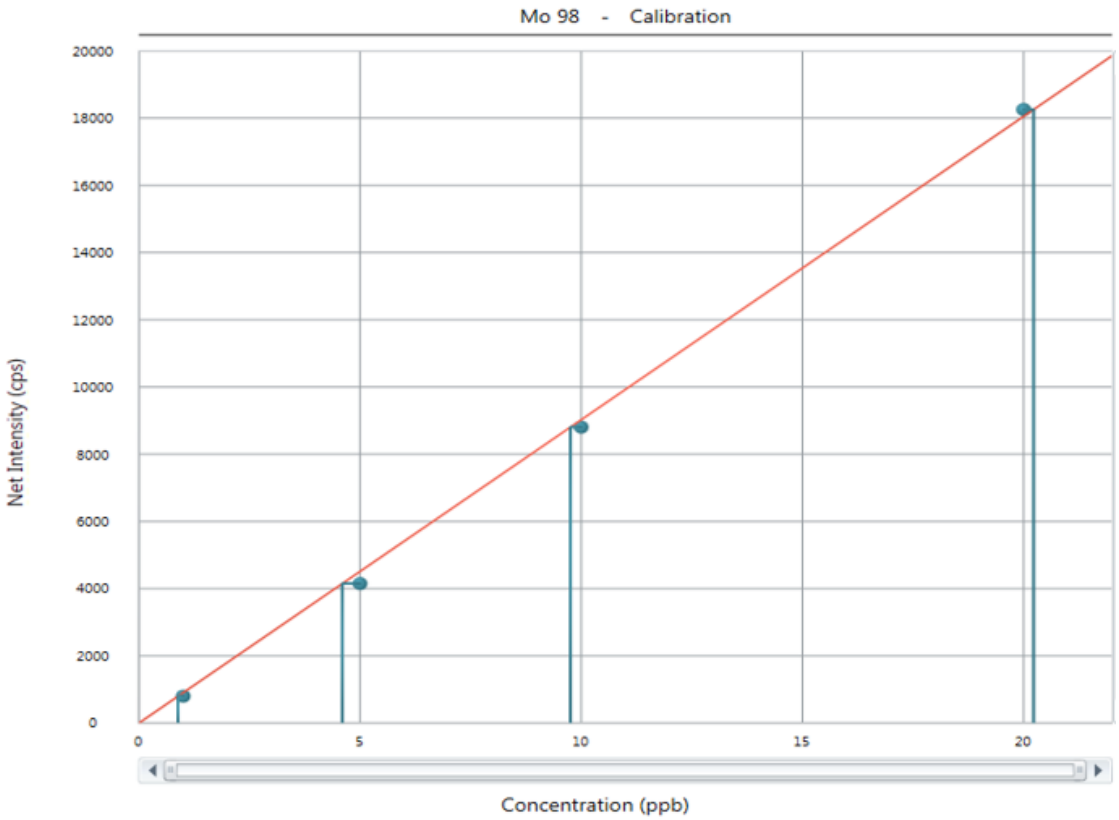

Statistics

Eqn. :	y = 903x + 0	
Cor.Coeff. :	0.999730	
BEC :	0.076857	ppb
DL :	0.026172	ppb

Calibration Table

	Net Intensity Mo 98 (cps)	Apparent Conc. Mo 98 (ppb)
Blank	69.4	
Cal. Std.1	800.5	0.9
Cal. Std.2	4151.0	4.6
Cal. Std.3	8808.0	9.8
Cal. Std.4	18259.3	20.2

Figure A-4.53. Calibration curve of the ICP-MS analyses of the leachates for Mo element.

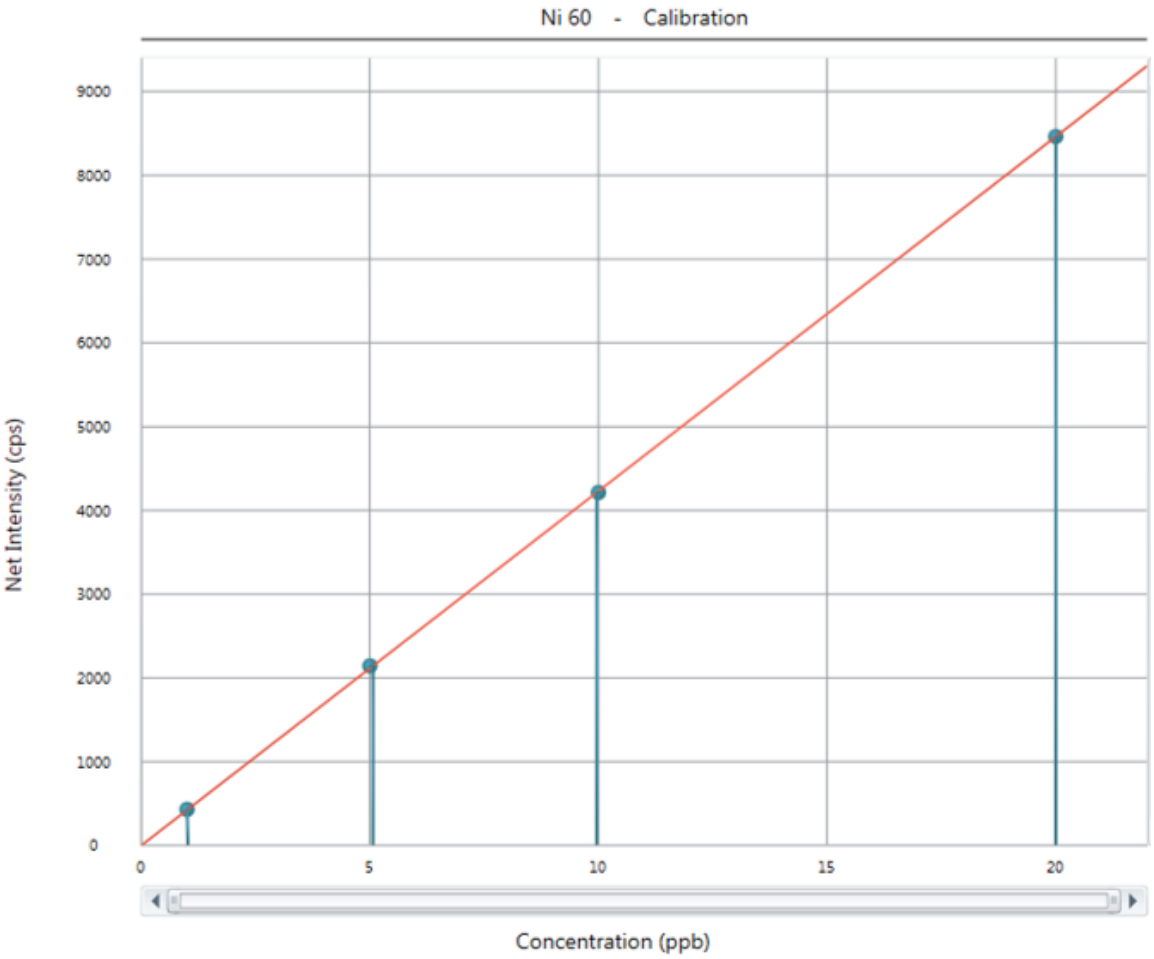

Statistics

Eqn. :	y = 423x + 0	
Cor.Coeff. :	0.999994	
BEC :	0.122115	ppb
DL :	0.065883	ppb

Calibration Table

	Net Intensity Ni 60 (cps)	Apparent Conc. Ni 60 (ppb)
Blank	51.7	
Cal. Std.1	431.3	1.0
Cal. Std.2	2144.2	5.1
Cal. Std.3	4214.6	10.0
Cal. Std.4	8462.5	20.0

Figure A-4.54. Calibration curve of the ICP-MS analyses of the leachates for Ni element.

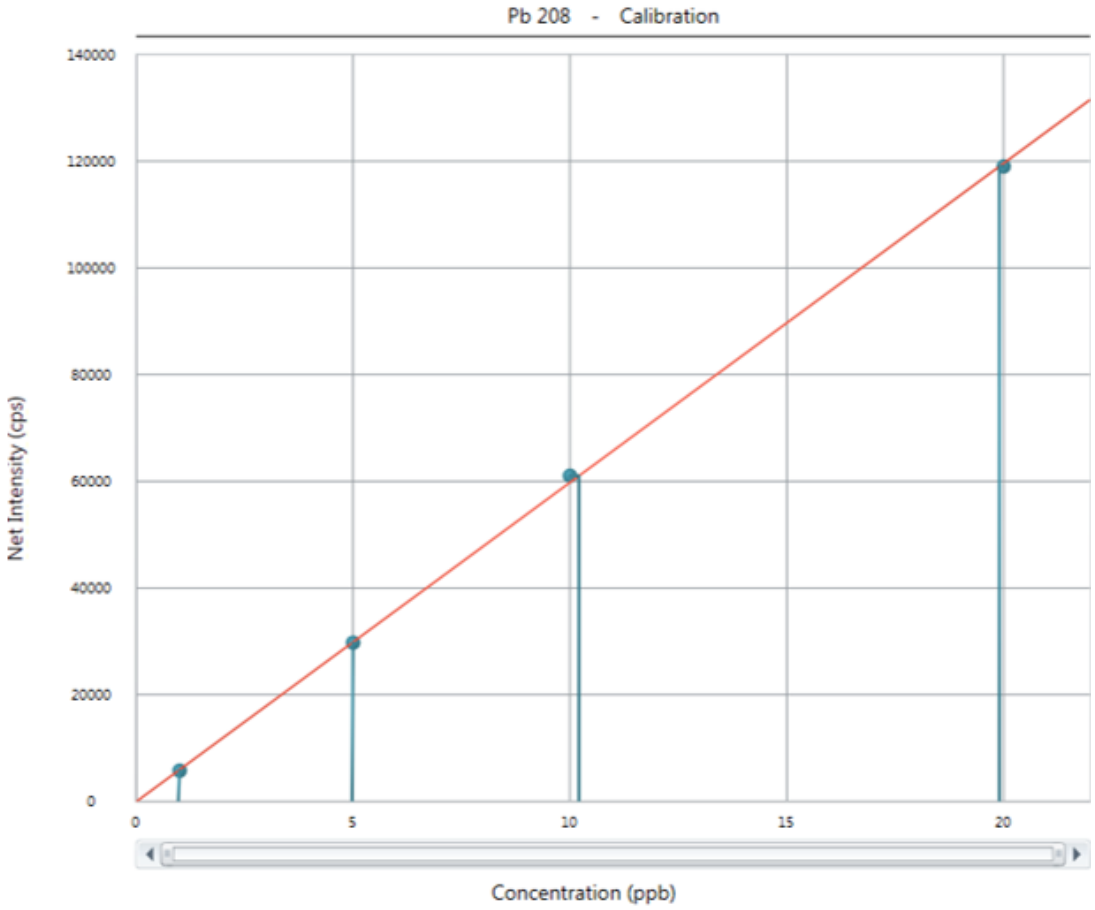

Statistics

Eqn. :	y = 5979x + 0	
Cor.Coeff. :	0.999948	
BEC :	0.031555	ppb
DL :	0.007615	ppb

Calibration Table

	Net Intensity Pb 208 (cps)	Apparent Conc. Pb 208 (ppb)
Blank	188.7	
Cal. Std.1	5806.9	1.0
Cal. Std.2	29762.7	5.0
Cal. Std.3	61041.3	10.2
Cal. Std.4	118994.1	19.9

Figure A-4.55. Calibration curve of the ICP-MS analyses of the leachates for Pb element.

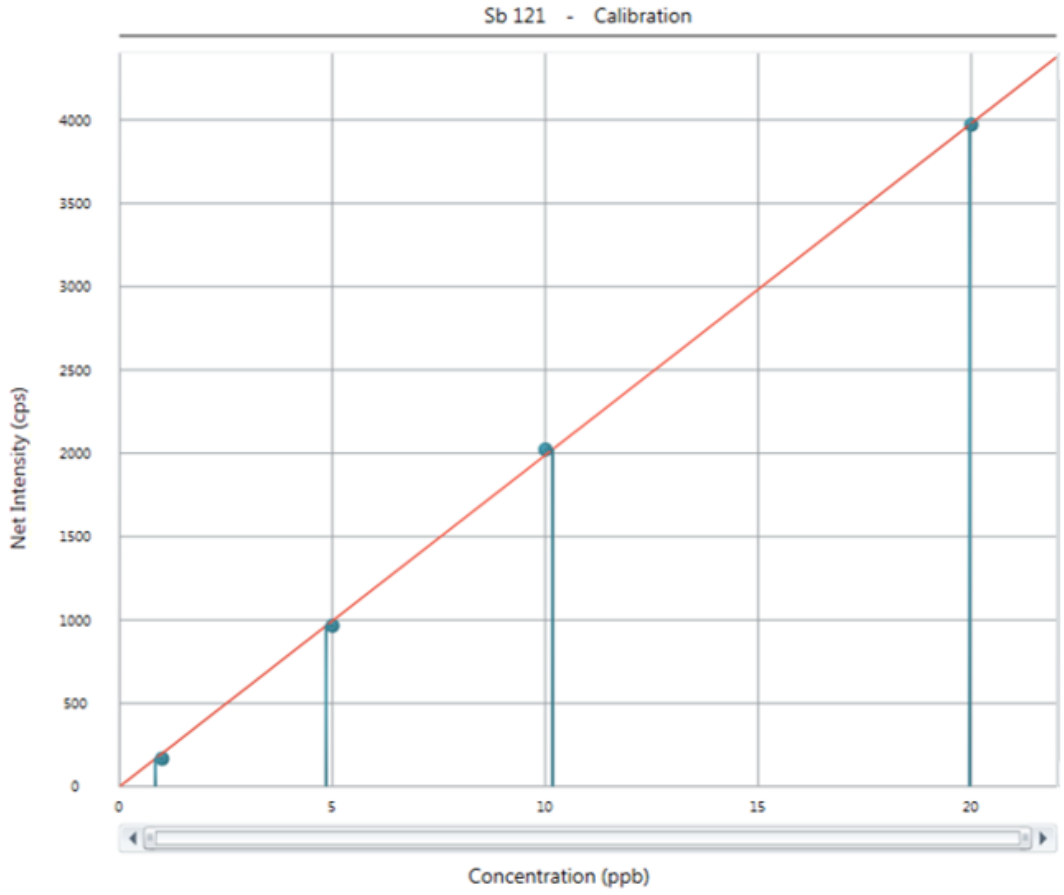

Statistics

Eqn. :	y = 199x + 0	
Cor.Coeff. :	0.999928	
BEC :	0.105548	ppb
DL :	0.098875	ppb

Calibration Table

	Net Intensity Sb 121 (cps)	Apparent Conc. Sb 121 (ppb)
Blank	21.0	
Cal. Std.1	167.7	0.8
Cal. Std.2	965.4	4.9
Cal. Std.3	2022.8	10.2
Cal. Std.4	3971.6	20.0

Figure A-4.56. Calibration curve of the ICP-MS analyses of the leachates for Sb element.

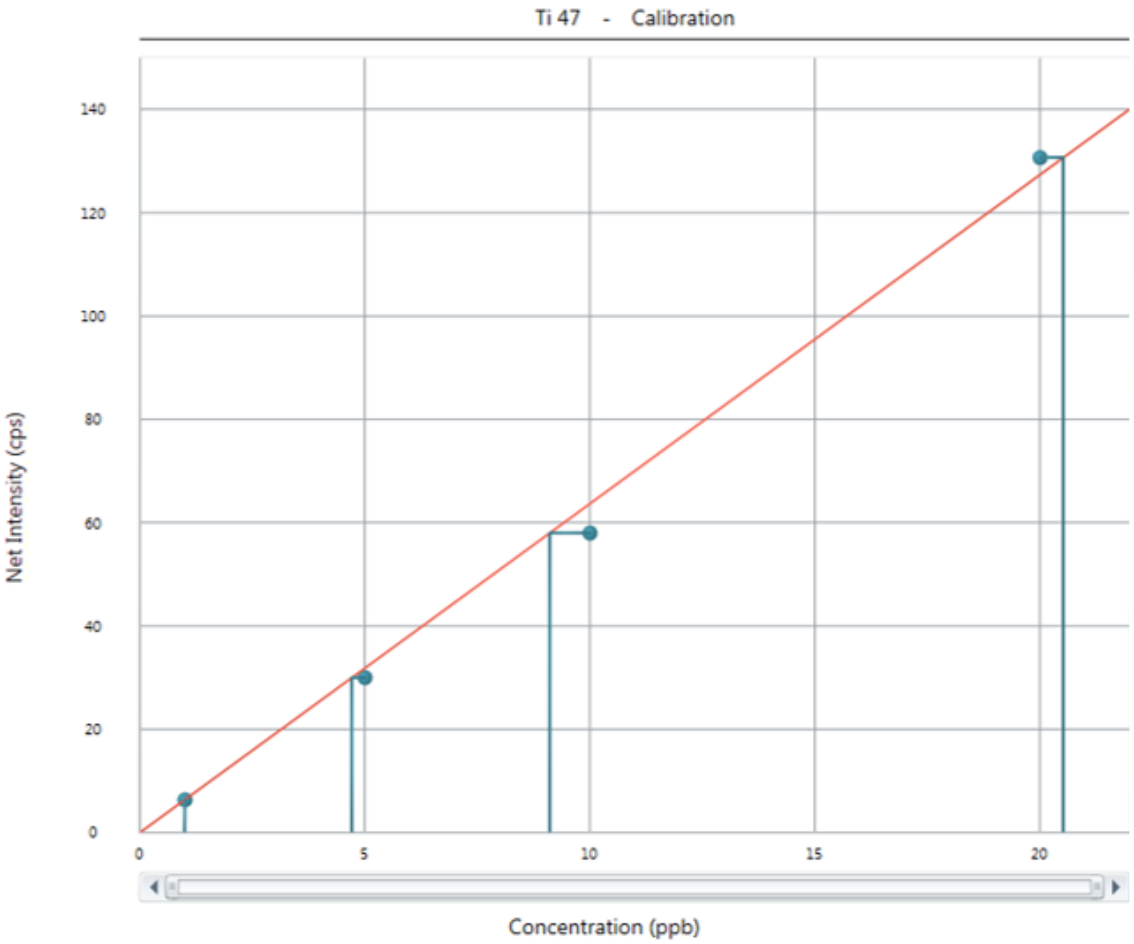

Statistics

Eqn. :	y = 6x + 0	
Cor.Coeff. :	0.998910	
BEC :	0.418746	ppb
DL :	0.980652	ppb

Calibration Table

	Net Intensity Ti 47 (cps)	Apparent Conc. Ti 47 (ppb)
Blank	2.7	
Cal. Std.1	6.3	1.0
Cal. Std.2	30.0	4.7
Cal. Std.3	58.0	9.1
Cal. Std.4	130.7	20.5

Figure A-4.57. Calibration curve of the ICP-MS analyses of the leachates for Ti element.

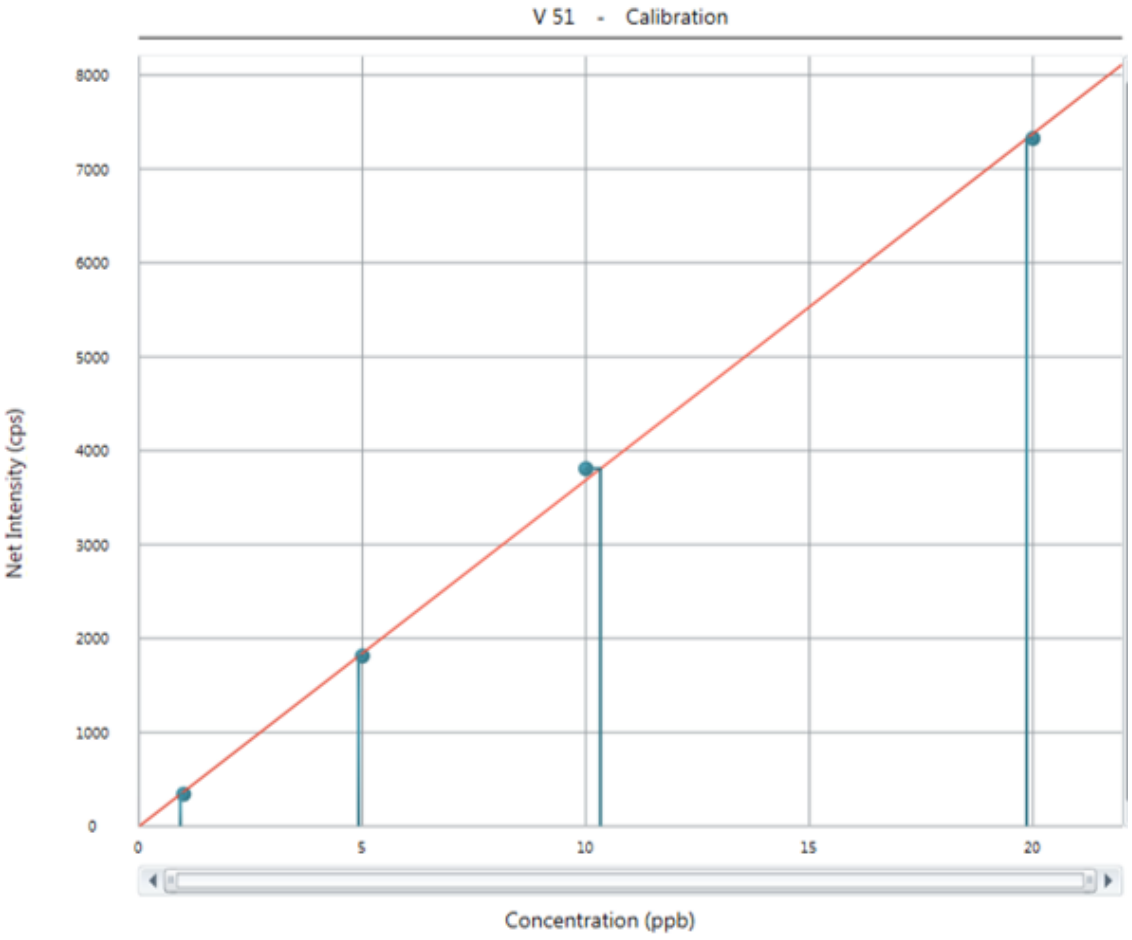

Statistics

Eqn. :	y = 369x + 0	
Cor.Coeff. :	0.999870	
BEC :	0.009942	ppb
DL :	0.009392	ppb

Calibration Table

	Net Intensity V 51 (cps)	Apparent Conc. V 51 (ppb)
Blank	3.7	
Cal. Std.1	343.0	0.9
Cal. Std.2	1814.4	4.9
Cal. Std.3	3808.2	10.3
Cal. Std.4	7325.2	19.9

Figure A-4.58. Calibration curve of the ICP-MS analyses of the leachates for V element.

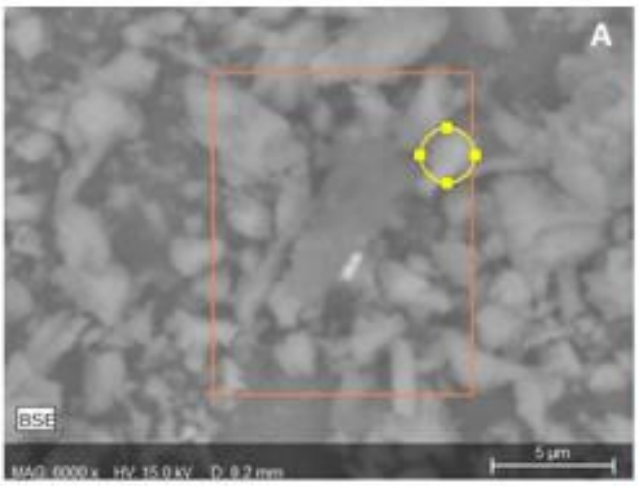

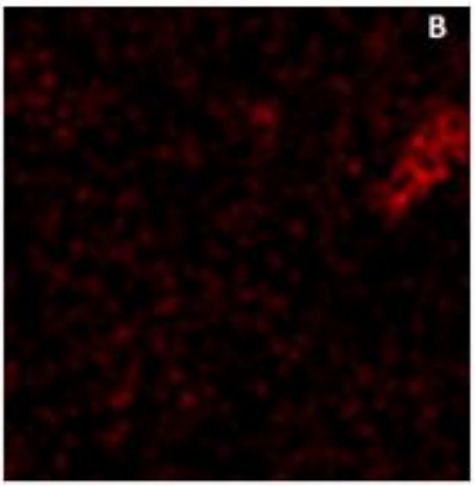

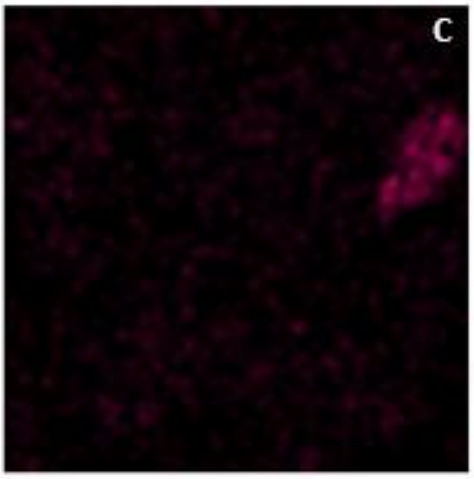

D

Spectrum: Point

Element	AN	Series	Net	unn. C [wt.%]	norm. C [wt.%]	Atom. C [at.%]	Error [%]
Silicon	14	K-series	373	13.75	34.21	67.32	0.6
Tin	50	L-series	176	11.97	29.76	13.86	0.4
Antimony	51	L-series	146	10.46	26.02	11.81	0.3
Selenium	34	L-series	68	4.01	9.97	6.98	0.2
Chlorine	17	K-series	0	0.00	0.00	0.00	0.0
Titanium	22	K-series	0	0.00	0.00	0.00	0.0
Vanadium	23	K-series	0	0.00	0.00	0.00	0.0
Chromium	24	K-series	0	0.00	0.00	0.00	0.0
Manganese	25	K-series	0	0.00	0.00	0.00	0.0
Iron	26	K-series	0	0.00	0.00	0.00	0.0
Nickel	28	K-series	0	0.00	0.00	0.00	0.0
Cobalt	27	K-series	0	0.00	0.00	0.00	0.0
Copper	29	K-series	0	0.00	0.00	0.00	0.0

Figure A-4.59. EDS data referring to the composition of a particle found in Baltic face mask. (A) is the image generated by the SEM at x6000, (B) is a false colour map for elemental Sb (C) is a false colour map for elemental Sn and (D) is the tabulated elemental composition data.

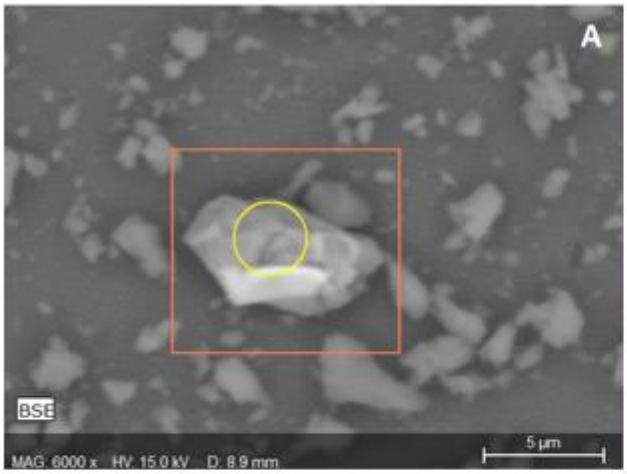

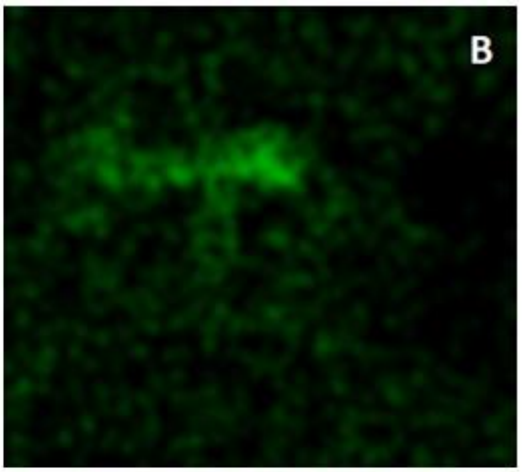

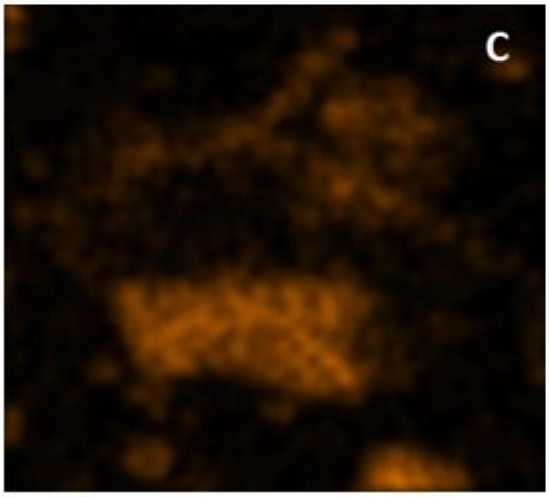

D

Spectrum: Point

Element	AN	Series	Net	unn. C [wt.%]	norm. C [wt.%]	Atom. C [at.%]	Error [%]
Oxygen	8	K-series	896	16.56	36.28	50.09	2.8
Carbon	6	K-series	188	7.80	17.08	31.40	1.9
Silicon	14	K-series	751	4.96	10.86	8.54	0.2
Selenium	34	L-series	420	4.26	9.34	2.61	0.2
Arsenic	33	L-series	343	3.57	7.83	2.31	0.2
Iron	26	K-series	124	2.57	5.63	2.23	0.1
Tellurium	52	L-series	247	3.12	6.83	1.18	0.1
Manganese	25	K-series	40	0.66	1.45	0.58	0.0
Nickel	28	K-series	9	0.32	0.69	0.26	0.0
Antimony	51	L-series	49	0.58	1.26	0.23	0.0
Chromium	24	K-series	13	0.17	0.38	0.16	0.0
Copper	29	K-series	4	0.18	0.40	0.14	0.0
Cadmium	48	L-series	18	0.19	0.41	0.08	0.0
Mercury	80	M-series	25	0.31	0.69	0.08	0.0
Lead	82	M-series	22	0.29	0.63	0.07	0.0
Tin	50	L-series	10	0.12	0.26	0.05	0.0
			Total:	45.66	100.00	100.00	

Figure A-4.60. EDS data referring to the composition of a particle found in Omnitex face mask. (A) is the image generated by the SEM at x6000, (B) is a false colour map for elemental As (C) is a false colour map for elemental Si and (D) is the tabulated elemental composition data.

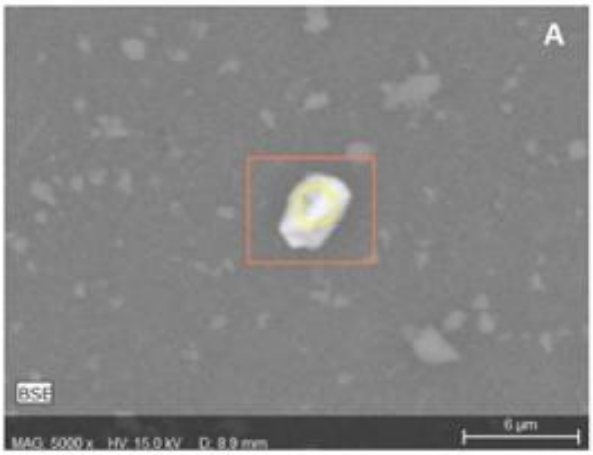

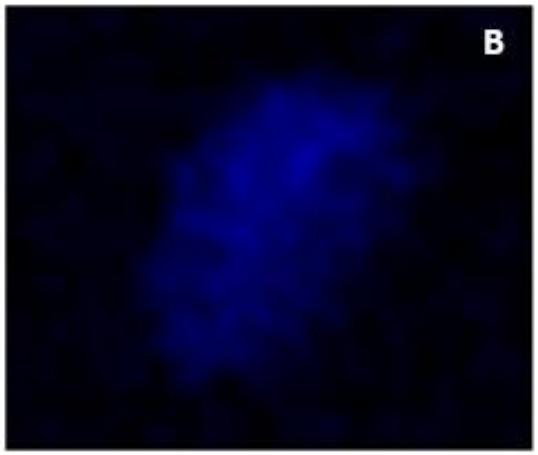

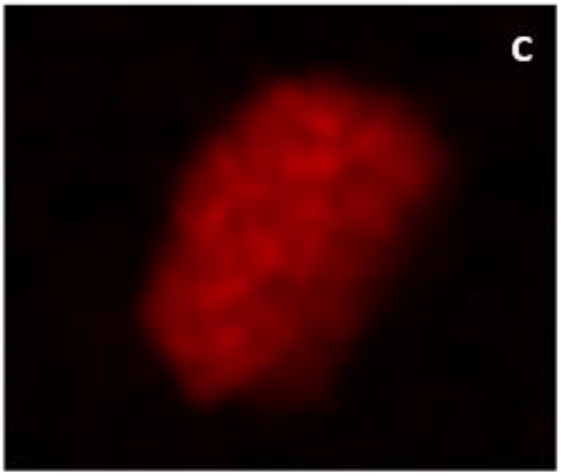

D

Spectrum: Point

Element	AN	Series	Net	unn. C [wt.%]	norm. C [wt.%]	Atom. C [at.%]
Copper	29	K-series	67	44.57	36.66	55.46
Lead	82	M-series	197	33.88	27.87	12.93
Selenium	34	L-series	145	23.21	19.09	23.24
Mercury	80	M-series	110	18.20	14.97	7.18
Cadmium	48	L-series	5	0.83	0.68	0.59
Antimony	51	L-series	4	0.82	0.67	0.53
Manganese	25	K-series	0	0.03	0.02	0.04
Vanadium	23	K-series	0	0.01	0.01	0.01
Scandium	21	K-series	0	0.00	0.00	0.00
Titanium	22	K-series	0	0.00	0.00	0.00
Chromium	24	K-series	0	0.00	0.00	0.00
Iron	26	K-series	0	0.00	0.00	0.00
Cobalt	27	K-series	0	0.00	0.00	0.00
Nickel	28	K-series	0	0.00	0.00	0.00
Zinc	30	K-series	0	0.00	0.00	0.00
Silver	47	L-series	0	0.00	0.00	0.00
Rhodium	45	L-series	0	0.00	0.00	0.00

Figure A-4.61. EDS data referring to the composition of a particle found in NHS face mask. (A) is the image generated by the SEM at x5000, (B) is a false colour map for elemental Hg. (C) is a false colour map for elemental Pb and (D) is the tabulated elemental composition data.